REPUBLIQUE DU CAMEROUN
Paix-Travail-Patrie
****
UNIVERSITÉ DE YAOUNDÉ I
****
FACULTÉ DES SCIENCES
****
CENTRE DE RECHERCHE ET DE FORMATION DOCTORALE EN SCIENCES, TECHNOLOGIES ET GEOSCIENCES
UNITE DE RECHERCHE ET DE FORMATION DOCTORALE PHYSIQUE ET APPLICATIONS
BP.812 Yaoundé
Email: crftstg@uy1.uninet.cm

REPUBLIC OF CAMEROON
Peace-Work-Fatherland
****
UNIVERSITY OF YAOUNDE I
****
FACULTY OF SCIENCES
****
POSTGRADUATES SCHOOL OF SCIENCE, TECHNOLOGY AND GEOSCIENCES
RESEARCH UNIT FOR PHYSICS AND APPLICATIONS
P.O.BOX.812 Yaoundé
Email: crftstg@uy1.uninet.cm

DEPARTMENT OF PHYSICS

LABORATORY OF NUCLEAR, ATOMIC, MOLECULAR PHYSICS AND BIOPHYSICS

DISSIPATIVE SOLITONS IN REACTION-DIFFUSION SYSTEMS WITH SELF-AND-CROSS DIFFUSION

THESIS

Submitted and defended in fulfillment of the requirements for the award of the degree of Doctorate/Ph.D. in Physics

Speciality: ATOMIC, MOLECULAR PHYSICS AND BIOPHYSICS

By:

TABI DZOU BLAISE
Registration number: 11W0812
Master of Science in Physics

Under the supervision of:

KOFANÉ TIMOLÉON CRÉPIN
Professor
University of Yaoundé I

MVOGO ALAIN
Associate Professor
University of Yaoundé I

Year : 2025

REPUBLIQUE DU CAMEROUN
Paix-Travail-Patrie
****
UNIVERSITÉ DE YAOUNDÉ I
****
FACULTÉ DES SCIENCES
****
CENTRE DE RECHERCHE ET DE FORMATION DOCTORALE EN SCIENCES, TECHNOLOGIES ET GEOSCIENCES
UNITE DE RECHERCHE ET DE FORMATION DOCTORALE PHYSIQUE ET APPLICATIONS
BP.812 Yaoundé
Email: crftstg@uy1.uninet.cm

REPUBLIC OF CAMEROON
Peace-Work-Fatherland
****
UNIVERSITY OF YAOUNDE I
****
FACULTY OF SCIENCES
****
POSTGRADUATES SCHOOL OF SCIENCE, TECHNOLOGY AND GEOSCIENCES
RESEARCH UNIT FOR PHYSICS AND APPLICATIONS
P.O.BOX.812 Yaoundé
Email: crftstg@uy1.uninet.cm

DEPARTMENT OF PHYSICS

LABORATORY OF NUCLEAR, ATOMIC, MOLECULAR PHYSICS AND BIOPHYSICS

DISSIPATIVE SOLITONS IN REACTION-DIFFUSION SYSTEMS WITH SELF-AND-CROSS DIFFUSION

THESIS

Submitted and defended in fulfillment of the requirements for the award of the degree of Doctorate/Ph.D. in Physics

Speciality: ATOMIC, MOLECULAR PHYSICS AND BIOPHYSICS

By:

TABI DZOU BLAISE
Registration number: 11W0812
Master of Science in Physics

Under the supervision of:

KOFANÉ TIMOLÉON CRÉPIN
Professor
University of Yaoundé I

MVOGO ALAIN
Associate Professor
University of Yaoundé I

Year : 2025

UNIVERSITÉ DE YAOUNDÉ I **Faculté des Sciences** Division de la Programmation et du Suivi des Activités Académiques		THE UNIVERSITY OF YAOUNDE I **Faculty of Science** Division of Programming and Follow-up of Academic Affaires
LISTE DES ENSEIGNANTS PERMANENTS		**LIST OF PERMANENT TEACHING STAFF**

ANNÉE ACADEMIQUE 2024/2025

(Par Département et par Grade)

DATE D'ACTUALISATION 30 septembre 2024

ADMINISTRATION

1. **DOYEN :** OWONO OWONO Luc Calvin, *Professeur*
2. **VICE-DOYEN / DPSAA:** NDJIGUI Paul-Désiré, *Professeur*
3. **VICE-DOYEN / DSSE :** NYEGUE Maximilienne Ascension, *Professeur*
4. **VICE-DOYEN / DRC :** NOUNDJEU Pierre, *Maître de Conférences*
5. **Chef Division Administrative et Financière :** NDOYE FOE Florentine Marie Chantal, *Maître de Conférences*
6. **Chef Division des Affaires Académiques, de la Recherche et de la Scolarité DAARS :** AJEAGAH Gidéon AGHAINDUM, *Professeur*

1- DÉPARTEMENT DE BIOCHIMIE (BC) (44)

N°	NOMS ET PRÉNOMS	GRADE	OBSERVATIONS
1.	BIGOGA DAIGA Jude	Professeur	En poste
2.	FEKAM BOYOM Fabrice	Professeur	En poste
3.	KANSCI Germain	Professeur	En poste
4.	MBACHAM FON Wilfred	Professeur	En poste
5.	MOUNDIPA FEWOU Paul	Professeur	*Chef de Département*
6.	NGUEFACK Julienne	Professeur	En poste
7.	NJAYOU Frédéric Nico	Professeur	En poste
8.	OBEN Julius ENYONG	Professeur	En poste
9.	ACHU Merci BIH	Maître de Conférences	En poste
10.	AKINDEH MBUH NJI	Maître de Conférences	En poste
11.	ATOGHO Barbara MMA	Maître de Conférences	En poste
12.	AZANTSA KINGUE GABIN BORIS	Maître de Conférences	En poste
13.	BELINGA née NDOYE FOE F. M. C.	Maître de Conférences	*Chef DAF / FS*
14.	DAKOLE DABOY Charles	Maître de Conférences	En poste
15.	DONGMO LEKAGNE Joseph Blaise	Maître de Conférences	En poste
16.	DJUIDJE NGOUNOUE Marceline	Maître de Conférences	En poste
17.	DJUIKWO NKONGA Ruth Viviane	Maître de Conférences	En poste
18.	EFFA ONOMO Pierre	Maître de Conférences	*VD/FS/Univ Ebwa*
19.	EWANE Cécile Annie	Maître de Conférences	En poste
20.	KENGNE NOUEMSI Anne Pascale	Maître de Conférences	En poste
21.	KOTUE TAPTUE Charles	Maître de Conférences	En poste
22.	LUNGA Paul KEILAH	Maître de Conférences	En poste
23.	MANANGA Marlyse Joséphine	Maître de Conférences	En poste
24.	MBONG ANGIE M. Mary Anne	Maître de Conférences	En poste
25.	MOFOR née TEUGWA Clotilde	Maître de Conférences	*Doyen FS / UDs*
26.	NANA Louise épouse WAKAM	Maître de Conférences	En poste
27.	NGONDI Judith Laure	Maître de Conférences	En poste
28.	Palmer MASUMBE NETONGO	Maître de Conférences	En poste
29.	PECHANGOU NSANGOU Sylvain	Maître de Conférences	En poste
30.	TCHANA KOUATCHOUA Angèle	Maître de Conférences	En poste
31.	BEBEE Fadimatou	Chargée de Cours	En poste
32.	BEBOY EDJENGUELE Sara N.	Chargé de Cours	En poste
33.	FONKOUA Martin	Chargé de Cours	En poste
34.	FOUPOUAPOUOGNIGNI Yacouba	Chargé de Cours	En poste
35.	KOUOH ELOMBO Ferdinand	Chargé de Cours	En poste
36.	MBOUCHE FANMOE Marceline J.	Chargé de Cours	En poste
37.	OWONA AYISSI Vincent Brice	Chargé de Cours	En poste
38.	WILFRED ANGIE ABIA	Chargé de Cours	En poste

39.	BAKWO BASSOGOG Christian Bernard	Assistant	En Poste
40.	ELLA Fils Armand	Assistant	En Poste
41.	EYENGA Eliane Flore	Assistant	En Poste
42.	MADIESSE KEMGNE Eugenie Aimée	Assistant	En Poste
43.	MANJIA NJIKAM Jacqueline	Assistant	En Poste
44.	WOGUIA Alice Louise	Assistant	En Poste

2- DÉPARTEMENT DE BIOLOGIE ET PHYSIOLOGIE ANIMALES (BPA) (50)

1.	AJEAGAH Gidéon AGHAINDUM	Professeur	*DAARS/FS*
2.	DIMO Théophile	Professeur	En Poste
3.	DJIETO LORDON Champlain	Professeur	En Poste
4.	DZEUFIET DJOMENI Paul Désiré	Professeur	En Poste
5.	ESSOMBA née NTSAMA MBALA	Professeur	*CD et Vice Doyen/FMSB/UYI*
6.	KEKEUNOU Sévilor	Professeur	*Chef de Département*
7.	NJAMEN Dieudonné	Professeur	En poste
8.	NOLA Moïse	Professeur	En poste
9.	TAN Paul VERNYUY	Professeur	En poste
10.	TCHUEM TCHUENTE Louis Albert	Professeur	*Inspecteur de service / Coord.Progr./MINSANTE*
11.	ZEBAZE TOGOUET Serge Hubert	Professeur	En poste

12.	ALENE Désirée Chantal	Maître de Conférences	*Vice Doyen/ Uté Ebwa*
13.	ATSAMO Albert Donatien	Maître de Conférences	En poste
14.	BILANDA Danielle Claude	Maître de Conférences	En poste
15.	DJIOGUE Séfirin	Maître de Conférences	En poste
16.	GOUNOUE KAMKUMO Raceline épse FOTSING	Maître de Conférences	En poste
17.	JATSA BOUKENG Hermine épse MEGAPTCHE	Maître de Conférences	En Poste
18.	KANDEDA KAVAYE Antoine	Maître de Conférences	En poste
19.	LEKEUFACK FOLEFACK Guy B.	Maître de Conférences	En poste
20.	MAHOB Raymond Joseph	Maître de Conférences	En poste
21.	MBENOUN MASSE Paul Serge	Maître de Conférences	En poste
22.	MEGNEKOU Rosette	Maître de Conférences	En poste
23.	MOUNGANG Luciane Marlyse	Maître de Conférences	En poste
24.	NOAH EWOTI Olive Vivien	Maître de Conférences	En poste
25.	MONY Ruth épse NTONE	Maître de Conférences	En Poste
26.	MVEYO NDANKEU Yves Patrick	Maître de Conférences	En poste
27.	NGUEGUIM TSOFACK Florence	Maître de Conférences	En poste
28.	NGUEMBOCK	Maître de Conférences	En poste
29.	TAMSA ARFAO Antoine	Maître de Conférences	En poste
30.	TOMBI Jeannette	Maître de Conférences	En poste

31.	AMBADA NDZENGUE GEORGIA ELNA	Chargé de Cours	En poste
32.	BASSOCK BAYIHA Etienne Didier	Chargé de Cours	En poste
33.	ETEME ENAMA Serge	Chargé de Cours	En poste
34.	FEUGANG YOUMSSI François	Chargé de Cours	En poste
35.	FOKAM Alvine Christelle Epse KENGNE	Chargé de Cours	En poste
36.	FOSSI TANKOUA Olivia Epse DJEUTCHOUANG SAYANG	Chargé de Cours	En poste (transfert Uté de Dla)
37.	GONWOUO NONO Legrand	Chargé de Cours	En poste
38.	KOGA MANG DOBARA	Chargé de Cours	En poste

39.	LEME BANOCK Lucie	Chargé de Cours	En poste
40.	MAPON NSANGOU Indou	Chargé de Cours	En poste
41.	METCHI DONFACK MIREILLE FLAURE EPSE GHOUMO	Chargé de Cours	En poste
42.	NGOUATEU KENFACK Omer Bébé	Chargé de Cours	En poste
43.	NJUA Clarisse YAFI	Chargée de Cours	*Chef Div. Uté Bamenda*
44.	NWANE Philippe Bienvenu	Chargé de Cours	En poste
45.	TADU Zephyrin	Chargé de Cours	En poste
46.	YEDE	Chargé de Cours	En poste
47.	YOUNOUSSA LAME	Chargé de Cours	En poste

48.	KODJOM WANCHE Jacguy Joyce	Assistante	En poste
49.	NDENGUE Jean De Matha	Assistant	En poste
50.	ZEMO GAMO Franklin	Assistant	En poste

3- DÉPARTEMENT DE BIOLOGIE ET PHYSIOLOGIE VÉGÉTALES (BPV) (32)

1.	AMBANG Zachée	Professeur	*Chef de Département*
2.	DJOCGOUE Pierre François	Professeur	En poste
3.	MBOLO Marie	Professeur	En poste
4.	MOSSEBO Dominique Claude	Professeur	En poste
5.	NDONGO BEKOLO	Professeur	En poste
6.	ZAPFACK Louis	Professeur	En poste

7.	ANGONI Hyacinthe	Maître de Conférences	En poste
8.	BIYE Elvire Hortense	Maître de Conférences	En poste
9.	MAHBOU SOMO TOUKAM. Gabriel	Maître de Conférences	En poste
10.	MALA Armand William	Maître de Conférences	En poste
11.	MBARGA BINDZI Marie Alain	Maître de Conférences	*DAAC /UDla*
12.	NGALLE Hermine BILLE	Maître de Conférences	En poste
13.	NGONKEU MAGAPTCHE Eddy L.	Maître de Conférences	*CT / MINRESI*
14.	TONFACK Libert Brice	Maître de Conférences	En poste
15.	TSOATA Esaïe	Maître de Conférences	En poste
16.	ONANA JEAN MICHEL	Maître de Conférences	En poste

17.	DJEUANI Astride Carole	Chargé de Cours	En poste
18.	GONMADGE CHRISTELLE	Chargé de Cours	En poste
19.	MAFFO MAFFO Nicole Liliane	Chargé de Cours	En poste
20.	MANGA NDJAGA JUDE	Chargé de Cours	En poste
21.	NNANGA MEBENGA Ruth Laure	Chargé de Cours	En poste
22.	NOUKEU KOUAKAM Armelle	Chargé de Cours	En poste
23.	NSOM ZAMBO EPSE PIAL ANNIE CLAUDE	Chargé de Cours	*En détachement/UNESCO MALI*
24.	GODSWILL NTSOMBOH NTSEFONG	Chargé de Cours	En poste
25.	KABELONG BANAHO Louis-Paul-Roger	Chargé de Cours	En poste
26.	KONO Léon Dieudonné	Chargé de Cours	En poste
27.	LIBALAH Moses BAKONCK	Chargé de Cours	En poste
28.	LIKENG-LI-NGUE Benoit C	Chargé de Cours	En poste
29.	TAEDOUNG Evariste Hermann	Chargé de Cours	En poste
30.	TEMEGNE NONO Carine	Chargé de Cours	En poste
31.	DIDA LONTSI Sylvere Landry	Assistant	En poste
32.	METSEBING Blondo-Pascal	Assistant	En poste

4- DÉPARTEMENT DE CHIMIE INORGANIQUE (CI) (27)

1.	GHOGOMU Paul MINGO	Professeur	*Ministre Chargé de Mission PR*
2.	NANSEU NJIKI Charles Péguy	Professeur	En poste
3.	NDIFON Peter TEKE	Professeur	*CT MINRESI*
4.	NENWA Justin	Professeur	En poste
5.	NGOMO Horace MANGA	Professeur	*Vice Chancelor/UB*
6.	NJIOMOU C. épse DJANGANG	Professeur	En poste
7.	NJOYA Dayirou	Professeur	En poste
8.	ACAYANKA Elie	Maître de Conférences	En poste
9.	EMADAK Alphonse	Maître de Conférences	En poste
10.	KAMGANG YOUBI Georges	Maître de Conférences	En poste
11.	KEMMEGNE MBOUGUEM Jean C.	Maître de Conférences	En poste
12.	KENNE DEDZO GUSTAVE	Maître de Conférences	En poste
13.	MBEY Jean Aime	Maître de Conférences	En poste
14.	NDI NSAMI Julius	Maître de Conférences	*Chef de Département*
15.	NEBAH Née NDOSIRI Bridget NDOYE	Maître de Conférences	*Sénatrice/SENAT*
16.	NYAMEN Linda Dyorisse	Maître de Conférences	En poste
17.	PABOUDAM GBAMBIE AWAWOU	Maître de Conférences	En poste
18.	TCHAKOUTE KOUAMO Hervé	Maître de Conférences	En poste
19.	BELIBI BELIBI Placide Désiré	Maître de Conférences	*Chef Service/ ENS Bertoua*
20.	CHEUMANI YONA Arnaud M.	Maître de Conférences	En poste
21.	KOUOTOU DAOUDA	Maître de Conférences	En poste
22.	MAKON Thomas Beauregard	Chargé de Cours	En poste
23.	NCHIMI NONO KATIA	Chargée de Cours	En poste
24.	NJANKWA NJABONG N. Eric	Chargé de Cours	En poste
25.	PATOUOSSA ISSOFA	Chargé de Cours	En poste
26.	SIEWE Jean Mermoz	Chargé de Cours	En Poste
27.	BOYOM TATCHEMO Franck W.	Assistant	En Poste

6- DÉPARTEMENT DE CHIMIE ORGANIQUE (CO) (33)			
1.	Alex de Théodore ATCHADE	Professeur	*DEPE/Univ. Bertoua*
2.	DONGO Etienne	Professeur	*Vice-Doyen/FSE/UYI*
3.	NGOUELA Silvère Augustin	Professeur	*Chef de Département UDS*
4.	PEGNYEMB Dieudonné Emmanuel	Professeur	*Recteur UBertoua/ Chef de Département*
5.	MBAZOA née DJAMA Céline	Professeur	En poste
6.	MKOUNGA Pierre	Professeur	En poste
7.	AMBASSA Pantaléon	Maître de Conférences	En poste
8.	EYONG Kenneth OBEN	Maître de Conférences	En poste
9.	FOTSO WABO Ghislain	Maître de Conférences	En poste
10	KAMTO Eutrophe Le Doux	Maître de Conférences	En poste
11	KENMOGNE Marguerite	Maître de Conférences	En poste
12	MVOT AKAK CARINE	Maître de Conférences	En poste
13	NGO MBING Joséphine	Maître de Conférences	*Chef de Cellule MINRESI*
14	NGONO BIKOBO Dominique Serge	Maître de Conférences	*C.E.A/ MINESUP*
15	NOTE LOUGBOT Olivier Placide	Maître de Conférences	*Dir ENS/Uté Bertoua*
16	NOUNGOUE TCHAMO Diderot	Maître de Conférences	En poste
17	TABOPDA KUATE Turibio	Maître de Conférences	En poste
18	TAGATSING FOTSING Maurice	Maître de Conférences	En poste
19	OUAHOUO WACHE Blandine M.	Maître de Conférences	En poste
20	ZONDEGOUMBA Ernestine	Maître de Conférences	En poste
21.	MESSI Angélique Nicolas	Chargé de Cours	En poste
22.	MUNVERA MFIFEN Aristide	Chargé de Cours	En poste
23.	NGNINTEDO Dominique	Chargé de Cours	En poste
24.	NGOMO Orléans	Chargée de Cours	En poste
25.	NONO NONO Éric Carly	Chargé de Cours	En poste
26.	OUETE NANTCHOUANG Judith Laure	Chargée de Cours	En poste
27.	SIELINOU TEDJON Valérie	Chargé de Cours	En poste
28.	TCHAMGOUE Joseph	Chargé de Cours	En poste
29.	TSAFFACK Maurice	Chargé de Cours	En poste
30.	TSAMO TONTSA Armelle	Chargé de Cours	En poste
31.	TSEMEUGNE Joseph	Chargé de Cours	En poste
32.	NDOGO ETEME Olivier	Assistant	En poste
33.	NGUEMDJO CHIMEZE Valery Wilfried	Assistant	En poste

6- DEPARTEMENT DES ENERGIES RENOUVELABLES (ER) (1)			
1.	BODO Bertrand	Professeur	*Chef de Département*

7- DÉPARTEMENT D'INFORMATIQUE (IN) (22)

1.	ATSA ETOUNDI Roger	Professeur	*Chef de Division des SI/ MINESUP*
2.	FOUDA NDJODO Marcel Laurent	Professeur	*Inspecteur Général Académique/ MINESUP*

3.	NDOUNDAM Réné	Maître de Conférences	En poste
4.	TSOPZE Norbert	Maître de Conférences	En poste

5.	ABESSOLO ALO'O Gislain	Chargé de Cours	*Chef de Cellule MINFOPRA*
6.	AMINOU HALIDOU	Chargé de Cours	*Chef de Département*
7.	DJAM Xaviera YOUH - KIMBI	Chargé de Cours	En Poste
8.	DOMGA KOMGUEM Rodrigue	Chargé de Cours	En poste
9.	EBELE Serge Alain	Chargé de Cours	En poste
10.	EKODECK Stéphane Gaël Raymond	Chargé de Cours	En poste
11.	HAMZA Adamou	Chargé de Cours	En poste
12.	JIOMEKONG AZANZI Fidel	Chargé de Cours	En poste
13.	KOUOKAM KOUOKAM E. A.	Chargé de Cours	En poste
14.	MELATAGIA YONTA Paulin	Chargé de Cours	En poste
15.	MESSI NGUELE Thomas	Chargé de Cours	En poste
16.	MONTHE DJIADEU Valery M.	Chargé de Cours	En poste
17.	NZEKON NZEKO'O ARMEL JACQUES	Chargé de Cours	En poste
18.	OLLE OLLE Daniel Claude Georges Delort	Chargé de Cours	*Directeur Adjoint ENSET Ebolowa*
19.	TAPAMO Hyppolite	Chargé de Cours	En poste

20.	BAYEM Jacques Narcisse	Assistant	En poste
21.	MAKEMBE. S . Oswald	Assistant	*Directeur CUTI*
22.	NKONDOCK. MI. BAHANACK.N.	Assistant	En poste

8- DÉPARTEMENT DE MATHÉMATIQUES (MA) (34)			
1.	AYISSI Raoult Domingo	Professeur	*Chef de Département*
2.	KIANPI Maurice	Maître de Conférences	En poste
3.	MBANG Joseph	Maître de Conférences	En poste
4.	MBEHOU Mohamed	Maître de Conférences	*Chef de Division/ENSPY*
5.	MBELE BIDIMA Martin Ledoux	Maître de Conférences	*Chef de Département de modélisation et applications industrielles/ENSPY*
6.	NOUNDJEU Pierre	Maître de Conférences	*VDRC/FS/UYI*
7.	TAKAM SOH Patrice	Maître de Conférences	En poste
8.	TCHAPNDA NJABO Sophonie B.	Maître de Conférences	*Directeur/AIMS Rwanda*
9.	TCHOUNDJA Edgar Landry	Maître de Conférences	En poste
10.	AGHOUKENG JIOFACK Jean Gérard	Chargé de Cours	*Chef Cellule MINEPAT*
11.	BOGSO ANTOINE Marie	Chargé de Cours	En poste
12.	BITYE MVONDO Esther	Chargé de Cours	En poste
13.	CHENDJOU Gilbert	Chargé de Cours	En poste
14.	DJIADEU NGAHA Michel	Chargé de Cours	En poste
15.	DOUANLA YONTA Herman	Chargé de Cours	En poste
16.	KIKI Maxime Armand	Chargé de Cours	En poste
17.	KOKOMO AYISSI Eric Brice	Chargé de Cours	En poste(transfert de l'université de Douala)
18.	LOUMNGAM KAMGA Victor	Chargé de Cours	En poste
19.	MBAKOP Guy Merlin	Chargé de Cours	En poste
20.	MBATAKOU Salomon Joseph	Chargé de Cours	En poste
21.	MENGUE MENGUE David Joël	Chargé de Cours	*Chef Dpt /ENS Université d'Ebolowa*
22.	MBIAKOP Hilaire George	Chargé de Cours	En poste
23.	NGUEFACK Bernard	Chargé de Cours	En poste
24.	NIMPA PEFOUKEU Romain	Chargée de Cours	En poste
25.	OGADOA AMASSAYOGA	Chargée de Cours	En poste
26.	POLA DOUNDOU Emmanuel	Chargé de Cours	*En stage*
27.	TENKEU JEUFACK Yannick Léa	Chargé de Cours	En poste
28.	TCHEUTIA Daniel Duviol	Chargé de Cours	En poste
29.	TETSADJIO TCHILEPECK M. Eric.	Chargé de Cours	En poste
30.	FOKAM Jean Marcel	Assistant	En poste
31.	GUIDZAVAI KOUCHERE Albert	Assistant	En poste
32.	MANN MANYOMBE Martin Luther	Assistant	En poste
33.	MEFENZA NOUNTU Thiery	Assistant	En poste
34.	NYOUMBI DLEUNA Christelle	Assistant	En poste

9- DÉPARTEMENT DE MICROBIOLOGIE (MIB) (24)

1.	ESSIA NGANG Jean Justin	Professeur	*Chef de Département*
2.	NYEGUE Maximilienne Ascension	Professeur	*Vice-Doyen / DSSE*
3.	SADO KAMDEM Sylvain Leroy	Professeur	En poste
4.	ASSAM ASSAM Jean Paul	Maître de Conférences	En poste
5.	BOUGNOM Blaise Pascal	Maître de Conférences	En poste
6.	KOUITCHEU MABEKU Epse KOUAM Laure Brigitte	Maître de Conférences	En poste
7.	MUNE MUNE Martin Alain	Maître de Conférences	En poste
8.	RIWOM Sara Honorine	Maître de Conférences	En poste
9.	NJIKI BIKOÏ Jacky	Maître de Conférences	En poste
10	TCHIKOUA Roger	Maître de Conférences	*Chef de Service de la Scolarité*
11	ESSONO Damien Marie	Chargé de Cours	En poste
12	LAMYE Glory MOH	Chargé de Cours	En poste
13	MEYIN A EBONG Solange	Chargé de Cours	En poste
14	MONI NDEDI Esther Del Florence	Chargé de Cours	En poste
15	NKOUDOU ZE Nardis	Chargé de Cours	En poste
16	NKOUE TONG Abraham	Chargé de Cours	En poste
17	TAMATCHO KWEYANG Blandine Pulchérie	Chargé de Cours	En poste
18	SAKE NGANE Carole Stéphanie	Chargé de Cours	En poste
19	TOBOLBAÏ Richard	Chargé de Cours	En poste
20	EZO'O MENGO Fabrice Télésfor	Assistant	En poste
21	EHETH Jean Samuel	Assistant	En poste
22	MAYI Marie Paule Audrey	Assistant	En poste
23	NGOUENAM Romial Joël	Assistant	En poste
24	NJAPNDOUNKE Bilkissou	Assistant	En poste

10. DEPARTEMENT DE PHYSIQUE (PHY) (42)

1.	BEN- BOLIE Germain Hubert	Professeur	En poste
2.	BIYA MOTTO Frédéric	Professeur	*DG/HYDRO Mekin*
3.	DJUIDJE KENMOE épouse ALOYEM	Professeur	En poste
4.	EKOBENA FOUDA Henri Paul	Professeur	*Vice-Recteur. Uté Ngaoundéré*
5.	ESSIMBI ZOBO Bernard	Professeur	En poste
6.	EYEBE FOUDA Jean sire	Professeur	En poste
7.	HONA Jacques	Professeur	En poste
8.	NANA ENGO Serge Guy	Professeur	En poste
9.	NANA NBENDJO Blaise	Professeur	En poste
10.	NDJAKA Jean Marie Bienvenu	Professeur	*Chef de Département*
11.	NJANDJOCK NOUCK Philippe	Professeur	En poste
12.	SAIDOU	Professeur	*Chef de centre/IRGM/MINRESI*
13.	SIMO Elie	Professeur	En poste
14.	TABOD Charles TABOD	Professeur	*Doyen FSUniv/Bda*
15.	TCHAWOUA Clément	Professeur	En poste
16.	WOAFO Paul	Professeur	En poste
17.	ZEKENG Serge Sylvain	Professeur	En poste

18.	ENYEGUE A NYAM épse BELINGA	Maître de Conférences	*Chef de Division de la formation continue et à distance/ENSPY*
19.	FEWO Serge Ibraïd	Maître de Conférences	En poste
20.	FOUEJIO David	Maître de Conférences	*Chef Cell/ MINADER*
21.	MBINACK Clément	Maître de Conférences	En poste
22.	MBONO SAMBA Yves Christian U.	Maître de Conférences	En poste
23.	MELI'I Joelle Larissa	Maître de Conférences	En poste
24.	MVOGO ALAIN	Maître de Conférences	En poste
25.	NDOP Joseph	Maître de Conférences	En poste
26.	SIEWE SIEWE Martin	Maître de Conférences	En poste
27.	VONDOU Derbetini Appolinaire	Maître de Conférences	En poste
28.	WAKATA née BEYA Annie Sylvie	Maître de Conférences	*Directeur/ENS/UYI*
29.	WOULACHE Rosalie Laure	Maître de Conférences	*En stage depuis février 2023*
30.	ABDOURAHIMI	Chargé de Cours	En poste
31.	AYISSI EYEBE Guy François Valérie	Chargé de Cours	En poste
32.	CHAMANI Roméo	Chargé de Cours	En poste
33.	DJIOTANG TCHOTCHOU Lucie Angennes	Chargée de Cours	En poste
34.	EDONGUE HERVAIS	Chargé de Cours	En poste

35.	KAMENI NEMATCHOUA Modeste	Chargé de Cours	En poste
36.	LAMARA Maurice	Chargé de Cours	En poste
37.	NGA ONGODO Dieudonné	Chargé de Cours	En poste
38.	OTTOU ABE Martin Thierry	Chargé de Cours	*Directeur Unité de production des réactifs/IMPM*
39.	TEYOU NGOUPO Ariel	Chargé de Cours	En poste
40.	TOGUEU MOTCHEYO Alain Bertrand	Chargé de Cours	En poste
41.	WANDJI NYAMSI William	Chargé de Cours	En poste
42.	SOUFFO TAGUEU Merimé	Assistant	En poste

11- DÉPARTEMENT DE SCIENCES DE LA TERRE (ST) (34)

1.	EKOMANE Emile	Professeur	*Chef Div./Uté Ebolowa*
2.	GANNO Sylvestre	Professeur	En poste
3.	NDJIGUI Paul-Désiré	Professeur	*Vice-Doyen /DPSAA*
4.	NGOS III Simon	Professeur	En poste
5.	NKOUMBOU Charles	Professeur	En poste
6.	ONANA Vincent Laurent	Professeur	*Chef de Département/Uté. Eb.*
7.	YENE ATANGANA Joseph Q.	Professeur	*Chef Div. /MINTP*

8.	BISSO Dieudonné	Maître de Conférences	*Chef de Département*
9.	Elisé SABABA	Maitre de Conférences	En poste
10.	EYONG John TAKEM	Maître de Conférences	En poste
11.	FUH Calistus Gentry	Maître de Conférences	*Sec. D'Etat/MINMIDT(ai)*
12.	MBIDA YEM	Maitre de Conférences	En poste
13.	MBESSE Cécile Olive	Maitre de Conférences	En poste
14.	METANG Victor	Maître de Conférences	En poste
15.	NGO BIDJECK Louise Marie	Maître de Conférences	En poste
16.	NGUEUTCHOUA Gabriel	Maître de Conférences	*CEA/MINRESI*
17.	NJILAH Isaac KONFOR	Maître de Conférences	En poste
18.	TCHAKOUNTE Jacqueline épse NUMBEM	Maître de Conférences	*Chef. Cell /MINRESI*
19.	TCHOUANKOUE Jean-Pierre	Maître de Conférences	En poste
20.	TEMGA Jean Pierre	Maître de Conférences	En poste
21.	ZO'O ZAME Philémon	Maître de Conférences	*DG/ART*

22.	ANABA ONANA Achille Basile	Chargé de Cours	En poste
23.	BEKOA Etienne	Chargé de Cours	En poste
24.	MAMDEM TAMTO Lionelle Estelle, épouse BITOM	Chargée de Cours	En poste
25.	NGO BELNOUN Rose Noël	Chargée de Cours	En poste
26.	NGO'O ZE ARNAUD	Chargé de Cours	En poste
27.	NOMO NEGUE Emmanuel	Chargé de Cours	En poste
28.	NTSAMA ATANGANA Jacqueline	Chargée de Cours	En poste
29.	TCHAPTCHET TCHATO De P.	Chargé de Cours	En poste
30.	TEHNA Nathanaël	Chargé de Cours	En poste
31.	FEUMBA Roger	Chargé de Cours	En poste
32.	MBANGA NYOBE Jules	Chargé de Cours	En poste

33.	KOAH NA LEBOGO Serge P.	Assistant	En poste
34.	TENE DJOUKAM Joëlle Flore, épouse KOUANKAP NONO	Assistante	En poste

Répartition chiffrée des Enseignants de la Faculté des Sciences de l'Université de Yaoundé I

NOMBRE D'ENSEIGNANTS					
DÉPARTEMENT	**Professeurs**	**Maîtres de Conférences**	**Chargés de Cours**	**Assistants**	**Total**
BCH	08 (01)	22 (13)	08 (03)	06 (04)	**44 (20)**
BPA	11 (01)	19 (09)	16 (05)	03 (01)	**49 (16)**
BPV	06 (01)	10 (02)	14 (07)	02 (00)	**32 (10)**
CI	07 (01)	14 (03)	05 (01)	01 (00)	**27 (05)**
CO	06 (01)	14 (05)	11 (03)	02 (00)	**33 (09)**
ER	01 (00)		/	/	**01 (0)**
IN	02 (00)	02 (00)	15 (01)	03 (00)	**22 (01)**
MAT	01 (00)	08 (00)	20 (01)	05 (01)	**34 (02)**
MIB	03 (01)	07 (03)	09 (05)	05 (02)	**24 (11)**
PHY	17 (01)	12 (04)	12 (01)	01 (00)	**42 (06)**
ST	07 (00)	14 (03)	11 (03)	02 (01)	**34 (07)**
Total	**69 (07)**	**122 (42)**	**121 (30)**	**30 (09)**	**342 (88)**

Soit un total de **342 (88)** dont :

- Professeurs **69 (07)**
- Maîtres de Conférences **123 (41)**
- Chargés de Cours **120 (30)**
- Assistants **30 (09)**

( ) = Nombre de Femmes **88**

ENSEIGNANTS SOUS CONTRAT DE COLLABORATION

1.	BELL JOSEPH MARTIN	547019U	17/06/1957	Sakbayeme	M	10/11/1986	RETRAITE - CONTRAT DE COLLABORATION	PR
2.	DJOUFAC WOUMFO EMMANUEL	547069Z	09/01/1957	Ngaoundéré	M	04/05/1990	RETRAITE - CONTRAT DE COLLABORATION	PR
3.	ELIMBI ANOINE.	546958X	30/11/1955		M		RETRAITE - CONTRAT DE COLLABORATION	PR
4.	FOMENA ABRAHAM	546778X	10/11/1958	Batcham	M	01/12/1986	RETRAITE - CONTRAT DE COLLABORATION	PR
5.	GHOGOMU TIH RAPH	547004-K	23/12/1956	BAMBALANG	M	13/10/1982	RETRAITE - CONTRAT DE COLLABORATION	PR
6.	KAMTCHOUING PIERRES	143299X	13/09/1955	Nkongsamba	M	01/10/1988	RETRAITE - CONTRAT DE COLLABORATION	PR
7.	LAMINSI SAMUEL	143149J	301/12/1953		M		RETRAITE - CONTRAT DE COLLABORATION	PR
8.	NGADJUI TCHALEU BONAVENTURE	546959-G	15/09/1953	FONTSIGA	M	12/08/1982	RETRAITE - CONTRAT DE COLLABORATION	PR
9.	NGO BILONG ANASTASIE épse TIH	546164-I	27/12/1955	MBANGA	F	28/07/2000	RETRAITE - CONTRAT DE COLLABORATION	MC
10.	NKENGFACK EPHRAIM AUGUSTIN	546948-F	17/06/1955	YAOUNDE	M	01/09/1983	RETRAITE - CONTRAT DE COLLABORATION	PR
11.	NDIKONTAR MAURICE KOR	169784G	09/05/1958	Mbaa	M	10/01/1991	RETRAITE - CONTRAT DE COLLABORATION-EN COURS DE SIGNATURE	PR
12.	NJIOKOU FLOBERT	547321H	11/06/1958	Nkongsamba	M	03/05/1993	RETRAITE - CONTRAT DE COLLABORATION-EN COURS DE SIGNATURE	PR
13.	BENG NEE NINTCHOM PENLAP VERONIQUE	546643B	07/01/1957	Melong I	F	02/10/1992	RETRAITE-CONTRAT DE COLLABORATION	PR
14.	FOKOU ELIE	546725J	08/06/1957	Fiéla-Bamendjinda	M	01/04/1988	RETRAITE-CONTRAT DE COLLABORATION EN COURS DE FINALISATION	PR
15.	TCHOUANKEU JEAN CLAUDE	547295-E	06/01/1959	Douala	M	01/12/1989	RETRAITE-CONTRAT DE COLLABORATION EN COURS DE FINALISATION	PR
16.	BOYOMO ONANA						CONTRATS TRAITES LORS DU CONSEIL D'UNIVERSITE DU 12 JUILLET 2024	MC
17.	WANDJI JEAN	162242M	09/06/1958	Bangou	M			UYI
18.	YOUMBI EMMANUEL	547332Z	12/02/1959	Bangou	M	Bangou		PR
19.	NGODO MELINGUI JEAN	500475X	05/09/1958	Endoum		20/10/2005		MC
20.	KOFANE TIMOLEON CREPIN							PR
21.	NGAMENI EMMANUEL	547277-C	24/04/1959	Mbanga	M			PR
22.	BITOM DIEUDONNE	547050X	23/11/1958	Ambam	M			PR

To my beloved parents: late OWONA
Fabien Didier and NGUINI Céline

ACKNOWLEDGEMENTS

Infinitely grateful that no human endeavor and effort can be accomplished without the blessing and grace of the Almighty God, I thank him for allowing me to undertake and complete this Thesis. Throughout the process, His grace in my life has inspired new ideas that have given me the desire and motivation to carry-out the research with consistency. I give God all the glory, honor and adoration.

I would like to express my deep gratitude to everyone who has contributed in any way to the success of this work. First of all, i will like to thank my thesis supervisors

- **Pr KOFANÉ Timoléon Crépin** for devoting his unvaluable time and resources for the completion of this thesis.
- **Pr MVOGO Alain** to who my warmest thanks go to, who give me the access to cardiology and many other domain on which this thesis is based. This fields of modern science have enabled me mechanism of transmission of electrical, magnetic impulses by heart wall in a well organized lattice.
- Secondly to the members of the jury.

- **Pr BEN-BOLIE Germain Hurbert**, Head of the laboratory of Nuclear, Atomic, Molecular and Biophysics of Yaoundé for his unvaluable advice and guidance, **Pr BOUETOU BOUETOU Thomas** head of Department of Computer Sciences at National Advanced School of Engineering of Yaoundé , **Pr NANA Engo Serge Guy** for all his encouragement, **Pr NGUENANG Jean Pierre** head of Department of Physics of University of Douala.
- Thirly, i would like to express my deep gratitude to the teachers of the Department and the Laboratory of Nuclear, Atomic, Molecular Physics and Biophysics, as they have also welcomed and trained many students, while improving the quality of their work and the image of our institution through remarkable scientific contributions:
- **Pr EKOBENA FOUDA Henri Paul**, Vice-Rector of University of Ngaoundéré in charge of Internal Control and Evaluation,
- **Pr OWONO OWONO Luc Calvin**, Dean of the Faculty of Sciences,

☞ **Pr NDJAKA Jean-Marie Bienvenu**, head of the Department of Physics,

☞ **Pr WOAFO Paul**, Chairman of the Cameroon Physical Society,.

☞ **Pr TABI Conrad Bertrand**, for all his unvaluable support

☞ **Pr SAÏDOU**, Head, Research Centre for Nuclear Science and Technology, IRGM, Cameroon,

☞ **Pr NANA NBENDJO Blaise Roméo**, President of the Cameroon Physical Society,

☞ **Pr EFFA Joseph Yves** responsable of Energy, Signal, Images, and Automation Laboratory, University of Ngaoundéré,

☞ **Pr BODO Bertrand**, Head of the Department of Renewable Energy, University of Yaoundé,

☞ **Dr BELOBO BELOBO Didier** for his warm welcome in his office, in his center at National Advanced School of Engineering of Yaoundé. For his passion for research, his love of a job well done, his particular interest in knowledge transfer and learner autonomy.

☞ **Dr DANG Koko Adamu** for advice and raising awareness. Furthermore, for improving the quality work and the image of our laboratory through remarkable scientific contributions.

☞ **Dr ETÉMÉ Armand Sylvin** for his clarity, motivation, consistency and uncompromising standards. Moreover, for his academic and social advice,

☞ **Dr TAKEMBO NTAHKIE Clovis** for all the teaching, advice and encouragement.

Additionally, I would like to thank the rest of people who supported me with various actions throughout my academic career. I am thinking mainly of **Dr ENYENGUE BALLA Nadine, Dr BANSI KAMDEM Delphin Christel, Dr KUIPOU Domgno William, Dr FORWAH TAH Amstrong, Dr NDJAWA YOMI Pavel Arnold, Dr FOUEDJI Chenceline, Dr TABAPSI KAMDEM Rostand, Mr ESSAGA ANABA Billy Armel, Mr DJOUODJO Lucien, Mrs KEPTA Aurore Cedrine.**

☞ To the Minister Delegate of the Presidency in charge of Defense, **Mr Joseph Beti Assomo** whom i would like to thank sincerely for his unvaluable opportunity, support and commitment to me and through the unwavering support of Colonel **KAOLE ALEOKOL Raymond**, the Sergeants **ESSAMA Joseph Christian, SEBEKREO Raissa Ivanov Esther**.

☞ To all the **reverend sisters of the Strasbourg Cross**, To the **readers of the Holy Trinity parish of Nsam** and to the Priest of Jesus Christ: **EBELA BALLA Louis-Marie, ETOUNDI Siméon Joel.**

☞ To all my brothers **ESSOMBA MBALA Nicolas Kevin, MBALA MBALA Alexis** and sisters **NKOA NGUINI Celine Jeanne**, aunts and

uncles for their psychological and material supports which have largely contributed to the success of this Thesis.

Last but not least, a big thank you to all those who, from near and far, have given me their moral, spiritual and intellectual support along the way.

CONTENTS

List of Figures

List of Tables

List of Abbreviations

HR	Hindmarsh-Rose
HH	Hodgkin-Huxley
FHN	FitzHugh-Nagumo
ML	Morris-Lecar
DNA	Deoxyribonucleic Acid
MF	Magnetic Flow
ATP	Adenosine Tri-Phosphate
EMI	Electromagnetic induction
MI	Modulational Instability
LSA	Linear Stability Analysis
NA	Neuronal Activity
NLS	Nonlinear Schrödinger
CCGL	Cubic Complex Ginzburg-Landau
CQCGL	Cubic-Quintic Complex Ginzburg-landau
ODEs	Ordinary Differential Equations
ECG	Electrocardiogram
MCG	Magnetocardiogram
MSA	Multiple-Scale Approximation
SDA	Semi-Discrete approximation
HBM	Hirota Bilinear Method
MKdV	Modified Kortheweg de Vries
RK4	Fourth-order Runge-Kutta
SA	Sino Atrial
AV	Atrio-Ventricular
RD	Reaction-Diffusion
IF	Integrate and Fire
AP	Aliev-Panfilov
AP	Action Potential
NN	Neural Network
BH	Bundle of His
PF	Purkinje Fibers
CAD	Coronary Artery Disease
HF	Heart Failure
HBP	Hight Blood Pressure
CHD	Congenital Heart Defects
PAD	Peripheral Artery Disease
RHD	Rheumatic Heart Disease
DNA	Deoxyribonuclei Acid
RNA	Ribonuclei Acid
CNS	Central Nervous System
pH	Hydrogen Potential
GABA	Gamma-Aminobutyric Acid

RÉSUMÉ

Cette thèse est consacrée à l'étude des excitations nonlinéaires de type soliton dans les modèles dissipatifs de FitzHugh-Nagumo, dans le but d'étudier l'activité électrique des cellules biologiques excitables. Ces modèles se présentent sous forme d'équations de réaction-diffusion et intègrent des phénomènes physiques tels que la diffusion croisée, l'induction électromagnétique et les variations de température. Ces phénomènes qui influencent de manière significative la dynamique des systèmes de Réaction-Diffusion (RD), se révèlent importants pour comprendre la dynamique des réactions chimiques, la propagation des ondes, la formation des motifs, l'activité cardiaque, ainsi que la neuromodulation. De plus, ils jouent un rôle crucial dans le métabolisme cellulaire et l'homéostasie thermique. À partir du modèle de RD de FitzHugh-Nagumo (FHN) nous développons, explorons et dérivons via la méthode des échelles multiples, l'équation régissant la dynamique de ces solitons, menant ainsi à l'équation CGL cubic-quintique. Une approche analytique, telle que la méthode bilinéaire de Hirota est utilisée pour identifier et valider les solutions solitoniques. Le spectre du gain d'instabilité modulationnelle est renforcé par l'analyse de stabilité linéaire du modèle, ainsi que sa résolution via la méthode de Ferrari. Les résultats analytiques sont confirmés par des simulations numériques appropriées, réalisées à l'aide de l'algorithme de RK4. Cela offre des perspectives prometteuses pour le contrôle et une stabilité des potentiels au sein des cellules excitables. Toutefois, en raison de la non-linéarité et des propriétés de dispersion des milieux, les résultats montrent que le champ électrique ou magnétique peut induire la formations des ondes solitaires. La génération d'impulsions et des comportements rythmiques, tels que la respiration, revêt une importance capitale dans la recherche sur les systèmes cardiaques et cérébraux. Ces phénomènes pourraient permettre une meilleure comprehension des symptômes d'insuffisance cardiaque soudaine, des arhythmies.

Mots clés: **Systèmes de réaction-diffusion; Solitons; diffusion croisée; induction électromagnétique; couplage thermoélectriques; motifs spatiotemporels; Méthode de Hirota.**

ABSTRACT

This thesis is devoted to the study of nonlinear soliton-like excitations in the dissipative FitzHugh-Nagumo models, with the aim of investigating the electrical activity of excitable biological cells. These models are formulated as reaction-diffusion equations and incorporate physical phenomena such as cross-diffusion, electromagnetic induction, and temperature variations. These phenomena, which significantly influence the dynamics of reaction-diffusion systems, are crucial for understanding processes such as chemical reaction dynamics, wave propagation, pattern formation, cardiac activity, as well as neuromodulation. Furthermore, they play a vital role in cellular metabolism and thermal homeostasis. From the FHN RD model, we develop, explore, and derive, through the method of multiple scales, the equation governing the dynamics of these solitons. The results lead to the cubic-quintic complex Ginzburg-Landau equation. An analytical approach, such as the Hirota bilinear method, is employed to identify and validate soliton solutions. The modulational instability gain spectrum is reinforced by linear stability analysis of the model, as well as its resolution via the Ferrari method. The analytical results are corroborated by appropriate numerical simulations, performed using the fourth-order Runge-Kutta algorithm. This offers promising prospects for the control and stability of potentials within excitable cell environments. However, due to the nonlinearity and dispersive properties of the media, pulses, the results show that electrical or magnetic field, can induce solitary waves formation. The generation of pulses and rhythmic behaviors, such as respiration, is of paramount importance in research on cardiac and cerebral systems. These phenomena could lead to a better understanding of symptoms such as sudden heart failure and arrhythmias.

Keywords : **Reaction-diffusion systems; Solitons; cross-diffusion; electromagnetic induction; thermoelectric coupling; spatiotemporal patterns; Hirota method.**

General Introduction

Excitable environments are spatially distributed systems that are of significant interest in the research community. These systems are essential components of living organisms, including humans. Excitable cells possess the unique ability to generate and transmit electrical impulses and, in some cases, blood, enabling rapid communication and coordination in various physiological processes. These cells are found in various tissues and organs, such as nerve cells in the brain, muscle cells (skeletal and cardiac) in the heart, and endocrine cells (insulin-releasing pancreatic β-cells) [1–3]. When these ecosystems interact, they produce specific types of waves due to the dynamics of various processes (biological, physical, and chemical) that can be studied from theoretical, experimental, analytical, and numerical perspectives. Their primary function is to receive, process, and transmit information, facilitating the execution of specific actions. This property is crucial in physiological functions like sensory perception, muscle contraction, and the generation of electrical signals in the nervous system. Understanding the brain and heart through nonlinear science methods is a significant branch of modern computational biology [4]. To study activity in these environments, tools like Reaction-Diffusion (RD) equations are used to elucidate the spatiotemporal progression of concentrations, where the nonlinear interplay among these morphogens deeply affects patterns and dynamics (speed, amplitude, shape). The thesis focuses on RD systems, a class of dissipative systems originating in chemistry but now found in many scientific fields. Experimental studies have observed pattern formation in controlled systems like chemical reactions in gels and semiconductor physics. Reaction-diffusion systems feature both localized and spatially-extended structures, specifically discussing localized solitary structures known as dissipative solitons (DSs).

Reaction-diffusion systems, formulated and applied in various dimensions, describe a wide range of phenomena. This theory of RD waves began in the 1930s with the works by Fisher [5] of dominant gene. The simplest one-component RD equation is the Kolmogorov-Petrovsky-Piskunov equation [6]. The two-component RD models [7–9] and more complex three-component systems like the Belousov-Zhabotinsky reaction

[10, 11] also exist and and finaly by Zeldovich, Frank-Kamenetskii in combustion theory [12]. These works were followed by many others where RD waves were studied in connection with various problems in Chemistry with Pattern formation in chemical reactions, like the Belousov-Zhabotinsky reaction, in Biology with Morphogenesis, where RD models explain how patterns like animal skins and shells form (Turing patterns), in Ecology with the spread of species, population dynamics and habitat fragmentation, in Physics with the formation of dissipative structures in non-equilibrium thermodynamic systems and in Medecine with Tumor Growth and Cancer Modeling, wound healing, drug delivery, cardiovascular diseases and neuroscience. Although known for a long time, the principles of these patterns were clarified by Turing's 1952 work on morphogenesis. Turing instability is a key concept explaining how spatial patterns emerge in such systems of RD, where a homogeneous steady state becomes unstable under small perturbations under certain conditions [13]. By understanding these components and using mathematical and computational tools, we can analyze and simulate complex pattern formation processes. Over several decades, the interest in using such spatial structures has grown, notably with the work of Zhabotinsky [14]. The generalization of RD theory has introduced concepts like self-diffusion, cross-diffusion, intra-diffusion, and inter-diffusion, depending on the biological problem at hand [15–20]. For example, in supercritical and subcritical RD equations, if the reaction kinetics allow the system to sustain large amplitude solutions, small perturbations can lead to traveling waves, oscillations, or chaotic dynamics. Otherwise, the system returns to a stable homogeneous state. The transition between these states is explained through bifurcation theory (e.g., Hopf bifurcation, Turing bifurcation), which is crucial for predicting and controlling the behavior of these RD systems [21–23].

Another perspective on RD systems involves activator-inhibitor reaction kinetics, where cross-diffusion is considered to determine how the concentration of one or more substances changes in space under the influence of local chemical reactions and diffusion. It has been observed that parameter spaces without cross-diffusion are subspaces of the cross-diffusion induced parameter spaces [24]. Additionally, in predator-prey systems, also known as the Lotka-Volterra model, with negative and positive taxis represented by nonlinear cross-diffusion terms, quasi-soliton interplay has been demonstrated, showing that the velocity of wave propagation depends on taxis with parabolic and linear forms [25, 26]. The concept of predator-prey dependence, subject to both self-diffusion and cross-diffusion, explores more realistic species interactions that generate complex behaviors [27]. Similar to subcritical and supercritical reaction kinetics, some

of these models are unstable with respect to small perturbations [28]. However, the presence of cross-diffusion can induce instability in systems that would otherwise be stable with self-diffusion alone [29].

In the early stages of research, mathematical models were developed to describe the dynamics and behavior of action potentials in cardiac cells and neurons. These models were based on their physical, biological, and chemical properties. Key models include the Hodgkin-Huxley (HH) model [30], which is widely used to understand ion channel behavior, and the FitzHugh-Nagumo (FHN) model [8, 9], a simplified version of the HH model. Other notable models are the Integrate-and-Fire model [31], the Morris-Lecar (ML) model [32], and the Hindmarsh-Rose (HR) model [33]. These models help explain how action potentials are generated and transmitted in neurons and cardiac cells. Various factors affect the excitability of these systems, such as self- and cross-diffusion, electromagnetic induction and temperature. Temperature impacts the amplitude and frequency of action potentials, and electromagnetic fields generated by fluctuating action potentials can affect conduction in excitable cells [34–40]. Researchers have recently explored how cross-diffusion influences wave propagation and pattern formation in the FHN model, revealing new behaviors like oscillating tails and complex wave structures [39–41]. In addition, electromagnetic induction, introduced by Faraday, affects how action potentials generate magnetic fields in cells, which in turn influences cellular excitability [42]. Understanding these effects is crucial for predicting and controlling complex electrophysiological behaviors in the heart, such as arrhythmias, using more realistic models. This thesis investigates how soliton-like excitations form and propagate in the FHN model, aiming to enhance knowledge of cardiac dynamics and potential medical applications.

Over the past century, human exposure to harmful factors such as self- and cross-diffusion, temperature changes, and electromagnetic radiation has increased due to medical advances, industrial growth, and new technologies. These factors have affected human cells, particularly in the brain and heart, raising concerns about their possible link to neurodegenerative diseases and heart conditions [43]. These health issues contribute to about one-third of global mortality. Takembo et al. [44, 45] have shown that waves in myocardial cells are influenced by exposure to electromagnetic radiation. However, fully understanding how these factors impact cardiac and neuronal damage, as well as disease detection and control, remains an ongoing area of research. Studies suggest that electromagnetic radiation [46–50] and temperature changes [51–53] can disrupt signaling in the heart and nervous systems, but the exact conditions for how

these energy fluctuations lead to harmful patterns in cells are not yet fully understood. This motivates further investigation.

In this thesis, we use both analytical and numerical methods to study wave propagation and synchronization in cardiac tissue and neural networks. Our research focuses on:

- Determining the key parameters value that control the existence, shape, stability and dynamics of dissipative solitons in RDs.
- Developing and analyzing mathematical models of reaction-diffusion systems that include both cross-diffusion electromagnetic induction and temperature to explain soliton-like structures in the FitzHugh-Nagumo (FHN) cardiac model using the complex cubic-quintic Ginzburg-Landau equation.
- Studying the characteristics of soliton propagation, such as speed, amplitude, and shape, under different parameters.
- Conducting analytical studies to understand the conditions needed for the existence and stability of dissipative solitons.
- Investigating the sensitivity of soliton properties to factors like reaction rates, diffusion coefficients, and initial conditions.
- Running numerical simulations to explore the formation, evolution, and interaction of dissipative solitons in these systems.
- Comparing theoretical and numerical findings with experimental data to validate the models and predictions.
- Applying the results to improve diagnostic tools and therapies for cardiac disorders, especially arrhythmias.

Organization of the Thesis

The document is divided into three main chapters, each concluding with a general summary.

✎ **Chapter one**, presents several prominent cellular models, culminating in the selection of the FHN model due to its extensively studied characteristics and explores the biology of excitable cells, detailing the properties and organization of

myocardial cells and neurons as the fundamental units of excitation and information processing in both systems. These networks are then analyzed as macroscopic structures for impulse transmission during signal encoding.

- **Chapter two**, entitled improved models of FHN and methodologies, discusses various mathematical techniques and models developed within this thesis. It covers both analytical approaches such as the multiple-scale expansion, the Hirota Bilinear Method and the modulational instability analysis. Numerical methods like the Finite difference and the Fourth-order Runge-Kutta are also taken into account. The immediate applications illustrate these methods, including their relevance in understanding cardiac excitability and spiking behavior, bifurcation analysis, oscillatory patterns, stimulation and control mechanisms, modeling of cardiac networks, and comprehending excitable media. The generic model produces discrete nonlinear Schrödinger (DNLS), cubic Complex Ginzburg-Landau (CCGL), and cubic-quintic Complex Ginzburg-Landau (CQCGL) equations. These models equations offer analytical expressions for modulational instability functions, encompassing critical amplitude, MI gain, and instability criteria.

- **Chapter three**, entitled results and discussion, presents the findings biological and physical implications. It begins with an analysis of soliton-like excitations observed from a discrete model of a one-dimensional FHN network.

- The thesis concludes with a general summary of the main results and future directions.

CHAPTER 1

LITTERATURE REVIEW

Contents

1.1 Introduction

Reaction-diffusion systems play a pivotal role in understanding the complex dynamics of excitable cells, such as those found in the heart and brain. Excitable cells are specialized tissues crucial for the proper functioning of both cardiac and neural systems. In the heart, myocardial cells, which include both contractile and conducting cells, ensure the heart's rhythmic contractions and the efficient circulation of blood. The precise coordination of these cells is essential to maintaining a healthy cardiac rhythm, with disruptions often leading to severe cardiovascular conditions. Similarly, neurons in the brain communicate via action potentials, creating intricate networks that govern cognitive and control functions. The electrical impulses generated by neurons are integral to processing nervous messages and maintaining the brain's overall functionality. Like cardiac cells, neurons rely on the intricate balance of electrical and chemical signals to perform their roles effectively.

To better understand these complex interactions, researchers have developed mathematical models that simulate the behaviors of neurons and myocardial cells. These models, rooted in reaction-diffusion theory, have proven effective in replicating the spike patterns observed in experimental studies, such as those by Hodgkin and Huxley, Aliev and Panfilov and FitzHugh-Nagumo. While these models provide valuable insights, some of them often lack the biological specificity necessary for a comprehensive understanding of these systems, as they are based on universal physical principles rather than the unique characteristics of individual cells.

This chapter is structured into three primary sections: The first section provides an overview of the most prominent mathematical models used to describe the electrical activity in both cardiac and neuronal cells. The second section delves into the anatomy of cardiac muscle, including the filament cross section, the components of the blood and electrical conduction systems responsible for distributing blood and electrical impulses throughout the heart. It also compares the effects of ion movement on the membrane potential of cardiac conductive and contractile cells, explores the features of an electrocardiogram in relation to the cardiac cycle, and identifies the cardiopathies cycle. The third section focuses on the neuron, the fundamental unit of the nervous system. It examines the neuron's structure, functions, classification, electrical activity, the nature of synapses, the characteristics of action potentials and the neurodegenerative disorders.

1.2 Mathematical models

Mathematical models serve as representations of real-world systems or phenomena, employing mathematical structures and relationships for this purpose. These models play a crucial role in gaining insights, making predictions, and comprehending the behavior of systems across various domains such as physics, biology, economics, engineering, and more. There exists a diverse array of mathematical models, broadly categorized into distinct types, including Deterministic Models, Stochastic Models, Discrete Models, Continuous Models, Analytical Models, Numerical Models, Empirical Models, and Mechanistic Models. The selection of a specific model type depends on the inherent nature of the system under investigation and the objectives of the analysis. Each model type offers unique advantages and applicability, tailored to suit the intricacies of the system being studied and the desired outcomes of the research endeavor. [54]

1.2.1 Reaction-Diffusion models

A RD model serves as a mathematical framework employed to elucidate the spatiotemporal progression of concentrations within a system characterized by both chemical reactions and diffusion phenomena. These models hold particular significance in disciplines encompassing chemistry, biology, physics, and ecology, where the interplay among diffusing substances significantly influences patterns and dynamics. Within this context, generic excitable media can be effectively characterized by a system comprising two coupled reaction-diffusion equations:

$$\begin{aligned} \frac{dv}{dt} &= D\frac{d^2v}{dx^2} + I(v,u,p_i), \\ \frac{du}{dt} &= R(v,u,p_i), \end{aligned} \tag{1.1}$$

The terms $v(x,t)$ represents a scaled transmembrane potential v, $u(x,t)$ denotes the recovery variable, representing slower physiological processes like ion channel recovery or ionic concentrations at position x and time t, and D serving as the diffusion coefficient governing the spatial spreading rate, respectively. $\frac{d^2v}{dx^2}$ signifies the spatial diffusion term. The term p_i represents one or more biophysical or physiological parameters that shape the dynamics of the excitation and recovery processes. These are essential for calibrating the model to match experimental or clinical observations. These parameters are typically constants that define physiological or biophysical properties of the model. Since their objective is not to achieve quantitative agreement, it is customary to simplify the functions $I(v,u,p_i)$ a nonlinear function representing ionic currents or

external inputs, and $R(v,u,p_i)$ another nonlinear function for the recovery process, as much as possible [8, 55–57].

Reaction-diffusion models are renowned for their capacity to replicate fundamental qualitative characteristics of cardiac excitation, including pulse generation and propagation, refractory properties, dispersion relation, and furthermore, to generate various spatial patterns such as traveling waves, stable formations, and irregular structures. They have been extensively utilized to investigate a broad spectrum of phenomena, ranging from chemical reactions and pattern formation in biological systems (e.g., animal coat patterns, chemical Turing patterns) to the dynamics of excitable media (e.g., cardiac tissue and neural networks).

1.2.2 Hodgkin-Huxley models

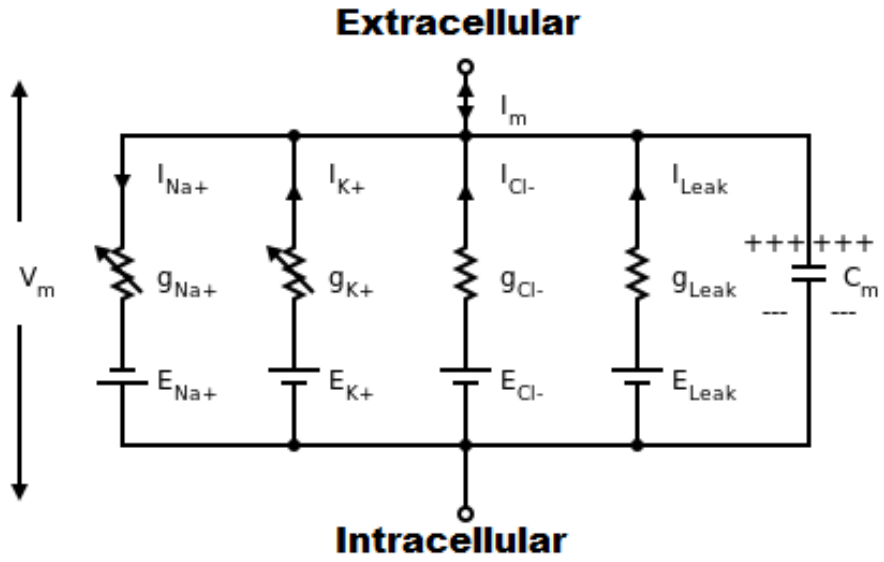

Figure 1.1: Hodgkin-Huxley electrical circuit [84].

The Hodgkin-Huxley (HH) model, also known as the conductance-based model, comprises a system of nonlinear differential equations formulated to elucidate the behavior of excitable cells like neurons and muscle cells during the initiation and transmission of action potentials. This model stands as a significant milestone in neurophysiology, constructed upon sound physiological principles, and offers an intricate elucidation of the ionic currents underlying the electrical excitability of neurons. [30, 58, 59]. The HH model treats each component of the circuit as an electrical entity, as depicted in Fig. 1.1. Here, the capacitance C_m represents the cell membrane's ability to store charge, while

the electrical resistance, denoted as $g_n(t,V)$ (where n signifies the specific ion channel), varies with both time and voltage. This resistance factor models the behavior of voltage-gated ion channels. Additionally, g_{leak} represents the conductance of leak channels. The electrochemical gradients E_n serve as voltage sources in the model, while I_n denotes current sources. Finally, V_m signifies the membrane potential, with specific numerical values (see Table 1.1).

Parameter	Unit	Value
C_m	$\mu F cm^{-2}$	1.0
E_K	mV	+12
E_{Na}	mV	−115
E_L	mV	−10.63
$\bar{g}_K$	$mS.cm^{-2}$	36
$\bar{g}_{Na}$	$mS.cm^{-2}$	120
$\bar{g}_L$	$mS.cm^{-2}$	0.3

Table 1.1: HH model parameters.

Using the fundamental principles of Kirchhoff's laws, HH formulated a model comprising four primary first-order ordinary differential equations:

$$\begin{aligned} C_m\frac{dV_m}{dt} &= I+\bar{g}_{Na}m^3h(E_{Na}-V_m)+\bar{g}_Kn^4(E_K-V_m)+\bar{g}_L(E_L-V_m)+\frac{d^2V_m}{dx^2},\\ \frac{dm}{dt} &= \alpha_m(V_m)(1-m)-\beta_m(V_m)m,\\ \frac{dh}{dt} &= \alpha_h(V_m)(1-h)-\beta_h(V_m)h,\\ \frac{dn}{dt} &= \alpha_n(V_m)(1-n)-\beta_n(V_m)n, \end{aligned} \tag{1.2}$$

where $a_m(V_m) = 0.1(25-V)/(\exp(-(25-V)/10)-1)$, $b_m(V_m) = 4\exp(-V/18)$, $a_h(V_m) = 0.07\exp(-V/10)$, $b_h(V_m) = 1/(\exp((30-V)/10)+1)$, $a_n(V_m) = 0.01(10-V)/(\exp((10-V)/10)-1)$, $b_n(V_m) = 0.125\exp(-V/80)$.

In the equation, $V = V_{rest} - V_m$, the variable V represents the negative depolarization measured in mV. As previously mentioned, the HH model stands out among neural models for its biological significance. Such models hold significance not only due to their parameters being biophysically meaningful and measurable, but also because they enable investigations into related questions. However, a notable drawback of the HH model lies in its multitude of time-dependent parameters. Additionally, the complexity arising from the integration of numerous ordinary differential equations poses challenges to its implementation. Nonetheless, the Hodgkin-Huxley model has played a pivotal role in laying the groundwork for understanding cellular electrical excitability and has greatly influenced the field of neuronal physiology.

1.2.3 Hindmarsh-Rose models

The Hindmarsh-Rose (HR) model is a mathematical model that describes the dynamics of neuronal activity, specifically the spiking behavior of the membrane potential of neurons. The HR is described as [60–63]

$$\begin{aligned}\frac{du}{dt} &= y - au^3 + bu^2 - w + I + D\frac{d^2u}{dx^2},\\ \frac{dv}{dt} &= c - du^2 - v + D\frac{d^2v}{dx^2},\\ \frac{dw}{dt} &= r[s(u - u_{th}) - w].\end{aligned} \tag{1.3}$$

with dimensionless variables x, y and z being membrane potential, fast and slow current, respectively. The variable I is taken as a control parameter that can lead to chaotic spiking. Other parameters: a, b, c, d, r are modeling the working of the fast ion channels and the slow ion channels, respectively. s, x_{th} are also fixed. The HR model provides insights into the mechanisms underlying the diverse firing patterns observed in real neurons. Its simplicity makes it a useful tool for studying the basic principles of neuronal dynamics and bifurcation analysis.

1.2.4 Aliev-Panfilov models

The Aliev-Panfilov (AP) model constitutes a mathematical framework aimed at describing the dynamics of excitation waves within cardiac tissue, with a particular focus on studying cardiac arrhythmias and wave propagation. This AP system combines a series of partial differential equations to describe the spatial and temporal evolution of electrical activity in cardiac tissue, employing two primary variables: the renormalized transmembrane potential v and the recovery variable u [64–69]. The equations are given by:

$$\begin{aligned}\frac{dv}{dt} &= D\frac{d^2v}{dx^2} + f(v,u) + I,\\ \frac{du}{dt} &= g(v,u).\end{aligned} \tag{1.4}$$

Herein, v denotes the renormalized transmembrane potential while u represents the recovery variable. The diffusion coefficient D and the Laplacian operator $\frac{d^2v}{dx^2}$ contribute to the description of spatial diffusion dynamics. Functions $f(v,u) = -p_0v(v-p_3)(v-1) - vu$ and $g(v,u) = (\epsilon_0 + \frac{p_1u}{v-p_2})(u - p_0v(v-p_3-1))$ describe the local excitation and recovery processes, respectively. This model captures the fundamental aspects of cardiac cell dynamics, including action potential generation and repolarization. Parameters ϵ_0, p_1,

and p_2 specify the relationship between v and the control variable w. Parameters p_0 and p_3 govern the shape of the cubic function controlling action potential dynamics, with the term vu mitigating hyperpolarization. The AP model is renowned for its capacity to simulate the initiation and propagation of excitation waves, as well as the emergence of spiral waves and other intricate spatiotemporal patterns conducive to arrhythmias. It has found widespread application in computational investigations aimed at elucidating the mechanisms underlying cardiac arrhythmias, such as reentrant waves and fibrillation. Furthermore, this model can be viewed as an extension of the FHN model, which will be discussed in the subsequent paragraph.

1.2.5 FitzHugh-Nagumo models

The FitzHugh-Nagumo model serves as a simplified two-dimensional mathematical representation of the HH model, focusing on the electrical activity of neurons. It aims to replicate the plateau phase observed in cardiac cells, a feature absent in the original HH model of nerve impulses. The FHN model constitutes a coupled system of two ODEs [70–73]:

$$\begin{aligned} \frac{dv}{dt} &= v - \frac{v^3}{3} - w + I_{ext} + D\frac{d^2v}{dx^2}, \\ \frac{dw}{dt} &= \epsilon(v + a - bw). \end{aligned} \tag{1.5}$$

Herein, parameters a and b specify the inhibitor kinetics. Notably, the model parameters adhere to certain constraints: $0 < a < 1$, $0 < \epsilon << 1$, $b > 0$, $1b - (1 - a + a^2)/3 > 0$ and $(1 - a + a^2)/3 - \epsilon b > 0$. The small parameter ϵ represents the ratio of temporal scales between v and w. The variable v signifies the membrane potential, w denotes a recovery variable and I serves as an external input current, respectively. The first equation captures the rapid dynamics of the membrane potential v, influenced by a cubic nonlinearity, the recovery variable w, and the external input current I. The second equation encapsulates the slower dynamics of the recovery variable w, modulated by the membrane potential v. Renowned for its excitability, the FHN model exhibits the capability to generate action potentials in response to external stimuli. Additionally, it has been postulated that electrical and chemical autapses, specific synapses forming closed loops with the body, can modulate the electrical behaviors of neural and myocardial cells, thereby regulating collective behaviors within networks through the induction of continuous pulses and wave fronts. The model holds particular utility in investigating the behavior of excitable cells and has found application across diverse contexts, including studies involving cardiac cells and neural networks. [4, 8, 9, 74, 75]

1.3 Soliton theory

A soliton is a self-reinforcing solitary wave that maintains its shape while traveling at a constant speed. From his Origins and Historical Background, the signal known as Solitons can be defined as solitary waves that asymptotically maintain their shape and velocity after a collision with other solitary waves. This observation was first recorded by J. Scott Russell in 1834 on the Edinburgh-Glasgow channel [76]. In 1895, Korteweg and de Vries [77–80] derived an equation, the so-called KdV equation which describes shallow water waves where the existence of solitary waves was verified mathematically. In 1955, Fermi, Pasta and Ulam (FPU) decided to numerically solve Newton's equations of motion for a one-dimensional chain of identical masses attached by nonlinear springs [81]. Their studies inspired Zabusky and Kruskal [82, 83] and they analyzed the KdV equation which had been arisen from the FPU problem. They observed that the localized waves preserve their shape and momentum in collisions. Evidence is presented that solitons may exist in a nonlinear system of RD equations and provides some key Characteristics such as:

- Stability: Unlike typical waves that dissipate over time, solitons are stable and can travel long distances without changing shape.
- Nonlinearity: Solitons arise in nonlinear systems where the wave speed depends on the wave amplitude.
- Balance between Dispersion and Nonlinearity: The shape-preserving nature of solitons is due to a balance between dispersive effects (which tend to spread the wave out) and nonlinear effects (which tend to focus the wave).

Solitons are present in fiber optics, used to transmit information over long distances without signal degradation; in biological processes, such as the propagation of nerve impulses, which can be modeled using soliton theory.

Dissipative solitons, are a more recent concept emerging from the study of nonlinear systems far from equilibrium, particularly in RD systems. These are systems where chemical reactions (reaction) and processes like diffusion (spatial distribution of substances) occur simultaneously. These solitons exist in systems where energy is constantly supplied and dissipated, resulting in stable, localized structures due to a balance between nonlinearity, dispersion, and dissipation.

The concept of dissipative solitons in RD systems emerged as researchers sought to understand how localized structures, such as chemical patterns (Turing patterns),

waves, and pulses, could form and persist in these systems despite the presence of dissipation. The study of dissipative solitons in RD systems gained significant attention in the late 20th century, particularly with the advent of experimental and computational techniques that allowed for the observation and simulation of these phenomena. Researchers like Alan Turing in the 1950s laid the groundwork by showing that RD equations could produce stable, spatially periodic patterns, which are now known as Turing patterns. These patterns are an early example of the complex behavior that can arise in RD systems. The extension of this concept to solitons occurred as researchers realized that under certain conditions, RD systems could support not just stationary patterns, but also moving localized structures that resemble solitons in conservative systems. These structures were termed ”dissipative solitons” because they required a constant input of energy or material to sustain themselves, distinguishing them from the classical solitons that are solutions to integrable systems like the KdV equation.

Dissipative solitons in RD systems have been observed and studied in a variety of contexts:

- Chemical reactions: One of the most well-known examples is the Belousov-Zhabotinsky (BZ) reaction, a chemical oscillator that can exhibit wave patterns and localized structures. In certain conditions, the BZ reaction can produce dissipative solitons that move through the medium without changing shape.
- Biological systems: RD models are used to describe processes like morphogenesis (the development of patterns and structures in organisms), neural activity (e.g., the propagation of nerve impulses), and cardiac activity (e.g., the formation of spiral waves and reentrant waves that can lead to arrhythmias).
- Optical systems: In nonlinear optics, dissipative solitons can occur in optical cavities where light interacts with a medium, leading to stable pulses of light that propagate without distortion. These are particularly important in the development of advanced laser systems and optical communication technologies.
- Ecological models: RD systems are also used in ecology to model the spread of species and the formation of spatial patterns in ecosystems.

Dissipative solitons in RD systems represent a fascinating intersection of nonlinear dynamics, pattern formation, and stability theory. Their origins lie in the study of solitons in conservative systems, but they have evolved into a critical concept for understanding a wide range of phenomena in both natural and engineered systems. Their

applicability spans from chemical reactions to biological systems and even optical and ecological models, making them a powerful tool for exploring complex behaviors in non-linear, dissipative environments.

1.4 Heart system

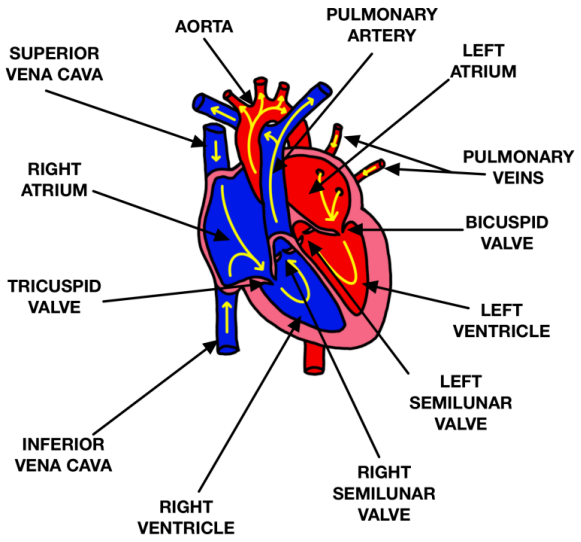

Figure 1.2: Structure of the heart [85].

1.4.1 Structure and function

The heart, a vital organ in the cardiovascular system, pumps blood throughout the body via a network of blood vessels. Positioned in the front of the chest, slightly behind and to the left of the sternum, it collaborates with other bodily systems to regulate heart rate and blood pressure. Various factors, including family history, personal health, and lifestyle choices, influence its efficiency. Comprised of four chambers made of muscle and powered by electrical impulses, the heart's primary function is blood circulation. Additionally,

- it controls heart rate rhythm and speed,
- maintains blood pressure,
- facilitates the transportation of oxygen, nutrients, and metabolic waste such as carbon dioxide to the lungs.

Working in conjunction with other bodily systems, particularly,

- The nervous system: aids in heart rate control by sending signals for adjustments based on rest or stress levels.
- The endocrine system: releases hormones that affect blood vessel constriction or relaxation, thus influencing blood pressure. Hormones from the thyroid gland also contribute to heart rate modulation.

1.4.2 Structure of the cardiac muscle

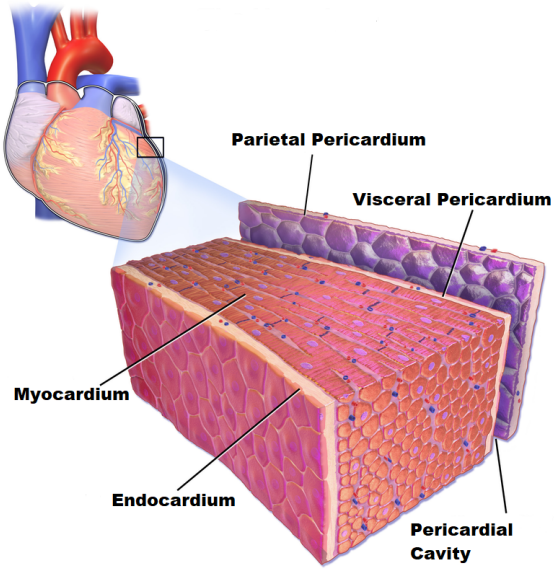

Figure 1.3: Heart Wall [86].

The heart is enclosed in a protective covering called the pericardium, which contains a small amount of fluid. Its wall consists of three layers: the epicardium, myocardium, and endocardium.

1.4.2.1 The pericardium comprises two main parts that surrounds and protects the heart:

- The fibrous pericardium, an outer layer of tough and inelastic connective tissue. It shields the heart, secures it in the chest, and prevents excessive stretching.
- The serous pericardium, an inner layer of delicate membrane. It forms a closed sac around the heart. It serves functions such as:
  - Protection from infections and external trauma.
  - Anchoring the heart within the chest cavity.
  - Facilitating smooth movement with lubricating pericardial fluid.

– Preventing overstretching particularly during changes in blood volume or pressure.

1.4.2.2 The myocardium, composed of involuntary striated muscle, constitutes the main tissue of the heart wall. Positioned between the pericardium and endocardium, his Key features and functions include:

- Muscular contractions are done rhythmically to pump blood throughout the body.
- Striated muscle similar to skeletal muscle. It displays a striped appearance under a microscope due to its organization.
- Contractile properties are regulated by electrical signals, and it requires a substantial blood supply via coronary circulation.
- The thickness of the myocardium varies in different regions of the heart, with the left ventricle possessing a thicker layer to pump blood effectively.

The coordinated contraction and relaxation of the myocardium create the pumping action of the heart, allowing it to efficiently circulate blood and fulfill the body oxygen and nutrient requirement

1.4.2.3 The endocardium, the innermost layer of the heart wall, lines the heart chambers with a thin, smooth membrane of endothelial cells and connective tissue. It serves several essential functions such as:

- The endothelial barrier that provides a smooth lining to the inside of the heart chambers, which helps reduce friction as blood flows through the heart.
- Protection: It forms a protective layer that separates the heart muscle from the blood within the chambers.
- Regulation of blood flow through the heart chambers. The smooth surface facilitates the smooth movement of blood without clotting.
- Conduction of electrical signals regulate the heartbeat. It contains specialized cells participating in the conduction of electrical signals that control the heartbeat.

1.4.3 Structure of the Filament cross section

Cardiac cells are called myocytes, having a length of $80-100$ μm and a diameter of $10-20$ μm. Each of these cells is separated from the extracellullar space by a phospholipid bilayer membrane. This membrane presents selective permitivity, allowing some

ions (Na^+, K^+, Ca^{+2}, etc) to flow between the extracellular and intracellular media through a set of specific ion channels. The resulting charge imbalance produces a transmembrane potential difference, whose evolution is governed by the balance between the electrical and chemical gradients across the membrane of the cell. Cardiac muscle is a specialized type of muscle tissue that makes up the myocardium, the muscular wall of the heart. Unlike skeletal muscle, cardiac muscle is involuntary, meaning its contractions are not under conscious control. Here are the key structural features of cardiac muscle:

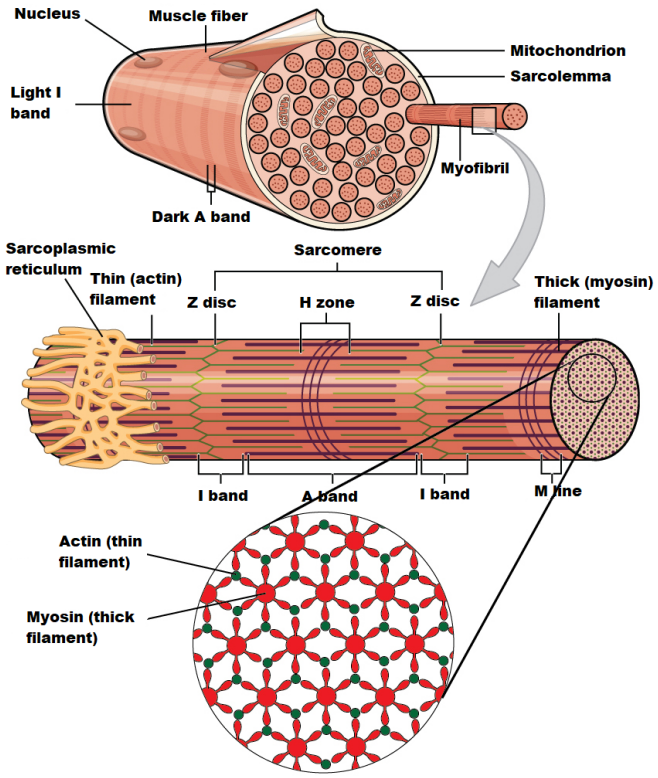

Figure 1.4: Filament cross section [87].

- Striated appearance: Similar to skeletal muscle, it has a striated (striped) appearance when viewed under a microscope. This striation is due to the organization of sarcomeres, which are the basic contractile units of muscle tissue.
- Branching cells: Cardiac muscle cells are branching cells that form a three-dimensional network. This branching allows for better communication and coordination between adjacent cells. The branches interconnect at junctions called intercalated discs.
- Intercalated Discs: are specialized regions where adjacent cardiac muscle cells con-

nect. The latter is produced by gap junctions, which allow for rapid electrical and chemical communication between cells. Gap junctions are located at the longitudinal ends of the myocytes, that are bundled in cardiac fibers along which the propagation speed is faster. This synchronization is crucial for the coordinated contraction of the entire heart.

- Single Nucleus: Unlike skeletal muscle cells, cardiac muscle cells typically have a single centrally located nucleus. The presence of a single nucleus per cell is a characteristic feature of cardiac muscle.
- Involuntary Contraction: The contraction of cardiac muscle is involuntary and is regulated by the autonomic nervous system. The heart contracts rhythmically to pump blood throughout the body. The impulses for contraction originate in the sinoatrial (SA) node and are conducted through the heart via the atrioventricular (AV) node.
- Rich Blood Supply: The heart has an extensive network of blood vessels to supply oxygen and nutrients to the cardiac muscle cells. Coronary arteries branch throughout the myocardium to ensure an adequate blood supply.
- Mitochondria Abundance: Cardiac muscle cells are rich in mitochondria, reflecting their high energy demands. The continuous pumping action of the heart requires a significant amount of energy for sustained contractions.
- Endomysium and Perimysium: Like skeletal muscle, cardiac muscle is also surrounded by connective tissue layers. The endomysium surrounds individual muscle fibers, while the perimysium separates and surrounds bundles of muscle fibers, forming fascicles.
- Adaptation to Continuous Contraction: Cardiac muscle cells are adapted to continuous and rhythmic contractions. They are resistant to fatigue, ensuring that the heart can pump blood consistently throughout an individual's lifetime.

The unique structural features of cardiac muscle contribute to its ability to contract rhythmically and pump blood effectively, maintaining the circulation of blood throughout the body. The coordinated contraction of cardiac muscle is essential for proper heart function and overall cardiovascular health.

1.4.4 Blood conduction system

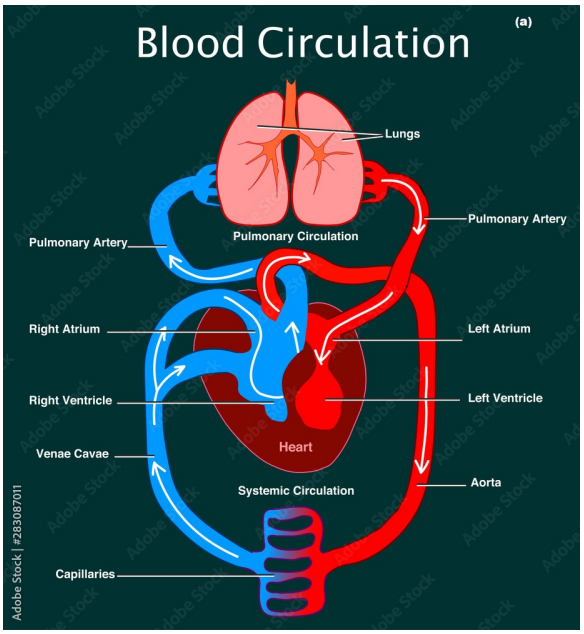

Figure 1.5: Blood conduction [88].

Blood circulation in the heart follows a defined pathway, involving the movement of blood through its four chambers and associated blood vessels. The human heart comprises two upper chambers called atria and two lower chambers known as ventricles. Valves within the heart ensure blood flows in one direction. Here's a summary of how blood moves through the heart:

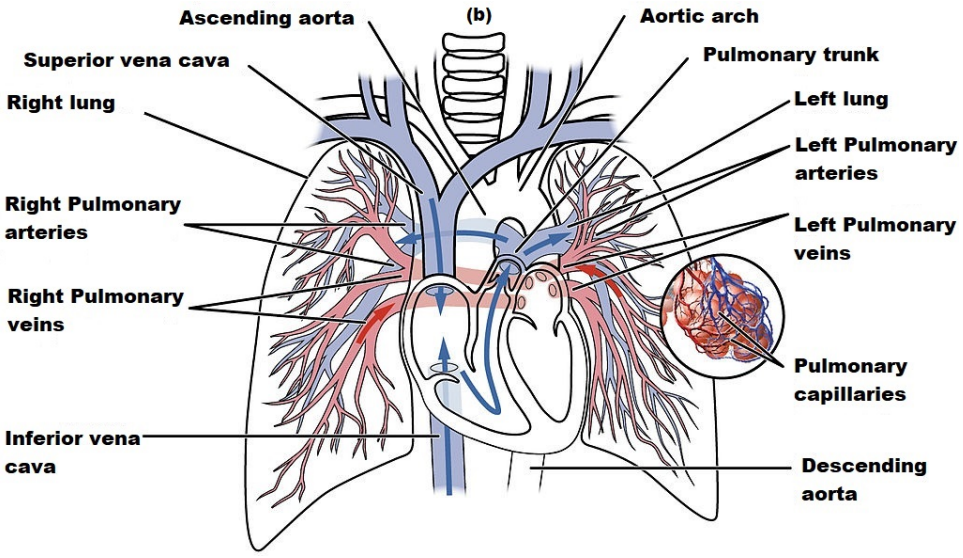

Figure 1.6: Pulmonary Circuit [89].

- The right atrium receives deoxygenated blood returning to the heart from the body through two major veins: the superior vena cava (from the upper body) and the inferior vena cava (from the lower body).
- Tricuspid valve: Blood moves from the right atrium into the right ventricle through the tricuspid valve. This valve ensures that blood flows in one direction, preventing any backward flow from the right ventricle to the right atrium during contraction.
- The right ventricle expels deoxygenated blood through the pulmonary valve into the pulmonary artery.
- The pulmonary artery transports deoxygenated blood to the lungs, where it undergoes pulmonary gas exchange. During this process, the blood picks up oxygen and releases carbon dioxide.
- Pulmonary Veins: Oxygenated blood returns from the lungs to the heart via the pulmonary veins, entering the left atrium.
- Blood moves from the left atrium into the left ventricle through the mitral (or bicuspid) valve. This valve prevents the backward flow of blood from the left ventricle to the left atrium during contraction.
- The left ventricle expels oxygenated blood through the aortic valve into the aorta.
- The aorta is the largest artery, distributes oxygenated blood to all tissues and organs, supplying them with oxygen and nutrients.
- Systemic Circulation: The oxygenated blood is disseminated to the body's tissues via smaller arteries, arterioles, and capillaries, facilitating the delivery of oxygen and the pickup of carbon dioxide within the capillary network.
- Venous return occurs as deoxygenated blood is conveyed back to the right atrium via the superior and inferior vena cava, perpetuating the cycle.

The ongoing movement of blood through the heart and the circulatory system constitutes the cardiac cycle. Valves within the heart are pivotal in directing blood flow in the proper direction, safeguarding against reverse flow, and sustaining optimal circulation throughout the body.

1.4.5 Electrical conduction system

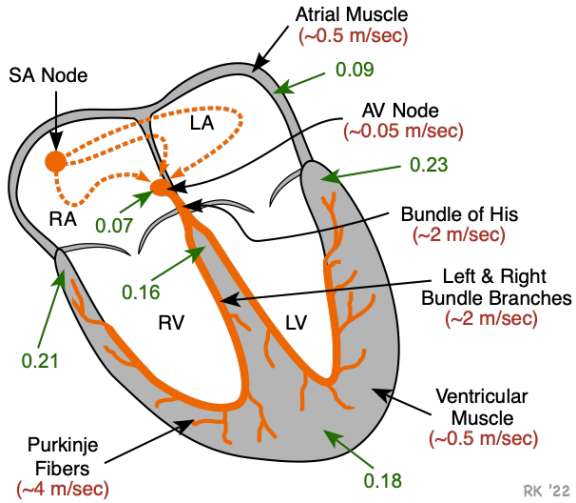

Figure 1.7: Electrical conduction [90].

If embryonic heart cells are isolated and sustained in a Petri dish, each cell can autonomously produce its own electrical impulse followed by contraction. When two embryonic cardiac muscle cells with independent beating patterns are brought together, the cell with the faster intrinsic rate dictates the rhythm, and its impulse propagates to the slower cell, prompting contraction. This hierarchy persists as more cells are aggregated, with the swiftest cell retaining control over the pace. In the fully developed adult heart, this mechanism persists, with the fastest cells initiating the electrical impulse as part of the cardiac conduction system. The cardiac conduction system orchestrates the rhythmic contractions of the heart muscle, ensuring efficient blood pumping. Comprising specialized cells, this system generates and conducts electrical signals. Here is an outline of the fundamental components and processes involved in the electrical conduction within the heart:

- The electrical impulse originates from the SA node, situated within the right atrium, earning it the moniker "natural pacemaker" due to its autonomous generation of electrical signals. These impulses, traveling at a velocity of approximately 0.5 m/sec, initiate the contraction of the atria.
- Upon the propagation of the electrical impulse, the atria undergo contraction, facilitating the pumping of blood into the ventricles within a timeframe of approximately 0.09 seconds.

- The electrical impulse reaches the AV node, positioned in the interatrial septum between the atria. Functioning as a delay mechanism, the AV node slows the impulse to approximately 0.05 m/sec, enabling the ventricles to adequately fill with blood before their contraction.
- Bundle of His (BH): From the AV node, the electrical impulse travels down the BH, a collection of specialized fibers located in the interventricular septum, at a rapid velocity of approximately 2 m/sec.
- Right and Left Bundle Branches: The BH then divides into right and left bundle branches, which extend along the septum towards the apex of the heart.
- Purkinje fibers (PF): subsequently, these branches further split into PF, which spread throughout the ventricles. The PF conduct the electrical impulse at a high velocity of about 4 m/sec, coordinating the contraction of the ventricles.
- Ventricular contraction: As a result of this electrical stimulation, the ventricles contract, leading to the pumping of blood into the pulmonary artery from the right ventricle and into the aorta from the left ventricle.
- Repolarization: Following contraction, the heart undergoes repolarization, a phase of electrical recovery, in preparation for the subsequent cardiac cycle.

This sequence of electrical processes forms the cardiac conduction cycle, ensuring the coordinated contraction of the atria and ventricles, which is essential for the efficient pumping of blood by the heart. Any disorders or irregularities in the electrical conduction system can lead to arrhythmias or other cardiac issues, underscoring the crucial role of this system in sustaining the heart's rhythmic function.

1.4.6 Membrane potential and ions movement

In panel (b), the principal ionic currents and channels responsible for the different phases of the action potential in a cardiac cell are displayed.

- During Phase 0, both chemical and electrostatic forces facilitate the entry of Na^+ into the cell through fast Na^+ channels, leading to the upstroke.
- Phase 1 is characterized by the efflux of K^+ through i_{to} channels, driven by both chemical and electrostatic forces, resulting in early partial repolarization.
- In Phase 2, the net influx of Ca^{+2} through Ca^{+2} channels is counterbalanced by the efflux of K^+ through i_K, i_{K1}, and i_{to} channels, sustaining the plateau.

- Phase 3 sees a predominance of chemical forces favoring the efflux of K^+ through i_K and i_{K1} channels over the electrostatic forces that promote the influx of K^+ through the same channels.
- During Phase 4, the efflux of K^+ through i_K and i_{K1} channels slightly surpasses the electrostatic forces facilitating the influx of K^+ through these same channels.

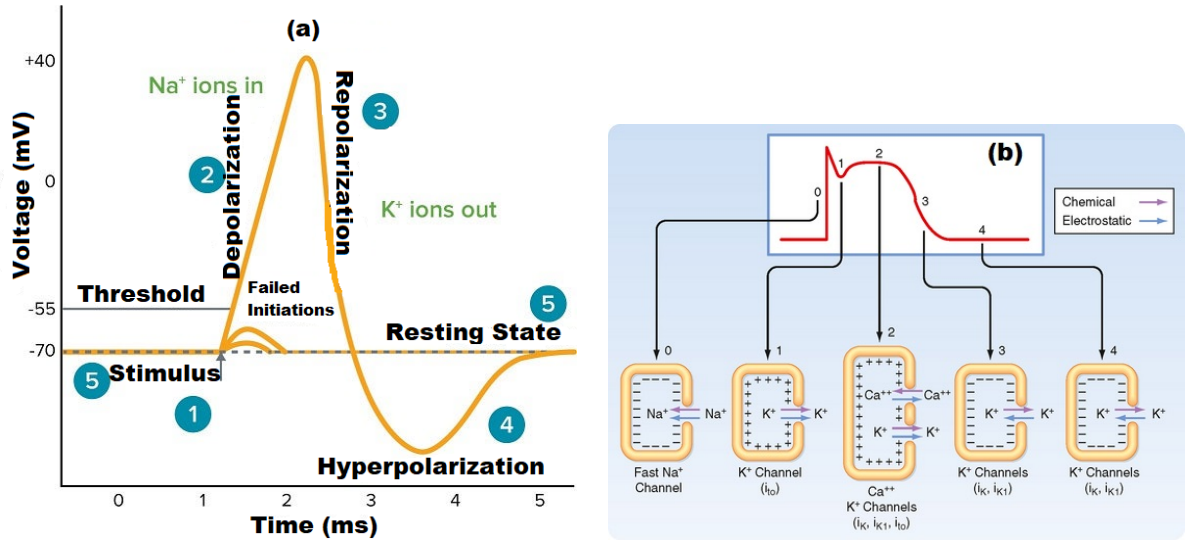

Figure 1.8: Panel (a) illustrates the action potential of heart nodal cells [91], while panel (b) depicts the action potential of cardiac muscle cells [92].

The membrane potential of cardiac cells signifies the variance in electrical charge across the cell membrane. This electrical potential plays a vital role in initiating and transmitting electrical signals within the heart, ultimately resulting in the contraction of cardiac muscle. Cardiomyocytes are the key cells responsible for generating the heart's electrical activity.

- Resting Membrane Potential: At rest, the membrane potential of a cardiac cell is negative, typically around −90 millivolts (mV) to −80 mV. This negative resting potential is maintained by the selective movement of ions across the cell membrane, primarily through ion channels.
- Depolarization Phase: When a cardiac cell is stimulated, typically by an electrical impulse from the SA node, sodium channels open, allowing an influx of sodium ions (Na^+) into the cell. The rapid influx of sodium ions causes a sharp rise in membrane potential, leading to depolarization. This is the rising phase of the action potential.

- Ion Movement: Sodium (Na^+), potassium (K^+), calcium (Ca^{2+}), and chloride (Cl^-) ions play essential roles in establishing and changing the membrane potential. The resting membrane potential is largely influenced by the movement of potassium ions through potassium channels, which are more permeable to K^+.
- Action Potential: When a cardiac cell undergoes stimulation, it initiates an action potential. During the depolarization phase, there's a rapid influx of sodium ions, causing the membrane potential to become less negative, approaching 0 mV. Subsequently, in the repolarization phase, potassium ions efflux, restoring the negative charge inside the cell.
- Calcium Influx: In addition to sodium and potassium, calcium ions play a pivotal role in the action potential of cardiac cells, particularly during the plateau phase. Calcium channels open during the action potential, allowing calcium to enter the cell and contribute to sustained depolarization.
- Role of Chloride Ions: Chloride ions (Cl^-) also contribute to maintaining electrical balance. While they have a relatively minor role during the action potential, they aid in overall ion balance within the cell.
- Plateau Phase: Unlike many other excitable cells, cardiac cells exhibit a distinctive plateau phase during the action potential. This plateau arises from a balance between calcium influx and potassium efflux. Following the initial depolarization, a brief plateau phase ensues during which calcium channels open, facilitating the entry of calcium ions (Ca^{+2}) into the cell, which prolongs the action potential and prevents rapid firing.
- Repolarization: After the plateau, further repolarization occurs due to continued potassium efflux, leading to the restoration of the resting membrane potential.
- Refractory Period: Following an action potential, there is a refractory period during which the cardiac cell becomes less responsive to additional stimuli. This period is crucial for preventing rapid and uncontrolled impulses.

The synchronized action potentials across cardiac cells, particularly in the SA node, AV node, and the BH, contribute to the rhythmic contractions of the heart. The sequence of depolarization and repolarization events ensures orderly and efficient blood pumping, maintaining the heart's function as a pump in the circulatory system. Any disruptions in the normal membrane potential and action potential sequence can lead to arrhythmias or other cardiac abnormalities.

1.4.7 Cardiopathies

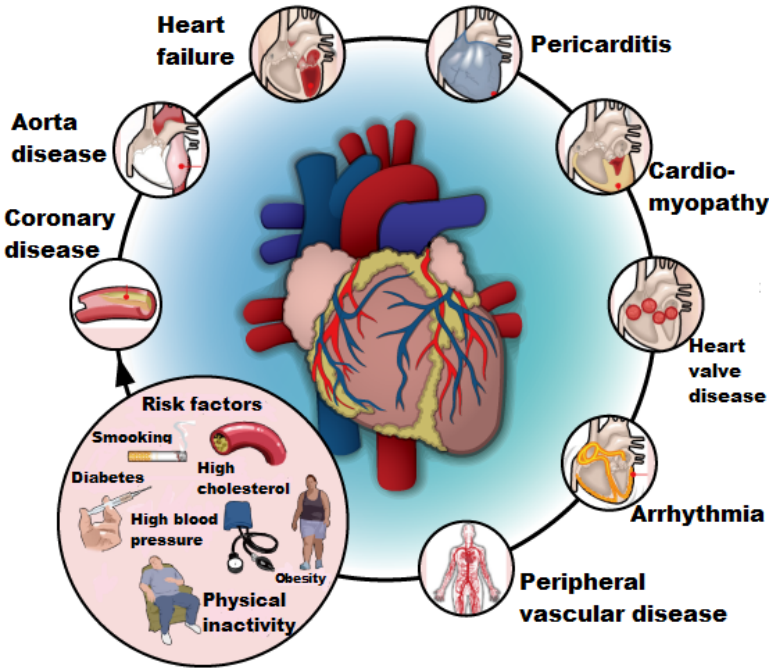

Figure 1.9: Cardiopathies [93].

Several conditions can affect the heart, ranging from congenital (present at birth) to acquired conditions that develop over time. Here are some common conditions that can impact the heart:

- Coronary Artery Disease (CAD): CAD occurs when the coronary arteries, which supply blood to the heart muscle, become narrowed or blocked by a buildup of plaque. This can lead to chest pain (angina) or a heart attack.
- Myocardial Infarction (Heart Attack): occurs when blood flow to a part of the heart muscle is blocked, usually due to a blood clot. This leads to damage or death of the affected heart muscle tissue.
- Heart Failure (HF): is a condition where the heart is unable to pump blood effectively, leading to inadequate circulation. It can result from various underlying causes, including coronary artery disease, hypertension, and cardiomyopathy.
- Hypertension (High Blood Pressure): Chronic HBP can lead to increased strain on the heart, potentially causing the heart muscle to thicken and weaken over time.

- Arrhythmias: are abnormalities in the heart's rhythm, manifest as irregular heartbeats, too fast (tachycardia) or too slow (bradycardia) heart rates. Atrial fibrillation is a common type of arrhythmia.
- Valvular Heart Disease: involves problems with the heart valves, which regulate blood flow within the heart. Conditions include valve stenosis (narrowing) or regurgitation (leakage).
- Cardiomyopathy: refers to diseases of the heart muscle, caused by various factors, including infections, genetics, and certain medications, leading to weakened heart muscle and impaired function.
- Congenital Heart Defects (CHD): CHD are structural abnormalities present at birth, affecting the heart's chambers, valves, or blood vessels.
- Peripheral Artery Disease (PAD): PAD involves the narrowing or blockage of arteries outside the heart, typically affecting the arteries that supply the limbs, resulting in reduced blood flow to the extremities.
- Endocarditis: is the inflammation of the inner lining of the heart chambers and valves, often caused by bacterial or fungal infections leading to damage of the heart valves.
- Rheumatic Heart Disease (RHD) : RHD is a complication of untreated streptococcal infections, particularly strep throat, leading to inflammation and damage to the heart valves.
- Pericarditis: is the inflammation of the pericardium, the sac surrounding the heart, causing chest pain and discomfort.

It is important to note that many heart conditions share risk factors, such as smoking, obesity, diabetes, and a sedentary lifestyle. Regular medical check-ups, a healthy lifestyle, and early detection and management of risk factors are crucial for maintaining heart health. Individuals experiencing symptoms such as chest pain, shortness of breath, or irregular heartbeats should seek prompt medical attention.

1.5 Neurons system

Neurons, also referred to as nerve cells, serve as the basic units of the nervous system, encompassing the brain, spinal cord, and peripheral nerves. These specialized cells are

responsible for conveying information via electrical and chemical signals. Their primary function involves processing and transmitting information, facilitating communication within the nervous system.

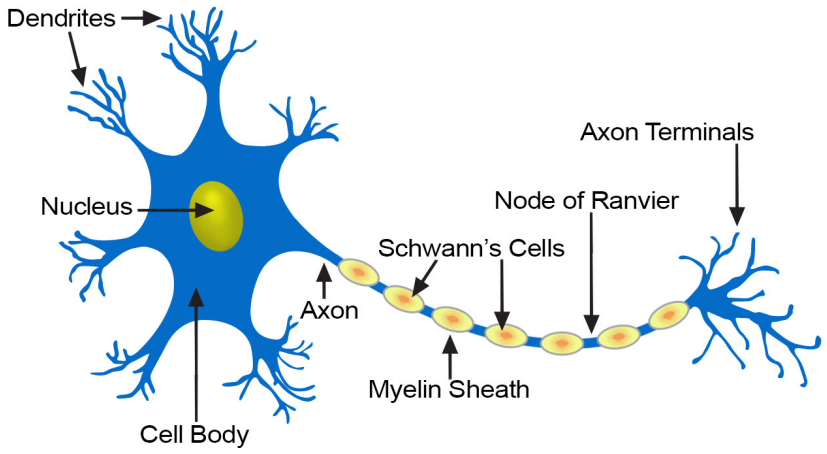

Figure 1.10: Neuron [94].

1.5.1 Structure and function

There is a wide variety of neurons, with various shapes and sizes. However, they all have a common structure (see Ref. [94] of 1.10) comprising:

- Cell Body (Soma): is the central part of the neuron containing essential components such as the nucleus, mitochondria, endoplasmic reticulum, ribosomes, and other organelles. Neurons typically consist of around 70-80 percent water, with the dry material comprising approximately 80 percent protein and 20 percent lipid. The soma uniquely houses the cell nucleus, where the DNA molecule is confined, and most RNA in a neuron is produced. It plays a crucial role in the overall maintenance and functioning of the cell.
- Dendrites: are branching extensions emerging from the cell body, responsible for receiving signals, whether chemical or electrical, from other neurons or sensory receptors. They ensure the propagation of these signals towards the cell body, with specialized protein molecules known as receptors present on the post-synaptic dendritic membrane, detecting neurotransmitters within the synaptic cleft.
- Axon: is a long, slender extension of the neuron that carries nerve impulses away from the cell body. Axons can vary in length, ranging from as short as 0.1mm to as

long as 2m, and are covered by a myelin sheath.

- Axon Hillock: is the region where the axon originates from the cell body, critical for integrating signals received from dendrites.
- Myelin Sheath: is a fatty insulation surrounding the axon in segments, formed by specialized cells called Schwann cells in the peripheral nervous system and oligodendrocytes in the central nervous system. The myelin sheath serves to protect the axon, prevent interference between axons, and enhance the speed of nerve impulse transmission.
- Nodes of Ranvier: are small gaps in the myelin sheath along the axon, crucial for the saltatory conduction of nerve impulses. They allow the signal to jump from one node to the next, speeding up transmission.
- Axon Terminals (Synaptic Endings): Are structures located at the end of the axon, forming synaptic connections with other neurons, muscle cells, or glands. Communication between neurons occurs at these synapses.
- Neurotransmitters: are Chemical substances that transmit signals across synapses, released from vesicles in the axon terminals and binding to receptors on the postsynaptic neuron, thereby initiating a response.
- Action Potential: is a brief electrical impulse traveling down the axon of a neuron, generated in response to a stimulus. It is essential for the transmission of signals over long distances.

1.5.2 Classification of neurons

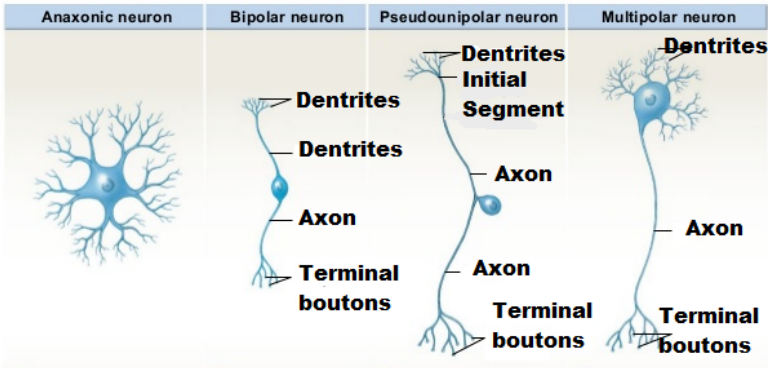

Figure 1.11: Structural categories of neurons [95].

Neurons, also known as nerve cells, can be categorized according to several criteria, such as their structure, function, and position within the nervous system. Below are some typical classifications of neurons, as illustrated in Fig. 1.11:

1.5.2.1 Based on Structure:

- Multipolar Neurons: These neurons feature multiple processes, comprising one axon and two or more dendrites, emanating from the cell body. They are predominantly located within the central nervous system (CNS), encompassing motor neurons and interneurons.
- Bipolar Neurons: These neurons possess two processes, an axon and a dendrite, extending from opposite ends of the cell body. They are typically found in specialized sensory organs such as the retina of the eye and the olfactory epithelium in the nose.
- Unipolar (Pseudounipolar) Neurons: Characterized by a single process that branches into a T-shape, with one branch serving as an axon and the other as a dendrite. They are primarily observed in sensory neurons, particularly those involved in touch and pain sensations.

1.5.2.2 Based on Function:

- Sensory Neurons (Afferent Neurons): These neurons relay signals from sensory receptors to the central nervous system (CNS), conveying information about both external and internal stimuli. They are primarily located in sensory organs and peripheral nerves.
- Interneurons (Association Neurons): Serving as intermediaries within the CNS, interneurons play a vital role in processing and integrating signals. They establish connections between sensory neurons, motor neurons, or other interneurons, facilitating communication within the central nervous system. Interneurons are predominantly found within the CNS.
- Motor Neurons (Efferent Neurons): These neurons transmit signals from the CNS to effectors such as muscles or glands, triggering a response. They are distributed throughout both the CNS and peripheral nerves, with axons extending to target muscles or glands.

1.5.2.3 Based on Location:

- Central Neurons: are neurons located within the central nervous system, comprising the brain and spinal cord. This category encompasses both interneurons, which facilitate communication within the CNS, and motor neurons.
- Peripheral Neurons: are neurons are situated outside the central nervous system, typically within peripheral nerves. They include sensory neurons, which convey sensory information to the CNS, and motor neurons, whose cell bodies reside in peripheral ganglia.

1.5.2.4 Based on Neurotransmitter Release:

- Cholinergic Neurons: These neurons release acetylcholine, a neurotransmitter commonly involved in the neuromuscular junction and certain regions of the autonomic nervous system.
- Adrenergic Neurons: These neurons release norepinephrine (also known as noradrenaline) and are primarily active in the sympathetic division of the autonomic nervous system.

These categorizations offer a structural model for comprehending the wide array of neurons present within the intricate framework of the nervous system. Neurons collaborate within intricate networks to relay and interpret information, facilitating the nuanced functionalities of the nervous system, encompassing processes such as perception, cognition, and motor regulation.

1.5.3 Electrical activity system

The electrical activity of a neuron is essential for its ability to transmit and process information. Neurons generate and conduct electrical signals, known as action potentials or nerve impulses, which allow them to communicate with other neurons and target cells. Here's an overview of the electrical activity of a neuron:

- Resting Membrane Potential: Neurons maintain a resting membrane potential, which is the electrical charge difference across the cell membrane when the neuron is at rest. The resting membrane potential is typically around -70 millivolts (mV) in neurons, with the interior of the cell being negatively charged compared to the extracellular fluid.

- Ion Channels: The resting membrane potential is influenced by the movement of ions across the neuron cells membrane. Ion channels, including sodium (Na^+), potassium (K^+), and chloride (Cl^-) channels, play a crucial role in regulating the flow of ions.
- Resting State: At rest, the neuron is permeable to potassium ions. Potassium channels allow a slow efflux of potassium out of the cell, contributing to the negative charge inside the neuron. Sodium and chloride channels are typically closed or less permeable, maintaining the resting membrane potential.

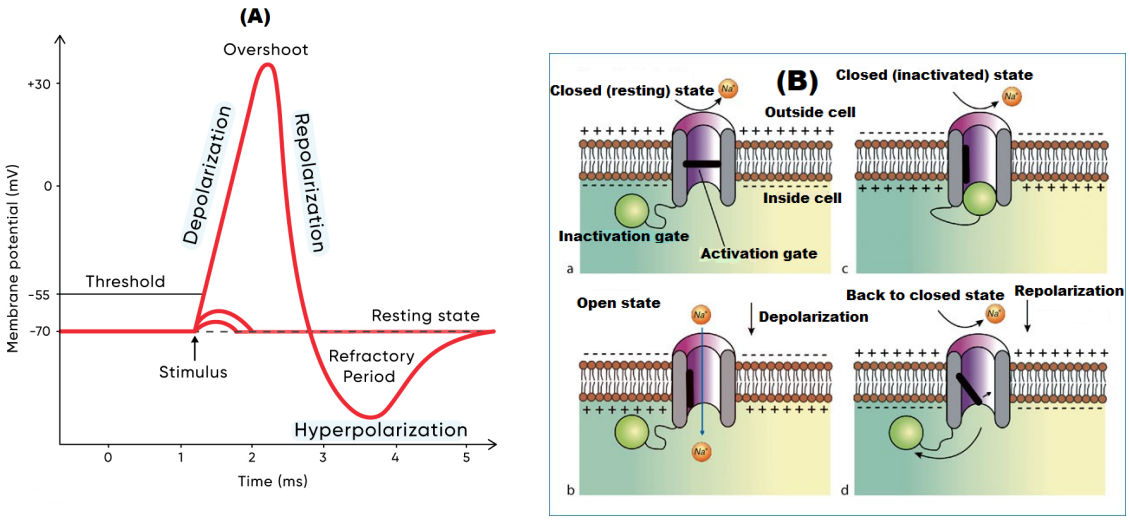

Figure 1.12: Neuron Action Potential in panel (a) [96] and ions flow in panel (b) [97].

- Action Potential Initiation: When a neuron receives a stimulus (e.g., from a neighboring neuron) the action potential which is between - 70 mV and - 55 mV, it may reach the threshold for action potential initiation. If the threshold is reached, voltage-gated sodium channels in the neuron membrane open, allowing an influx of sodium ions into the cell.
- Depolarization: As the action potential increases from - 55 mV to +30 mV, sodium influx induces membrane depolarization, diminishing intracellular negativity. This rapid change in voltage alteration constitutes the rising phase of the action potential.
- Threshold and All-or-None Principle: Adhering to the all-or-none principle, once the threshold is reached, an action potential follows with consistent amplitude and

duration. Subthreshold stimuli fail to elicit an action potential.[98, 99]

- Propagation of Action Potential: Depolarization in one membrane segment triggers the opening of voltage-gated sodium channels in adjacent regions, thereby propagating the action potential.
- Repolarization: Following its peak, the neuron experiences repolarization, returning from its summit of +30 mV to the resting state of -70 mV. Voltage-gated potassium channels open, permitting potassium efflux and restoration of intracellular negativity.
- Hyperpolarization: Certain neurons exhibit a transient hyperpolarization phase post-repolarization, driven by continued potassium efflux, resulting in a membrane potential more negative than the resting state.
- Refractory Period: Subsequent to an action potential, a refractory period results, during which the neuron's responsiveness to additional stimuli diminishes. This interval is critical for preventing the generation of successive action potentials in close succession.
- Sodium-Potassium Pump: The sodium-potassium pump actively transports sodium ions outward the cell and transports potassium ions inward, facilitating the restoration of ion gradients and the resting membrane potential.

The recurrent generation and transmission of action potentials along neuronal axons facilitate signal propagation over extended distances, enabling inter-neuronal communication within the nervous system. The precise control of ion dynamics and membrane potential alterations are fundamental of neuronal electrical activity.

1.5.4 Synapses

A synapse denotes the point of connection between the axon terminal of one neuron and the dendrite or cell body of another neuron. The transmission of signals across this synaptic junction is orchestrated by neurotransmitters, which serve as chemical mediators discharged from the presynaptic neuron to engage with receptors situated on the postsynaptic neuron. The categorization of synapses often hinges upon the nature of the signaling mechanism, the structural attributes, or the involvement of specific neurotransmitters. Below are several methodologies for classifying synapses

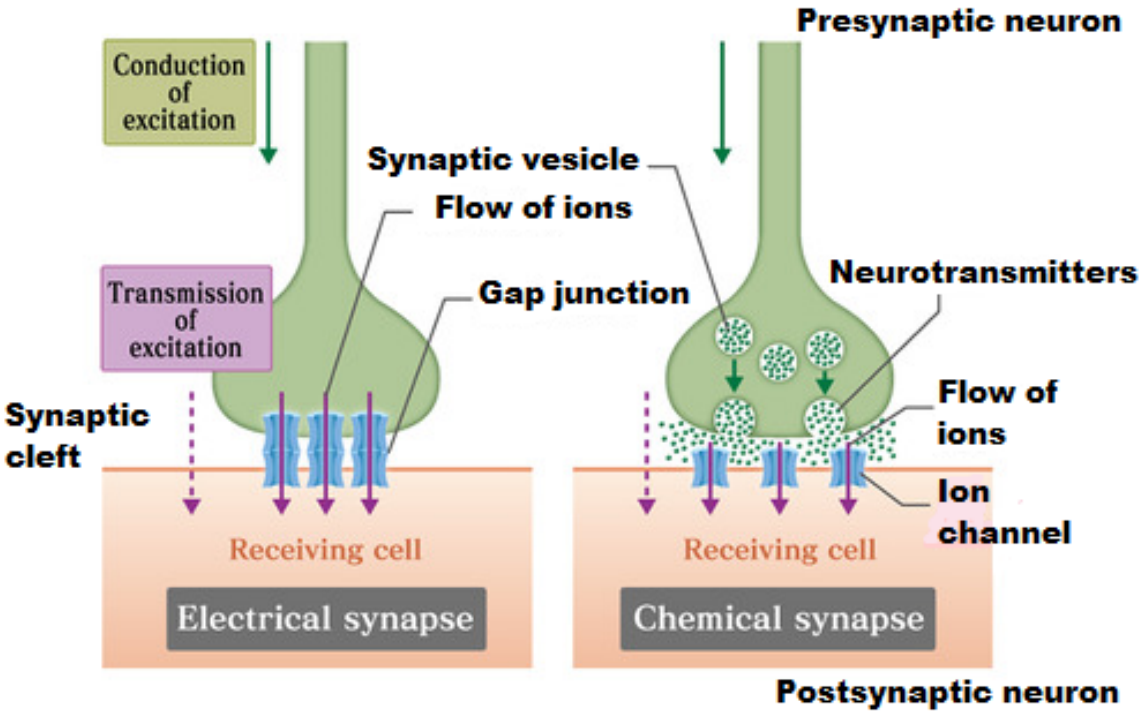

Figure 1.13: Comparison between Electrical and Chemical synapses [100].

1.5.4.1 Based on Signal Direction:

- Axodendritic: Between the axon terminal of one neuron and the dendrite of another.
- Axosomatic: Between the axon terminal of one neuron and the cell body (soma) of another.
- Axoaxonic: Between the axon terminal of one neuron and the axon of another.

1.5.4.2 Based on Structural Characteristics:

- Gray Type I (Asymmetric): Postsynaptic density is thicker, often excitatory synapses.
- Gray Type II (Symmetric): Postsynaptic density is thinner, often inhibitory synapses.

1.5.4.3 Based on Neurotransmitter release:

- Chemical Synapses, as depicted in Fig. 1.13, represent the most prevalent type of synaptic connection. They comprise a presynaptic terminal, a synaptic cleft, and a postsynaptic membrane. These synapses facilitate the transmission of information across the synaptic cleft through the use of chemical messengers known as neurotransmitters. Upon release, neurotransmitters bind to receptors situated on the postsynaptic membrane, thereby eliciting alterations in the membrane potential of the postsynaptic cell. Such modifications may culminate in the initiation of an action potential within the postsynaptic neuron, thereby perpetuating the transmission of the signal [101, 102].
- Electrical Synapses as portrayed in Fig. 1.13, involve the presence of gap junctions, facilitating direct interconnection between the cytoplasm of neighboring neurons. These specialized junctions enable swift electrical communication between neurons, enhancing the speed of signal transmission. Ion channels located at these gap junctions facilitate the direct exchange of ions between cells, facilitating rapid propagation of electrical signals from one neuron to another, bypassing the requirement for chemical neurotransmitters [103, 104].

1.5.4.4 Based on Neurotransmitter Function:

- Excitatory Synapses: These synapses release neurotransmitters such as glutamate or aspartate, which result in depolarization of the postsynaptic membrane. This depolarization allows for the passage of sodium Na^+ and potassium K^+ ions, thereby increasing the likelihood of generating an action potential. Excitatory synapses are notably significant within the brain, particularly in the formation of memories, as they enhance synaptic activity and strength.
- Inhibitory Synapses: These synapses release neurotransmitters such as Gamma-Aminobutyric Acid (GABA) and glycine, which hyperpolarize the postsynaptic membrane, thereby reducing the probability of generating an action potential due to the negative charge of chloride Cl^- ions.

1.5.4.5 Based on Structural complexity:

- Simple (Axosomatic or Axodendritic): One presynaptic terminal contacts one postsynaptic element.

- Complex (Axoaxonic or Multiple Contacts): One presynaptic terminal contacts multiple postsynaptic elements.

1.5.4.6 Based on Synaptic transmission Modulation:

- Facilitatory Synapses: Enhance the postsynaptic cell's response to neurotransmitters.
- Depressant Synapses: Decrease the postsynaptic cell's response to neurotransmitters.

1.5.4.7 Based on Location:

- Central Synapses: Occur within the central nervous system (brain and spinal cord).
- Peripheral Synapses: Occur outside the central nervous system, connecting peripheral nerves to muscles or glands.

1.5.4.8 Based on Timing:

- Temporal Summation: Accumulation of signals from the same presynaptic neuron over time.
- Spatial Summation: Integration of signals from multiple presynaptic neurons that synapse on the same postsynaptic neuron.

These categorizations help in understanding the diverse characteristics of synapses and their impact on the intricacy of neural transmission. The assorted categories of synapses assume pivotal roles in configuring neuronal networks, processing information, and governing the comprehensive functionality of the nervous system. In summary, the comparative table 1.2 outlining the distinctions between electrical and chemical synapses is provided below.

Electrical synapse	Chemical synapse
Essentially no synaptic delay	Significant synaptic delay
Typically bidirectional	Unidirectional
Direct communication among neurons	Indirect communication among neurons
Temperature-insensitive	Temperature-sensitive
Communicating agent is ionic current	Communicating agent is a chemical transmitter
Transmission of information occurs at high speed	Transmission of information is slow
Post synaptic signal is similar to pre-synaptic	Post synaptic signal can be different
Transmission is by gap junctions or low resistance bridges	Transmission is by Neurotransmitters
Synchronized activity	Specificity: point to point communication
Direct connections between neurons	Indirect connections between neurons
Insensitive to hypoxia and pH	Sensitive to hypoxia and pH
Rare in complex animals	Common in complex animals

Table 1.2: Comparison between electrical and chemical synapses.

1.5.5 Functional and behavioral properties

The human brain comprises an estimated 10^{15} neural networks. While these networks can function autonomously, they collaborate to execute diverse functions and exhibit analogous behaviors. Although neurons possess the capacity to produce, analyze, and convey information independently, their influence is confined to the microscopic realm. Participation within a network allows them to modulate their functions and acquire advantageous attributes across various cerebral regions. Below are several principal cognitive functions linked with neural networks. [105]

1.5.5.1 Perception:

Neural networks undertake the processing of sensory data received from the environment, which is then transmitted to the brain, analyzed, and subsequently deciphered to enable individuals to perceive and interpret various stimuli, including visual, auditory, tactile, olfactory, and gustatory inputs.

1.5.5.2 Attention:

Neural networks empower individuals to direct their focus toward specific stimuli while effectively filtering out extraneous information through attentional mechanisms that entail the selective activation and modulation of neural pathways.

1.5.5.3 Memory:

Neural networks are indispensable for the encoding, storage, and retrieval of information. Various forms of memory, encompassing short-term, long-term, episodic, and procedural memory, are supported by distinct neural circuits and structures.

1.5.5.4 Learning:

Neural networks facilitate the process of learning by modulating the strength of synaptic connections. Learning, characterized by the acquisition of new knowledge, skills, and behaviors through experience, relies on the dynamic adjustment of neuronal connectivity.

1.5.5.5 Language Processing:

Neural networks localized in language-associated brain regions enable individuals to comprehend and produce spoken and written language. Language processing entails intricate interactions among cortical regions such as Broca's and Wernicke's areas.

1.5.5.6 Emotional Processing:

Interactions among diverse brain regions mediate emotional responses, encompassing feelings of fear, joy, and sadness. Neural networks, including components of the limbic system, play a key roles in the processing of emotions.

1.5.5.7 Motor Control:

Neural networks situated in the motor cortex and related motor areas govern both voluntary and involuntary movements. These networks are responsible for the planning, execution, and coordination of precise motor actions.

1.5.5.8 Social Cognition:

Neural networks contribute to social cognition, enabling individuals to comprehend and interpret the thoughts, intentions, and emotions of others. Regions such as the mirror neuron system are implicated in processes of empathy and social interaction.

1.5.5.9 Consciousness and Self-awareness:

Neural networks are implicated in the generation of consciousness and self-awareness. The orchestrated activity of diverse brain regions underpins the subjective experience of existence and self-awareness.

These cognitive functions are intricately interconnected, and their harmonious interplay enables individuals to navigate their environment, adapt to challenges, and engage in complex cognitive endeavors. The exploration of neural networks and their functionalities constitutes a multidisciplinary pursuit, amalgamating insights from neuroscience, psychology, and computational modeling to unravel the complexities of cerebral cognitive processes.

1.5.5.10 Neurodegenerative Diseases

Neurodegenerative diseases are a class of progressive diseases caused by abnormalities in the structure and function of nerves. This type of disease is characterized by the loss of specific neurons in large numbers, which can lead to cognitive and behavioral disorders, even death in severe cases, and it is very difficult to cure. The incidence of many neurodegenerative diseases will increase with age, and the ever-increasing life expectancy of modern life makes it urgent to develop new and more effective treatment strategies to combat these destructive diseases.

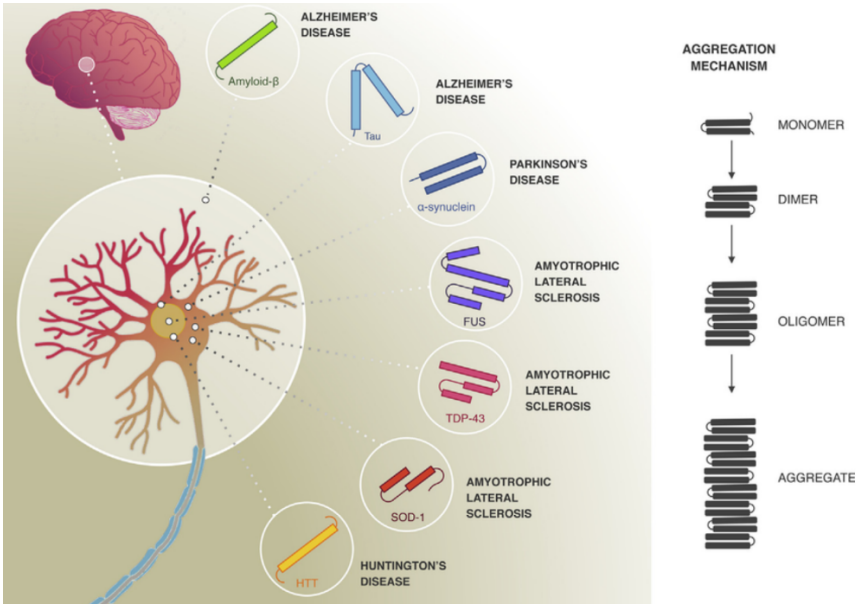

Figure 1.14: Neurodegenerative Diseases [106].

Neurodegenerative diseases can be divided into two types: acute neurodegenerative diseases and chronic neurodegenerative diseases. Although the lesions and causes of these diseases are different, with the progress of research, most neurodegenerative diseases have many common characteristics. The common neurodegenerative diseases are listed as follows:

- Alzheimer's disease (AD)is the most common neurodegenerative disorder, primarily affecting memory, thinking, and behavior, and characterized by the accumulation of amyloid plaques and tangles in the brain, leading to the death of neurons [107, 108].
- Parkinson's disease (PD) primarily affects movement, and it is caused by the degeneration of dopamine-producing neurons in the substantia nigra, a region of the brain responsible for controlling movement [109, 110].
- Amyotrophic Lateral Sclerosis (ALS) also known as Lou Gehrig's disease (LGD), is a condition that affects motor neurons, the cells that control voluntary muscle movement, and leading to muscle weakness and atrophy, difficulty speaking (dysarthria), difficulty swallowing (dysphagia), and eventually, respiratory failure [111, 112].
- Huntington's Disease (HD) is a genetic disorder that causes the progressive breakdown of nerve cells in the brain, due to a mutation in the huntingtin gene, leading to abnormal protein production, uncontrolled movements (chorea), emotional disturbances, and cognitive decline [113, 114].

Neurodegenerative disorders result from a combination of genetic, environmental, and lifestyle factors, though the exact causes remain largely unknown. Age is a major risk factor, with these disorders being more common in older populations. There is currently no cure, and treatments focus on symptom management and slowing disease progression. These treatments, including medications, therapies (Deap Brain Stimulation for Parkinson, Vague Nerve Stimulation for the refractory epilepsy, Transcranian Magnetic stimulation for depression, Transcranian Direct Curent Stimulation for post-CDV), and lifestyle changes, aim to improve quality of life but often require long-term care and support.

Finally, neurodegenerative disorders represent a major challenge in modern medicine due to their progressive nature and the lack of curative treatments. Understanding these disorders' mechanisms and developing effective interventions is a critical area of research that holds promise for improving the lives of millions of affected individuals worldwide.

1.6 Conclusion

This chapter has provided a comprehensive review of the historical context surrounding excitable cells, elucidating their anatomy and physiology, with particular emphasis on inter-cellular communication via membrane cells and synapses. Moreover, it has delved into extensive research conducted on prominent computational models aimed at replicating various patterns of electrical activity observed in cardiac cells and neurons, including soliton-like phenomena, spikes, bursts, and localized patterns. It is important to stress that among these models, namely the HH, ML, and FHN models, possess biologically plausible properties, as their parameters have been derived from experimental data. Conversely, other models strive to simulate the biological behavior of neurons and cardiac cells but lack empirical validation, which fails to fulfill this criterion. These models can be investigated analytically and numerically using various methods, promising interesting results that will significantly enhance our comprehension of the triadic system's functionality, as elucidated in the subsequent chapter.

CHAPTER 2

MATHEMATICAL BACKGROUND AND METHODOLOGIES

Contents

2.1 Introduction

During recent years, dissipative solitons has long been intensively studied both theoretically and experimentally. Several perturbation techniques have been

used to reduce the FHN model equations combined with linear self-and cross-diffusion, thermoelectric coupling and feedback gain of electromagnetic induction terms to the amplitude equation in one or more dimensions. Depending on the excitation modes, the problem of nonlinear waves propagating in cardiac cells can be described by NLS, CCGL and CQCGL equations, etc., leading to envelope or non-envelope soliton wave structures. These cited equations are derived from model equations by techniques such as the multiple scale expansion method, the reductive perturbation method and other asymptotic expansions [115]. Generally, these equations are written into complex forms in order to obtain exact solutions by using some methods such as Painlevé method, Hirota bilinear method and so on [116–121, 187].

Otherwise, for envelope solitons, they have been found greatly interesting in studying the MI of different wave modes in cardiac tissue, due to its importance in stable wave propagation. According to the linear stability analysis, a set of equations describing the evolution of the perturbation amplitude is derived, and an analysis of the MI gain spectrum is presented.

Our aims in this work is to analyze the effects of self-and-cross diffusion, feedback gain of the electromagnetic induction, thermoelectric coupling of the temperature, in the formation, propagation and stability of the solitary waves in cardiac media. To reach our purpose, it is convenient to rewrite FHN equations in a more tractable amplitude equation, for 1D and 2D, respectively. In so doing, we present by turns the Multiple-scale expansion technique, Analytical method with the HBM for finding solitary wave solution, hole wave solution, the discrete approximation, the MI, numerical schemes with the Finite difference method, the fourth-order Runge-Kutta method (RK4) the Pseudo Spectral method, and the Absorbing boundary conditions, respectively.

2.2 Mathematical Background and methodology

2.2.1 Soliton-like nonlinear excitation in the FitzHugh-Nagumo cardiac model

The new simple two variables FHN model for excitable media and electrical dynamics we investigate is governed by the following system of RD equations:

$$\frac{\partial u}{\partial t} = -u^5 + (a+b)u^4 + (1-ab)u^3 - (a+b)u^2 + abu - v + d_1\frac{\partial^2 u}{\partial x^2} + h_1\frac{\partial^2 v}{\partial x^2}, \tag{2.1a}$$

$$\frac{\partial v}{\partial t} = \sigma u - \sigma\gamma v + d_2\frac{\partial^2 v}{\partial x^2} - h_2\frac{\partial^2 u}{\partial x^2}. \tag{2.1b}$$

The system of equations given above is an extension of the FHN model [122], recently proposed by Zemskov et al. [17], in which a and b are the excitation thresholds that control the amplitude and the shape of the pulse ($0 < a < 1/2, -1/2 < b < 0$). The parameter ($\sigma \ll 1$), which is the ratio of the time scales and γ a free positive parameter, are taken both according to these conditions inter alia $((1-a-a^2)/3 - \sigma\gamma) > 0$, and $((1/\gamma) - (1-a-a^2)/3) > 0$. In Eq. 2.1a and Eq. 2.1b, the parameters d_1 and d_2 stand for the self-diffusion coefficients, while h_1 and h_2 represent the positive and negative cross-diffusion coefficients. The variable $u = u(x,t)$ represents the fast variable trans-membrane potential and $v = v(x,t)$ is the recharge variable ionic current. Although Eq. 2.1b does not contain any nonlinearity, the corresponding property is brought by the term $-u^5+(a+b)u^4+(1-ab)u^3-(a+b)u^2$ in Eq. 2.1a which denotes the trans-membrane ionic currents per unit area [17, 123, 124]. We rewrite Eqs. 2.1a-2.1b in a more general form from which will be used many techniques of resolution.

$$\frac{\partial u}{\partial t} = \lambda_5 u^5 + \lambda_4 u^4 + \lambda_3 u^3 + \lambda_2 u^2 + \lambda_1 u + \lambda_0 v + d_1\frac{\partial^2 u}{\partial x^2} + h_1\frac{\partial^2 v}{\partial x^2}, \tag{2.2a}$$

$$\frac{\partial v}{\partial t} = \mu_1 u + \mu_2 v + d_2\frac{\partial^2 v}{\partial x^2} - h_2\frac{\partial^2 u}{\partial x^2}. \tag{2.2b}$$

where auxiliary parameters are given by $\lambda_0 = -1$, $\lambda_1 = ab$, $\lambda_2 = -(a+b)$, $\lambda_3 = 1-ab$, $\lambda_4 = a+b$, $\lambda_5 = -1$, $\mu_1 = \sigma$, and $\mu_2 = -\sigma\gamma$.

2.2.2 The 1D diffusive FHN myocardial lattice under thermoelectric coupling

We elaborate from the modified FHN introduced in [125] an add tempereture-dependent coefficients. The generalized modified FHN obtained reads:

$$\frac{\partial u}{\partial t} = \frac{F(u,v)}{T_1} + d_1\frac{\partial^2 u}{\partial x^2} + h_1\frac{\partial^2 v}{\partial x^2}, \tag{2.3a}$$

$$\frac{\partial v}{\partial t} = \frac{G(u,v)}{T_2} + d_2\frac{\partial^2 v}{\partial x^2} - h_2\frac{\partial^2 u}{\partial x^2}. \tag{2.3b}$$

In Eqs. (2.3a)-(2.3b), the function $u = u(x,t)$ denotes the fast-variable transmembrane potential, while $v = v(x,t)$ corresponds to the slow-variable governing the excitation-recovery cycle. The terms $F(u,v)/T_1$ and $G(u,v)/T_2$ in Eqs. 1 are phenomenologically introduced to account for temperature as in Ref [126–130]. In this vein $T_1 = \tau_u^0/\eta(T)$, $(\eta(T) = \alpha[1+\beta(T-T_0)])$ describes the thermo-electric coupling between the membrane potential and the temperature of the heart. $\tau_u^0 = 2.5$, $\alpha = 1.12$ the ratio between the ionic conductance of the tissue, $\beta = 0.05853$ the rate of change of conductance with temperature and $T_0 = 37°C$ the reference temperature of the tissue [126–130]. If $T \in\ ]37.3-39]°C$, then $T_1 \in [1.99-2.10]$. Similarly, $T_2 = \tau_v^0/\phi(T)$, ($\phi(T) = [Q_{10}^{(T-T_0)/10}]$) represents the thermo-electric coupling between the recovery variable and the temperature of the heart. Here we set $\tau_v^0 = 2.5$, $Q_{10} = 3$ and $T_2 \in [2.00-2.23]$ as in [126–130]. The parameters d_1 and d_2 quantify the self-diffusion coefficients. Additionally, h_1 and h_2 represent the positive and negative cross-diffusion coefficients, respectively, which account for molecular and ionic interactions occurring across different cellular domains through gap junctions. The functions $G(u,v)$ and $F(u,v)$ are given by $G(u,v) = \mu_1 u + \mu_2 v$ and $F(u,v) = -u^5 + (a+b)u^4 + (1-ab)u^3 - (a+b)u^2 + abu - v$ as defined in [125], where the parameters a and b correspond to excitation thresholds that regulate both the amplitude and waveform of the pulse, with $0 < a < 1/2$ and $-1/2 < b < 0$. Setting $h_1 = h_2 = 0$, $\tau_u^0 = \alpha = Q_{10} = 1$, $\beta = 0$ one recovers the standard FHN model [9, 131]. The system of Eqs. (2.3a-2.3b) even in the absence of temperature and cross-diffusion terms is considered as a basic model of excitation and propagation in various active physical, chemical, and biological media [71, 126]. Knowledge of the analytical solutions remains an important task and challenge. Hence, to solve Eqs. (2.3a-2.3b), we first rewrite them in the form:

$$T_1\frac{\partial u}{\partial t} = \lambda_0 v + \lambda_1 u + \lambda_2 u^2 + \lambda_3 u^3 + \lambda_4 u^4 + \lambda_5 u^5 + d_1 T_1 \frac{\partial^2 u}{\partial x^2} + h_1 T_1 \frac{\partial^2 v}{\partial x^2}, \tag{2.4a}$$

$$T_2\frac{\partial v}{\partial t} = \mu_1 u + \mu_2 v + d_2 T_2 \frac{\partial^2 v}{\partial x^2} - h_2 T_2 \frac{\partial^2 u}{\partial x^2}. \tag{2.4b}$$

with coefficients given by $\lambda_0 = -1$, $\lambda_1 = ab$, $\lambda_2 = -(a+b)$, $\lambda_3 = 1-ab$, $\lambda_4 = a+b$, $\lambda_5 = -1$, $\mu_1 = \sigma$, $\mu_2 = -\sigma\gamma$, $a = 0.25$, $b = -0.15$, $\sigma = 0.01$, $\gamma = 3.6$.

2.2.3 The 1D diffusive FHN myocardial lattice under electromagnetic induction coupling

Within this framework, we introduce new set of independent variables of time and space following the approach outlined in [46, 125]. The generic system of RD equations is

given by:

$$\frac{\partial u}{\partial t} = -Ku(1-u^2)(u-a)(u-b) - v - k_0\cos(\phi)u + d_1\frac{\partial^2 u}{\partial x^2}, \tag{2.5a}$$

$$\frac{\partial v}{\partial t} = \epsilon_0(u - \sigma v) + d_2\frac{\partial^2 v}{\partial x^2}, \tag{2.5b}$$

$$\frac{\partial \phi}{\partial t} = k_1 u - k_2\phi. \tag{2.5c}$$

System of Eqs. 2.5a-2.5b-2.5c has been derived from FHN model [8, 9]. This system is considered as a basic model of excitation and propagation in various active physical, chemical, and biological medium [71]. To solve this problem, we plan to reduce the above system into the CQCGL equation, whose analytical solutions are well-known [136, 137]. a, b and K are constant model parameters adjusted to fit real biological situations : $K = 8.0$, $(0 < a < 1/2, -1/2 < b < 0)$. During the motion of ions amount in cells, a time varying electromagnetic can be set up. In the above stated model, k_0 represents the feedback gain which bridges the coupling and modulation on gap junction membrane potential from magnetic field. k_1 calculates the effect of electromagnetic induction induced by the transport of ions in the cell. k_2 is the degree of polarization and magnetization of the media looked as a physical parameter adjusting saturation of ϕ. ϕ represents the flux variable used to describe the effect of the electromagnetic induction. The nonlinear term $\cos(\phi) = \alpha - 3\beta\phi^2 + 5\Gamma\phi^4$, is a flux-controlled memristor and α, β and Γ are parameters of the magnetic flux-controlled memristor. The term $-k_0\cos(\phi)u$ describes the relation of modulation on membrane potential, and it is dependent on the variation in magnetic flux by generating additive faradic current.

The parameter $\epsilon_0 \ll 1$ which is the ratio of the time scales, and γ, a free positive parameter, are taken both according to the conditions inter alia $((1-a-a^2)/3 - \epsilon_0\sigma) > 0$, and $((1/\sigma) - (1-a-a^2)/3) > 0$. d_1 and d_2 are the diffusion coefficients. The variable $u = u(x,t)$ represents the fast variable trans-membrane potential, and $v = v(x,t)$ is the slow variable for current. The first equation is the finite difference discretized ordinary differential FHN equation with quadratic and quartic terms in u and no nonlinearities in v and ϕ. In Eq. 2.5a, $-u^5 + (a+b)u^4 + (1-ab)u^3 - (a+b)u^2 + abu$ [119], corresponds to a nonlinear term denoting the total trans-membrane ionic currents per unit area. To reach this aim, we derive the Eq. 2.5a of the system as a function of time without the change of generality, to obtain the Liénard form of the system above, and we get,

$$\frac{\partial^2 u}{\partial t^2} = (\lambda_0 + \lambda_1 u + \lambda_2 \phi^2 + \lambda_3 u^2 + \lambda_4 u^3 + \lambda_5 u^4 + \lambda_6 \phi^4)\frac{\partial u}{\partial t} + \alpha_0 u + \alpha_1 u^2 + \alpha_2 u\phi^2 + \alpha_3 \phi u^2 + \alpha_4 u^3 + \alpha_5 u^4 + \alpha_6 u^5 + \alpha_7 u\phi^4 + \alpha_8 u^2\phi^3 + (\beta_0 + \beta_1 u + \beta_2 \phi^2 + \beta_3 u^2 + \beta_4 u^3 + \beta_5 u^4 + \beta_6 \phi^4)\frac{\partial^2 u}{\partial x^2} + (\gamma_0 + \gamma_1 u + \gamma_2 u^2 + \gamma_3 u^3)(\frac{\partial u}{\partial x})^2 + (j_0 u\phi + j_1 u\phi^3)\phi_{xx} + (j_2 u + j_3 u\phi^2)(\frac{\partial \phi}{\partial x})^2 + (j_4\phi + j_5\phi^3)\frac{\partial u}{\partial x}\frac{\partial \phi}{\partial x} + j_6\frac{\partial^4 u}{\partial x^4} + j_7\frac{\partial^3 u}{\partial t \partial x^2}, \tag{2.6a}$$

$$\frac{\partial v}{\partial t} = \mu_1 u + \mu_2 v + d_2\frac{\partial^2 v}{\partial x^2}, \tag{2.6b}$$

$$\frac{\partial \phi}{\partial t} = k_1 u - k_2 \phi. \tag{2.6c}$$

Indeed, by perturbing λ_0 and $j_7\frac{\partial u}{\partial t \partial x^2}$ to a fourth-order perturbation parameter, i.e., $\lambda_0, j_7\frac{\partial u}{\partial t \partial x^2} \longleftarrow \epsilon^4\lambda_0$, using the semi-discrete approximation, we therefore derive analytically localized excitations propagating in the lattice of cardiac tissue model. We begin the application of this method by first transforming for better convenience, the dynamical system of Eqs. 2.6a-2.6b-2.6c into the waveform. Through the differentiation of Eq. 2.6a, we write the second-order differential equation with a small damping term ϵ that control the expansion order of the equation into a Liénard form, that is

$$\frac{\partial^2 u}{\partial t^2} = (\epsilon^4\lambda_0 + \lambda_1 u + \lambda_2 \phi^2 + \lambda_3 u^2 + \lambda_4 u^3 + \lambda_5 u^4 + \lambda_6 \phi^4)\frac{\partial u}{\partial t} + \alpha_0 u + \alpha_1 u^2 + \alpha_2 u\phi^2 + \alpha_3 \phi u^2 + \alpha_4 u^3 + \alpha_5 u^4 + \alpha_6 u^5 + \alpha_7 u\phi^4 + \alpha_8 u^2\phi^3 + (\beta_0 + \beta_1 u + \beta_2 \phi^2 + \beta_3 u^2 + \beta_4 u^3 + \beta_5 u^4 + \beta_6 \phi^4)\frac{\partial^2 u}{\partial x^2} + (\gamma_0 + \gamma_1 u + \gamma_2 u^2 + \gamma_3 u^3)(\frac{\partial u}{\partial x})^2 + (j_0 u\phi + j_1 u\phi^3)\frac{\partial^2 \phi}{\partial x^2} + (j_2 u + j_3 u\phi^2)(\frac{\partial \phi}{\partial x})^2 + (j_4\phi + j_5\phi^3)\frac{\partial u}{\partial x}\frac{\partial \phi}{\partial x} + j_6\frac{\partial^4 u}{\partial x^4} + \epsilon^4 j_7\frac{\partial^3 u}{\partial t \partial x^2}, \tag{2.7a}$$

$$\frac{\partial v}{\partial t} = \mu_1 u + \mu_2 v + d_2\frac{\partial^2 v}{\partial x^2}, \tag{2.7b}$$

$$\frac{\partial \phi}{\partial t} = k_1 u - k_2 \phi. \tag{2.7c}$$

with

$$\lambda_0 = -(abK + \alpha k_0 - \mu_2), \lambda_1 = 2(a+b)K, \lambda_2 = -3\beta k_0, \lambda_3 = -3(1-ab)K,$$
$$\lambda_4 = -4(a+b)K, \lambda_5 = 5K, \lambda_6 = -5\Gamma k_0, \alpha_0 = -\mu_1 + \mu_2 \alpha k_0 + abK\mu_2,$$
$$\alpha_1 = -(a+b)\mu_2 K, \alpha_2 = 3\beta k_0(2k_2 + \mu_2), \alpha_3 = -6\beta k_0 k_1, \alpha_4 = (1-ab)\mu_2 K,$$
$$\alpha_5 = (a+b)\mu_2 K, \alpha_6 = -\mu_2 K, \alpha_7 = 5k_0\Gamma(4k_2 + \mu_2), \alpha_8 = 20\Gamma k_0 k_1,$$

$$\beta_0 = -\mu_2 d_1 + (abK + \alpha k_0)d_2, \beta_1 = -2(a+b)Kd_2, \beta_2 = 3\beta k_0 d_2, \beta_3 = 3(1-ab)Kd_2,$$
$$\beta_4 = 4(a+b)Kd_2, \beta_5 = -5Kd_2, \beta_6 = 5\Gamma k_0 d_2, \gamma_0 = -2(a+b)Kd_2, \gamma_1 = 6(1-ab)Kd_2,$$
$$\gamma_2 = 12(a+b)Kd_2, \gamma_3 = -20Kd_2, j_0 = 12\beta k_0 d_2, j_1 = 40\Gamma k_0 d_2, j_2 = 6\beta k_0 d_2,$$
$$j_3 = 60\Gamma k_0 d_2, j_4 = 6\beta k_0 d_2, j_5 = 20\Gamma k_0 d_2, j_6 = -d_1 d_2, j_7 = d_1 + d_2,$$
$$\mu_1 = \epsilon_0, \mu_2 = -\epsilon_0\sigma, \alpha = 1.0, \beta = -1/6, \Gamma = 1/120.$$

The above dynamical equations are similar to those generally used in modeling the dynamics of atomic chain. Approximate solutions is possible by means of a perturbation technique.

Generally speaking, the described models will be used to characterize the 1D and 2D FHN myocardial lattice

2.3 Analytical methods

Analytical methods in the context of mathematics, physics, engineering, and other sciences involve the use of mathematical techniques to obtain approximate exact solutions to the problems. These methods contrast with numerical methods, which rely on approximations and computations. Analytical methods often provide closed-form expressions, allowing for a deeper understanding of the underlying mathematical structure. Here are some common analytical methods:

2.3.1 Multiple-scale expansion

The multiple-scale expansion, also known as the perturbation or asymptotic expansion, is a mathematical technique used to solve differential equations or systems of equations that involve parameters with different scales. This method is particularly valuable in problems involving fast and slow processes interacting within the system, and one wishes to study the dynamics over different time or spatial scales. Built by Bender and Nayfeh [138, 139], the multiple-scale allows to deduce simplified equations from a basic model without loosing its characteristics. The key concepts of the multiple scale expansion method are:

- In the separation of scales: The idea behind this method is to introduce multiple scales (e.g., time or spatial scales) in the problem by assuming that the solution depends on several independent variables that evolve at different rates. For example, in a temporal problem, you might introduce ($t_1 = \epsilon t$) and ($t_2 = \epsilon^2 t$), where (ϵ) is a small parameter, indicating that the solution evolves on both a fast and slow timescale.

- In the perturbative approach: The solution to the differential equation is expanded as a power series in terms of a small parameter (ϵ), which separates different orders of approximation:$[u(t) = u_0(t_1, t_2, ...) + \epsilon u_1(t_1, t_2, ...) + \epsilon^2 u_2(t_1, t_2, ...) + \cdots]$ Here, (u_0, u_1, u_2), etc., represent the solutions at different orders of approximation.
- Eliminating secular terms: During the expansion, certain terms may grow unbounded, referred to as secular terms. The goal of multiple scale expansion is to eliminate these terms to ensure that the solution remains uniformly valid over time.

In the context of reaction-diffusion (RD) systems, the multiple scale expansion method can be employed to study the formation and propagation of dissipative solitons or wavefronts. For instance, using the Complex Ginzburg-Landau equation (CGL), which is a common model for pattern formation, the method helps in deriving amplitude equations that govern the slow evolution of these patterns across multiple scales. Solutions of the modified FHN equation are looked for in the forms [140]:

$$u(x,t) = \sum_{n=1}^{\infty} \epsilon^n \sum_{\ell=-n}^{n} u_n^{(\ell)}(\xi_1, \xi_2, \tau_1, \tau_2) A^{\ell}(x,t), \tag{2.8a}$$

$$v(x,t) = \sum_{n=1}^{\infty} \epsilon^n \sum_{\ell=-n}^{n} v_n^{(\ell)}(\xi_1, \xi_2, \tau_1, \tau_2) A^{\ell}(x,t). \tag{2.8b}$$

Terms in $u_n^{(\ell)}$ and $v_n^{(\ell)}$ are given such a way that $u_n^{(-\ell)} = (u_n^{(\ell)})^*$ and $v_n^{(-\ell)} = (v_n^{(\ell)})^*$, with the star $''*''$ being the complex conjugate. The new independent variables ξ_p and τ_p, are defined as $\xi_p = \epsilon^p(x - v_g t)$, and $\tau_p = \epsilon^{2p} t$, with $p = 1, 2$, and $\epsilon \ll 1$ being the small perturbation parameter. The carrier wave $A^{\ell}(x,t) = e^{i\ell\theta(x,t)}$, where the phase $\theta = kx - \omega t$, with k and ω being its wavenumber and angular frequency, respectively [42, 141, 142].

2.3.2 Case 1

By substitution of solution Eqs. 2.8a-2.8b into Eqs. 2.1a-2.1b, we obtain at the leading order $(1, \ell)$ for $\ell = 0$, an homogeneous set of equations with non-zero determinant. Consequently, only the trivial solutions exist, so that $u_1^{(0)} = v_1^{(0)} = 0$. At the same order, for $\ell = 1$, we obtain a linear system for $u_1^{(1)}$ and $v_1^{(1)}$, yielding the following dispersion relation

$$(i\omega)^2 + (\mu_2 + \lambda_1 - (d_1 + d_2)k^2)(i\omega) + (d_1 d_2 + h_1 h_2)k^4 + (\mu_1 h_1 - \mu_2 d_1 - \lambda_1 d_2)k^2 + \lambda_1 \mu_2 = 0, \tag{2.9}$$

where the solutions $u_1^{(1)} \equiv \psi$, $v_1^{(1)} = \alpha_0 u_1^{(1)}$, $\alpha_0 = \dfrac{i\omega + \lambda_1 - d_1 k^2}{h_1 k^2} = \dfrac{-(\mu_1 + h_2 k^2)}{i\omega + \mu_2 - d_2 k^2}$ are found. It is worth noting that $u_1^{(1)}$ is an arbitrary function which will be defined later.

The order $(2, \ell)$, when $\ell = 0$, admits the solutions

$$u_2^{(0)} = \alpha_1 |\psi|^2, \; v_2^{(0)} = \alpha_2 |\psi|^2, \tag{2.10}$$

with $\alpha_1 = \dfrac{-2\lambda_2}{\lambda_1}$ and $\alpha_2 = \dfrac{-\mu_1}{\mu_2}$. The case $\ell = 1$ leads to an inhomogeneous linear system for $u_2^{(1)}$ and $v_2^{(1)}$. As the determinant of the associated homogeneous system is equal to zero due to the dispersion relation (2.9), the system will have a solution under the Fredholm solvability condition, which is satisfied for:

$$v_g = \frac{1}{(2i\omega + \mu_2 + \lambda_1 - (d_1 + d_2)k^2)} (4ik^3(d_1 d_2 + h_1 h_2) + 2k((d_1 + d_2)\omega + i(h_1\mu_1 - d_1\mu_2 - d_2\lambda_1))), \tag{2.11}$$

with v_g being the group velocity. The corresponding solutions are given by:

$$u_2^{(1)} = u_2^{(1)}, v_2^{(1)} = \alpha_0 u_2^{(1)} + \frac{(2ih_2 k - (v_g + 2id_2 k)\alpha_0)}{(i\omega\mu_2 - d_2 k^2)} \frac{\partial \psi}{\partial \xi_1}. \tag{2.12}$$

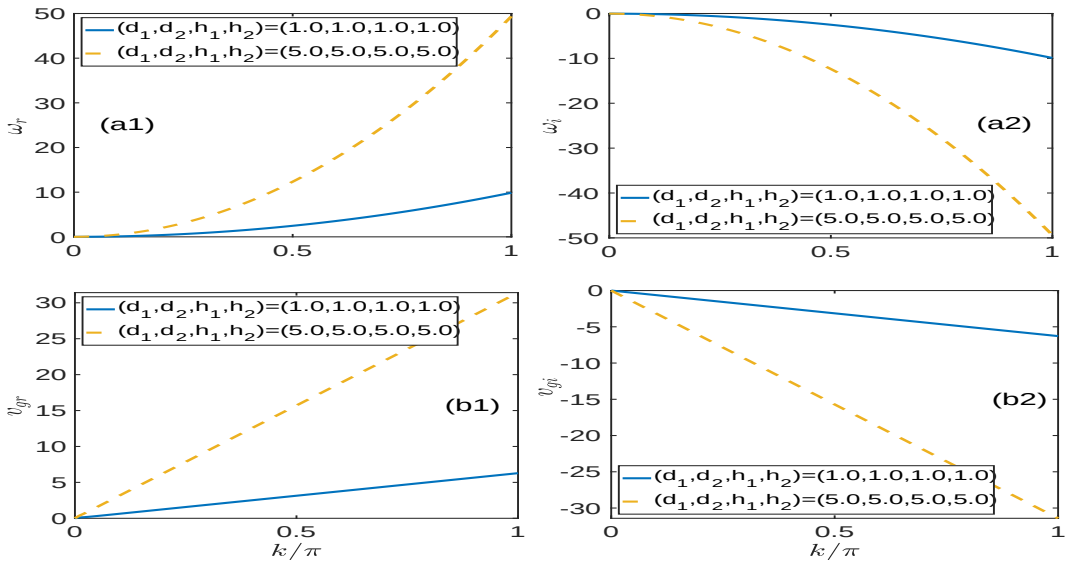

Figure 2.1: Panels $(aj)_{j=1,2}$ show plots of the real and imaginary parts of the frequency ω, while panels $(bj)_{j=1,2}$ display real and imaginary parts of the group velocity v_g versus the wavenumber k. The plots are generated by changing values of self- and cross-diffusion coefficients with $a = 0.25$, $b = -0.15$, $\gamma = 3.6$ and $\sigma = 0.01$. Real parts of ω and v_g are increasing functions of d_1, d_2, h_1 and h_2, while their imaginary components decrease when the self-and cross-diffusion coefficients are increased.

The angular frequency and the group velocity of Fig. 2.1 display the behavior of the real parts that increases with k at the same time with increasing values of d_1, d_2, h_1

and h_2. Biologically, a lower diffusion reduces the propagation speed or conductivity and local instabilities risk more exists.

For the same order, it remains to consider $\ell = 2$. For this, one obtains the solutions:

$$u_2^{(2)} = \alpha_3 \psi^2, \; v_2^{(2)} = \alpha_4 \psi^2, \tag{2.13}$$

where $\alpha_3 = -\dfrac{(2i\omega + \mu_2 - 4d_2k^2)\lambda_2}{\Delta_1}$, $\alpha_4 = \dfrac{(\mu_1 + 4h_2k^2)\lambda_2}{\Delta_1}$, $\Delta_1 = (2i\omega)^2 + (\mu_2 + \lambda_1 - 4(d_1 + d_2)k^2)(2i\omega) + 16(d_1d_2 + h_1h_2)k^4 + 4(\mu_1h_1 - \mu_2d_1 - \lambda_1d_2)k^2 + \lambda_1\mu_2$. Similarly, calculations at the order $(3,\ell)$, when $\ell = 0$, lead to the solutions

$$u_3^{(0)} = \alpha_5 \frac{\partial |\psi|^2}{\partial \xi_1}, \; v_3^{(0)} = \alpha_6 \frac{\partial |\psi|^2}{\partial \xi_1}. \tag{2.14}$$

where $\alpha_5 = -\dfrac{\alpha_0 v_g}{\lambda_1}$ and $\alpha_6 = \dfrac{(\alpha_0\mu_1 - \alpha_1\lambda_1)v_g}{\lambda_1\mu_2}$. At the same order ϵ^3, for $\ell = 1$, we obtain an inhomogeneous system of equations for $u_3^{(1)}$ and $v_3^{(1)}$. Taking into account the previous results, we therefore obtain the cubic CGL equation which reads:

$$i\frac{\partial \psi}{\partial \tau_1} + p\frac{\partial^2 \psi}{\partial \xi_1^2} + q|\psi|^2\psi = 0, \tag{2.15}$$

where

$$\begin{aligned} p = {} & \frac{1}{(2\omega - i(\mu_2 + \lambda_1 - (d_1 + d_2)k^2))}(h_1\mu_1 - (i\omega + \mu_2 - d_2k^2)d_1 - (i\omega + \lambda_1 - d_1k^2)d_2 + 6h_1h_2k^2 \\ & + 2ih_1k\alpha_0(v_g + 2id_2k) - \frac{(v_g + 2id_2k)^2(i\omega + \lambda_1 - d_1k^2)^2}{(\mu_1 + h_2k^2)h_1k^2} + 2ih_2k\frac{(v_g + 2id_2k)(i\omega + \lambda_1 - d_1k^2)}{(\mu_1 + h_2k^2)}), \\ q = {} & -\frac{(i\omega + \mu_2 - d_2k^2)(3\lambda_3 + 2\lambda_2(\alpha_1 + \alpha_3))}{(2\omega - i(\mu_2 + \lambda_1 - (d_1 + d_2)k^2))}. \end{aligned} \tag{2.16}$$

Still at the order $(3,\ell)$, for $\ell = 1$, the solutions of the obtained inhomogeneous system are given by:

$$\begin{aligned} u_3^{(1)} = {} & u_3^{(1)}, \\ v_3^{(1)} = {} & \frac{1}{(i\omega\mu_2 - d_2k^2)}\Big(-(\mu_1 + h_2k^2)u_3^{(1)} + \alpha_0\frac{\partial \psi}{\partial \tau_1} + (2ih_2k - (v_g + 2id_2k)\alpha_0)\frac{\partial \psi}{\partial \xi_2} + ((h_2 \\ & - d_2\alpha_0) - (v_g + 2id_2k)\frac{(2ih_2k - (v_g + 2id_2k)\alpha_0)}{(i\omega + \lambda_1 - d_1k^2)})\frac{\partial^2 \psi}{\partial \xi_1^2}(2ih_2k - (v_g + 2id_2k)\alpha_0)\frac{\partial u_2^{(1)}}{\partial \xi_1}\Big). \end{aligned} \tag{2.17}$$

where $u_3^{(1)}$ is an another arbitrary function. We follow up in the same order, with $\ell = 2$ and $\ell = 3$, one obtains the solutions:

$$\begin{aligned} u_3^{(2)} &= \frac{det\left(u_3^{(2)}\right)}{\Delta_1}, \\ v_3^{(2)} &= \frac{1}{(2i\omega + \mu_2 - 4d_2k^2)}(-(\mu_1 + 4h_2k^2)u_3^{(2)} + ((4ih_2k\alpha_3 - v_g + 4id_2k)\alpha_4)\frac{\partial\psi^2}{\partial\xi_1}), \end{aligned} \tag{2.18}$$

with $det\left(u_3^{(2)}\right) = (((2i\omega + \mu_2 - 4d_2k^2)\alpha_3 + 4h_1k^2\alpha_3\alpha_4)v_g + 16i\alpha_3(d_1d_2 + h_1h_2 + (h_1d_2 - h_1d_1)\alpha_4)k^3 + 4\alpha_3((2d_1 + 2h_1\alpha_4)\omega - i\mu_2(d_1 + h_1\alpha_4))k)\frac{\partial\psi^2}{\partial\xi_1}$

$$u_3^{(3)} = \alpha_7\psi^3, v_3^{(3)} = \alpha_8\psi^3, \tag{2.19}$$

where $\alpha_7 = -\frac{(3i\omega + \mu_2 - 9d_2k^2)(\lambda_3 + 2\lambda_2\alpha_3)}{\Delta_2}$ and $\alpha_8 = \frac{(\mu_1 + 9h_2k^2)\alpha_7}{\Delta_2}$, with $\Delta_2 = (3i\omega)^2 + (\mu_2 + \lambda_1 - 9(d_1 + d_2)k^2)(3i\omega) + 81(d_1d_2 + h_1h_2)k^4 + 9(\mu_1h_1 - \mu_2d_1 - \lambda_1d_2)k^2 + \lambda_1\mu_2$. At the order $(4, \ell)$, when $\ell = 0$, by neglecting the nonlinear terms of higher-order such as, $\frac{\partial u_3^{(0)}}{\partial\xi_1}$, $\frac{\partial u_2^{(0)}}{\partial\xi_2}$, $\frac{\partial u_2^{(0)}}{\partial\tau_1}$, $\frac{\partial^2 u_2^{(0)}}{\partial\xi_1^2}$ and $\frac{\partial^2 v_2^{(0)}}{\partial\xi_1^2}$. we get the following solutions

$$u_4^{(0)} = \alpha_9|\psi|^4, \; v_4^{(0)} = \alpha_{10}|\psi|^4, \tag{2.20}$$

where $\alpha_9 = -\frac{(6\lambda_4 + 3\lambda_3(2\alpha_1 + \alpha_3^* + \alpha_3) + \lambda_2(2|\alpha_3|^2 + \alpha_1^2))}{\lambda_1}$, and $\alpha_{10} = -\frac{\mu_1}{\mu_2}\alpha_9$. The order $(4, \ell)$, when $\ell = 1$, the obtained system of algebraic equations is such that, setting its determinant to zero and cancelling the higher-order nonlinearities terms like $\frac{\partial u_3^{(1)}}{\partial\xi_1}$, $\frac{\partial u_2^{(1)}}{\partial\xi_2}$ and $\frac{\partial|\psi|}{\partial\xi_1}\psi$, and yields

$$\begin{aligned} & i\frac{\partial u_2^{(1)}}{\partial\tau_1} + p\frac{\partial^2 u_2^{(0)}}{\partial\xi_1^2} = 0, \; u_4^{(1)} = u_4^{(1)}, \\ v_4^{(1)} &= \frac{1}{(i\omega + \mu_2 - d_2k^2)}(-(\mu_1 + h_2k^2)u_4^{(1)} - \alpha_0\frac{\partial u_2^{(1)}}{\partial\tau_1} + (2ih_2k - (v_g + 2id_2k)\alpha_0)\frac{\partial u_3^{(1)}}{\partial\xi_1} \\ & + (2ih_2k - (v_g + 2id_2k)\alpha_0)\frac{\partial u_2^{(1)}}{\partial\xi_2} + ((h_2 - d_2\alpha_0) \\ & - (v_g + 2id_2k)(\frac{(2ih_2k - (v_g + 2id_2k)\alpha_0)}{(i\omega + \mu_2 - d_2k^2)})\frac{\partial^2 u_2^{(1)}}{\partial\xi_2^2}). \end{aligned} \tag{2.21}$$

with $u_4^{(1)}$ another arbitrary function. Equation 2.21 looks like the heat equation which mimic the metabolic activity in the heart. In the same order, with $\ell = 2$, one gets

$$u_4^{(2)} = \alpha_{11}|\psi|^2\psi^2, v_4^{(2)} = \alpha_{12}|\psi|^2\psi^2. \tag{2.22}$$

where $\alpha_{11} = -\frac{1}{\Delta_1}((4\lambda_4 + 3\lambda_3(2\alpha_3 + \alpha_1) + \lambda_2(2\alpha_1\alpha_3 + \alpha_7))(2i\omega + \mu_2 - 4d_2k^2))$ and $\alpha_{12} = \frac{(\mu_1 + 4h_2k^2)\alpha_{11}}{(2i\omega + \mu_2 - 4d_2k^2)}$. However, for $\ell = 3$, one obtains:

$$u_4^{(3)} = \alpha_{13}\frac{\partial\psi^3}{\partial\xi_1}, v_4^{(3)} = \alpha_{14}\frac{\partial\psi^3}{\partial\xi_1}. \tag{2.23}$$

with $\alpha_{13} = det(u_4^{(3)})/(\Delta_2\frac{\partial\psi^3}{\partial\xi_1})$, $\alpha_{14} = \frac{1}{(3i\omega + \mu_2 - 9d_2k^2)}(-(\mu_1+9h_2k^2)\alpha_{13}+(6ih_2k\alpha_7-(v_g+6id_2k)\alpha_8))$, $det\left(u_4^{(3)}\right) = (((3i\omega+\mu_2-9d_2k^2)+9h_1k^2\alpha_8)v_g+54i(h_2\alpha_7-d_2\alpha_8)k^3+18\omega(d_1\alpha_7+h_1\alpha_8)k+(6id_2k^3-6i\mu_2k)(d_1\alpha_7+h_1\alpha_8))\frac{\partial\psi^3}{\partial\xi_1}$. Still at the same order, for $\ell = 4$, we get

$$u_4^{(4)} = \alpha_{15}\psi^4, v_4^{(4)} = \alpha_{16}\psi^4, \tag{2.24}$$

with $\alpha_{15} = det(u_4^{(4)})/(\Delta_3\psi^4)$, $\alpha_{16} = -\frac{(\mu_1 + 16h_2k^2)\alpha_{15}}{(4i\omega + \mu_2 - 16d_2k^2)}$, $\Delta_3 = (4i\omega)^2 + (\mu_2 + \lambda_1 - 16(d_1 + d_2)k^2)(4i\omega)+256(d_1d_2+h_1h_2)k^4+16(\mu_1h_1-\mu_2d_1-\lambda_1d_2)k^2+\lambda_1\mu_2$, and $det(u_4^{(4)}) = -(4i\omega+\mu_2-16d_2k^2)(\lambda_4+3\lambda_3\alpha_3+2\lambda_2(\alpha_3^2+\alpha_7))\psi^4$.

The order $(5,\ell)$, for $\ell = 0$, admits the solutions:

$$u_5^{(0)} = \alpha_{17}\frac{\partial|\psi|^4}{\partial\xi_1}, v_5^{(0)} = \alpha_{18}\frac{\partial|\psi|^4}{\partial\xi_1}. \tag{2.25}$$

where $\alpha_{17} = -\frac{\alpha_9 v_g}{\lambda_1}$ and $\alpha_{18} = -\frac{(\alpha_{10}v_g + \mu_1\alpha_{17})}{\mu_2}$. At the same order for $\ell = 1$, taking into account the previous results and making some simplifications, we derive the following reduced equation:

$$i\frac{\partial\psi}{\partial\tau_2} + p\frac{\partial^2\psi}{\partial\xi_2^2} + i\frac{\partial\psi}{\partial\tau_1} + p\frac{\partial^2\psi}{\partial\xi_1^2} + r|\psi|^4\psi = i\gamma\psi. \tag{2.26}$$

From Eq. 2.15, with the expression $i\frac{\partial\psi}{\partial\tau_1} + p\frac{\partial^2\psi}{\partial\xi_1^2} = -q|\psi|^2\psi$, and letting, $\xi = \xi_2$, $\tau = \tau_2$, we derive the CQCGL equation as:

$$i\frac{\partial\psi}{\partial\tau} + p\frac{\partial^2\psi}{\partial\xi^2} - q|\psi|^2\psi + r|\psi|^4\psi = i\gamma\psi, \tag{2.27}$$

where ψ, $p = p_r + ip_i$, $q = q_r + iq_i$, $r = r_r + ir_i$ denotes the complex envelope, dispersion cubic nonlinear and the quintic nonlinear coefficients, respectively. $\gamma = \gamma_r + i\gamma_i$ is the

complex dissipation coefficient, which is responsible for damping in the action potential of myocardial cells, with

$$\begin{aligned} r &= \frac{-1}{(2\omega - i(\mu_2 + \lambda_1 - (d_1+d_2)k^2))}((i\omega + \mu_2 - d_2k^2)(10\lambda_5 + 4\lambda_4(\alpha_3^* + 3(\alpha_1+\alpha_3)) \\ &\quad + 3\lambda_3(2|\alpha_3|^2 + \alpha_1^2 + \alpha_7) + 2\lambda_2(\alpha_{11} + \alpha_9 + \alpha_7))), \\ \gamma &= \frac{(\omega - i(\mu_2 + d_2k^2))\lambda_0\alpha_0}{(2\omega - i(\mu_2 + \lambda_1 - (d_1+d_2)k^2))}. \end{aligned} \tag{2.28}$$

It is important to note that the cqCCGL equation Eq. 2.27 allow to capture more intricate dynamics, offering insights into phenomena like phase transition and pattern formation. In biological contexts, it describes spatial patterns in developing tissues, the emergence of spiral waves in heart tissue, the formation of structures in biological membranes.

2.3.3 Case 2

Inserting Eqs. 2.8a-2.8b into Eqs. 2.3a-2.3b, then collecting powers of ϵ, setting coefficients of each power of ϵ to zero, and considering different harmonics related to ℓ, we obtain at the leading order $(1,\ell)$, for $\ell = 0$, $u_1^{(0)} = v_1^{(0)} = 0$. At the same order, but for $\ell = 1$, we obtain a linear system for $u_1^{(1)}$ and $v_1^{(1)}$, from which, we retrieve the following dispersion relation:

$$\begin{aligned} &(i\omega)^2 T_1T_2 + (\mu_2T_1 + \lambda_1T_2 - (d_1+d_2)k^2T_1T_2)(i\omega) + (d_1d_2 + h_1h_2)k^4T_1T_2 + ((\mu_1h_1 \\ &- \mu_2d_1)T_1 - \lambda_1d_2T_2)k^2 + \lambda_1\mu_2 = 0. \end{aligned} \tag{2.29}$$

This allows the determination of the group velocity, from the Fredholm solvability condition, leading to:

$$\begin{aligned} v_g = &\frac{1}{(2i\omega T_1T_2 + \mu_2T_1 + \lambda_1T_2 - (d_1+d_2)k^2T_1T_2)} \times (4ik^3(d_1d_2 + h_1h_2)T_1T_2 \\ &+ 2k((d_1+d_2)T_1T_2\omega + i((h_1\mu_1 - d_1\mu_2)T_1 - d_2T_2\lambda_1))). \end{aligned} \tag{2.30}$$

Fig. 2.2 illustrates the behavior of the real parts of $(a1)$ $w(k) = w_r(k)$ and $(b1)$ $v_g(k) = v_{g_r}(k)$, for different values of T_1. While $w_r(k)$ increases with increasing values of k and T_1, $v_{g_r}(k)$ also increases with k, but decreases with increasing values of T_1. The influence of T_2 on $w_r(k)$ $(a2)$ and v_{g_r} $(b2)$ presents similar behaviors as for T_1. From a biological standpoint, variations in thermal coupling induce fluctuations in ionic transport, ultimately influencing the collective electrical activity near the cell membrane. To be precise, a lower temperature degrades the effectiveness of the electrical wave propagation in the heart.

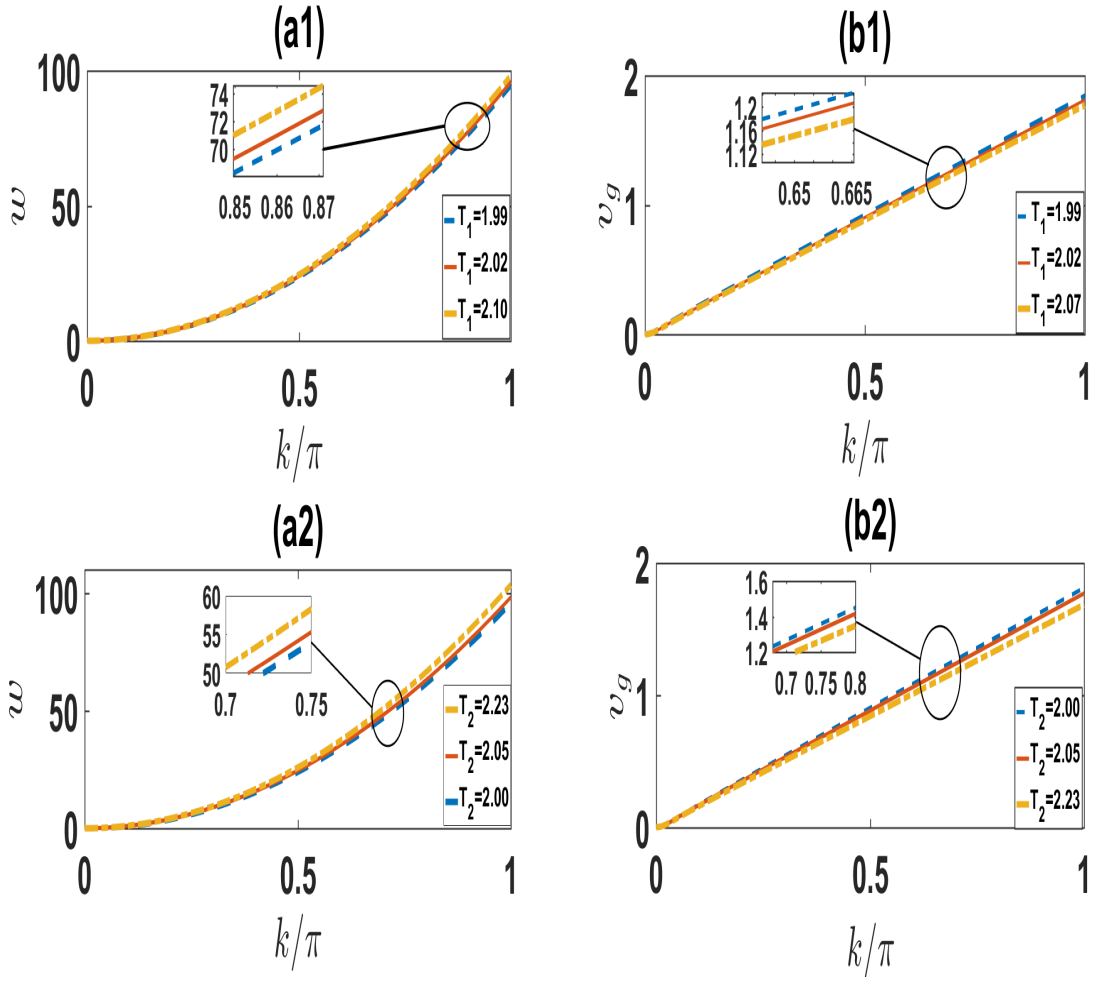

Figure 2.2: (Color online) Dispersion relation: ($a1$) $T_2 = 2.05$ and ($a2$) $T_1 = 2.02$. Group velocity: ($b1$) $T_2 = 2.05$ and ($b2$) $T_1 = 2.02$. The other parameters are $d_1 = d_2 = h_1 = h_2 = 2.1$, $k = 0.018\pi$, $a = 0.25$, $b = -0.15$, $\gamma = 3.6$ and $\sigma = 0.01$.

Solving then the system for $u_3^{(1)}$ and $v_3^{(1)}$, the unknown function$u_3^{(1)} \equiv \psi(\varphi, \tau)$ cancels out, and the system eventually reduces to CCGL equation:

$$i\frac{\partial \psi}{\partial \tau_1} + P\frac{\partial^2 \psi}{\partial \xi_1^2} + Q|\psi|^2\psi = 0, \tag{2.31}$$

with

$$P = \frac{1}{(2\omega T_1 T_2 - i(\mu_2 T_1 + \lambda_1 T_2 - (d_1 + d_2)T_1 T_2 k^2))}(h_1\mu_1 T_1 - (i\omega T_2 + \mu_2 - d_2 T_2 k^2)T_1 d_1$$
$$-(i\omega T_1 + \lambda_1 - d_1 T_1 k^2)T_2 d_2 + 6h_1 h_2 T_1 T_2 k^2 + 2ih_1 T_1 T_2 k\alpha_0(v_g + 2id_2 k)$$

$$- T_2^2\left(\frac{(v_g+2id_2k)^2(i\omega T_1+\lambda_1-d_1T_1k^2)^2}{(\mu_1+h_2T_2k^2)h_1k^2T_1}\right)+2ih_2T_2^2\left(\frac{(v_g+2id_2k)(i\omega T_1+\lambda_1-d_1T_1k^2)}{(\mu_1+h_2T_2k^2)}\right),$$

$$Q=-\frac{(i\omega T_2+\mu_2-d_2T_2k^2)(3\lambda_3+2\lambda_2(\alpha_1+\alpha_3))}{(2\omega T_1T_2-i(\mu_2T_1+\lambda_1T_2-(d_1+d_2)T_1T_2k^2))}. \tag{2.32}$$

At the order $(4,\ell)$, when $\ell=1$, the obtained system of algebraic equations is such that setting its determinant to zero, cancels the following higher-order nonlinearities terms $\frac{\partial u_3^{(1)}}{\partial\xi_1}$, $\frac{\partial u_2^{(1)}}{\partial\xi_2}$ and $\frac{\partial|\psi|}{\partial\xi_1}\psi$, one retrieves:

$$i\frac{\partial u_2^{(1)}}{\partial\tau_1}+P\frac{\partial^2u_2^{(1)}}{\partial\xi_1^2}=0, \tag{2.33}$$

At the order, $(5,\ell)$, when $\ell=1$, we obtain an inhomogeneous system for $u_5^{(1)}$ and $v_5^{(1)}$. Thus, taking into account the previous results and making some simplifications, we derive the following reduced equation.

$$i\frac{\partial\psi}{\partial\tau_2}+P\frac{\partial^2\psi}{\partial\xi_2^2}+i\frac{\partial\psi}{\partial\tau_1}+P\frac{\partial^2\psi}{\partial\xi_1^2}+R|\psi|^4\psi=i\gamma\psi. \tag{2.34}$$

From Eq. 2.31, with the expression $i\frac{\partial\psi}{\partial\tau_1}+P\frac{\partial^2\psi}{\partial\xi_1^2}=-Q|\psi|^2\psi$, and by setting $\xi=\xi_2$ $\tau=\tau_2$, we derive the following CQCGL equation:

$$i\frac{\partial\psi}{\partial\tau}+P\frac{\partial^2\psi}{\partial\xi^2}-Q|\psi|^2\psi+R|\psi|^4\psi=i\gamma\psi. \tag{2.35}$$

With $P=P_r+iP_i$, $Q=Q_r+iQ_i$, $R=R_r+iR_i$, the complex dispersion, cubic nonlinear and quintic nonlinear coefficients, respectively, while $\gamma=\gamma_r+i\gamma_i$ is the complex dissipation coefficient which is responsible for damping in the action potential of myocardial cells. While P and Q are given in Eq. 2.31, the explicit expressions for the other coefficients are

$$\begin{aligned}R&=\frac{-1}{(2\omega T_1T_2-i(\mu_2T_1+\lambda_1T_2-(d_1+d_2)T_1T_2k^2))}\times((i\omega T_2+\mu_2-d_2T_2k^2)\\&\times(10\lambda_5+4\lambda_4(\alpha_3^*+3(\alpha_1+\alpha_3))+3\lambda_3(2|\alpha_3|^2+\alpha_1^2+\alpha_7)+2\lambda_2(\alpha_{11}+\alpha_9+\alpha_7))),\\\gamma&=\frac{(\omega T_2-i(\mu_2+d_2T_2k^2))\lambda_0\alpha_0}{(2\omega T_1T_2-i(\mu_2T_1+\lambda_1T_2-(d_1+d_2)T_1T_2k^2))}.\end{aligned} \tag{2.36}$$

Eq. 2.35 is a well known model for boundary value problems. It has been reported in other biophysical settings such as in calcium and cardiac wave propagation [157]

2.3.4 Case 3

The tree-variables model of FHN equation Eqs. (2.37a)-(2.37b)-(2.37c) detects essence of electrical activity and memory effect, holding more bifurcation parameters and can reproduce similar dynamical behaviors like the original FHN model. The general solution of such equations, according to the multiple scale expansion, is given by

$$u(x,t) = \sum_{n=1}^{\infty} \epsilon^n \sum_{\ell=-n}^{n} u_n^{(\ell)}(\xi_1,\xi_2,\tau_1,\tau_2) A^{\ell}(x,t), \tag{2.37a}$$

$$v(x,t) = \sum_{n=1}^{\infty} \epsilon^n \sum_{\ell=-n}^{n} v_n^{(\ell)}(\xi_1,\xi_2,\tau_1,\tau_2) A^{\ell}(x,t), \tag{2.37b}$$

$$\phi(x,t) = \sum_{n=1}^{\infty} \epsilon^n \sum_{\ell=-n}^{n} \phi_n^{(\ell)}(\xi_1,\xi_2,\tau_1,\tau_2) A^{\ell}(x,t). \tag{2.37c}$$

For the leading order $(1,\ell)$, for $\ell = 0$, yields an homogeneous set of equations with non-zero determinant. Consequently, only the trivial solutions exist, so that $u_1^{(0)} = v_1^{(0)} = \phi_1^{(0)} = 0$. At the same order, for $\ell = 1$, we obtain a linear system for $u_1^{(1)}$, $v_1^{(1)}$ and $\phi_1^{(1)}$, yielding the following dispersion relation:

$$\omega^2 + \alpha_0 + j_6 k^4 - \beta_0 q^2 = 0. \tag{2.38}$$

At the order $(2,\ell)$, for the case $\ell = 1$, leads to an inhomogeneous linear system for $u_2^{(1)}$, $v_2^{(1)}$ and $\phi_2^{(1)}$, and the system will have a solution from the Fredholm solvability condition, which is satisfied by the group velocity

$$v_g = \frac{k\beta_0 - 2k^3 j_6}{\omega}. \tag{2.39}$$

where v_g refers to the group velocity.

Notably, both the dispersion relation w and group velocity v_g are real-valued and are depicted as functions of the wavenumber k. Figure 2.3 displays the behavior of $w(k)$ and the group velocity $v_g(k)$, both of which increase with the wavenumber k and with higher values of electromagnetic induction, as modulated by the feedback gain k_0. From a biological point of view, this suggests that fluctuations in k_0 may initiate the destabilization of wave propagation, impair cardiac contraction, and alter the sensitivity of the cell membrane thereby reinforcing the significant role of electromagnetic induction in this context.

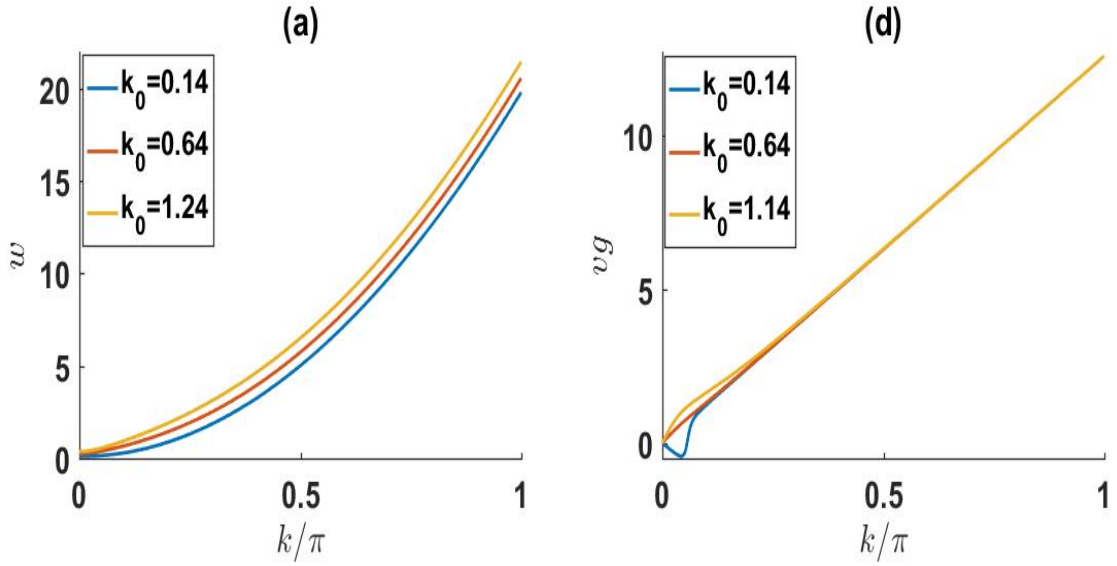

Figure 2.3: Dispersion relation in (a) and Group velocity (b) versus the wave number of the plane wave for $k_0 = 0.14, 0.64, 1.24$. The other parameters are a = 0.25, b = -0.15, $\gamma = 3.6$, $\epsilon_0 = 0.01$, $d_1 = 2.0$, $d_2 = 2.0$, K = 8.0, $\alpha = 1.0$, $\beta = -1/6$, $\Gamma = 1/120$, $k_1 = 0.5$, $k_2 = 1.0$. $d_1 = d_2 = 2.0$.

At the order $(3,\ell)$, with $\ell = 1$, we obtain a nonlinear equation in which the terms in $u_3^{(1)}$ on the one hand, and the derivatives $\frac{\partial u_2^{(1)}}{\partial n_1}$ and $\frac{\partial u_1^{(1)}}{\partial n_2}$ on the other hand, cancel out due to the dispersion relation and the Fredholm solvability condition, respectively. Hence, the leading cubic CGL equation reads:

$$i\frac{\partial \psi}{\partial \tau_1} + p\frac{\partial \psi}{\partial n_1^2} + q|\psi|^2\psi = 0. \tag{2.40}$$

where,

$$\begin{aligned} p &= -\frac{\left(v_g^2 - \beta_0 + 6k^2 j_6\right)}{2\omega}, \\ q &= -\frac{1}{2\omega}(i\omega\left(\lambda_1(r_2+r_5) + \lambda_2(r_1^2+r_4) + \lambda_3(1+r_2)\right) - 2\alpha_1(r_2+r_5) - 2\alpha_2|r_1|^2 - \alpha_3(2r_1+r_1^*) \\ &\quad - 3\alpha_4 + k^2(\beta_1(r_2+5r_5) + \beta_2(r_1^2+2|r_1|^2) + 3\beta_3 + \gamma_1 - j_0 r_1^2 + j_2 r_1^2 + j_4(r_1^2+2|r_1|^2))). \end{aligned} \tag{2.41}$$

At the order $(4,\ell)$, when $(\ell = 1)$, the obtained system of algebraic equations is such that setting its determinant to zero cancels the higher-order nonlinear terms such that $u_4^{(1)}$, $\frac{\partial u_2^{(1)}}{\partial n_2}$ and $\frac{\partial u_3^{(1)}}{\partial n_1}$ are canceled due to the dispersion relation and the group velocity, respectively, and we obtain

$$i\frac{\partial u_1^{(2)}}{\partial \tau_1} + p\frac{\partial u_1^{(3)}}{\partial^2 n_1} = 0. \tag{2.42}$$

At the final order $(5,\ell)$, with $\ell = 1$, we obtain an inhomogeneous system in $u_5^{(1)}$, $v_5^{(1)}$ and $\phi_5^{(1)}$. Terms with derivatives in $\left(u_4^{(1)}\right)_{n_1}$ and $\left(u_3^{(1)}\right)_{n_2}$ will be canceled due to the Fredholm solvability condition on the one hand and term in $u_5^{(1)}$ due to the dispersion relation on the other hand. Thus, taking into account previous results, and making some simplifications, the following reduced equation is derived:

$$i\frac{\partial\psi}{\partial\tau_2} + p\frac{\partial^2\psi}{\partial n_2^2} + i\frac{\partial\psi}{\partial\tau_1} + p\frac{\partial^2\psi}{\partial n_1^2} + r|\psi|^4\psi = i\gamma\psi. \tag{2.43}$$

From Eq. 2.40, with the expression $i\frac{\partial\psi}{\partial\tau_1} + p\frac{\partial^2\psi}{\partial n_1^2} = -q|\psi|^2\psi$, and by letting $n = n_2$ and $\tau = \tau_2$, we derive the CQCGL equation:

$$i\frac{\partial\psi}{\partial\tau} + p\frac{\partial^2\psi}{\partial n^2} + q|\psi|^2\psi + r|\psi|^4\psi = i\gamma\psi. \tag{2.44}$$

The parameter γ denotes the real dissipation coefficient, while $r = r_r + ir_i$ corresponds to the complex quintic nonlinear complex coefficient, with r_r the real part and r_i the imaginary one. Additionally, $s_i = (1,...28)$ and $s_i^* = (1,...7)$ represent real and complex coefficients, with the specific expressions of r and γ available in **Appendix (A)**. It is worth emphasizing that Eq. 2.44 and its modified forms have been widely explored in many scientific discipline. This equation has valuable characteristics in numerous physical and biological phenomena, notably in excitability and contractility in cardiac tissue and nonlinear transmission in neural networks [9]. Furthermore, it finds applications in plasma physics [143], fluid mechanics [144], nonlinear optics [145], and Bose-Einstein condensates in three-body interactions [146]. From a biological standpoint, the quintic term allows the equation to capture the realistic correction of saturation effects and nonlinear damping, which are essential for accurately modeling wave stability of ionic channels in the heart. This can correspond to reentrant waves, fibrillation, or alternans. The cqCGL equation thus serves as an essential tool for obtaining exact analytical solutions and conducting modulational instability analysis, offering a deeper understanding of nonlinear wave phenomena in excitable systems.

All these coefficients are expressed by this relation below

$$\begin{aligned} r = -\frac{1}{2\omega}(&i\omega(\lambda_1(r_5^*r_{14} + r_{17}) + \lambda_2(3r_{19} - 2r_1^3 + r_1^*(4r_4r_5 + 3r_1^*r_{14}) + 4r_1r_5r_7^*) \\ &+ \lambda_3(2 + 2r_2r_5 + 2|r_5|^2 + r_{14} + 3r_{17}) + \lambda_4(3r_2(1 + r_5) + 3r_5 + r_5^* + 3r_{17}) \\ &+ \lambda_5(2 + 6r_2 + r_{17}) + \lambda_6(6|r_1|^4 + r_{19} + 12r_4|r_1|^2 - 6r_1r_4 - 4r_1|r_1|^2)) - (2\alpha_1(r_5^*r_{14} + r_{17} + r_{20}) \end{aligned}$$

$$
\begin{aligned}
&+2\alpha_2(r_1 r_5^* r_7 + r_1^*(r_{16} + r_2 r_7)) + 2\alpha_3(r_1^*(r_{14} + r_2 r_5) + r_1|r_5|^2 + r_2 r_4 + r_4 r_5 + r_5 r_7^*) \\
&+3\alpha_4(2r_2 r_5 + 2|r_5|^2 + r_{14}) + 4\alpha_5(3r_2 r_5 + r_5^* + 3r_{17} + 3r_2) + 10\alpha_6 \\
&+\alpha_7(r_{19} + 4r_1^2|r_1|^2 + 12r_4|r_1|^2 + 6|r_1|^4 + 6r_4 r_1^2) + 6\alpha_8 r_1|r_1|^2) \\
&+k^2(\beta_1(13r_5^* r_{14} + 5r_{20} + r_{17}) + \beta_2(2r_1^* r_{16} + 2r_4 r_7 + 2|r_7|^2 - 3r_{19}) \\
&+\beta_3(2r_2 r_5 + 10|r_5|^2 + 2r_{14} + 3r_{17}) + \beta_4(9r_2 + 7r_5^* + 9r_5) - 5\beta_5 \\
&+\beta_6(4r_1^2|r_1|^2 + 12r_4|r_1|^2 + r_{19} + 6|r_1|^4 + r_4 r_1^2) - \gamma_1(4r_2 r_5 + 8|r_5|^2 \\
&-5r_{14}) - 2\gamma_2(2r_2 + 2r_5^* + 5r_5) - 5\gamma_3 - j_0(2r_1^3 + 2r_1 r_5 r_7^* + r_1^*(2r_4 r_5 + 2r_{16} + 3r_1^* r_{14}) \\
&+2r_4 r_7 + 6r_1 r_5^* r_7) + j_1(3|r_1|^4 + 2r_1^2|r_1|^2) + j_2(r_1^*)^2 r_{14} - 3j_3|r_1|^4 + j_4(r_1(5r_5^* r_7 + r_2 r_4 + 5r_5 r_7^*) \\
&+r_1^*(10r_{16} + r_4 r_5 + 5r_2 r_7) + 4r_4 r_7 + 2r_1^3 + (r_1^*)^2 r_{14} + 8|r_7|^2) + j_5(3|r_1|^4 + 4|r_1|^2 r_1^2))), \\
\gamma = &\frac{(\lambda_0 - k^2 j_7)}{2}.
\end{aligned}
\tag{2.45}
$$

This equation highlights the qualitative and quantitative character of various physical and biological phenomena, particularly in excitability and contractility in cardiac tissue and neural network. The multiple scale expansion method is indispensable for handling complex, nonlinear systems where interactions across different scales need to be understood in a controlled, approximate manner.

2.3.5 Hirota Bilinear Method (HBM)

In 1971, Ryogo Hirota unveiled a novel ”direct method” for the development of multisoliton solutions to integrable nonlinear evolution equations. The core concept of this method was to implement a transformation into new variables. This transformation allowed for multisoliton solutions to be represented in a notably straightforward manner within these new variables. All derivatives emerged as Hirota's bilinear derivatives, a term now recognized as the ”Hirota Bilinear form”. HBM is a mathematical technique utilized in the exploration of integrable systems. It is particularly effective in the context of soliton equations. The primary advantage of Hirota's method over other methods is its algebraic nature. The first step of this method is to make suitable transformations of nonlinear partial differential and difference equations which provide that the equations are in quadratic form in dependent variables. This new form is called bilinear form. We introduce a special differential operator called Hirota Operator in the CQCGLE, which is used to write the bilinear form of the equation as a polynomial of D-operator which we call the Hirota bilinear form. Let S : $C_n \longrightarrow$ C be a space of differentiable functions. Then; the Hirota D-operator D : $S \times S \longrightarrow$ S is defined asM

$$
\begin{aligned}
D^m_{n,\xi}(g\cdot f) &= (\frac{\partial}{\partial\xi} - n\frac{\partial}{\partial\xi'})^m g(\xi,\tau)\times f(\xi',\tau')_{|_{\xi=\xi',\tau=\tau'}},\\
D^m_{n,\xi}D^{m'}_{n,\tau}(g\cdot f) &= (\frac{\partial}{\partial\xi} - n\frac{\partial}{\partial\xi'})^m(\frac{\partial}{\partial\tau} - n\frac{\partial}{\partial\tau'})^{m'} g(\xi,\tau)\times f(\xi',\tau')_{|_{\xi=\xi',\tau=\tau'}}:
\end{aligned}
\tag{2.46}
$$

were $m = m' = 0,1,2,3,...$ are positive integers and ξ, τ, ... are independent variables which was introduced in [135] and applied by Nozaki and Bekki [116, 119, 121, 136].

Accordingly, the constitutive derivatives, in terms of Hirota's operator, can be written as

$$
\begin{aligned}
D_{n,\tau}(g\cdot f) &= \left[\left(\frac{\partial}{\partial\tau} - n\frac{\partial}{\partial\tau'}\right) g(\xi,\tau)f(\xi',\tau')\right]_{\xi=\xi',\tau=\tau'},\\
D^2_{n,\xi}(g\cdot f) &= \left[\left(\frac{\partial}{\partial\xi} - n\frac{\partial}{\partial\xi'}\right)^2 g(\xi,\tau)f(\xi',\tau')\right]_{\xi=\xi',\tau=\tau'},\\
D^2_{\xi}(f\cdot f) &= \left[\left(\frac{\partial}{\partial\xi} - n\frac{\partial}{\partial\xi'}\right) f(\xi,\tau)f(\xi',\tau')\right]_{\xi=\xi',\tau=\tau'}.\\
D^n_x D^m_t(f\cdot g) &= \left(\frac{\partial}{\partial x} - \frac{\partial}{\partial x'}\right)^n \left(\frac{\partial}{\partial t} - \frac{\partial}{\partial t'}\right)^m f(x,t)g(x',t')\Big|_{x=x',t=t'}.
\end{aligned}
\tag{2.47}
$$

We take exemple on the Modified KdV (MKdV) equation, well-known as a nonlinear partial differential equation given as:

$$
\frac{\partial u}{\partial t} + 6u^2\frac{\partial u}{\partial x} + \frac{\partial^3 u}{\partial x^3} = 0. \tag{2.48}
$$

This equation describes the evolution of solitary waves (or solitons) and is a well-known equation in fluid dynamics and nonlinear wave theory. The goal of Hirota's method is to transform this nonlinear equation into a simpler bilinear form as:

$$
u(x,t) = 2\frac{\partial}{\partial x}\log(f(x,t)) \tag{2.49}
$$

where $f(x,t)$ is a new function used to linearize the equation. We rewrite the mKdV equation and the substitution results in the following equation for $f(x,t)$ are:

$$
(D_tD_x + D^4_x)(f\cdot f) = 0 \tag{2.50}
$$

We now use a trial solution for $f(x,t)$ to simplify the equation. For a one-soliton solution, assume the following trial function: $f(x,t) = 1 + e^{\theta}$ where $\theta = kx - \omega t$, with k being the wave number and ω the frequency. Now, we apply the bilinear differential operatorsD_t and D_x to the trial solution by substituting $f = 1 + e^{kx-\omega t}$, we compute:

$$
(D_tD_x + D^4_x)(f\cdot f) \quad = (-\omega k + k^4)e^{kx-\omega t} = 0 \tag{2.51}
$$

For this equation to hold, the coefficient of $e^{kx-\omega t}$ must be zero, giving us the dispersion relation: $-\omega k + k^4 = 0$. For the one-soliton solution is:

$$u(x,t) = 2\frac{\partial_x f}{f} = 2k\,\mathrm{sech}(kx - k^3 t) \tag{2.52}$$

This represents a one-soliton solution for the mKdV equation, where sech denotes the hyperbolic secant function, which gives the shape of the soliton wave. The HBM has been applied successfully to many integrable equations, including the NLS and the Sine-Gordon equation.

We take another exemple on the Nonlinear Schrödinger (NLS) equation, let's go step-by-step. The NLS equation is a key model for describing solitons in various fields like optics, plasma physics, and fluid dynamics. Its simplest form is:

$$i\frac{\partial \psi}{\partial t} + \frac{\partial \psi}{\partial x^2} + 2|\psi|^2\psi = 0 \tag{2.53}$$

where $\psi(x,t)$ is a complex-valued wave function, and the terms describe the evolution of nonlinear waves, such as optical pulses in fibers. We first rewrite the NLS equation using a dependent variable transformation. We introduce a transformation of the form: $\psi(x,t) = \frac{g(x,t)}{f(x,t)}$, where $g(x,t)$ and $f(x,t)$ are new complex functions with g^* and f^* the complex conjugate of g and f, that will help linearize the equation through bilinear operators. We substitute $\psi(x,t) = \frac{g}{f}$ into the NLS equation to obtain the bilinear form after some algebraic manipulation as:

$$(D_t + D_x^2)(g \cdot f) = 0, \tag{2.54}$$

$$D_x^2(f \cdot f) = 2(g \cdot g^*). \tag{2.55}$$

where D_x and D_t are Hirota's bilinear operators, defined above. For a one-soliton solution, we assume the following trial functions for $g(x,t)$ and $f(x,t)$ such as $g(x,t) = e^{\theta}$ and $f(x,t) = 1 + e^{\theta+\theta^*}$, where $\theta = kx - \omega t + \delta$, θ^* is the complex conjugate, and k, ω, and δ are constants. As application, on this equation, $(D_t + D_x^2)(g \cdot f)$, we first compute: $D_t(g \cdot f) = \frac{\partial g}{\partial t} f - g\frac{\partial f}{\partial t}$. We proceed in the same manner with $D_x^2(f \cdot f) = 2(g \cdot g^*)$. Substituting the trial solutions for $g(x,t)$ and $f(x,t)$, we calculate the operator terms. The time derivative of (g) gives: $\frac{\partial g}{\partial t} = -\omega e^{\theta}$. Similarly, applying (D_x^2) to the trial function gives: $D_x^2(g \cdot f) = k^2 e^{\theta}$. Substituting the computed terms into the bilinear form, we get:

$$(-\omega + k^2)e^{\theta} = 0. \tag{2.56}$$

For this to hold, the coefficient must vanish, which gives the dispersion relation: $\omega = k^2$. The trial functions now yield a one-soliton solution for the NLS equation. Substituting

$\omega = k^2$ back into the solution, we obtain the one-soliton solution:

$$\psi(x,t) = \frac{e^{kx - ik^2 t + \delta}}{1 + e^{2kx}}, \tag{2.57}$$

This describes a localized wave packet (soliton) that maintains its shape and travels at a constant velocity, a characteristic feature of solitons in nonlinear systems. To obtain a multi-soliton solution, we extend the trial function for $f(x,t)$ and $g(x,t)$ by including more exponential terms. For a two-soliton solution, for example: $g(x,t) = e^{\theta_1} + e^{\theta_2}$ and $f(x,t) = 1 + e^{\theta_1+\theta_1^*} + e^{\theta_2+\theta_2^*} + Ae^{\theta_1+\theta_2}$, where A is a constant that takes into account the interaction between the two solitons. The corresponding multi-soliton solutions can be found similarly by applying the bilinear operators and solving for the constants.

In summary the steps for solving equations via the Hirota's methods are :

- Transform the original equation using a dependent variable transformation $\psi(x,t) = \frac{g(x,t)}{f(x,t)}$.
- Rewrite the equation in terms of bilinear operators $(D_t + D_x^2)(g \cdot f) = 0$.
- Assume a trial solution for $g(x,t)$ and $f(x,t)$, typically using exponential functions.
- Apply the bilinear operators to the trial functions.
- Solve the dispersion relation and obtain the soliton solution.
- Extend the trial functions to find multi-soliton solutions.

This process simplifies solving complex nonlinear equations like the NLS using Hirota's method, making it a powerful tool in soliton theory.

2.3.6 Modulational Instability Phenomenon

Modulational instability, also known as the Benjamin-Feir instability, refers to a phenomenon in which a stable continuous wave or periodic solution of a nonlinear partial differential equation PDE becomes unstable under the influence of small perturbations. In other words, it is a nonlinear effect that leads to the evolution or growth of larger-scale perturbations beyond the linear regime on a stable solution, often resulting in the emergence of modulated patterns in the system. The process has been addressed, under different contexts, in a broad range of physical systems, including biophysics [144, 177] to nonlinear optics [117, 158], through electrical transmission line [147], plasma systems [169, 170] and Bose-Einstein condensates [148, 149]. When studying the NLSE with perturbations in amplitude, we are particularly interested in understanding how

small amplitude variations can lead to the exponential growth of certain modes and the development of complex wave patterns.

2.3.6.1 Case 1 : Perturbation in amplitude

The standard form of the NLSE is given by:

$$\frac{\partial \psi}{\partial \tau} + \frac{1}{2}\frac{\partial \psi}{\partial x^2} + |\psi|^2 \psi = 0. \tag{2.58}$$

where $\psi(x,t)$ represents the complex envelope of the wave field. This equation describes the evolution of slowly varying packets of quasi-monochromatic waves in weakly nonlinear dispersive media. To analyze MI, we consider a plane wave solution of the NLSE:

$$\psi(x,t) = \psi_0 e^{i(kx-\omega t)}. \tag{2.59}$$

with k and ω corresponding to the wavenumber and angular frequency of the unperturbed plane wave, that are related by the equation:

$$\omega = -\frac{1}{2}k^2 + \psi_0^2. \tag{2.60}$$

To examine the stability of the plane wave solution, we modulate it with a small perturbation as:

$$\psi(x,t) = \left(\psi_0 + \delta\psi\right) e^{i(kx-\omega t)}. \tag{2.61}$$

where $\delta\psi$ accounts for the perturbation and its amplitude is supposed to be small in comparison to the plane wave amplitude ψ_0. Inserting the perturbed solution into Eq. 2.58, and linearizing the equation around ψ_0, we obtain the following equation for the perturbation field:

$$\delta\frac{\partial \psi}{\partial \tau} + \frac{1}{2}\delta\frac{\partial \psi}{\partial x^2} + 2\psi_0^2\delta\psi + \psi_0^2\delta\psi^* = 0. \tag{2.62}$$

A solution to the above equation can be taken in the form:

$$\delta\psi = \delta\psi_1 e^{i(\Gamma x-\Omega t)} + \delta\psi_2^* e^{-i(\Gamma x-\Omega^* t)}, \tag{2.63}$$

with Γ and Ω being the wavenumber and the angular frequency of the perturbation, respectively. Making use of this in the perturbation Eq. 2.63, one obtains the following homogeneous system for $\delta\psi_1$ and $\delta\psi_2$:

$$\delta\psi_1 = \psi_a e^{i(\Gamma x+\Omega_1 t)} + \psi_b e^{-i(\Gamma x-\Omega_1 t)}, \quad \delta\psi_1^* = \psi_a e^{-i(\Gamma x-\Omega_1 t)} + \psi_b e^{i(\Gamma x+\Omega_1 t)}. \tag{2.64}$$

Making use of the above equations, we get the system :

$$\begin{aligned}(-i\Omega_1 + c_{11})\psi_a + c_{12}\psi_b = 0,\\ c_{21}\psi_a + (i\Omega_2 + c_{22})\psi_2 = 0.\end{aligned} \tag{2.65}$$

where

$$\begin{aligned}c_{11} = -\frac{1}{2}\Gamma^2 - \frac{1}{2}k^2 + 3\psi_0^2, \qquad c_{12} = i\Gamma k + \omega_0,\\ c_{21} = \omega_0 - i\Gamma k, \qquad c_{22} = -\frac{1}{2}\Gamma^2 - \frac{1}{2}k^2 + 3\psi_0^2.\end{aligned} \tag{2.66}$$

The system above will admit non-trivial solutions under the condition that its determinant equal to zero, which allows obtaining the nonlinear dispersion relation:

$$\Omega^2 + A\Omega + B = 0, \tag{2.67}$$

where $A = -i(\Gamma^2 + k^2 - 6\psi_0^2)$ and $B = -(\frac{1}{4}\Gamma^4 - \frac{1}{2}\Gamma^2 k^2 - 3\Gamma^2\psi_0^2 + 9\psi_0^4 + \frac{1}{4}k^4 - 3k^2\psi_0^2 - w_0^2)$.

In summary, modulational instability phenomenon in the context of the NLSE with amplitude perturbations is a rich area of study, offering insights into the fundamental processes governing the formation and evolution of localized wave structures in nonlinear dispersive media.

2.4 Numerical Schemes

2.4.1 Finite difference method

The finite difference method is a numerical technique commonly used for solving partial differential equations (PDEs) and ordinary differential equations (ODEs). It discretizes the spatial domain into a grid and approximates derivatives with finite difference approximations. This method is widely applied in various fields, including physics, engineering, finance, and environmental modeling. Here are the key concepts and steps involved in the finite difference method:

- Problem Formulation: Begin with the given (PDE) or (ODE), along with appropriate initial or boundary conditions.
- Grid Discretization: Discretize the spatial domain by dividing it into a grid. For one spatial dimension, this involves defining a set of points; for two or three dimensions, a grid of points is used. The spacing between these points is called the grid spacing (∇x).

- Discretization of Derivatives: Replace spatial and temporal derivatives in the differential equation with finite difference approximations. The choice of finite difference schemes (e.g., forward, backward, central differences) depends on the specific requirements of the problem.
- Temporal Discretization (if applicable): If the problem involves time-dependent equations, a time-stepping method (e.g., explicit or implicit Euler method, Runge-Kutta methods) is used to advance the solution in time.
- Discretized Equations: Formulate the discretized system of algebraic equations by applying finite difference approximations to the differential equation. The resulting system relates the values of the solution at discrete points.
- Solution of the System: Solve the system of algebraic equations, either explicitly or implicitly, to obtain the numerical solution at each grid point.
- Boundary Conditions: Enforce boundary conditions to ensure the numerical solution satisfies the given conditions at the boundaries of the spatial domain.
- Convergence Analysis: Analyze the convergence of the numerical solution as the grid is refined. This involves studying how the numerical solution approaches the exact solution as the grid spacing decreases.
- Post-Processing: Evaluate and analyze the numerical solution. This may involve visualizing the results, computing derived quantities, or extracting relevant information from the simulation.

The finite difference method is relatively easy to implement and has broad applicability. It is especially effective for problems with regular geometries and simple boundary conditions. However, its accuracy depends on the chosen grid spacing, and stability considerations may impose constraints on the time step in time-dependent problems

2.4.2 The Fourth-order Runge-Kutta method (RK4)

The Fourth-order Runge-Kutta method is a numerical technique for solving ODEs numerically. It is a widely used and versatile method that provides a good balance between accuracy and computational efficiency. The method is particularly popular for solving initial value problems, where the ODE is given together with initial conditions. The general form of a first-order ODE is:

$$\begin{aligned}
&\frac{du_i}{dt} = F(t,u_i(t),v_i(t),u_{i+1}(t),u_{i-1}(t),v_{i+1}(t),v_{i-1}(t)), \quad u_i(t=0)=u_{i0}, \quad t>0,\\
&\qquad \text{where} \quad u_i(t)=u(x_i=i\cdot dx,t).\\
&\frac{dv_i}{dt} = F(t,u_i(t),v_i(t),u_{i+1}(t),u_{i-1}(t),v_{i+1}(t),v_{i-1}(t)), \quad v_i(t=0)=v_{i0}, \quad t>0,\\
&\qquad \text{where} \quad v_i(t)=v(x_i=i\cdot dx,t).
\end{aligned} \tag{2.68}$$

Then, integrating Eq. 2.68 using the RK4 scheme requires to calculate the intermediary variables and used the latter ones to extract the values of $u(x,t)$ and $v(x,t)$. The algorithm writes down as:

$$\begin{aligned}
L1_i &= dt\cdot F(t,u_i(t),v_i(t)),\\
M1_i &= dt\cdot F(t,u_i(t),v_i(t)),\\
L2_i &= dt\cdot F(t+1/2,u_i(t)+L1_i/2,v_i(t)+M1_i/2),\\
M2_i &= dt\cdot F(t+1/2,u_i(t)+L1_i/2,v_i(t)+M1_i/2),\\
L3_i &= dt\cdot F(t+1/2,u_i(t)+L2_i/2,v_i(t)+M2_i/2),\\
M3_i &= dt\cdot F(t+1/2,u_i(t)+L2_i/2,v_i(t)+M2_i/2),\\
L4_i &= dt\cdot F(t,u_i(t)+L3_i,v_i(t)+M3_i),\\
M4_i &= dt\cdot F(t,u_i(t)+L3_i,v_i(t)+M3_i).\\
u_i(t+dt) &= u_i(0)+\frac{1}{6}(L1_i+2(\cdot L2_i+L3_i)+L4_i).\\
v_i(t+dt) &= v_i(0)+\frac{1}{6}(M1_i+2(\cdot M2_i+M3_i)+M4_i).
\end{aligned}$$

Here, dt is the time step, and u_i and v_i are the approximate solutions at time t_i. The intermediate values $L1_i$, $L2_i$, $L3_i$, $L4_i$, $M1_i$, $M2_i$, $M3_i$ and $M4_i$ are used to estimate the slope at different points in the time interval. Explanation of the Steps:

- $L1_i$ represents the slope at the beginning of the interval (i.e., at t_n).
- $L2_i$ represents the slope at the midpoint of the interval using the value of u predicted by $L1_i$).
- $L3_i$ is another midpoint slope but now based on the estimate from $L2_i$.
- $L4_i$ is the slope at the endpoint of the interval (t_n+h), based on the estimate from $L3_i$.

The final value of u_{n+1} is calculated as a weighted average of these slopes, giving more weight to the slopes in the middle of the interval, which improves accuracy. The key features are :

- Fourth-order accuracy: The method has an error term of $O(h^5)$, which means the local error per step is proportional to h^5, and the global error is proportional to h^4, making it a highly accurate method.
- Stability: RK4 is generally stable for many types of problems but may require small time steps for stiff problems.
- Computational cost: Each time step involves four evaluations of the function $F(t,y)$, making it more computationally expensive than simpler methods like Euler's method but with significantly better accuracy.

The RK4 method is widely used for both initial value problems and time-stepping schemes in various fields, including fluid dynamics, celestial mechanics, and other scientific applications where accuracy and stability are critical , making it a popular choice for solving ODEs in various scientific and engineering applications.

2.4.3 The Pseudo Spectral method

The term "pseudo" in Pseudo Spectral Method (PSM) indicates that it combines elements of both finite difference and spectral methods. The PSM is a powerful numerical technique used for solving partial differential equations (PDEs), especially those involving wave-like phenomena or problems where high accuracy is required. This method combines the spectral method's high accuracy in spatial discretization with efficient techniques for handling nonlinear terms in real space. Rather than discretizing spatial derivatives as in the previous approach, Fourier transforms are used to transform the partial differential into an ordinary differential equation, hence:

$$\frac{d\hat{u}(k,t)}{dt} = F(k,t,\hat{u}(k,t)), \quad \hat{u}(k,t=0) = \hat{u}(k,0), \quad t>0,$$
$$\hat{u}(k,t) = \frac{1}{2\pi}\int_{-\infty}^{+\infty} u(x,t)e^{-2\pi ikx}dx.$$

The pseudo-spectral method combines the "global accuracy" of spectral methods, which use global basis functions, with the "efficiency" of performing nonlinear operations in real space. The general procedure involves:

- Transforming the solution to spectral space (e.g., using the Fourier transform) to compute spatial derivatives efficiently.

- Applying nonlinear operations in real space to avoid the computational complexity of performing these operations in spectral space.

Steps in the Pseudo-Spectral Method:

- Define the spatial domain and discretize it using points x_n, where $n = 0, 1, ..., N$. The number and distribution of these points depend on the boundary conditions and the choice of basis functions, such as the Fourier basis for periodic problems or Chebyshev polynomials for non-periodic problems.
- Transform the equation into spectral space, where it is represented by its Fourier or Chebyshev coefficients: $\hat{u}(k) = \mathscr{F}\{u(x)\}$
- In spectral space, spatial derivatives become simple multiplications by powers of the wavenumber k. For example, the first derivative becomes: $\frac{\partial u}{\partial x} \rightarrow ik\hat{u}(k)$
- The second derivative is expressed as: $\frac{\partial^2 u}{\partial x^2} \rightarrow -k^2\hat{u}(k)$
- Since spatial derivatives are efficiently computed in spectral space (due to simple multiplication by powers of k), the linear terms in the equation (e.g., diffusion or advection terms) are calculated directly in this space.
- Apply the inverse Fourier (or Chebyshev) transform to return the solution from spectral space to real space: $u(x) = \mathscr{F}^{-1}\{\hat{u}(k)\}$. This step is necessary because nonlinear terms, such as $f(u)$
- Once back in real space, compute the nonlinear terms (e.g., u^2, u^3, or any other nonlinear function of $u(x)$) directly. Nonlinear operations are generally more efficient in real space since they involve pointwise multiplication, which is computationally expensive in spectral space due to convolutions.
- Time-stepping iteration: For time-dependent problems, evolve the solution forward in time using an appropriate time-stepping method (e.g., Runge-Kutta, Crank-Nicolson). After each time step, repeat the process of transforming to spectral space to solve the linear terms, then applying the nonlinear terms in real space.

Advantages of the Pseudo-Spectral Method

- **High accuracy**: Spectral methods provide exponential or very high algebraic convergence (depending on the smoothness of the solution) with relatively few grid points. This makes the pseudo-spectral method (PSM) much more accurate than finite difference methods for the same grid resolution.

- **Efficient handling of derivatives**: In spectral space, spatial derivatives are computed as simple multiplications by powers of the wavenumber, making this operation computationally cheap.
- **Efficient treatment of nonlinearities**: By computing nonlinear terms in real space, the method avoids the complexities of convolutions that would otherwise arise in spectral space.

Limitations of the Pseudo-Spectral Method

- **Periodic boundary conditions**: The pseudo-spectral method is most efficient for problems with periodic boundary conditions, as the Fourier transform naturally accommodates periodic domains. For non-periodic boundary conditions, other basis functions like Chebyshev polynomials are required, which can introduce additional complications.
- **Aliasing errors**: Nonlinear operations can lead to aliasing errors, where high-frequency components (modes) interfere with lower frequencies due to undersampling. These errors can be mitigated using techniques such as "dealiasing" (e.g., the 2/3 rule, where two-thirds of the highest modes are discarded after computing the nonlinear terms).
- **Computational cost for large grids**: While pseudo-spectral methods are efficient for relatively smooth solutions and moderate grid sizes, they can become computationally expensive for very large grids, particularly when performing Fourier transforms or handling large datasets.

Dealiasing in the Pseudo-Spectral Method

- In nonlinear problems, aliasing can occur when performing nonlinear operations like squaring or cubing a function. This results from the "Nyquist limit," which restricts the maximum resolvable frequency. To mitigate aliasing, several dealiasing techniques are used:
- **2/3 rule**: When computing nonlinear terms, only the lower two-thirds of the modes are kept, while the upper one-third of the modes are set to zero before performing the inverse Fourier transform.
- **Padding**: Another approach is to pad the Fourier coefficients with zeros to artificially increase the resolution during nonlinear computations, then truncate the result afterward.

When solving time-dependent PDEs with the pseudo-spectral method, various time-stepping schemes can be employed:

- **Explicit methods** (e.g., Runge-Kutta): These are straightforward to implement but may require small time steps for stability, particularly in stiff problems.
- **Implicit methods** (e.g., Crank-Nicolson): These allow for larger time steps and are useful for stiff problems but require solving implicit equations at each step, which can introduce additional computational complexity.
- **Split-Step methods**: These combine both explicit and implicit methods, treating linear terms with an implicit scheme and nonlinear terms explicitly (similar to the "Split-Step Fourier Method").

The pseudo-spectral method is widely used in many fields, especially where wave-like or fluid dynamic behavior needs to be simulated with high precision:

- **Fluid dynamics**: Simulations of turbulence, vortex dynamics, and other fluid phenomena governed by the Navier-Stokes equations.
- **Nonlinear wave equations**: Solving problems like the nonlinear Schrödinger equation (NLS), Korteweg-de Vries (KdV) equation, or the cubic complex Ginzburg-Landau equation.
- **Quantum mechanics**: Solving the Gross-Pitaevskii equation for Bose-Einstein condensates or other wavefunction-based problems.
- **Astrophysics and plasma physics**: Modeling wave propagation, instabilities, and pattern formation in various systems.

The pseudo-spectral method is a highly accurate and efficient numerical technique for solving PDEs, particularly when high accuracy is required for problems with smooth solutions or periodic boundary conditions. It combines the strengths of spectral methods for linear terms with the simplicity of real-space operations for nonlinear terms, making it suitable for a wide range of applications, including fluid dynamics and wave propagation. Despite some limitations, such as aliasing and the need for periodic boundaries, the pseudo-spectral method remains a powerful tool in computational physics and applied mathematics.

2.4.4 Absorbing Boundaries Conditions

Absorbing Boundary Conditions (ABCs) are special types of boundary conditions used in numerical simulations to minimize artificial reflections from the edges of the computational domain. They are especially important when simulating wave propagation (e.g., electromagnetic waves, sound waves, reaction-diffusion waves, Cardiac electrophysiology, Quantum mechanics, Fluid dynamics) in an open or infinite space, using a finite computational grid.

- **General Idea:** When waves reach the boundary of a finite domain, standard boundary conditions (like Dirichlet or Neumann) tend to reflect the wave back into the domain. Absorbing boundary conditions aim to simulate an "open domain" where waves can exit the computational domain smoothly, as if the domain were infinite.

Types of Absorbing Boundary Conditions

- **First-Order Absorbing Conditions (Sommerfeld radiation condition)**: Basic and easy to implement, but may not be very effective for complex waveforms or multi-dimensional domains. Example in 1D:

$$\frac{\partial u}{\partial t} + c\frac{\partial u}{\partial x} = 0 \tag{2.69}$$

- **Higher-Order ABCs** Improve the absorption performance by matching the outgoing wave solution more accurately. However, they are more complex and computationally demanding.

- **Perfectly Matched Layers (PMLs)** Widely used in wave propagation problems, especially in computational electromagnetics. PMLs are artificial layers surrounding the computational domain that absorb incident waves without reflection. For a PDE like: $\frac{\partial u}{\partial t} = D\frac{\partial^2 u}{\partial x^2} + f(u)$

  we introduce a damping term in a PML region near the boundary:

$$\begin{aligned} \frac{\partial u}{\partial t} &= D\frac{\partial^2 u}{\partial x^2} - \sigma(x)u + f(u) \\ \sigma(x) &= \sigma_{\max}\left(\frac{x - x_{\text{PML start}}}{L_{\text{PML}}}\right)^2. \end{aligned} \tag{2.70}$$

  Where:

  1. $\sigma(x) = 0$ in the interior,

2. $\sigma(x) > 0$ increases gradually toward the edge,
3. $\sigma(x)$ is often quadratic or exponential:

- **Sponge Layers or Damping Layers** A region near the boundary is added where damping terms gradually reduce the wave amplitude. This is simpler than PMLs and can be effective in some cases.

$$\begin{aligned} \frac{\partial u}{\partial t} &= D_u \nabla^2 u + f(u,v) - \alpha(x)u, \\ \frac{\partial v}{\partial t} &= D_v \nabla^2 v + g(u,v) - \alpha(x)v, \\ \alpha(x) &= \alpha_0 \left[1 - \cos\left(\frac{\pi(x - x_0)}{L_{\text{damp}}}\right)\right], \end{aligned} \tag{2.71}$$

  where: $\alpha(x) = 0$ in the interior, and $\alpha(x)$ increases smoothly near the boundary.

- **Transparent Boundary Conditions (TBCs)** Theoretically ideal ABCs derived from the exact solution of the wave equation outside the domain. Very accurate but often difficult to implement and computationally expensive. For: $\frac{\partial u}{\partial t} = D\frac{\partial^2 u}{\partial x^2}$, the TBC at the boundary $x = L$ is:

$$\frac{\partial u}{\partial x}(L,t) = -\frac{1}{\sqrt{\pi D}} \int_0^t \frac{\partial u}{\partial t}(L,\tau) \cdot \frac{1}{\sqrt{t-\tau}}\, d\tau. \tag{2.72}$$

  This integral expression absorbs outgoing signals ”perfectly”, but it’s ”nonlocal” and requires ”storing the entire time history” of the solution

Key Features

- **Non-reflecting:** Prevents artificial reflections from boundaries.
- **Stability:** Should not introduce numerical instabilities.
- **Accuracy:** Should not alter the solution inside the domain.
- **Efficiency:** Should be computationally manageable.
- **Implementation:** Should be compatible with the numerical scheme (e.g., finite difference, finite element, spectral methods).

This mimics the behavior of a wave moving out of the domain without reflecting back.

2.5 Conclusion

This chapter was devoted to the presentation of the FHN model equations governing the dynamics of excitable membranes, particularly in the context of cardiac cell action potentials. We have also presented analytical methods used in this thesis. Asymptotic expansion techniques, like the reductive perturbation and the multiple-scale expansion methods, have been also presented. Using these methods, we were able to derive the amplitude equations like the cqCGL equation. We note that, coefficients of these equations depend on the self and cross diffusion, themoelectric coupling and the feedback gain of electromagnetic induction. The stability conditions have been discussed, using the linear stability analysis of the plane wave solution for the amplitude equations. Also, we have explored the Hirota Bilinear scheme to show how to derive soliton solutions and explain the phase transition in some specific context.

CHAPTER 3

RESULTS AND DISCUSSION

Contents

3.1 Introduction

Over the last twenty years, there has been growing interest in solitons, which are phenomena observed in various fields of physics, like nonlinear optics [117, 150] and Biophysics [151–154]. Solitons play a significant role in influencing how systems behave, including the way action potentials work in the heart [155, 156]. In this chapter, we have looked into the behavior of approximate solitary waves, specifically hole-type wave solitons, in the context of an improved model of the FitzHugh-Nagumo (FHN) equation used for cardiac dynamics. We aim to understand how factors such as diffusion, thermoelectric coupling, and feedback from electromagnetic induction affect the dynamics of electrical and chemical propagation in the modified FHN model. We will also explore how new types of waves, such as solitary waves and dark envelope solitons, can emerge under certain conditions. Modulated waves can form due to a phenomenon called modulation instability, which occurs when nonlinear and dispersive effects interact [152, 157]. Additionally, we will assess the stability of soliton solutions through numerical methods. This will help us understand how electrical and magnetic signals spread through the medium of cardiac cells and how they influence the heart's functioning.

3.2 Soliton-like nonlinear excitation in the FitzHugh-Nagumo cardiac model through the cubic-quintic complex Ginzburg-Landau equation

3.2.1 Modulational instability processess : Case 1 : Perturbation in amplitude

In the cited work [117], the authors have elegantly deduced the Modulational Instability (MI) criterion via the generalized cqCGL equation. In this discourse, we employ a comparable methodology to investigate the MI phenomenon through the lens of the cqCGL equation Eq. 2.27. To advance our analysis, we postulate that the plane wave serves as a solution to Eq. 2.27:

$$\psi(\xi,\tau) = \psi_0 e^{i(\nu\xi-\eta\tau)}. \tag{3.1}$$

with ν and η denoting to the wavenumber and angular frequency of the unperturbed plane wave, respectively, that are interconnected via the equation:

$$-\eta - p\nu^2 + q|\psi_0|^2 + r|\psi_0|^4 = i\gamma. \tag{3.2}$$

which can also be expressed in the form the real and imaginary parts, respectively.

$$-\eta - p_r\nu^2 + q_r|\psi_0|^2 + r_r|\psi_0|^4 = -\gamma_i. \tag{3.3}$$

$$-p_i v^2 + q_i|\psi_0|^2 + r_i|\psi_0|^4 = \gamma_r, \tag{3.4}$$

To examine the stability of the plane wave solution, we modulate it with a small perturbation as

$$\psi(\xi,\tau) = \left(\psi_0 + \delta\psi\right) e^{i(\nu\xi - \eta\tau)}, \tag{3.5}$$

where $\delta\psi$ represents the perturbation and its amplitude is supposed to be dimunitive in comparison to the plane wave amplitude ψ_0. By Incorporating the perturbed solution into Eq. 2.27, linearizing around the unperturbed plane wave and considering Eq. 3.2, we derive the subsequent equation for the perturbation field:

$$i\frac{\partial\delta\psi}{\partial\tau} + p\frac{\partial^2\delta\psi}{\partial\xi^2} + 2i\nu p\frac{\partial\delta\psi}{\partial\xi} + q\psi_0(\psi_0\delta\psi^* + \psi_0^*\delta\psi) + 2r|\psi_0|^2\psi_0(\psi_0\delta\psi^* + \psi_0^*\delta\psi) = 0. \tag{3.6}$$

A solution to the above equation can be taken in the form

$$\delta\psi = \delta\psi_1 e^{i(\Gamma\xi + \Omega\tau)} + \delta\psi_2^* e^{-i(\Gamma\xi + \Omega^*\tau)}, \tag{3.7}$$

with Γ and Ω being the wavenumber and the angular frequency of the perturbation, respectively. Using the perturbation Eq. 3.5, one leads to the following homogeneous system for $\delta\psi_1$ and $\delta\psi_2$:

$$2(\Omega + c_{11})\delta\psi_1 + c_{12}\delta\psi_2 = 0, \tag{3.8}$$

$$c_{21}\delta\psi_1 + (\Omega + c_{22})\delta\psi_2 = 0, \tag{3.9}$$

where

$$\begin{aligned} c_{11} &= (2\nu\Gamma + \Gamma^2)p - (q + 2r|\psi_0|^2)|\psi_0|^2, \\ c_{12} &= -(q + 2r|\psi_0|^2)\psi_0^2,\ c_{21} = (q^* + 2r^*|\psi_0|^2)(\psi_0^*)^2, \\ c_{22} &= (2\nu\Gamma - \Gamma^2)p^* + (q^* + 2r^*|\psi_0|^2)|\psi_0|^2. \end{aligned}$$

The aforementioned system will concede non-trivial solutions provided that its determinant equates to zero, thereby facilitating the derivation of the nonlinear dispersion relation:

$$\Omega^2 + X\Omega + Y = 0, \tag{3.10}$$

where $X = c_{11} + c_{22}$ and $Y = c_{11}c_{22} - c_{12}c_{21}$. Solutions of Eq. 3.8-3.9 are investigated via its discriminant given by:

$$\begin{aligned} \Delta &= (2\nu\Gamma p_r)^2 + (\Gamma^2 p_i - (q_i + 2r_i|\psi_0|^2)|\psi_0|^2)^2 + (4\nu^2\Gamma^2 - \Gamma^4)|p|^2 - 2\Gamma^2(p_r q_r + p_i q_i)|\psi_0|^2 \\ &- 4\Gamma^2(p_r r_r + p_i r_i)|\psi_0|^2 + 4i\nu\Gamma p_r(\Gamma^2 p_i - (q_i + 2r_i|\psi_0|^2))|\psi_0|^2 \\ &+ 4i\nu\Gamma[(p_i q_r - p_r q_i) + 2(p_i r_r - p_r r_i)|\psi_0|^2]|\psi_0|^2, \end{aligned} \tag{3.11}$$

that can be separated into its real and imaginary parts as follows:

$$\begin{aligned}\Delta_r = {} & (2\nu\Gamma p_r)^2 + (\Gamma^2 p_i - (q_i + 2r_i|\psi_0|^2)|\psi_0|^2)^2 + (4\nu^2\Gamma^2 - \Gamma^4)|p|^2 - 2\Gamma^2(p_r q_r + p_i q_i)|\psi_0|^2 \\ & - 4\Gamma^2(p_r r_r + p_i r_i)|\psi_0|^2,\end{aligned}$$

$$\begin{aligned}\Delta_i = {} & 4\nu\Gamma p_r(\Gamma^2 p_i - (q_i + 2r_i|\psi_0|^2)|\psi_0|^2) - 4\nu\Gamma[(p_r q_i - p_i q_r) \\ & + 2(p_i r_r - p_r r_i)|\psi_0|^2]|\psi_0|^2.\end{aligned}$$

Based on the above discriminant, the solution of Eq. 3.10, the angular frequency is a complex function that can be written in a simplified way as:

$$\Omega = (\chi \pm e_1) + i(\phi \pm e_2), \tag{3.12}$$

where $\chi = 2\nu\Gamma p_r$, $\phi = \left(\Gamma^2 p_i - q_i|\psi_0|^2 - 2r_i|\psi_0|^4\right)$, with

$$e_1 = \sqrt{\frac{1}{2}\left(\Delta_r + \sqrt{\Delta_r^2 + \Delta_i^2}\right)}, e_2 = \sqrt{\frac{1}{2}\left(-\Delta_r + \sqrt{\Delta_r^2 + \Delta_i^2}\right)}.$$

The previously determined expression of Ω permits us to examine two scenarios that are related upon the sign of the imaginary part of the discriminant Δ_i. Specifically, when $\Delta_i < 0$, the solutions of Eq. 3.10 are Ω_1 and Ω_2 on the one hand. Conversely, when $\Delta_i > 0$, solutions of Eq. 3.10 are $\Omega_1^{'}$ and $\Omega_2^{'}$. Consequently, the two-pairs of solutions are expressed as follows:

$$\begin{aligned}\Omega_1 &= (\chi + e_1) + i(\phi - e_2), \quad \Omega_2 = (\chi - e_1) + i(\phi + e_2), \\ \Omega_1^{'} &= (\chi - e_1) + i(\phi - e_2), \quad \Omega_2^{'} = (\chi + e_1) + i(\phi + e_2).\end{aligned} \tag{3.13}$$

It is noteworthy to emphasize that solutions $\Omega_1^{'}$ and $\Omega_2^{'}$ exhibit identical asymptotic behavior to that of Ω_1 and Ω_2. As is widely recognized [117], the sign of the imaginary component of the angular frequency allows us to qualify the evolution of the MI in the system under investigation. To better understand, let us insert the initial relation of Eq. 3.13 into the expression of the perturbation $\delta\psi$ and by doing so, we obtain the following

$$\delta\psi = \delta\psi_1 e^{i(\Gamma\xi + (\chi + e_1)\tau)} e^{-(\phi - e_2)\tau} + \delta\psi_2^* e^{-i(\Gamma\xi + (\chi + e_1)\tau)} e^{(\phi - e_2)\tau}. \tag{3.14}$$

Evidently, the behavior of the $\delta\psi$-function is influenced by the sign of $(\phi - e_2)$, which signifies $Im(\Omega_1)$. Upon analyzing the sign of $(\phi - e_2)$, we observe that if $\phi < 0$, then $(e_2 - \phi) > 0$. As a result, the CQCGL equation undergoes exponential growth over time, leading to the instability of the plane wave under modulation. However, if $\phi > 0$, we have $(\phi - e_2) < 0$, i.e., $Im(\Omega_1) < 0$, the CQCGL equation diverges without limit as τ increases,

and the system is deemed to be modulationally unstable. The explicit expression of the imaginary part of Ω_1 is provided by:

$$\phi - e_2 \quad = \phi - \sqrt{\tfrac{1}{2}\{e_3 + 2\Gamma^2(p_r q_r + p_i q_i)|\psi_0|^2 + 4\Gamma^2(p_r r_r + p_i r_i)|\psi_0|^4 + e_4\}}, \tag{3.15}$$

with, $e_3 = -4\nu^2\Gamma^2 p_r^2 - \Gamma^4|p|^2$, $e_4 = (\Gamma^2 p_i - (q_i + 2r_i|\psi_0|^2)|\psi_0|^2)^2 + 4\nu^2\Gamma^2|p|^2 + \sqrt{\Delta_r^2 + \Delta_i^2}$. As the quantity $e_4 > 0$, it happens that: $\phi - e_2 \leq \phi - \sqrt{\tfrac{1}{2}\{e_3 + 2\Gamma^2(p_r q_r + p_i q_i)|\psi_0|^2 + 4\Gamma^2(p_r r_r + p_i r_i)|\psi_0|^4\}}$. Moreover, the inequality $Im(\Omega_1) < 0$ is satisfied if $\phi - \sqrt{\tfrac{1}{2}\{e_3 + 2\Gamma^2(p_r q_r + p_i q_i)|\psi_0|^2 + 4\Gamma^2(p_r r_r + p_i r_i)|\psi_0|^4\}} < 0$. By giving that, $\phi > 0$ and $e_3 < 0$, the above condition is fulfilled as soon as we have:

$$(p_r q_r + p_i q_i) + 2(p_r r_r + p_i r_i)|\psi_0|^2 > 0. \tag{3.16}$$

The inequality Eq. 3.16 which represents the MI criterion is similar to the finding of Mohamadou et *al*. [158] in their exploration of pattern formation within the generalized CQCGL equation. From Eq. 3.16, the threshold amplitude of an unstable monochromatic wave, beyond which the plane wave breaks into nonlinear patterns is determined as follows:

$$|\psi_0|^2 > |\psi_{0,cr}|^2 = -\frac{(p_r q_r + p_i q_i)}{2(p_r r_r + p_i r_i)}. \tag{3.17}$$

It is worth noticing that the plane wave amplitude expressed in Eq. 3.1 as:

$$|\psi_0|^2 = (-q_i - \sqrt{q_i^2 + 4r_i(\nu^2 p_i + \gamma_r)})/2r_i, \tag{3.18}$$

verifies the above condition Eq. 3.18, when $\nu > 2.8\pi$. Furthermore, the instability function $\varpi(k) = (p_r q_r + p_i q_i) + 2(p_r r_r + p_i r_i)|\psi_0|^2$ is provided, in accordance with Eq. 3.17. This takes into account the global Benjamin-Feir instability [144], illustrating that certain wave types could lead in the formation of solitons in 1960s.

As shown, Fig. 3.1 the $\varpi(k)$-function remains positive regardless of the value of the wavenumber k along with the diffusion coefficients, thus attesting that the plane wave is trivially modulationally unstable. Obviously, $\varpi(k)$ increases with both self-diffusion coefficients [see panels (a1) and (a2)]. This suggests that these parameters can be used to monitor the appearance of nonlinear localized structures for the action potential within the cardiac cells. On the other hand, when the cross-diffusion coefficients h_1 and h_2 are increased in panels (b1) and (b2), respectively, the instability function decreases, which predicts a decrease of the MI growth rate [159]. Concerning the model under study, the projection is indicative of the membrane trying to adjust for the perturbation to bring the potential back down to the steady state. To ensure a comprehensive analysis, the MI growth rate is expressed as follows:

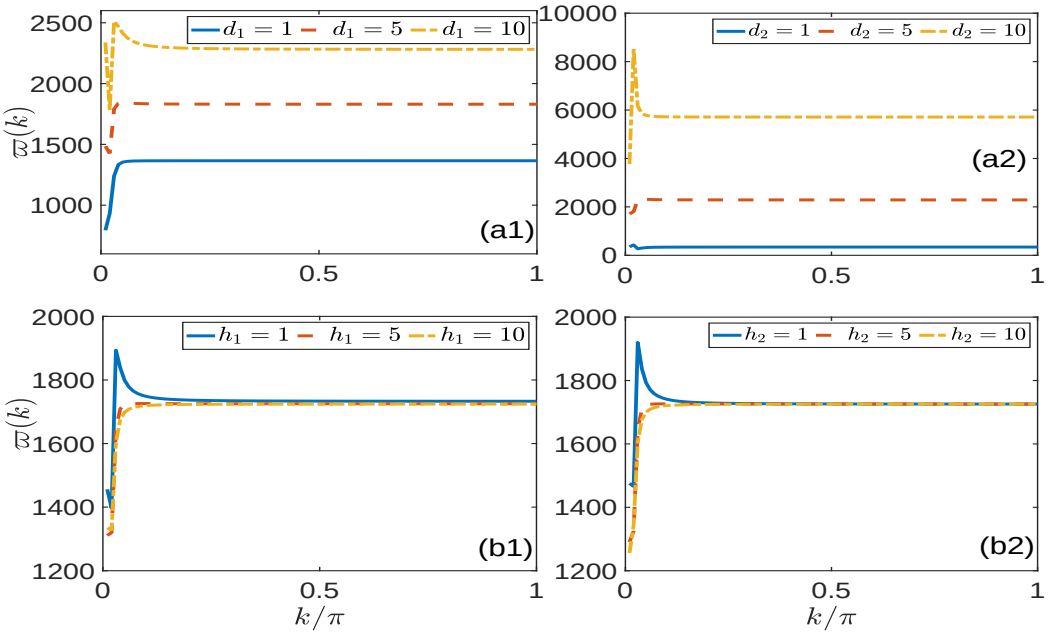

Figure 3.1: The panels show plots of the instability function $\varpi(k) = (p_r q_r + p_i q_i) + 2(p_r r_r + p_i r_i)|\psi_0|^2$ against the wavenumber k, under the respective effects of the self-diffusion coefficients [panels (a1) and (a2)] and cross-diffusion coefficients [panels (b1) and (b2)]. For (a1), $d_2 = h_1 = h_2 = 1$, for (a2) $d_1 = h_1 = h_2 = 1$, for (b1) $d_1 = d_2 = h_2 = 1$ and (b2) $d_1 = d_2 = h_1 = 1$, with the other parameter values being: $a = 0.25$, $b = -0.15$, $\gamma = 3.6$ and $\sigma = 0.01$.

$$G(\Gamma) = \left| \Gamma^2 p_i - q_i|\psi_0|^2 - 2r_i|\psi_0|^4 - \sqrt{\frac{1}{2}\left(-\Delta_r + \sqrt{\Delta_r^2 + \Delta_i^2}\right)} \right|. \tag{3.19}$$

Some features of the MI growth rate, using Eq. (3.18), are displayed in Fig. 3.2, where different combinations of self- and cross-diffusion parameter values have been used as in Fig. 2.1. Our discussion in this part emphasizes the maximum growth rate of instability that appears to be very sensitive to changes in d_1, d_2, h_1, and h_2. For example, the impact of varying d_1 is given by Fig. 3.2 $(\text{aj})_{j=1,2,3}$, where it is clear that increasing d_1 amplifies the maximum growth rate, in a context where nonlinear patterns are likely to appear in regions of weak wavenumber Γ. Similar calculations are repeated in Fig. 3.2 $(\text{bj})_{j=1,2,3}$, where d_1, h_1, and h_2 are fixed with d_2 changing. We also observe the same spectrum of behaviors which can be specifically attributed to the variations of self-diffusion coefficients. Now, fixing d_1, d_2, and h_2, the impact of h_1 is pictured in Fig. 3.2 $(\text{cj})_{j=1,2,3}$, where increasing its value does not importantly impact the growth rate magnitude, but rather contribute to reducing its parametric expansion in the Γ-direction. The same behavior of the growth rate remains ostensible when h_2 is changed,

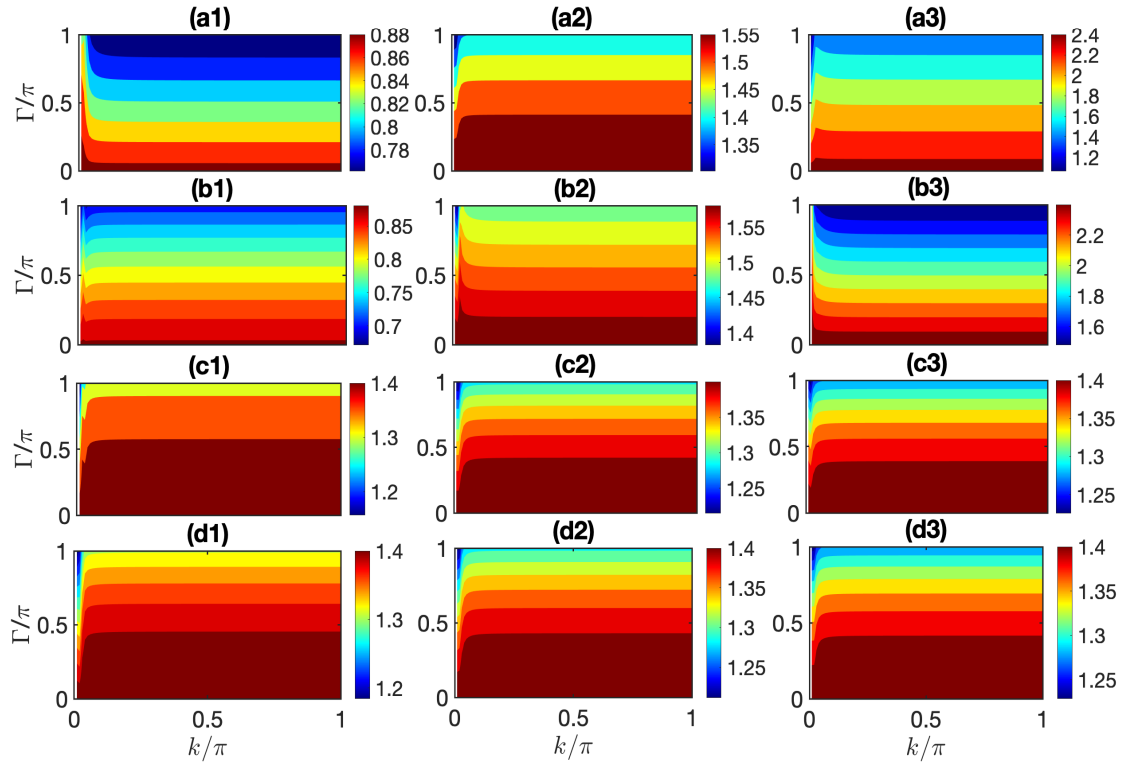

Figure 3.2: Panels (aj)$_{j=1,2,3,}$ and (bj)$_{j=1,2,3,}$ show the growth rate of MI versus the wavenumbers k and Γ, under the effect of the self-diffusion coefficients d_1 and d_2, respectively. Panels (cj)$_{j=1,2,3,}$ and (dj)$_{j=1,2,3,}$ display the MI growth rate under the effect of the cross-diffusion coefficients h_1 and h_2, respectively. It is worth noticing that when one of the self- or cross-diffusion coefficients varies, its values are selected in the $\{1,5,10\}$ range and the remaining coefficients are fixed to 4. The other parameters are given by: $a = 0.25$, $b = -0.15$, $\gamma = 3.6$ and $\sigma = 0.01$.

keeping d_1, d_2, and h_1 constant as shown in Fig. 3.2 (dj) $_{j=1,2,3}$. When parameters are chosen properly within the instability zone, the transmembrane potential is expected to exhibit nonlinear oscillations. These oscillations are crucial in understanding cardiac signals and electrocardiograms. If the magnitude of the MI growth rate decreases, the instability tends to disappear. Since the SA node generates the soliton train, energy decreases over time, preventing wave pattern formation in cardiac tissue. Tabi et *al*. [50] discussed the importance of plane wave perturbation to generate spiral waves in the FHN cardiac model, celebrating balanced contributions from nonlinear and dispersive effects. However, instead of cross-diffusion, the application of an induced magnetic field was shown to drastically modify the appearance of MI through the growth rate and spatiotemporal evolution. This reinforces the idea that MI and solitary waves are straightforwardly related and share the same parameter space [160]. That constitutes a profound motivation to look for exact envelope solutions for the studied model, as

proposed in the next section.

3.2.2 Hirota Bilinear Method. Case 1 : K, Ω = 0.

A solitary wave solution can be obtained for this case, following system of equations:

$$\begin{aligned} &\frac{f^3}{rg}(iD_{n,\tau}+pD^2_{n,\xi}-\lambda-\mu)(g\cdot f)=hf,\\ &f^2\{(\frac{n(n+1)pD^2_{n,\xi}}{2r}+\frac{i\gamma-\lambda}{r})(f\cdot f)+\frac{(q-\mu)|g|^2}{r}\}+|g|^4=hg. \end{aligned} \tag{3.20}$$

Here, h is an arbitrary function introduced with the intention of decoupling the equation. By setting the system to zero, we can individually constrain the terms of each bracket to be zero and partition Eq. 3.20

$$(iD_{n,\tau}+pD^2_{n,\xi}+\Lambda-pK^2-\lambda-\mu)(g\cdot f)=0, \tag{3.21a}$$

$$f^2\left\{\left(\frac{n(n+1)pD^2_{n,\xi}}{2r}+\frac{i\gamma-\lambda}{r}\right)(f\cdot f)+\frac{(q-\mu)|g|^2}{r}\right\}+|g|^4=0. \tag{3.21b}$$

Accordingly, the constitutive derivatives, in terms of Hirota's operator, can be written as:

$$\begin{aligned} D_{n,\tau}(g\cdot f)&=\left[\left(\frac{\partial}{\partial\tau}-n\frac{\partial}{\partial\tau'}\right)g(\xi,\tau)f(\xi',\tau')\right]_{\xi=\xi',\tau=\tau'},\\ D^2_{n,\xi}(g\cdot f)&=\left[\left(\frac{\partial}{\partial\xi}-n\frac{\partial}{\partial\xi'}\right)^2 g(\xi,\tau)f(\xi',\tau')\right]_{\xi=\xi',\tau=\tau'},\\ D^2_{\xi}(f\cdot f)&=\left[\left(\frac{\partial}{\partial\xi}-n\frac{\partial}{\partial\xi'}\right)f(\xi,\tau)f(\xi',\tau')\right]_{\xi=\xi',\tau=\tau'}. \end{aligned} \tag{3.22}$$

As we seek for the solitary wave solution, the functions f and g are supposed to be in the form:

$$g=g_0e^{\theta_3},f=1+e^{\theta_3+\theta_3^*}, \tag{3.23}$$

where $\theta_3=\kappa\xi-\Lambda\tau$, $\theta_3^*=\kappa^*\xi-\Lambda^*\tau$, $\kappa=\kappa_r+i\kappa_i$, and $\Lambda=\Lambda_r+i\Lambda_i$ being a complex constant. The presence of the term $|g|^4$, on the right-hand-side of Eq. (3.21b) implied that all coefficients of the corresponding equation should real. Therefore, $Im\left(\frac{n(n+1)p}{2r}\right)=Im\left(\frac{i\gamma-\lambda}{r}\right)=Im\left(\frac{q_r-\mu}{r}\right)=0$, leads to:

$$\begin{aligned} &\alpha=-\beta\pm\sqrt{\beta^2+2},\ \beta=\frac{3(p_rr_r+p_ir_i)}{2(p_rr_i-p_ir_r)},\\ &r_i(\lambda_r+\gamma_i)=r_r(\lambda_i-\gamma_r),\ r_r(q_i-\mu_i)=r_i(q_r-\mu_r). \end{aligned} \tag{3.24}$$

Here, we assume that $\lambda_r = -\gamma_i$, $\lambda_i = \gamma_r$, $\mu_i = q_i$ and $\mu_r = q_r$. Furthermore, solving the remainder of Eq. 3.21b at the order $e^{2(\theta_3+\theta_3^*)}$, yields:

$$|g_0|^4 = \frac{8\kappa_r^2}{A},\ A = \frac{(p_r r_r + p_i r_i)}{|p|^2(2-\alpha^2)}. \tag{3.25}$$

On the other hand, from Eq. 3.21a, at the order $e^{2\theta_3+\theta_3^*}$, taking into account the order e^{θ_3}, leads to:

$$\Lambda_r - 2p\kappa_r\kappa_i + 2p\kappa_r^2\alpha = 0. \tag{3.26}$$

After separating Eq.3.26 into real and imaginary parts, one obtains $\kappa_i = \alpha\kappa_r$, $\Lambda_r = 0$. Moreover, at the order e^{θ_3}, the same Eq.3.21a, yields:

$$\begin{aligned} \Lambda_i &= \kappa_r^2(2p_i\alpha - p_r\left(1-\alpha^2\right)) - \gamma_i + q_r, \\ \kappa_r^2 &= \frac{(\gamma_r + q_i)}{2p_r\alpha + p_i\left(1-\alpha^2\right)}. \end{aligned} \tag{3.27}$$

We finally get the solitary wave solution as:

$$\psi(\xi,\tau) = \frac{g_0 e^{((\kappa_r+i\kappa_i)\xi - i\Lambda_i\tau)}}{(1+e^{((\kappa_r+i\kappa_i)\xi - i\Lambda_i\tau)} + e^{((\kappa_r-i\kappa_i)\xi + i\Lambda_i\tau)})^{1+i\alpha}}, \tag{3.28}$$

Based on the above results on the Hirota's scheme and taking into consideration Eq. 2.8a and Eq. 2.8b, the solutions for the generic model Eq. 2.1a and Eq. 2.1b are expressed as:

$$u(x,t) = 2\epsilon(\cos(kx-\omega_r t)\psi_r - \sin(kx-\omega_r t)\psi_i)e^{\omega_i t} + O(\epsilon^2), \tag{3.29a}$$

$$v(x,t) = 2\epsilon((\alpha_r\psi_r - \alpha_i\psi_i)\cos(kx-\omega_r t) - (\alpha_r\psi_i + \alpha_i\psi_r)\sin(kx-\omega_r t))e^{\omega_i t} + O(\epsilon^2). \tag{3.29b}$$

with $\psi_r = Re(\psi)$ and $\psi_i = Im(\psi)$. In remainder, the relationship between the pair of variables (ξ,τ) and (x,t) is given by $(\xi,\tau) = \left(\epsilon^2(x - v_g t), \epsilon^4 t\right)$ which implied that above solutions (3.31) only depends on the state variables (x,t).

Obviously, the solutions given by Eqs. (3.29a)-(3.29b) are solitary pulses propagating from left to right. Eteme previously found a similar form of solutions [160] in the context of MI and energy localization in a time-delayed memristive neural network. As shown in Fig. 3.3, the corresponding analytical solutions are clearly depicted where panels (a) and (b) show the activator variable $u(x,t)$, and inhibitor variable $v(x,t)$, respectively. In other words, the recorded diagrams deliver the features of the fast variable trans-membrane potential $u(x,t)$ and slow variable potential in a spatiotemporal context, where the self-and-cross diffusion constants (d_1,d_2,h_1,h_2) have equal values, with $k = 0.01\pi$. The solution exhibits two peaks, normal and inverted, resulting from a change in the sign

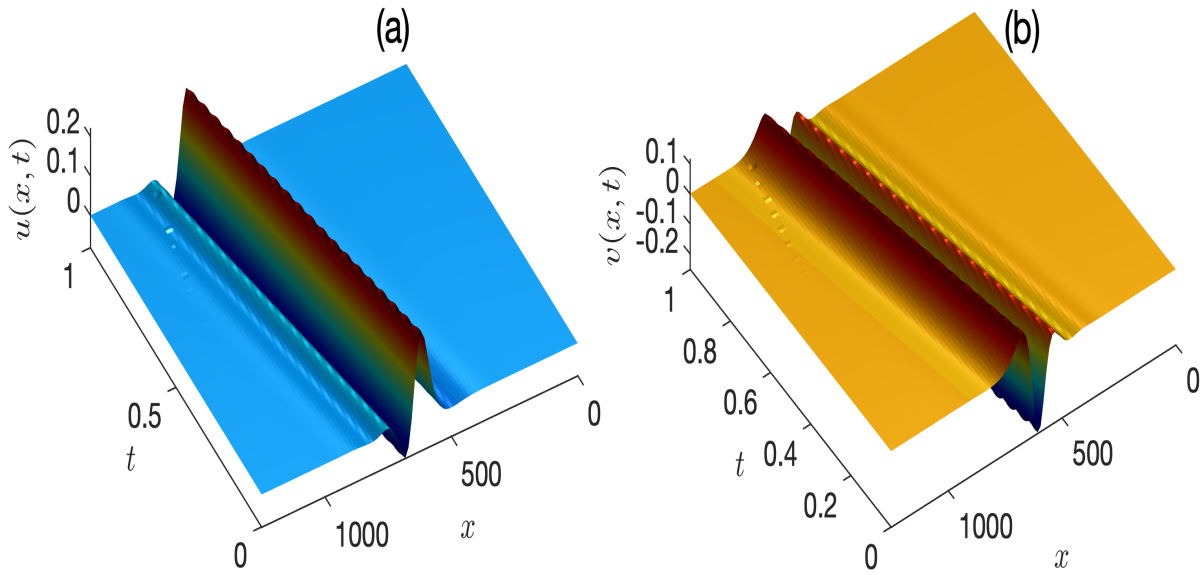

Figure 3.3: Space-time plots of the analytical solutions (3.29a), where the evolution of cardiac ionic wave of analytical solutions for $u(x,t)$ is shown in panels (a), and panels (b) displays the plot for the ionic current $v(x,t)$. The features are captured for fixed values of self- and cross diffusion parameters ($d_1, d_2, h_1, h_2 = 10, 10, 10, 10$).

of the same coefficients. These envelope solitons have an oscillatory profile and transmit information between nodes for better coordination of important cardiac functions downstream and pathological situations upstream [161, 162]. Additionally, the action potential starts with a sudden change in membrane potential to -0.05V, followed by a rapid upstroke approaching the sodium equilibrium potential. Finally, there is a fairly quick depolarisation to approximately -0.05V. The potential then moves in a positive direction to $+0.2$V, generating the characteristic "notch" that regulates cardiomyocyte electrical differentiation and intracellular signaling mechanism, as observed in many experimental records [163, 164].

3.2.3 Discussion 1

Electrical processes in the heart are initiated in the SA node due to the movement of charged particles. These processes spread to other components of the heart under various factors, including self-and cross-diffusive effects. Meanwhile, from a physical point of view, dissipative effects affect information stability and the energy that propagates across the cardiac tissue. The purpose of this section is to test the accuracy of the pro-

posed solution by numerically integrating Eqs. (2.1a)-(2.1b) of the generic FHN cardiac model using the standard fourth-order Runge-Kutta computational scheme. The time-step $\Delta t = 10^{-3}$, the spatial dimension coordinate step $\Delta x = 0.25$, the carrier wavenumber $k = 0.01\pi$, and the speed of propagation $v_0 = 0.1/\Delta t$ have been adopted. The parameter v_0 has been introduced here to regulate the propagation speeds of both analytical and numerical solutions. As said so far, the initial conditions are given by Eqs. (3.29a)-(3.29b), and the numerical integration is conducted using Neumann boundary conditions for both $u(x,t)$ and $v(x,t)$. For technical purposes, analytical results are superposed to numerical ones under the context where the phase plane of the global dynamics is unveiled.

To start, Fig. 3.4 displays the space evolution of the two components $u(x,t)$ and $v(x,t)$, which are the fast traveling pulse and the slow traveling pulse, at different instants $t = 0$ [panels (aj)$_{j=1,2}$], $t = 86$ [panels (bj)$_{j=1,2}$] and $t = 300$ [panels (cj)$_{j=1,2}$]. For $t = 0$ and $t = 86$, there is an accurate correlation between analytical and numerical results, which confirms the effectiveness of our solution. As predicted, the propagation features show direct pulses for $u(x,t)$ and inverted pulses for $v(x,t)$, with additional oscillations. In this case, when $(d_1, d_2, h_1, h_2) = (6,6,6,6)$, there is a slight mismatch between the analytical and numerical pulses of $u(x,t)$ at $t = 300$, but the resulting zigzag-shaped profiles are still recognized as the normal propagation of electrical impulses throughout myocardial cells, with familiar wave regimes such as depolarization, repolarization, and hyperpolarization, which help restore the pulse to its normal state by resetting the blocking mechanism in the system. The panels illustrate the scenario where the upper peaks occur at critical values lower than the lower peak. The graph of $v(x,t)$ in each panel (bj)$_{j=1,2,3}$) shows two upper peaks that have a substantially smaller amplitude than the lower, bigger peak. This indicates an equilibrium of ion particles random movement at the SA membrane level. Optical solitonic waves show a similar shape represented by the bright and dark soliton. There is no specific requirement for small values of σ for wave propagation. Analytical and numerical solutions have no amplitude gap due to ion regulation at gap junctions.

Figure 3.5 shows that the effect of the self-diffusion parameter d_1 on membrane potentials is stable upon propagation, meaning there is a perfect correlation between numerical and analytical results, for $d_1 = 1$ [panels (aj)$_{j=1,2}$] and $d_1 = 10$ [panels (bj)$_{j=1,2}$]. The difference in the sharpnesses of the profiles also testify to the sensitivity of the analytical and numerical solutions to changes in d_1. Obviously, the regimes of solitons are different in terms of amplitudes and increase progressively, i.e., $u(x,t)$ and $v(x,t)$ are

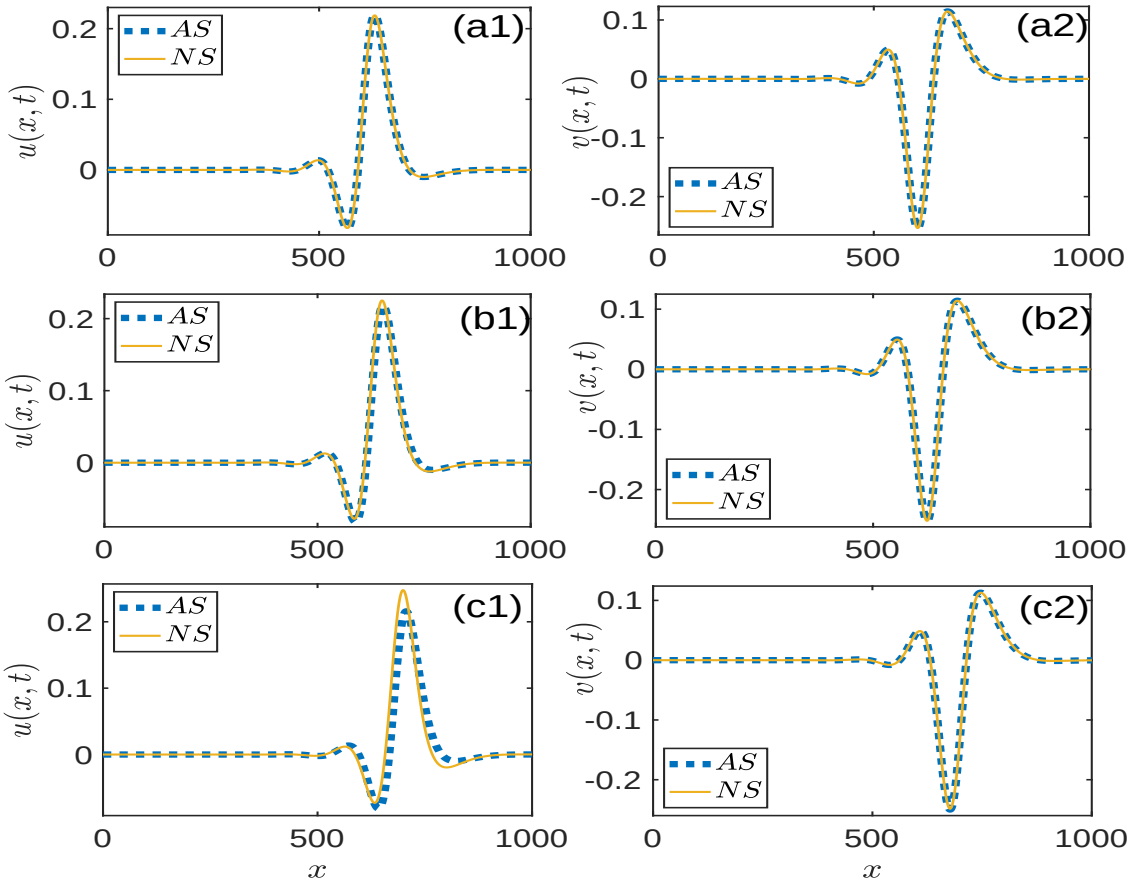

Figure 3.4: The panels compare analytical and numerical solitary pulses from solutions (3.29a)-(3.29b) giving $u(x,t)$ and $v(x,t)$. Plots (a1)-(a2) are generated at time $t = 0$. Panels (b1) and (b2) are obtained at time $t = 86$ and panels (c1)-(c2) are obtained at time $t = 300$, with the other parameters being $(d_1, d_2, h_1, h_2) = (6,6,6,6)$, $k = 0.01\pi$, $a = 0.25$, $b = -0.15$, $\gamma = 3.6$ and $\sigma = 0.01$. AS refers to analytical solution (dotted blue line) and NS refers to numerical solution (solid yellow line).

increasing functions. From another angle, we can say that the medium may absorb the inward and the outward concentration of ion currents among the gap junction of the cell membrane. However, in some cardiac diseases, there is an expansion of the protein molecules forming the gate channels from intercalated disc to lateral cell borders and reduces conduction velocity [165]. The phase planes of the corresponding components also show some propagative features, from which oscillations in the pulse profiles are materialized by minor nodes along with some manifestations of asymmetric profiles, also sensitive to changes in d_1 [see Figs.3.5 (a3) and (b3)].

For the case displayed in Fig. 3.6, all other parameters are kept constant, except d_2

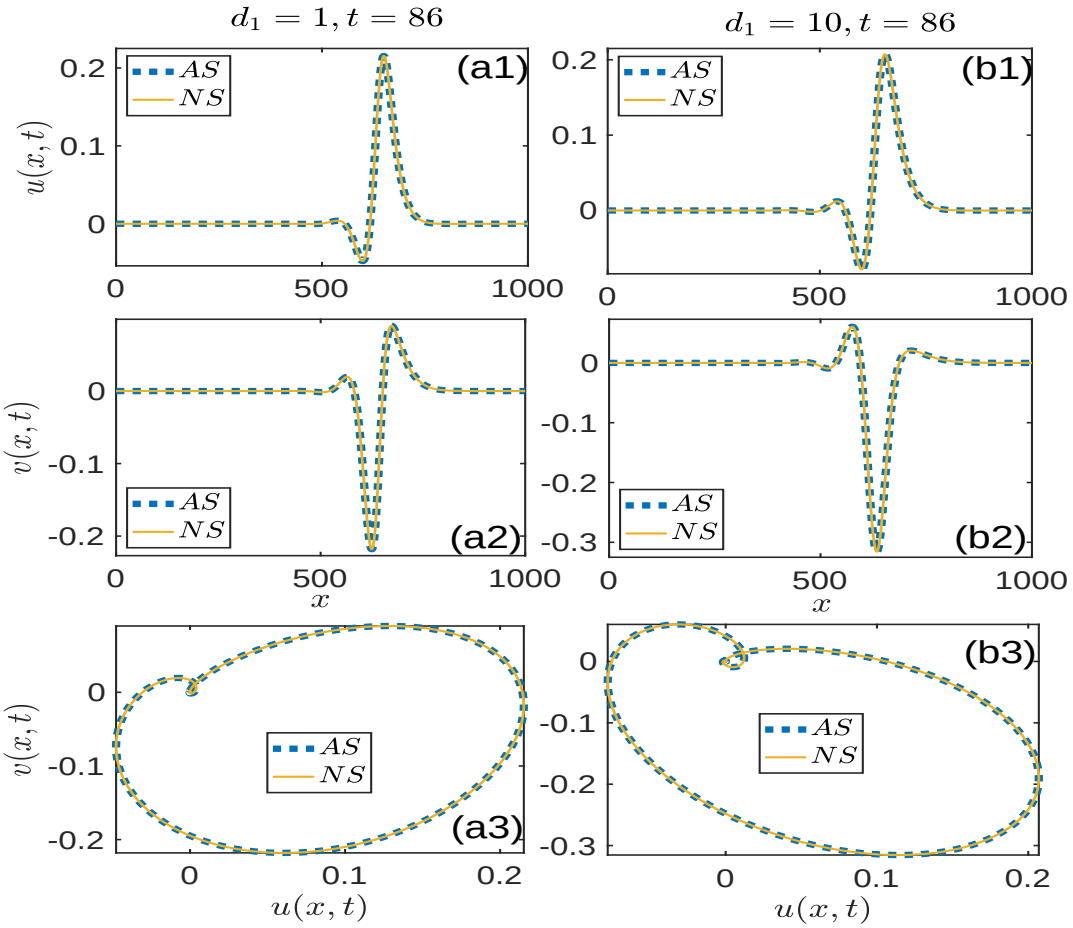

Figure 3.5: Comparison between analytical and numerical solitary pulse profiles of $u(x,t)$ and $v(x,t)$ under the effect of the self-diffusion coefficient d_1, with $d_1 = 1$ [panels (aj)$_{j=1,2,3}$] and $d_1 = 10$ [panels (bj)$_{j=1,2,3}$]. Panels (a3) and (b3) give the phase planes, respective to values of d_1, with the other parameter values being: $(d_2, h_1, h_2 = 6, 6, 6)$, $k = 0.01\pi$, $a = 0.25$, $b = -0.15$, $\gamma = 3.6$, and $\sigma = 0.01$. AS refers to analytical solution (dotted blue line) and NS refers to numerical solution (solid yellow line).

that takes the respective values $d_2 = 1$ [panels (aj)$_{j=1,2}$] and $d_2 = 10$ [panels (bj)$_{j=1,2}$]. In general, as the self-diffusion coefficient d_2 increases, so does the amplitude of cardiac impulse $u(x,t)$. Additionally, the more random the distribution of the ions across the membrane, the narrower the width of the action potential and the larger its amplitude [166]. The random wavering in the sequence of cardiac firing times induces this phenomenon. Moreover, we notice an exact correlation between the analytical and numerical solutions whose amplitude increases, therefore confirming the results in Fig. 3.4 and Fig. 3.5. In addition, the phase planes of Figs. 3.6 (a3) and (b3) support the fact that increasing d_2 tends to suppress lateral oscillations around the main pulses, a behavior

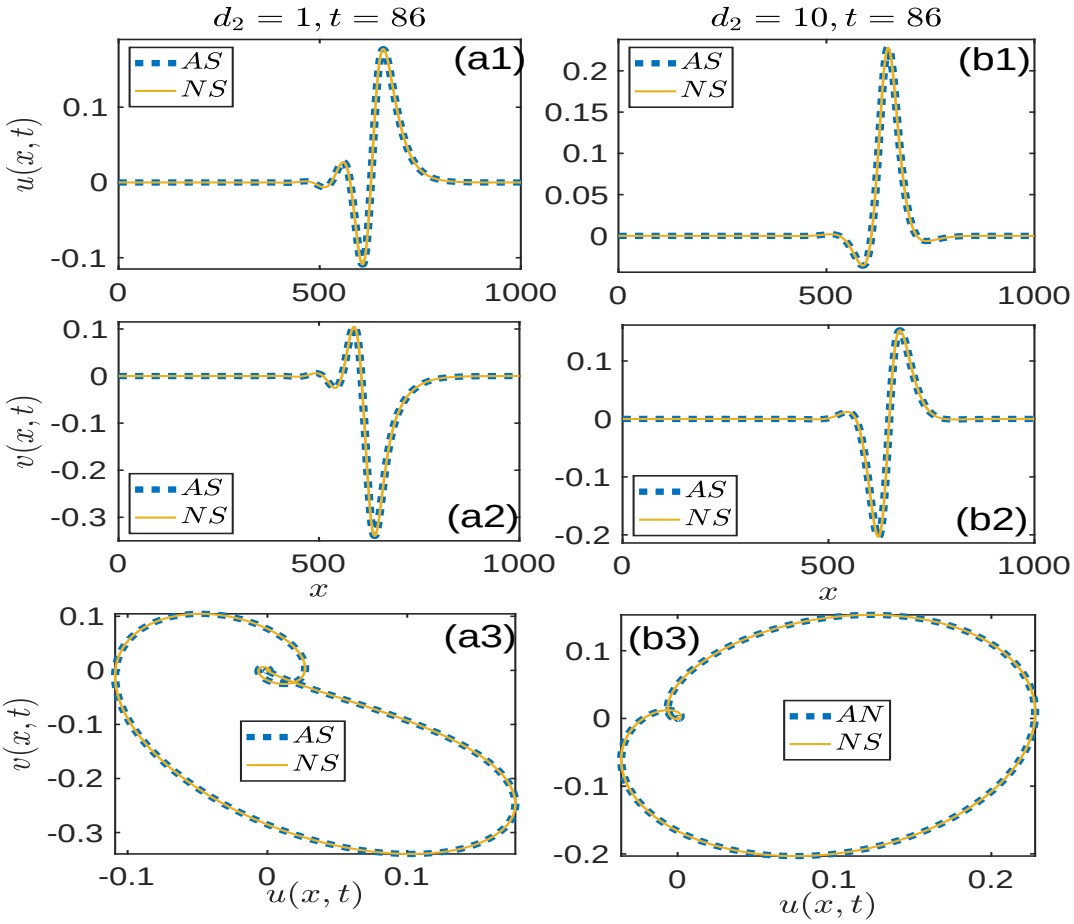

Figure 3.6: Comparison between analytical and numerical solitary pulse profiles of $u(x,t)$ and $v(x,t)$ under the effect of the self-diffusion coefficient d_2, with $d_2 = 1$ [panels (aj)$_{j=1,2,3}$] and $d_2 = 10$ [panels (bj)$_{j=1,2,3}$]. Panels (a3) and (b3) give the phase planes, respective to values of d_1, with the other parameter values being: $(d_1, h_1, h_2 = 6,6,6)$, $k = 0.01\pi$, $a = 0.25$, $b = -0.15$, $\gamma = 3.6$, and $\sigma = 0.01$. AS refers to the analytical solution (dotted blue line), and NS refers to the numerical solution (solid yellow line).

that is mainly triggered by the dynamics of the slow component $v(x,t)$. However, the dynamics remains periodic in both cases.

Figure 1.7 points out the impact and contribution of changing the cross-diffusion parameter h_1. Like in Figs. 3.5 and 3.6, analytical results and numerical simulations are confronted, where $h_1 = 1$ is supported by Fig. 3.7(aj)$_{j=1,2}$ and $h_1 = 10$ is depicted in Fig. 3.7(bj)$_{j=1,2}$. While the pulses' dynamics remains robust for the compound of the FHN model, one notices an increase in the pulse amplitudes, which clearly shows that the action potential of the cardiac tissue is an increasing function of the cross-diffusion coefficient h_1. However, further increasing h_1 leads to slight oscillations around the

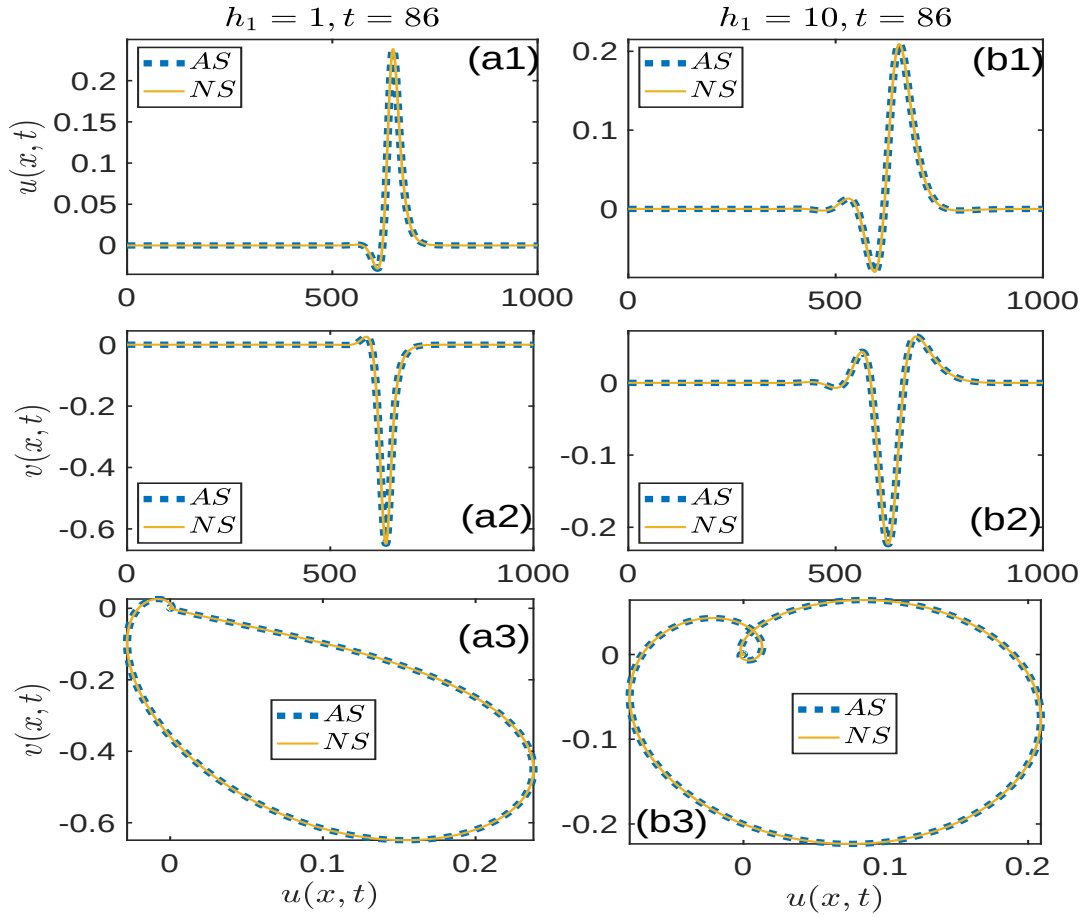

Figure 3.7: Comparison between analytical and numerical solitary pulse profiles of $u(x,t)$ and $v(x,t)$ under the effect of the cross-diffusion coefficient h_1, with $h_1 = 1$ [panels (aj)$_{j=1,2,3}$] and $h_1 = 10$ [panels (bj)$_{j=1,2,3}$]. Panels (a3) and (b3) give the phase planes, respective to values of h_1, with the other parameter values being: $(d_1, d_2, h_2 = 6, 6, 6)$, $k = 0.01\pi$, $a = 0.25$, $b = -0.15$, $\gamma = 3.6$, and $\sigma = 0.01$. AS refers to analytical solution (dotted blue line) and NS refers to numerical solution (solid yellow line).

main pulse peaks as shown in Fig. 3.7(bj)$_{j=1,2}$. On confronting the behaviors of the phase planes corresponding to the two used values of h_1, the phase plane between $u(x,t)$ and $v(x,t)$ shows one cycle for $h_1 = 1$, while the main loop is complemented by a minor inner one for $h_1 = 10$, showing the appearance of additional oscillations around the main pulses [see Figs. 3.7 (a3) and (b3)] as discussed earlier. Along the same line, the impact of the cross-diffusion coefficient is addressed in Fig. 3.8, where panels (aj)$_{j=1,2}$ and (bj)$_{j=1,2}$ correspond to the respective values $h_2 = 1$ and $h_2 = 10$, with all the other parameters being kept fixed. Indeed, the same spectrum of behaviors as in Fig. 3.7 is delivered and confirms the cross-diffusive effects to bring about more oscillations into

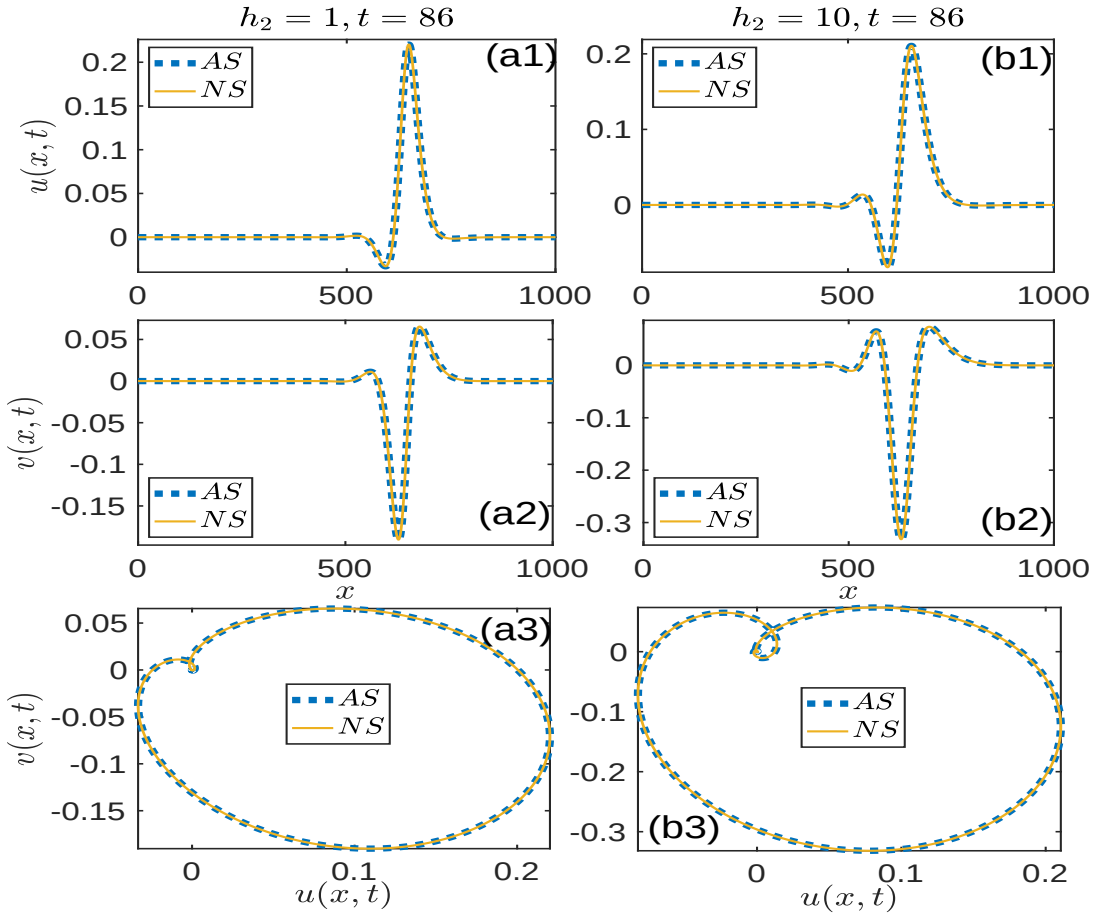

Figure 3.8: Comparison between analytical and numerical solitary pulse profiles of $u(x,t)$ and $v(x,t)$ under the effect of the cross-diffusion coefficient h_2, with $h_2 = 1$ [panels (aj)$_{j=1,2,3}$] and $h_2 = 10$ [panels (bj)$_{j=1,2,3}$]. Panels (a3) and (b3) give the phase planes, respective to values of h_2, with the other parameter values being: $(d_1, d_2, h_1 = 6,6,6)$, $k = 0.01\pi$, $a = 0.25$, $b = -0.15$, $\gamma = 3.6$, and $\sigma = 0.01$. AS refers to analytical solution (dotted blue line) and NS refers to numerical solution (solid yellow line).

the pulse profiles, as testified by the enclosed phase planes. Such behaviours also give the room to discuss the bistability brought by the cross-dispersion that was already identified in Ref. [167] as a direct signature of asymmetric wave trains, also known as caused by some fluctuations in the sequences of myocardial cells firing instants [168].

In order to assess the nontrivial effects of the cross-diffusion described so far, we have switched off self-diffusive effects, i.e., $d_1 = d_2 = 0$, in the system for the results of Fig. 3.9 to be recorded. In such a context, when $h_1 = h_2 = 1$, one observes the features of Fig. 3.9 (aj)$_{j=1,2}$, where the action potential dynamics is governed by a breather soliton, also known in many physical systems, in the reductive perturbation method, as the solution

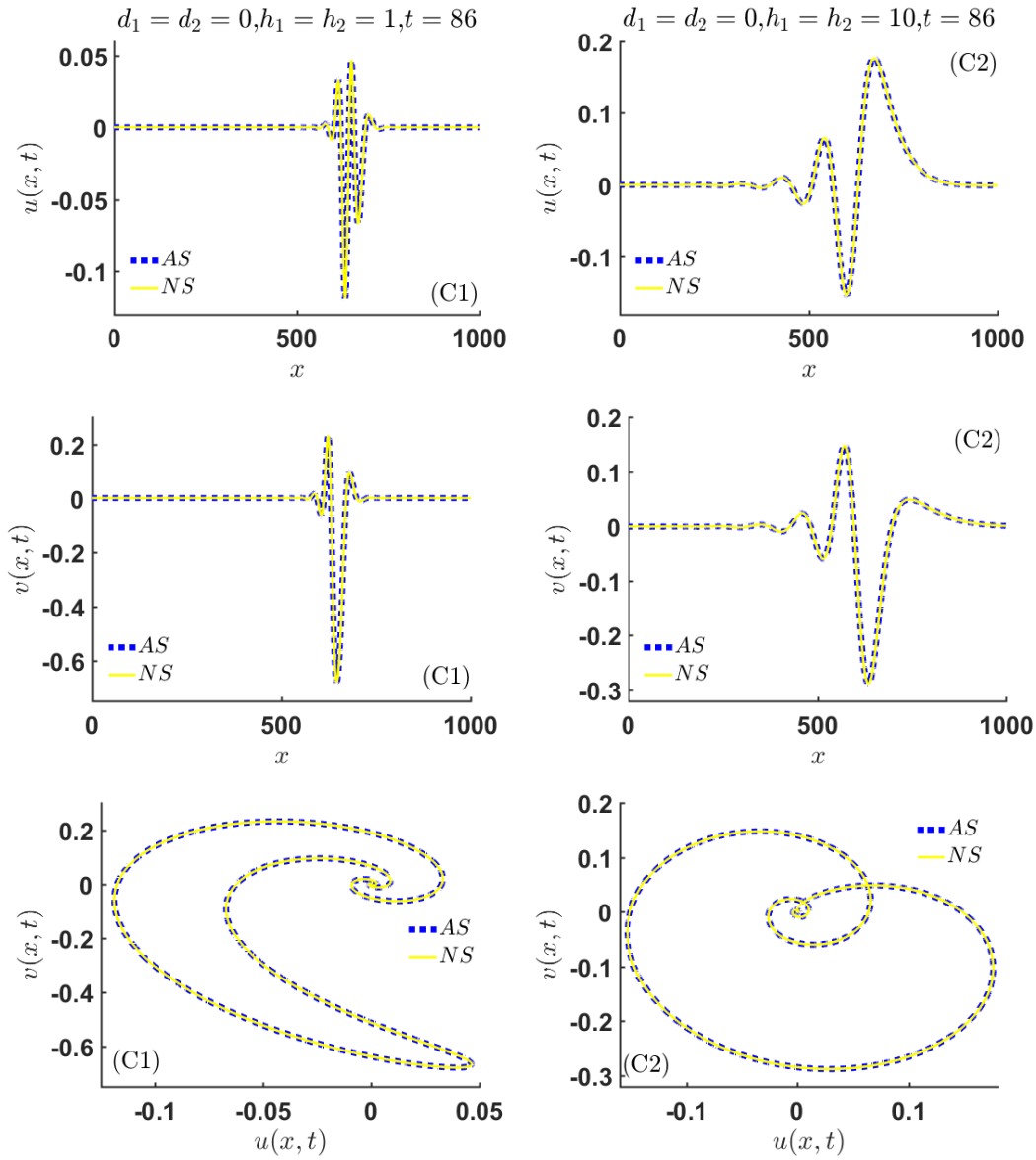

Figure 3.9: Comparison between analytical and numerical solitary pulse profiles of $u(x,t)$ and $v(x,t)$ under the effect of the cross-diffusion coefficients h_1 and h_2 in the absence of self-diffusive effects, i.e., $d_1 = d_2 = 0$, with $h_1 = h_2 = 1$ [panels (aj)$_{j=1,2,3}$] and $h_1 = h_2 = 10$ [panels (bj)$_{j=1,2,3}$]. Panels (a3) and (b3) give the phase planes, respective to values of $h_1 = h_2$, with the other parameter values being: $k = 0.01\pi$, $a = 0.25$, $b = -0.15$, $\gamma = 3.6$, and $\sigma = 0.01$. AS refers to analytical solution (dotted blue line) and NS refers to numerical solution (solid yellow line).

of the NLS equation [169–171]. Compared to other results in the paper, the number of oscillations in the pulse's profile has increased due to the absence of the self-diffusions. The same behaviour is also perceptible in the profile of $v(x,t)$, and more interestingly, in their subsequent phase plane that shows a curved single orbit, characteristics of

complex periodic dynamics. On the other hand, the panels of Fig. 3.8 $(\mathrm{bj})_{j=1,2}$ display extended breather solitons along with their asymmetric character, with oscillations in their profiles. This gives rise to two inner loops in their typical phase plane of Fig. 3.8 (b3). One may therefore suspect that the smaller h_1 and h_2, the faster the action potential in the studied model. Indeed, as predicted so far in the linear stability of a plane wave, one may conclude that the obtained patterns may share the same parameter areas with the unstable plane wave solution in the context of MI. This, once more, brings about the evidence shared by the soliton and MI concepts. In the meantime, the reader should be aware that for the MI phenomenon to be efficiently assessed, one should use a perturbed plane wave as the initial condition and observe its longtime evolution. This has been performed in a broad range of RD systems [172–176], with exciting results, and does not constitute the primary objective of this work.

3.3 Effect of the temperature variation in the FitzHugh-Nagumo cardiac model through the cubic-quintic Complex Ginzburg-Landau equation

3.3.1 Hirota Bilinear Method. Case 2 : K, $\Omega \neq 0$.

A hole wave solution for this case, can be obtained following the system of equations

$$\frac{f^3}{rg}(iD_{n,\tau} + 2iKpD_{n,x} + pD_{n,\xi}^2 + \Omega - pK^2 - \lambda - \mu)(g\cdot f) = hf, \tag{3.30a}$$

$$f^2\{(\frac{n(n+1)pD_{n,\xi}^2}{2r} + \frac{i\gamma-\lambda}{r})(f\cdot f) + \frac{(q-\mu)|g|^2}{r}\} + |g|^4 = hg. \tag{3.30b}$$

Here, h is a random function which is introduced in order to decouple the equation. By configuring the system to be zero, we are able to impose restrictions on the terms of each bracket seperately. We obtain a system involving two distinct bilinear components:

$$(iD_{n,\tau} + 2iKpD_{n,\xi} + pD_{n,\xi}^2 + \Lambda - pK^2 - \lambda - \mu)(g\cdot f) = 0, \tag{3.31a}$$

$$f^2\left\{\left(\frac{n(n+1)pD_{n,\xi}^2}{2r} + \frac{i\gamma-\lambda}{r}\right)(f\cdot f) + \frac{(q-\mu)|g|^2}{r}\right\} - |g|^4 = 0. \tag{3.31b}$$

To look for the hole type wave solution, we assume that the functions f and g can be written as:

$$g = g_1(1-e^{\theta_0}),\ f = 1+e^{\theta_0}, \tag{3.32}$$

where $\theta_0 = 2\kappa x$. Because of the presence of the term $|g|^4$, the right hand-side of Eq. (3.31b) suggests that all coefficients of the corresponding equation should be real.

By taking into account Eq. (3.31b) at the order $e^{0\times\theta_0}$, $Im\left(\frac{n(n+1)p}{2r}\right) = Im\left(\frac{i\gamma-\lambda}{r}\right) = Im\left(\frac{q_r-\mu}{r}\right) = 0$, leads to:

$$\begin{aligned} &\alpha = -\beta \pm \sqrt{\beta^2+2},\ \beta = \frac{3(p_r r_r + p_i r_i)}{2(p_r r_i - p_i r_r)}, \\ &r_i(\lambda_r+\gamma_i) = r_r(\lambda_i-\gamma_r),\ r_r(q_i-\mu_i) = r_i(q_r-\mu_r) \end{aligned} \tag{3.33}$$

with ($\lambda_r = -\gamma_i$, $\lambda_i = \gamma_r$, $\mu_i = q_i$,$\mu_r = q_r$). Additionally, solving the remainder of Eq. ((3.31b) at the order e^{θ_0}, yields

$$|g_1|^4 = -\frac{\kappa^2}{A}, with\ A = \frac{(p_r r_r + p_i r_i)}{|p|^2(2-\alpha^2)}. \tag{3.34}$$

Eq. (3.31b) at the order $e^{0\times\theta_0}$, after separating into real and imaginary parts, gives:

$$\Lambda = p_r K^2 - \lambda_r - \mu_r, \tag{3.35a}$$

$$\lambda_i = -(p_i K^2 + \mu_i). \tag{3.35b}$$

Writting Eq. ((3.31b) at the order e^{θ_0}, reads:

$$K = \alpha\kappa. \tag{3.36}$$

While, at the order $e^{0\times\theta_0}$, using Eq. (3.32) one obtains:

$$|g_1|^4 = \frac{\gamma_r - \lambda_i}{r_i}, \tag{3.37a}$$

$$|g_1|^4 = -(\frac{\gamma_i + \lambda_r}{r_r}). \tag{3.37b}$$

Inserting Eq. (3.37b) into Eq. (3.35a), and Eq. (3.36) into Eq. (3.34), then equating Eq. (3.34) and Eq. (3.37b), one arrives at the following results:

$$\Lambda = p_r K^2 - r_r|g_1|^4 + \gamma_i - q_r, \tag{3.38}$$

$$-\frac{\kappa^2}{A} = \frac{\gamma_r + p_i K^2 + q_i}{r_i}, \tag{3.39}$$

$$\kappa^2 = -\frac{A(\gamma_r + q_i)}{r_i + A\alpha^2 p_i}. \tag{3.40}$$

Hence we get a soliton solution as:

$$\psi(\xi,\tau) = \frac{g_1(1-e^{2\kappa\xi})e^{i(K\xi-\Lambda\tau)}}{(1+e^{2\kappa\xi})^{(1+i\alpha)}}. \tag{3.41}$$

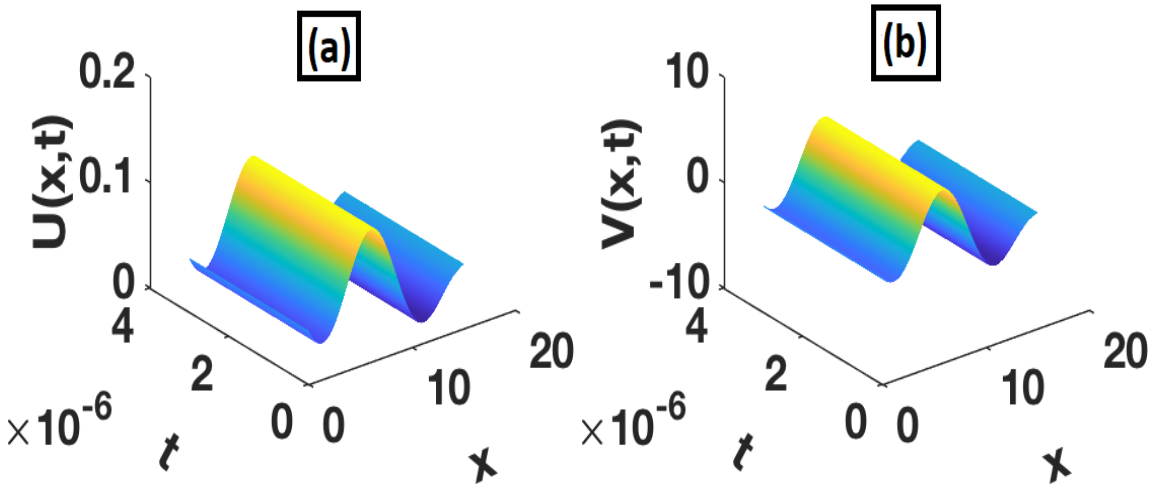

Figure 3.10: (Color online) Spatiotemporal evolutions of (a) $u(x,t)$ and (b) $v(x,t)$, with $T_1 = 2.02$, $T_2 = 2.05$. Other parameters are as in Fig. 2.3 .

Based on the above results on the Hirota's scheme and taking into consideration Eqs.(2.8a)-(2.8b), the solutions for the generic model Eqs.(2.3a)-(2.3b) are expressed as

$$u(x,t) = 2\epsilon(\cos(kx-\omega_r t)\psi_r - \sin(kx-\omega_r t)\psi_i)e^{(\omega_i t)} + O(\epsilon^2), \tag{3.42a}$$

$$v(x,t) = 2\epsilon((\alpha_r\psi_r - \alpha_i\psi_i)\cos(kx-\omega_r t) - (\alpha_r\psi_i + \alpha_i\psi_r)\sin(kx-\omega_r t))e^{(\omega_i t)} + O(\epsilon^2). \tag{3.42b}$$

With $\psi_r = Re(\psi)$ and $\psi_i = Im(\psi)$. In the remainder, the relationship between the pair of variables (ξ,τ) and (x,t) is given by $(\xi,\tau) = \left(\epsilon^2(x-v_g t), \epsilon^4 t\right)$ which implies that solutions Eqs. (3.42a)-(3.42b) only depends on x and t. This envelope have and oscillatory profile and show that it carries information between nodes with a better coordination of some important cardiac undertaking downstream, and pathological situations upstream [161, 162].

The solutions for the generic model Eqs.(2.3a)-(2.3b) are obtained using Eqs.(2.8a)-(2.8b). Figures (3.10a) and (3.10b) illustrate the spatiotemporal evolutions of $u(x,t)$ and $v(x,t)$ of Eqs. (3.42a)-(3.42b). These profiles provide insights into the bioelectrical dynamics, including wave propagation and substance diffusion within the cardiac system. Furthermore, they are indeed similar to the signals observed in electrocardiograms [161, 162].

3.3.2 Modulational instability processess. Case 2 : Perturbation in amplitude and phase

In Ref.[151, 177], the MI criterion has been derived through the discrete CCGL equation. Here, we apply the similar approach to investigate the MI phenomenon through the CQCGL equation Eq. (2.35). We then, propose to construct the solution of the Eq. (2.35)in the form of a plane wave with

$$\psi(\xi,\tau) = \phi_0 e^{i\theta_1}. \tag{3.43}$$

where, $\theta_1 = qx - \omega_0 t$, q and ω_0 corresponding to the wave number and angular frequency of the unperturbed plane wave. We performed linear stability analysis on Eq. (2.35) and we introduce Eq. (3.43) into it by deriving the plane wave on the aforementioned variables and we obtain:

$$(\omega_0 - Pq^2 + Q|\phi_0|^2 + R|\phi_0|^4 - i\gamma)\phi_0 = 0. \tag{3.44}$$

We split the above equation into real and imaginary parts and we have:

$$\omega_0 - P_r q^2 + Q_r|\phi_0|^2 + R_r|\phi_0|^4 + \gamma_i = 0, \tag{3.45a}$$

$$-P_i q^2 + Q_i|\phi_0|^2 + R_i|\phi_0|^4 - \gamma_r = 0. \tag{3.45b}$$

Eq. (3.45a) point out the nonlinear dispersion relation since it depends on both ω_0 and the wave amplitude ϕ_0. The stability of the above-mentioned solutions is examined and modulated with a slight perturbed system given by [178]:

$$\psi(\xi,\tau) = (\phi_0 + b(x,t))e^{(i\phi(x,t)+i\theta_1)} + cc. \tag{3.46}$$

in which, $b(x,t)$ and $\phi(x,t)$ account for perturbation and phase perturbation and are supposed to be small in comparison to the plane wave amplitude ϕ_0 and the angle θ_1 [160, 177, 179]. That is $b_c(x,t) = b^*(x,t)$ and $\phi_c(x,t) = \phi^*(x,t)$ where star * represent the complex conjugate. Assuming this, we introduce Eq. (3.46) into Eq. (2.35), and taking into account Eq. (3.45a) (retracted twice), then separating the obtained equation into real and imaginary parts, we get:

$$\begin{aligned}
&-\phi_0\left(\frac{\partial}{\partial t}\phi(x,t)\right) - 2P_m q\left(\frac{\partial}{\partial x}b(x,t)\right) - 2P_r q\phi_0\left(\frac{\partial}{\partial x}\phi(x,t)\right) - P_m\phi_0\left(\frac{\partial^2}{\partial x^2}\phi(x,t)\right) + P_r\frac{\partial^2}{\partial x^2}b(x,t)\\
&+(\gamma_r\phi_0 - 2Q_m{\phi_0}^3 + q^2P_m\phi_0 - 3R_m{\phi_0}^5)\phi(x,t) + (Q_m{\phi_0}^3 + 2R_m{\phi_0}^5)\phi_c(x,t)\\
&+(\omega_0 + \gamma_m + 2Q_r{\phi_0}^2 - q^2P_r + 3R_r{\phi_0}^4)b(x,t) + (Q_r{\phi_0}^2 + 2R_r{\phi_0}^4)b_c(x,t) = 0.
\end{aligned} \tag{3.47}$$

$$-(\frac{\partial}{\partial t}b(x,t))-2P_mq\phi_0(\frac{\partial}{\partial x}\phi(x,t))+2P_rq(\frac{\partial}{\partial x}b(x,t))+P_m(\frac{\partial^2}{\partial x^2}b(x,t))+P_r\phi_0\frac{\partial^2}{\partial x^2}\phi(x,t)$$
$$+(-\gamma_r+2Q_m{\phi_0}^2-q^2P_m-3R_m{\phi_0}^4)b(x,t)+(Q_m{\phi_0}^2+2R_m{\phi_0}^4)b_c(x,t)$$
$$+(\omega_0\phi_0+\gamma_m+2Q_r{\phi_0}^3-q^2P_r\phi_0+3R_r{\phi_0}^5)\phi(x,t)-(Q_r{\phi_0}^3+2R_r{\phi_0}^5)\phi_c(x,t)=0. \tag{3.48}$$

These equations are the perturbation equations which admits solution in the form of a combination of progressive and progressive waves:

$$\begin{bmatrix} b(x,t) \\ \phi(x,t) \\ b_c(x,t) \\ \phi_c(x,t) \end{bmatrix} = \begin{bmatrix} b_1 & b_2 \\ \phi_1 & \phi_2 \\ b_2 & b_1 \\ \phi_2 & \phi_1 \end{bmatrix} \begin{bmatrix} e^{i\theta_2} \\ e^{-i\theta_2^*} \end{bmatrix}. \tag{3.49}$$

Herein, $\theta_2 = \Gamma x + \Omega_1 t$, and θ_2^* the conjugate complex; where Γ and Ω_1 represent the wave number and the angular frequency of the perturbation, respectively and $\Omega_2 = -\Omega_1$. Furthermore, b_1, ϕ_1 and b_2, ϕ_2 stating the constant complex amplitudes and phases likewise their complex conjugate, respectively. By inserting solution Eq. (3.49) into Eqs. (3.47)-(3.48) and after linearization around the disturbed plane wave, yields the linear system:

$$\begin{bmatrix} a_{11} & a_{12} & a_{13} & a_{14} \\ a_{21} & a_{22} & a_{23} & a_{24} \\ a_{31} & a_{32} & a_{33} & a_{34} \\ a_{41} & a_{42} & a_{43} & a_{44} \end{bmatrix} \begin{bmatrix} \phi_1 \\ b_1 \\ \phi_2 \\ b_2 \end{bmatrix} = \begin{bmatrix} 0 \\ 0 \\ 0 \\ 0 \end{bmatrix}. \tag{3.50}$$

Taking into account that all the coefficients are given in the Appendix **(B)**, the system of Eqs. (3.47)-(3.48), admits a nontrivial solution if its determinant is nil. This thus, leads us to a dispersion relation with a fourth-order polynomial:

$$A_0\Omega_1^4 + A_1\Omega_1^3 + A_2\Omega_1^2 + A_3\Omega_1 + A_4 = 0. \tag{3.51}$$

The expressions of the coefficients of Eq. (3.51) , A_0, A_1, A_2, A_3 and A_4 are expressed in Appendix **(C)**. To solve this quartic polynomial given by Eqs. (3.51), we use the Ferrari's method [180], and find the reduced solution of this equation. In contrast to the analogous condition for a continuous system, the stability condition depends on the wave vector q and the perturbation wave vector Γ. This is specific to the discretized complex Ginzburg-Landau equation. It is worth noticing that, $\Omega_i < 0$, so that $\lim_{t\to\infty} e^{-\Omega_i t} \longrightarrow \infty$ and that the instability criterion holds. The MI growth rate is reduced into $G = Max(-\Omega_i)$ $(i = 1,2,3,4)$ [151]. The mathematical expression are given in Appendix **(D)**.

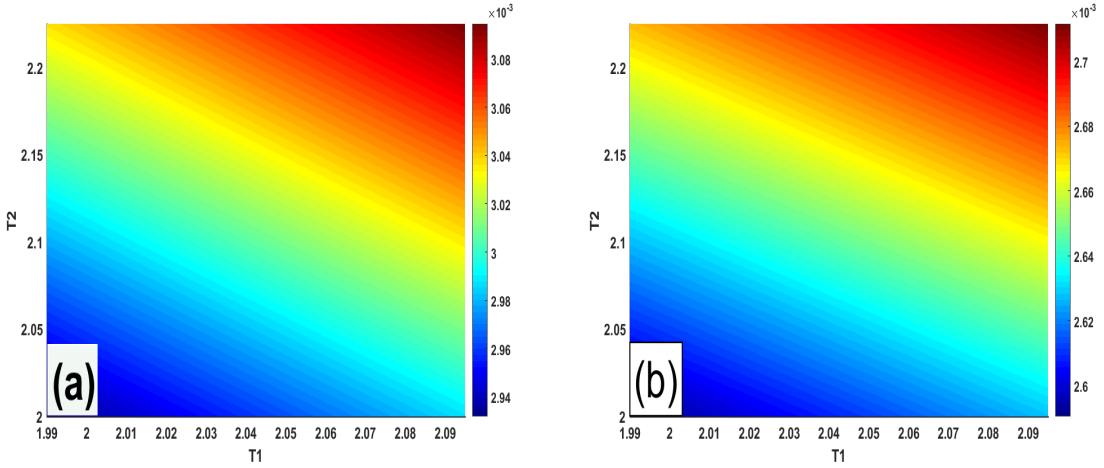

Figure 3.11: (Color online) Growth rate as a function of thermo-electric couplings T_1 and T_2. (a) presence of cross-diffusion $h_1 = h_2 = 2.1$, (b) absence of cross-diffusion $h_1 = h_2 = 0$. Other parameters are the same as in Fig. 3.10 .

Figure 3.11 presents the growth rate as a function of the thermo-electric couplings T_1 and T_2. One clearly observes that the amplitude of the MI growth rate increases with T_1 and T_2. However, the MI growth rate takes larger values in the presence of cross-diffusion terms in Fig. 3.11(a) than in Fig. 3.11(b) where there are no cross-diffusion terms. This suggest that cross-diffusion coupled to temperature terms leads to the destabilization of the system. From a biological point of vue, such couplings could impact the normal excitability, ionic imbalances, nature of the proteins and energy efficiency.

3.3.3 Discussion 2

In this section, we numerically solve the system Eqs. (2.3a)-(2.3b) as numerical simulations mimic the experiment. The motivation is to verify the validity of the analytical solutions constructed above since only stable solutions are likely to be seen in experiments. To this end, we use the fourth-order Runge-Kutta computational scheme applied to the spatial discretization employing the central difference formula with absorbing boundary conditions. We set the temporal and the spatial coordinates discretization steps to $\Delta t = 10^{-6}$ and $\Delta x = 0.01$, respectively. The initial conditions are solutions Eqs. (3.42a)-(3.42b) at $t = 0$. Panels (a)-(d) and (e)-(h) of Fig. 3.12 display snapshots at $t = 101, 201, 301, 401$ μs of $u(x,t)$ and $v(x,t)$, respectively. Our analytical predictions corroborate the numerical solutions with a pretty much good agreement. Top peaks of $U(x,t)$ reflects depolarization, while it return to baseline marks repolarization. Since the duration of standard electrocardiograms of $u(x,t)$ lies in the interval $[200, 400]$ ms,

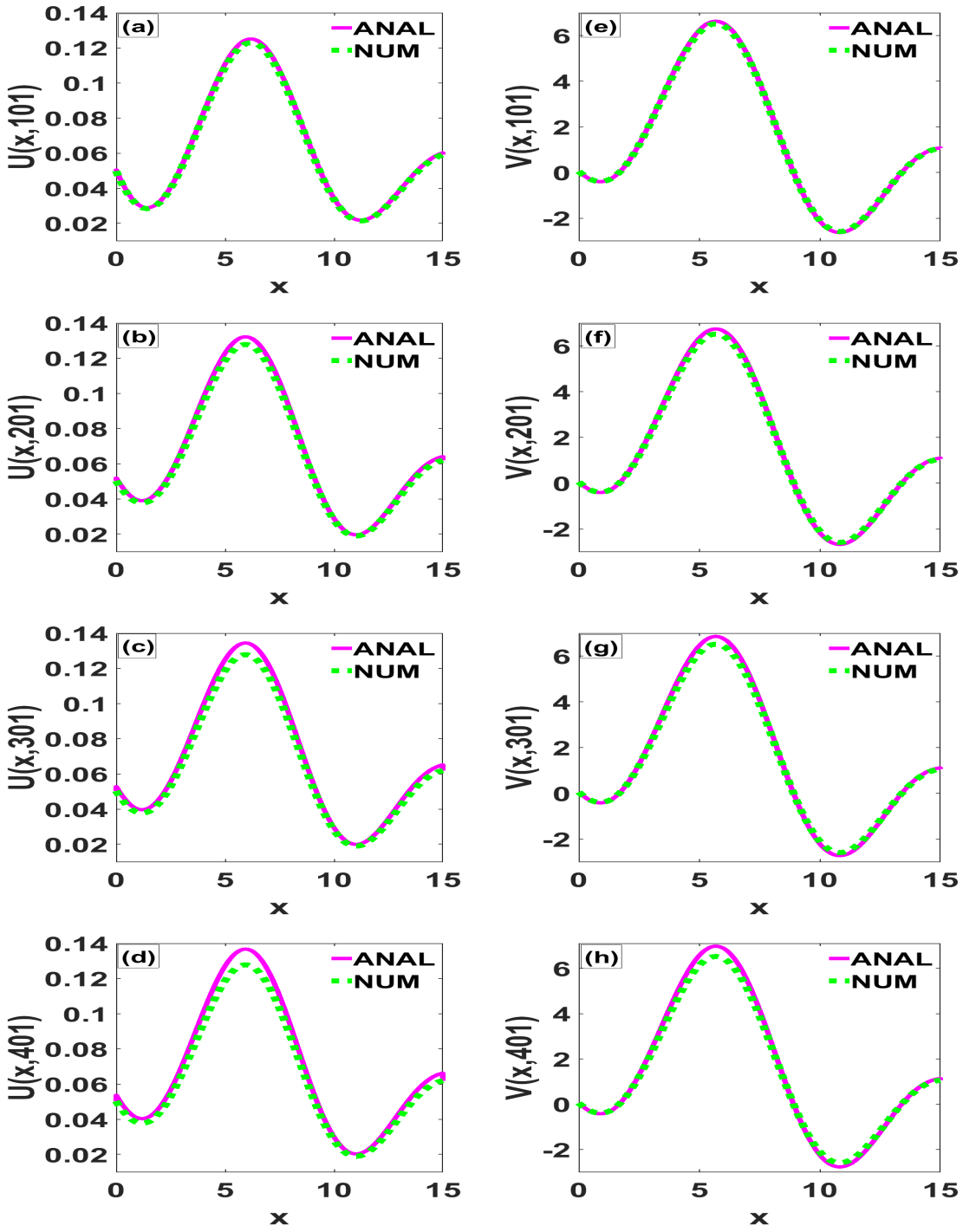

Figure 3.12: (Color online) Snapshots at different times of analytical vs numerical solutions. Panels $(a)-(d)$ for $u(x,t)$, $(e)-(h)$ for $v(x,t)$. $T_1 = 1.99$ and $T_2 = 2.05$. Other parameters are as in Fig. 3.10 . Analytical solutions agreed to numerical ones with high accuracy.

this suggests that our solutions are good candidates, that could better explain electrocardiograms of persons. It highlights the emergence of travelling waves, characteristic

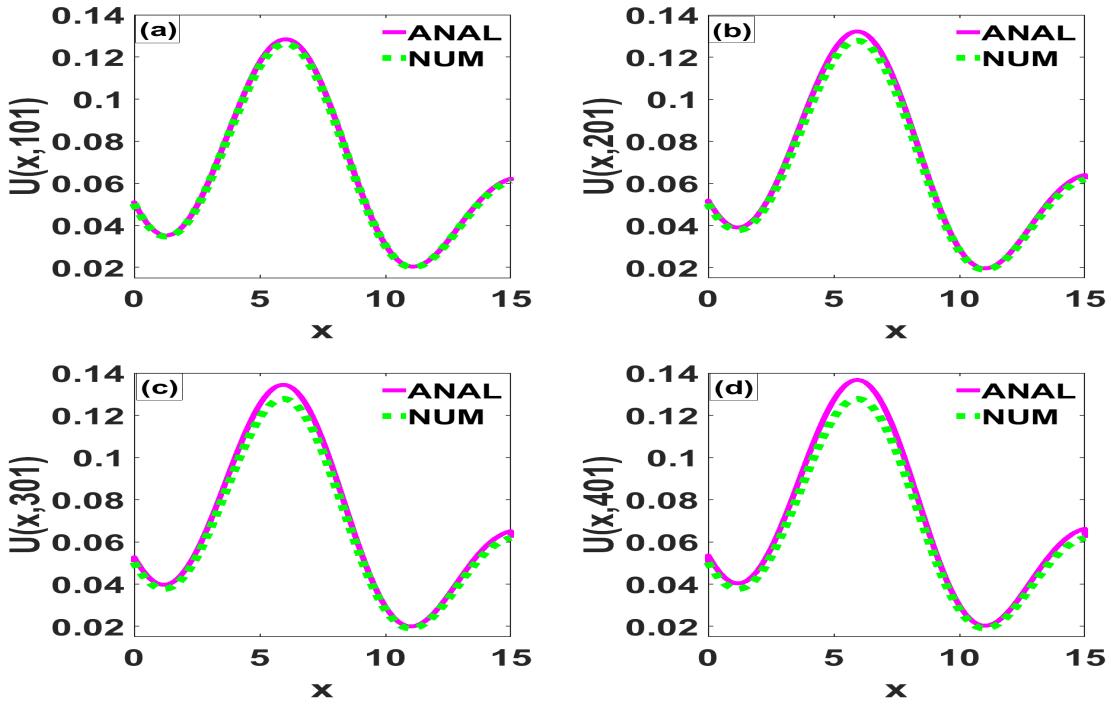

Figure 3.13: (Color online) Snapshots at different times of analytical vs numerical solutions of $u(x,t)$. $T_1 = 2.02$, $T_2 = 2.05$. Other parameters are as in Fig. 3.10 . Analytical solutions agreed to numerical ones with high accuracy.

of excitable media and linked to action potential propagation. We observe in Figs. 3.13 ($T_1 = 2.02$) and 3.14 ($T_1 = 2.10$) that the amplitude of the action potential decreases accompanied by a rightward shift of the peaks compared to Fig. 3.12 ($T_1 = 1.99$). As a result, the intensity of the electrical impulse diminishes, which slows down myocardial activity. When T_1 increases, the durations of depolarization and repolarization also increase, respectively. Such a situation suggests an increase of risk of fibrillation which prevents effective contraction of the atria and ventricles [181]. It is well known that a change on the membrane potential behavior stems from a modification of enzymatic activity. One may infer that a shrink of the membrane potential amplitude induces a reduction of the enzymes activity in other words an energy reduction involved in the regulation of ionic concentrations such as Na^+/K^+−ATPase and Ca^{2+}−ATPase. This ionic imbalance affects the conductance of ions channels, particularly K^+ transport across the membrane.

Regarding Fig. 3.15 ($T_2 = 2.00$) compared to Fig. 3.12 ($T_2 = 2.05$), the amplitude behavior remains unchanged above $x > 5$, with a slight decrease in amplitude and a minor rightward shift [182], confirming that the amplitude increases with increasing values of

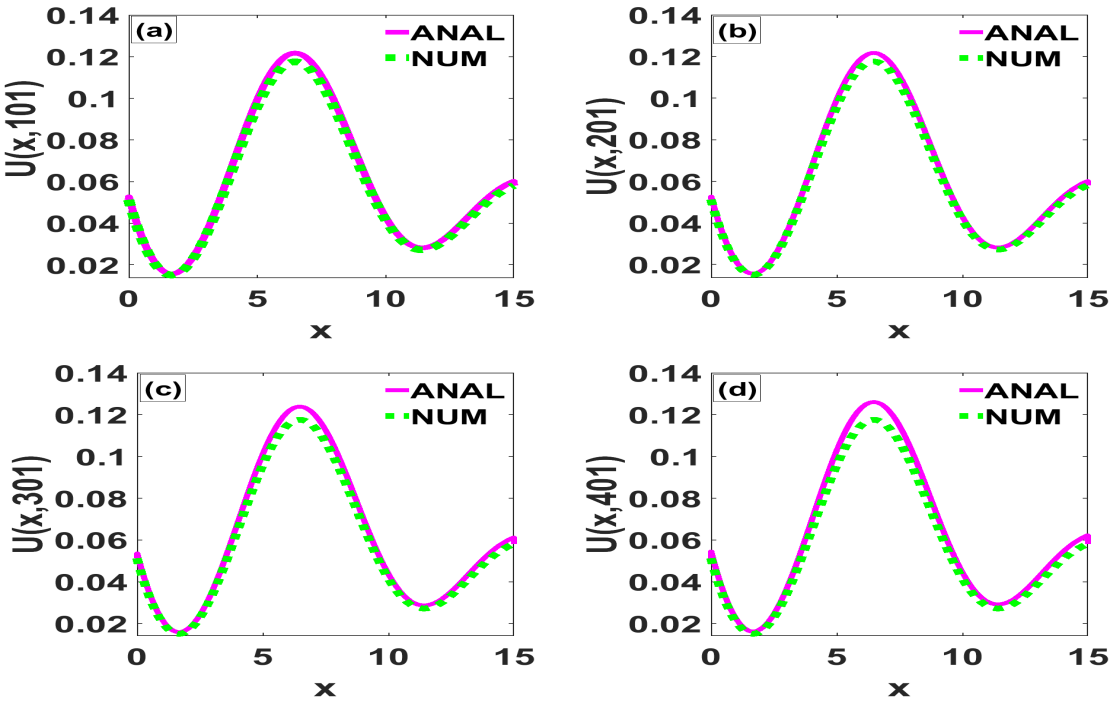

Figure 3.14: (Color online) Snapshots at different times of analytical vs numerical solutions of $u(x,t)$. $T_1 = 2.10$, $T_2 = 2.05$. Other parameters are as in Fig. 3.10 . As T_1 increases, the amplitude of the action potential decreases in comparison to lower values (see Fig. 3.10 , $T_1 = 1.99$).

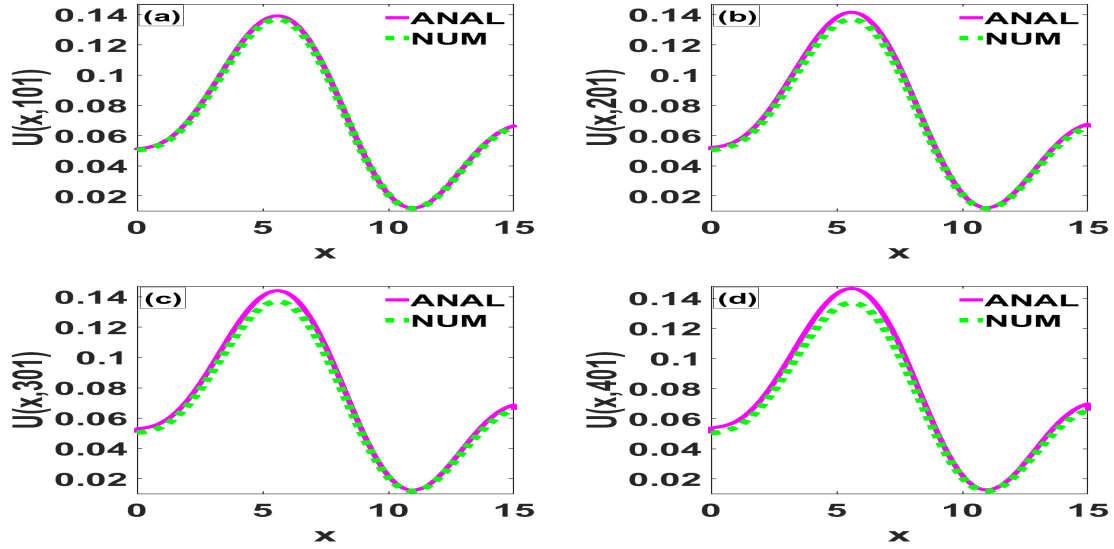

Figure 3.15: (Color online) Snapshots at different times of analytical vs numerical solutions of $u(x,t)$. $T_2 = 2.00$, $T_1 = 2.02$. Other parameters are as in Fig. 3.14 . At large value of T_2, absence of the Q-wave and amplitude increases in comparison to lower values as in Fig. 3.10 where $T_1 = 1.99$.

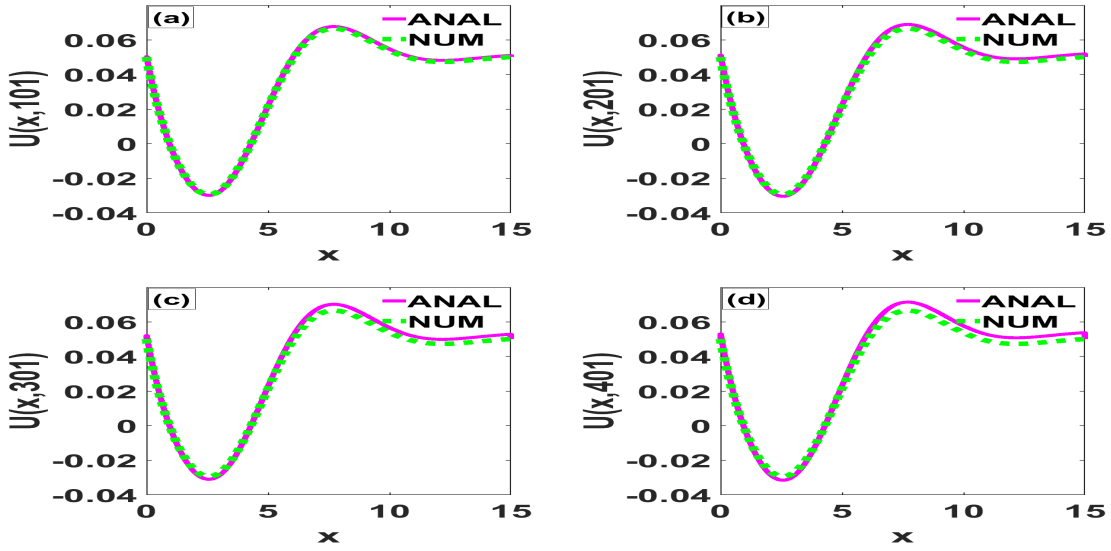

Figure 3.16: (Color online) Snapshots at different times of analytical vs numerical solutions of $u(x,t)$. $T_2 = 2.23$, $T_1 = 2.02$. Other parameters are as in Fig. 3.10 . Action potential becomes negative as T_2 increases in comparison to lower values (see Fig. 3.15 , $T_2 = 2.00$).

T_2. This indicates a reduction in cellular excitability, likely due to an insufficient stimulus at the plasma membrane. Furthermore, the absence of the $Q-$wave when $x < 3$, suggests that the alteration of the initial depolarization of the left ventricle reduces the visible impact of the initial phase. Biologically, this may be due to ischemia or infartus. Moreover, upon closer examination of panels (a)-(d) of Fig. 3.16 ($T_2 = 2.23$), the action potential appears negative for some value of x due to the predominance of intracellular K^+ ions [183]. This reduces the cell's excitability and corresponds to the activation treshold of L-type voltage-dependent Ca^{2+} channels at approximately -30 mV [184]. Negative action potential translates to cardiac rhythm disturbance, conduction delay, genetic mutations, primarily caused by hyperkalemia, hyponatremia, and the desynchronization of electrical conduction, in the excitation-recovery dynamics, which are characteristic precursors of arrhythmias such as cardiac fibrillation.

In cardiac electrophysiology, as this error applies to membrane potential measured in volts, a deviation of 0.03 V (30 mV) could represent a substantial shift, possibly altering the timing of action potentials or the excitability of cardiac cells.

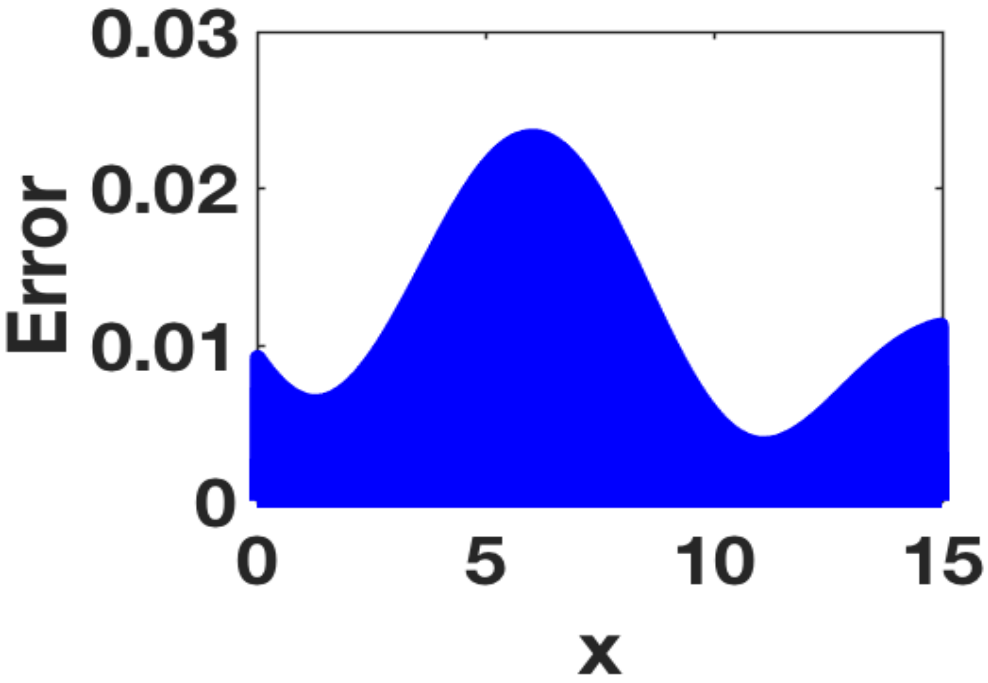

Figure 3.17: (Color online) Snapshot at of the absolute error of $u(x,t)$.

3.4 Effect of Electromagnetic induction in the FitzHugh-Nagumo cardiac model through the cubic-quintic Complex Ginzburg-Landau equation

3.4.1 Hirota Bilinear Method. Case 3 : K, $\Omega \neq 0$.

A hole-type solution for this case, can be obtained following the system of equations

$$\frac{f^3}{rg}\Big\{(iD_{n,\tau}+2iKpD_{n,x}+pD^2_{n,\xi}+\Omega-pK^2-\lambda-\mu)(g\cdot f)\Big\}=hg \tag{3.52a}$$

$$f^2\Big\{(\frac{n(n+1)pD^2_{n,\xi}(f\cdot f)}{2r}+\frac{i\gamma-\lambda}{r})(f\cdot f)+\frac{(q-\mu)|g|^2}{r}\Big\}-|g|^4=hf. \tag{3.52b}$$

h is an arbitrary function which is introduced in order to decouple the equation. Setting the system to be zero, we can restrict terms of each bracket individually and we get:

$$\Big(iD_{n,\tau}+2iKpD_{n,\xi}+pD^2_{n,\xi}+\Lambda-pK^2-\lambda-\mu\Big)(g\cdot f)=0, \tag{3.53a}$$

$$f^2\Big\{(\frac{n(n+1)pD^2_{n,\xi}(f\cdot f)}{2r}+\frac{i\gamma-\lambda}{r})(f\cdot f)+\frac{(q-\mu)|g|^2}{r}\Big\}-|g|^4=0. \tag{3.53b}$$

According to Hirota method the bilinear the operator $D^m_{n,\xi}(g\cdot f)$ is defined by:

$$D^m_{\xi}(g\cdot f)=(\frac{\partial}{\partial n}-z\frac{\partial}{\partial n'})^m g(n,\tau)f(n',\tau')_{|_{n=n',\tau=\tau'}}. \tag{3.54}$$

where, $m=0,1,2$ is a positive integer. Accordingly, the constitutive derivatives, in terms of Hirota's operator are given in [187]. To look for the hole type wave solution, we assumed that the functions f and g can be written as:

$$g=g_1(1-e^{\theta_0}),\ and\ \ f=1+e^{\theta_0}, \tag{3.55}$$

where $\theta_0=2\kappa x$. Because of the presence of the term $|g|^4$, the right hand-side of Eq. 3.53b suggested that all coefficients of the corresponding equation should be real. By taking into account Eq. 3.53b at the order $e^{0\times\theta_0}$, $Im\left(\frac{n(n+1)p}{2r}\right)=Im\left(\frac{i\gamma-\lambda}{r}\right)=Im\left(\frac{q_r-\mu}{r}\right)=0$, which leads to:

$$\begin{aligned}&\alpha=-\beta\pm\sqrt{\beta^2+2},\ \ \beta=\frac{3r_r}{2r_i},\\ &r_i\lambda_r=r_r(\lambda_i-\gamma_r),\\ &r_r(q_i-\mu_i)=r_i(q_r-\mu_r).\end{aligned} \tag{3.56}$$

Herein, we assume that $\lambda_r=0$, $\lambda_i=\gamma_r$, $\mu_i=q_i$ and $\mu_r=q_r$. Additionally, solving the remainder of Eq. 3.53b at the order e^{θ_0}, yields:

$$|g_1|^4=-\frac{\kappa^2}{A},with\ \ A=\frac{r_r}{|p_r|(2-\alpha^2)}. \tag{3.57}$$

The Eq. 3.53a at the order $e^{0\times\theta_0}$, after separating into real and imaginary parts, gives:

$$\Lambda=p_rK^2-\mu_r, \tag{3.58a}$$

$$\lambda_i=-\mu_i. \tag{3.58b}$$

Writing the Eq. 3.53a at the order e^{θ_0}, reads:

$$K=\alpha\kappa. \tag{3.59}$$

While at the order $e^{0\times\theta_0}$, using Eq. 3.53b we derive also:

$$|g_1|^4=\frac{\gamma_r-\lambda_i}{r_i}, \tag{3.60a}$$

$$|g_1|^4=-\frac{\lambda_r}{r_r}. \tag{3.60b}$$

We introduce Eq. 3.60b into Eq. 3.56, and we obtain:

$$\Lambda=p_rK^2-r_r|g_1|^4-q_r. \tag{3.61}$$

On the one hand, substituting λ_i from Eq. 3.55 into Eq. 3.57 one gets:

$$|g_1|^4 = \frac{\gamma_r - \mu_i}{r_i}. \tag{3.62}$$

On the other hand, we equalize the above relation Eq. 3.55 with the one of Eq. Eq. 3.62, we obtain the following results:

$$\kappa^2 = -\frac{A(\gamma_r + q_i)}{r_i}. \tag{3.63}$$

We finally get a Hole-type soliton solution as

$$\psi(\xi,\tau) = \frac{g_1(1-e^{2\kappa\xi})e^{i(K\xi-\Lambda\tau)}}{(1+e^{2\kappa\xi})^{(1+i\alpha)}}. \tag{3.64}$$

Based on the above results on the Hirota's scheme and taking into consideration Eq. (2.37a)-(2.37b)-(2.37c) , the solutions for the generic model Eq. (2.5a)-(2.5b)-(2.5c), are expressed as:

$$\begin{aligned} u(x,t) &= 2\epsilon(\cos(kx-\omega_r t)\psi_r \\ &\quad -\sin(kx-\omega_r t)\psi_i)e^{(\omega_i t)} + O(\epsilon^2), \end{aligned} \tag{3.65a}$$

$$\begin{aligned} v(x,t) &= 2\epsilon((\alpha_r\psi_r - \alpha_i\psi_i)\cos(kx-\omega_r t) \\ &\quad -(\alpha_r\psi_i + \alpha_i\psi_r)\sin(kx-\omega_r t))e^{(\omega_i t)} + O(\epsilon^2), \end{aligned} \tag{3.65b}$$

$$\begin{aligned} \phi(x,t) &= 2\epsilon((\alpha_r\psi_r - \alpha_i\psi_i)\cos(kx-\omega_r t) \\ &\quad -(\alpha_r\psi_i + \alpha_i\psi_r)\sin(kx-\omega_r t))e^{(\omega_i t)} + O(\epsilon^2). \end{aligned} \tag{3.65c}$$

With $\psi_r = Re(\psi)$ and $\psi_i = Im(\psi)$. In remainder, the relationship between the pair of variables (ξ,τ) and (x,t) is given by $(n,\tau) = \left(\epsilon^2(x-v_g t), \epsilon^4 t\right)$ which implied, that the solutions of Eq. (2.37a)-(2.37b)-(2.37c), only depends on the state variables (x,t).

This Fig. 3.18 illustrates the magnetic field characterizing the influence of a moving electric charge and its reciprocal impact on other mobile charges, such as Na^+, K^+, Cl^- and Ca^{2+}. Regarding the latter, the regulation of intracellular calcium by cardiomyocytes plays a crucial role, not only in immediate alterations to action potentials that may lead to potentially arrhythmogenic changes in the myocardium but also in long-term heart failure, as documented in previous studies [188, 189]. The spatiotemporal profiles of the analytical solution as presented in panels (a), (b), and (c) highlight the propagation at the level of cardiac cells. It is observed that the wave is localized in space and propagates in time. Weak vibrations are observed within a certain interval. When the magnetic field significantly approaches this portion of space, strong oscillations emerge due to the high intensity of the electrical current caused by the movement

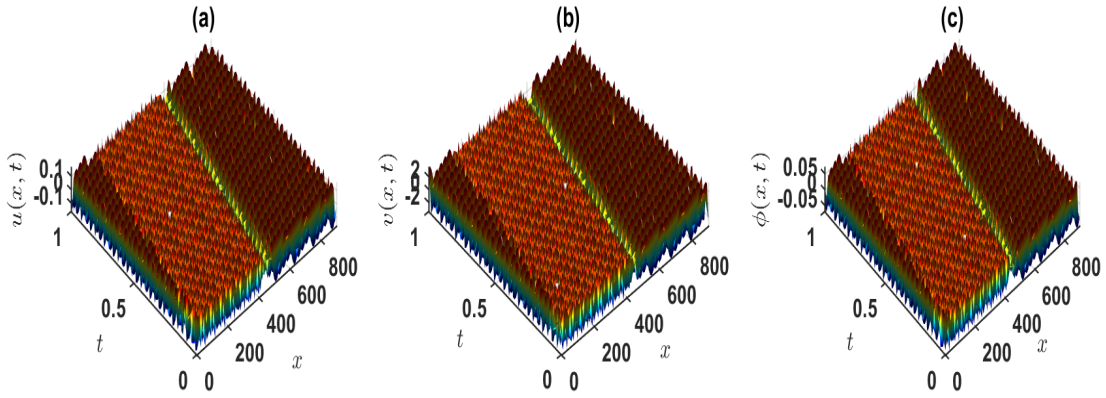

Figure 3.18: Space-time plots of the analytical solutions of Eq. (2.37a)-(2.37b)-(2.37c) are presented for a system comprising 6000 cells. In panel (a), the evolution of the cardiac ionic wave is depicted through the analytical solution for $u(x,t)$. Panel (b) illustrates the plot for the ionic current $v(x,t)$, while panel (c) show cases the flux variable $\phi(x,t)$. The respective planes for these variables are displayed in panels (d), (e) and (f) at a fixed time. These features are captured under fixed parameter values, where a = 0.25, b = -0.15, $\gamma = 3.6$, $\epsilon_0 = 0.01$, $d_1 = 2.0$, $d_2 = 2.0$, K = 8.0, $\alpha = 1.0$, $\beta = -1/6$, $\Gamma = 1/120$, ka0 = 0.64, ka1 = 0.5, ka2 = 1.0.

of charged particles. After the singularity, oscillations are restored and stabilized, resulting in weak interaction.

3.4.2 Modulational instability processess. Case 3 : Perturbation in amplitude and phase

To proceed with our analysis, we assume the plane wave to be solution of Eq. (2.44)

$$\psi(\xi,\tau) = \phi_0 e^{i\theta_1}, \tag{3.66}$$

where, $\theta_1 = q_0 x - \omega_0 t$, q and ω_0 corresponding to the new wave number and angular frequency. We introduce Eq. (3.66) into Eq. (2.44), by deriving the plane wave on the aforementioned variables and we obtain:

$$(\omega_0 - p q_0^2 + q|\phi_0|^2 + r|\phi_0|^4 - i\gamma)\phi_0 = 0. \tag{3.67}$$

We split the above equation into real and imaginary parts and we have:

$$\omega_0 - p_r q_0^2 + q_r|\phi_0|^2 + r_r|\phi_0|^4 = 0, \tag{3.68a}$$

$$q_i|\phi_0|^2 + r_i|\phi_0|^4 - \gamma_r = 0. \tag{3.68b}$$

The Eq. (3.68a), point out the nonlinear dispersion relation since it depends on both ω_0 and the wave amplitude ϕ_0. The stability of the above-mentioned solutions, is examined for slight perturbed system given by [178, 190]:

$$\psi(\xi,\tau) = \left(\psi_0 + \delta\psi\right) e^{i(\nu\xi - \eta\tau)}. \tag{3.69}$$

Where, $\delta\psi$ accounts for the perturbation and its amplitude is supposed to be small in comparison to the plane wave amplitude ψ_0. Supposing this, we introduce Eq. (3.69) into Eq. (2.44), and then separate the obtained equation into real and imaginary parts, leads to:

$$i\frac{\partial\delta\psi}{\partial\tau}+p\frac{\partial^2\delta\psi}{\partial\xi^2}+2i\nu p\frac{\partial\delta\psi}{\partial\xi}+q\psi_0(\psi_0\delta\psi^*+\psi_0^*\delta\psi)+2r|\psi_0|^2\psi_0(\psi_0\delta\psi^*+\psi_0^*\delta\psi)=0. \tag{3.70}$$

A solution to the above equation can be taken in the form:

$$\delta\psi=\delta\psi_1 e^{i(\Gamma\xi+\Omega\tau)}+\delta\psi_2^* e^{-i(\Gamma\xi+\Omega^*\tau)}. \tag{3.71}$$

where, Γ and Ω represent the wavenumber and the angular frequency of the perturbation, respectively. Making use of this in the perturbation Eq. (3.71), one obtains the following homogeneous system for $\delta\psi_1$ and $\delta\psi_2$:

$$(\Omega+c_{11})\delta\psi_1+c_{12}\delta\psi_2=0, \tag{3.72a}$$

$$c_{21}\delta\psi_1+(\Omega+c_{22})\delta\psi_2=0. \tag{3.72b}$$

where

$$\begin{aligned}
c_{11}&=(2\nu\Gamma+\Gamma^2)p-(q+2r|\psi_0|^2)|\psi_0|^2,\\
c_{12}&=-(q+2r|\psi_0|^2)\psi_0^2,\ c_{21}=(q^*+2r^*|\psi_0|^2)(\psi_0^*)^2,\\
c_{22}&=(2\nu\Gamma-\Gamma^2)p^*+(q^*+2r^*|\psi_0|^2)|\psi_0|^2.
\end{aligned}$$

The above system will admit non-trivial solutions under the condition, that its determinants equal to zero, which allows to obtain the nonlinear dispersion relation:

$$\Omega^2+X\Omega+Y=0, \tag{3.73}$$

where $X=c_{11}+c_{22}$ and $Y=c_{11}c_{22}-c_{12}c_{21}$. Solutions of Eq. (3.73) are investigated via its discriminant given by:

$$\begin{aligned}
\Delta=&(2\nu\Gamma p_r)^2-((q_i-2r_i|\psi_0|^2)|\psi_0|^2)^2+(4\nu^2\Gamma^2-\Gamma^4)|p_r|^2-2\Gamma^2(p_rq_r)|\psi_0|^2\\
&-4i\nu\Gamma p_r(q_i+2r_i|\psi_0|^2)|\psi_0|^2+4i\nu\Gamma[-p_rq_i+2(p_rr_i)|\psi_0|^2]|\psi_0|^2-4\Gamma^2(p_rr_r)|\psi_0|^2.
\end{aligned} \tag{3.74}$$

that can be separated into its real and imaginary parts as follows:

$$\begin{aligned}
\Delta_r=&(2\nu\Gamma p_r)^2+(-(q_i+2r_i|\psi_0|^2)|\psi_0|^2)^2+(4\nu^2\Gamma^2-\Gamma^4)|p_r|^2-2\Gamma^2(p_rq_r)|\psi_0|^2\\
&-4\Gamma^2(p_rr_r)|\psi_0|^2,
\end{aligned} \tag{3.75a}$$

$$\Delta_i=4\nu\Gamma p_r(-(q_i+2r_i|\psi_0|^2)|\psi_0|^2)+4\nu\Gamma[(p_rq_i)-2(p_rr_i)|\psi_0|^2]|\psi_0|^2. \tag{3.75b}$$

Based on the above discriminant, the solution of Eq. (3.75b)-(3.76) giving the perturbation angular frequency, is a complex function that can be written in a simplified way as:

$$\Omega = (\chi \pm e_1) + i(\phi \pm e_2). \tag{3.76}$$

Where,

$$\chi = 2\nu\Gamma p_r, \quad \phi = -\left(q_i|\psi_0|^2 + 2r_i|\psi_0|^4\right),$$
$$e_1 = \sqrt{\frac{1}{2}\left(\Delta_r + \sqrt{\Delta_r^2 + \Delta_i^2}\right)}, \quad e_2 = \sqrt{\frac{1}{2}\left(-\Delta_r + \sqrt{\Delta_r^2 + \Delta_i^2}\right)},$$

The previously determined expression of Ω allows us to examine two cases that are related to the sign of the imaginary part of the discriminant Δ_i. So, when $\Delta_i < 0$, the solutions of Eq. (3.78) are Ω_1 and Ω_2 on the one hand. On the other hand, when $\Delta_i > 0$, solutions of Eqs. (3.77a) are $\Omega_1^{'}$ and $\Omega_2^{'}$. Therefore, the two-pairs of solutions are expressed by:

$$\Omega_1 = (\chi + e_1) + i(\phi - e_2), \tag{3.77a}$$
$$\Omega_2 = (\chi - e_1) + i(\phi + e_2), \tag{3.77b}$$
$$\Omega_1^{'} = (\chi - e_1) + i(\phi - e_2), \tag{3.77c}$$
$$\Omega_2^{'} = (\chi + e_1) + i(\phi + e_2). \tag{3.77d}$$

It is remarkable to stress that, solutions $\Omega_1^{'}$ and $\Omega_2^{'}$ have the same asymptotic behavior as those of Ω_1 and Ω_2. As it is well known [117], the sign of the imaginary part of the angular frequency allows us to qualify the development of the MI in the system under studied. To gain a better understanding, let us insert the Eq. (3.71) into the expression of the perturbation $\delta\psi$, and doing so, we obtain:

$$\delta\psi = \delta\psi_1 e^{i(\Gamma\xi + (\chi + e_1)\tau)} e^{-(\phi - e_2)\tau} + \delta\psi_2^* e^{-i(\Gamma\xi + (\chi + e_1)\tau)} e^{(\phi - e_2)\tau}. \tag{3.78}$$

Obviously, the behaviour of the $\delta\psi$ function is influenced by the sign of $(\phi - e_2)$, which represents $Im(\Omega_1)$. Analysing the sign of $(\phi - e_2)$, we observe that if $\phi < 0$, then $(e_2 - \phi) > 0$. As a consequence, the CQCGL equation grows exponentially with time, leading to the instability of the plane wave under modulation. However, if $\phi > 0$, we have $(\phi - e_2) < 0$, i.e. $Im(\Omega_1) < 0$, the CQCGL equation diverges indefinitely as τ increases, and the system is considered to be modulationally unstable. The explicit expression for the imaginary part of Ω_1 is given by:

$$\phi - e_2 = \phi - [\frac{1}{2}\{e_3 + 2\Gamma^2(p_r q_r)|\psi_0|^2 + 4\Gamma^2(p_r r_r)|\psi_0|^4 + e_4\}]^{1/2}. \tag{3.79}$$

with, $e_3 = -\Gamma^2 p_r^2(4\nu^2+\Gamma^2)$, $e_4 = (-(q_i+2r_i|\psi_0|^2)|\psi_0|^2)^2 + 4\nu^2\Gamma^2|p|^2 + \sqrt{\Delta_r^2+\Delta_i^2}$. As the quantity $e_4 > 0$, it happens that: $\phi - e_2 \leq \phi - [\frac{1}{2}\{e_3 + 2\Gamma^2(p_r q_r)|\psi_0|^2 + 4\Gamma^2(p_r r_r)|\psi_0|^4\}]^{1/2}$. Moreover, the inequality $Im(\Omega_1) < 0$ is satisfied if:

$$\phi - [\frac{1}{2}\{e_3 + 2\Gamma^2(p_r q_r)|\psi_0|^2 + 4\Gamma^2(p_r r_r)|\psi_0|^4\}]^{1/2} < 0. \tag{3.80}$$

By giving that, $\phi > 0$ and $e_3 < 0$, the above condition is fulfilled as soon as we have:

$$p_r(q_r + 2r_r|\psi_0|^2) > 0. \tag{3.81}$$

The inequality Iq. (3.81), which represents the MI criterion, while investigating pattern formation in the generalized CQCGL equation. From Eq. (3.68b), the threshold amplitude of an unstable monochromatic wave above which the plane wave breaks into nonlinear patterns is found as:

$$|\psi_0|^2 > |\psi_{0,cr}|^2 = -\frac{q_r}{2r_r}. \tag{3.82}$$

It is important to emphasise that the plane wave amplitude in is expressed as: $|\psi_0|^2 = -(q_i + \sqrt{q_i^2 + 4r_i\gamma_r})/2r_i$, verifies the above condition of Eq. (3.82), when $\nu > 2.8\pi$. In Fig. 2.3, the instability function $\varpi(k) = p_r(q_r + 2r_r|\psi_0|^2)$, according to Eq. (3.81), is plotted against the wavenumber k of the carrier wave for different values of the feedback gain.

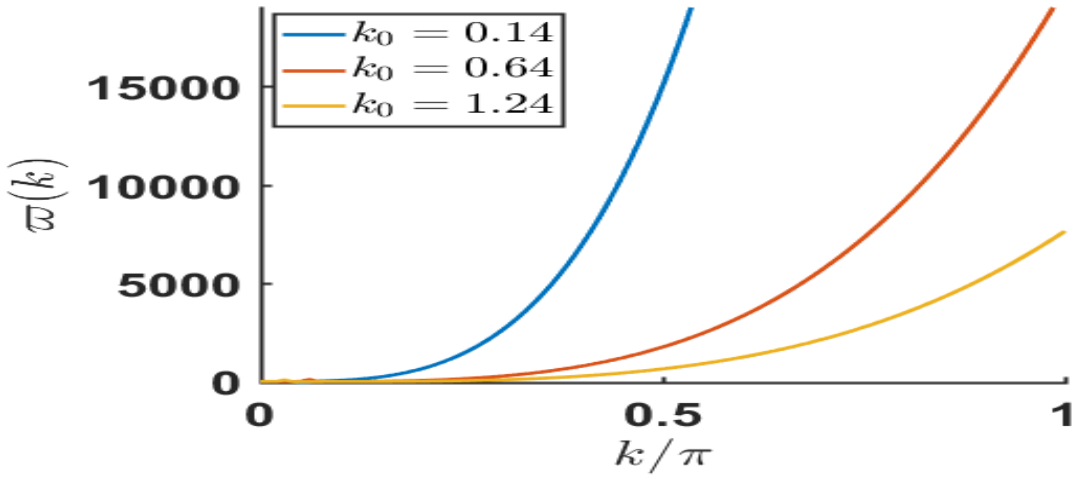

Figure 3.19: The panel show plots of the instability function $\varpi(k) = p_r q_r + 2(p_r r_r)|\psi_0|^2$ against the wavenumber k, under the respective effects of the feedback gain coefficient. Its values are selected in $\{0.14, 0.64, 1.24\}$ range and the remaining parameters are fixed and given by: $d_1 = d_2 = 2$, $\alpha = 1.0$, $\beta = -1/6$, $\Gamma = 1/120$, $a = 0.25$, $b = -0.15$, $\gamma = 3.6$, $\sigma = 0.01$, $K = 8.0$, $ka1 = 1.0$ and $ka2 = 0.5$.

As can be seen, in Fig. 3.19, the $\varpi(k)$ function remains positive regardless of the value of the wavenumber k together with the feedback gain coefficient, thus demonstrating that the plane wave is trivially modulationally unstable. This suggests that these parameters can be used to monitor the appearance of nonlinear localised structures for the action potential within the cardiac cells. For the model studied, the projection indicates that the membrane is trying to adapt to the perturbation, in order to bring the potential back to the steady state. To complete this linear stability analysis, the growth rate of the MI is expressed as:

$$G(\Gamma) = \left| -q_i|\psi_0|^2 - 2r_i|\psi_0|^4 - \sqrt{\frac{1}{2}\left(-\Delta_r + \sqrt{\Delta_r^2 + \Delta_i^2}\right)}\right|. \tag{3.83}$$

Some features of the MI growth rate, using Eq. (3.83), are displayed in Fig. 3.20, where different combinations of the feedback gain parameter values have been used as in Fig. 3.19. Our discussion in this part gives importance to the maximum growth rate of instability that appears to be very sensitive to changes in k_0. For example, the impact of varying k_0 is given by Fig. 3.20, where it is clear that increasing k_0 amplifies the maximum growth rate, in a context where nonlinear patterns are likely to appear in regions of weak wavenumber Γ. We also observe the same spectrum of behaviors which can be specifically attributed to the variations of the feedback gain coefficient. When parameters are chosen properly within the instability zone, the transmembrane potential is expected to exhibit nonlinear oscillations. These oscillations are crucial in understanding cardiac signals, magneto-cardiograms and electrocardiograms [191]. If the magnitude of the MI growth rate decreases, the instability tends to disappear. Since the soliton train is generated by the SA node, energy decreases over time, preventing wave pattern formation in cardiac tissue. Tabi et *al*. [124] discussed the importance of plane wave perturbation to generate spiral waves in the FHN cardiac model, celebrating balanced contributions from nonlinear and dispersive effects. However, the application of an induced magnetic field was shown to drastically modify the appearance of MI through the growth rate and spatiotemporal evolution. This reinforces the idea that MI and solitary waves are straightforwardly related and share the same parameter space [160]. That constitutes a profound motivation to look for comparison between numerical and analytical solutions for the studied model, as proposed in the next section.

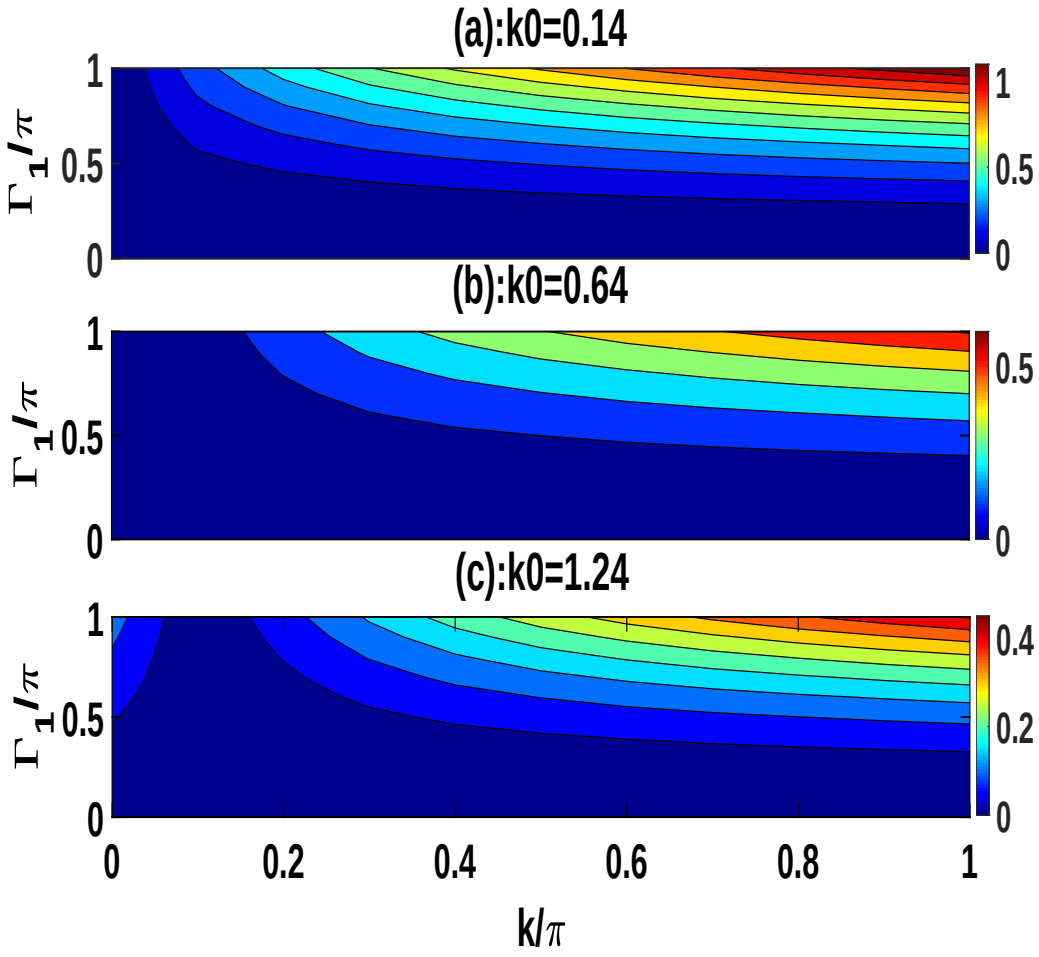

Figure 3.20: Panels (a), (b) and (c) show the growth rate of MI versus the wavenumbers q and Γ, under the effect of the electromagnetic induction. It is worth noticing that, when the feedback gain vary, its values are selected in $\{0.14, 0.64, 1.24\}$ range and the remaining coefficients are fixed. The other parameters are given by: $\alpha = 1.0$, $\beta = -1/6$, $\Gamma = 1/120$, $a = 0.25$, $b = -0.15$, $\gamma = 3.6$ and $\sigma = 0.01$.

3.4.3 Discussion 3

According the law of electromagnetic induction, electromagnetic field [47] can be set up during the fluctuation of electrical activities in cardiac tissue. From biological point of view, the magnetic flux can used to measure the changes of electromagnetic field if possible. As a consequence, the changes of magnetic flux can adjust the excitability and the spatial distribution of membrane potentials of cells. Herein, a memristor [192] is used to realize the coupling and modulation on membrane potential from magnetic flux so that the consistency of physical ans chemical dimension can be conserve. In this section, numerical simulations are realized in the CQCGL equation, with amount of several parameters widely given by Eq. 2.44, that highlight the influence of thermal

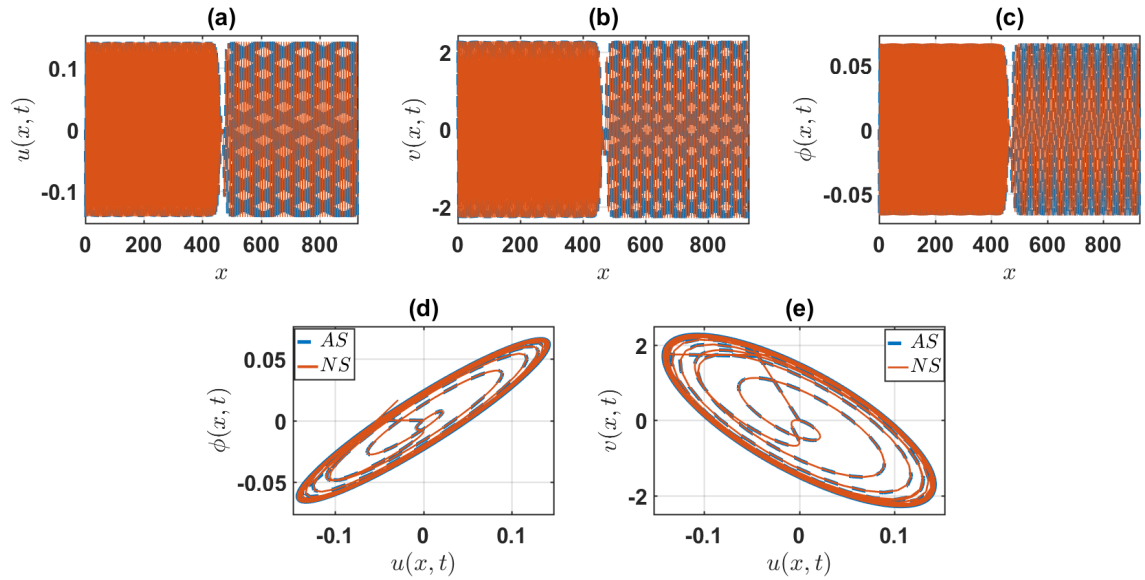

Figure 3.21: Comparison of the analytical and numerical solutions of Eqs. (3.67a)-(3.67b)-(3.67c) for 6000 cells and for a fixed time $t = 0.0$, where the evolution of cardiac ionic wave of both solutions for $u(x,t)$ is shown in panel (a), displays the plot for the ionic current $v(x,t)$ in panel (b) and the flux variable $\phi(x,t)$ in panel (c) and the phase portray in panels (d) and (e). The features are captured for fixed values of a = 0.25, b = -0.15, $\gamma = 3.6$, $\epsilon_0 = 0.01$, $d_1 = 2.0$, $d_2 = 2.0$, K = 8.0, $\alpha = 1.0$, $\beta = -1/6$, $\Gamma = 1/120$, ka0 = 0.14, ka1 = 0.5, ka2 = 1.0

.

coupling coefficients. The motivation included is to verify the validity of the generic FHN cardiac model that support the type of analytical solution obtained above. For this process, we make use of the standard Fourth-order Runge-Kutta computational scheme. We settle the discretized time step to $\Delta t = 0.001$, the spatial dimension coordinate step to $\Delta x = 0.18$, and the wave number $k = 0.11\pi$. Initial conditions as declare previously are stated using Eqs. (3.65a)-(3.65b)-(3.65c) and the numerical intergration making use of Neumann boundary conditions for both $u(x,t)$ and $v(x,t)$.

Figures 3.21 and 3.22 stated the comparison between analytical and numerical solutions and displays the space evolution of the three components $u(x,t)$, $v(x,t)$ and $\phi(x,t)$, which are the fast variable representing the transmembrane potential, the slow current for recovery variable and the magnetic flow , respectively, of the breather solution at different instants $t = 0$ [panels (a), (b), (c), (d), (e)] in Fig. 3.2 and $t = 100$ [panels (a), (b), (c), (d), (e)] in Fig. 3.3 for $k_0 = 0.14$ and for $N = 6000$ cells. According to this frame, there is pretty good agreements between analytical predictions and numerical results, which confirms the effectiveness of our explanation. In this case, when $k_0 = 0.14$, knots narrow over time for $u(x,t)$ and widen for $v(x,t)$ and $\phi(x,t)$, respectively. this can be explained

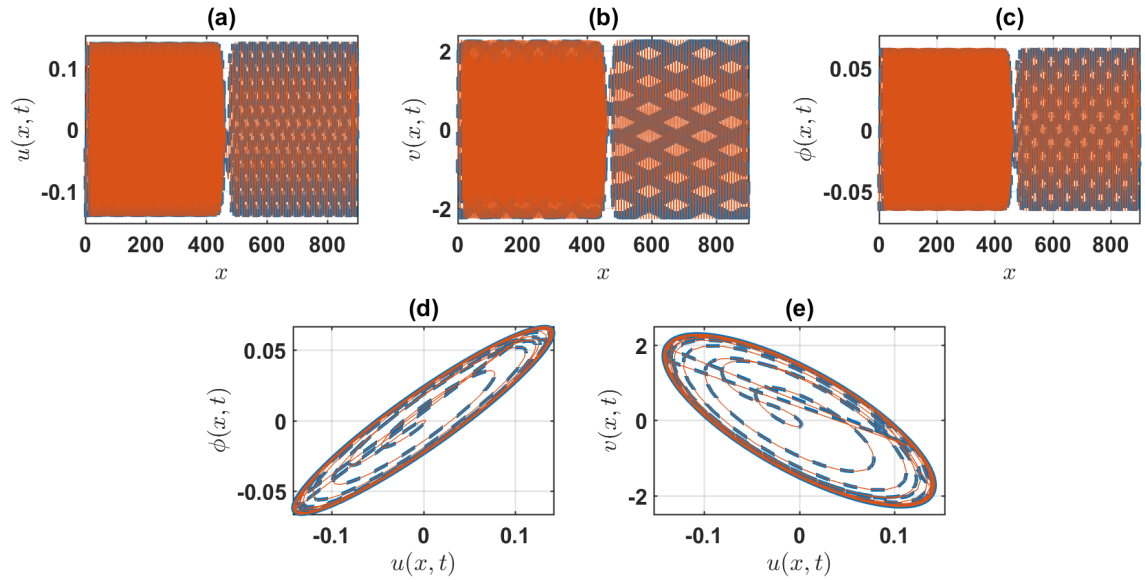

Figure 3.22: Comparison of the analytical and numerical solutions Eqs. (3.67a)-(3.67b)-(3.67c) for 6000 cells and for a fixed time $t = 100.0$, where the evolution of cardiac ionic wave of both solutions for u(x,t) is shown in panel (a), displays the plot for the ionic current v(x,t) in panel (b) and the flux variable $\phi(x,t)$ in panel (c) and the phase portray in panels (d) and (e). The features are captured for fixed values of a = 0.25, b = -0.15, $\gamma = 3.6$, $\epsilon_0 = 0.01$, $d_1 = 2.0$, $d_2 = 2.0$, K = 8.0, $\alpha = 1.0$, $\beta = -1/6$, $\Gamma = 1/120$, ka0 = 0.14, ka1 = 0.5, ka2 = 1.0.

from biological point of view as the cholesterol deposits that leads to ischemic cardiomyopathy and that contributes to the heart's inability to pump blood and which possible treatment can be surgery, defibrillator, pacemaker, coronary artery bypas (CABG) and heart transplant [193]. As far as phase portraits are concerned, [panels (d) and (e)] illustrate the scenario where the oscillations are materialized by nodes that widen with time with the present of lateral oscillations tails.

Figures 3.23 and 3.24 points out the impact and the contribution of changing the value of the feedback gain. We observe that out of having nodes, we have patterns similar to cardiac oscillations showing that the system after a slight perturbation become stable for the compound of the FHN model, which clearly show that the amplitudes of the cardiac tissue is an increasing function for the feedback gain. Furthermore, the corresponding phase planes of [panels (d), (e)] for Fig. 3.24 tends to suppress lateral oscillations around the main pulses, triggered by the dynamics of the slow variable.

Figures 3.25 and 3.26 shed some light on the dynamics of cardiac cells based on these profiles. For $u(x,t)$, $v(x.t)$ and $\phi(x,t)$, we observe an almost perfect correlation between the analytical and numerical solutions on the one hand and oscillations similar to those of heartbeats with time evolution on the other.

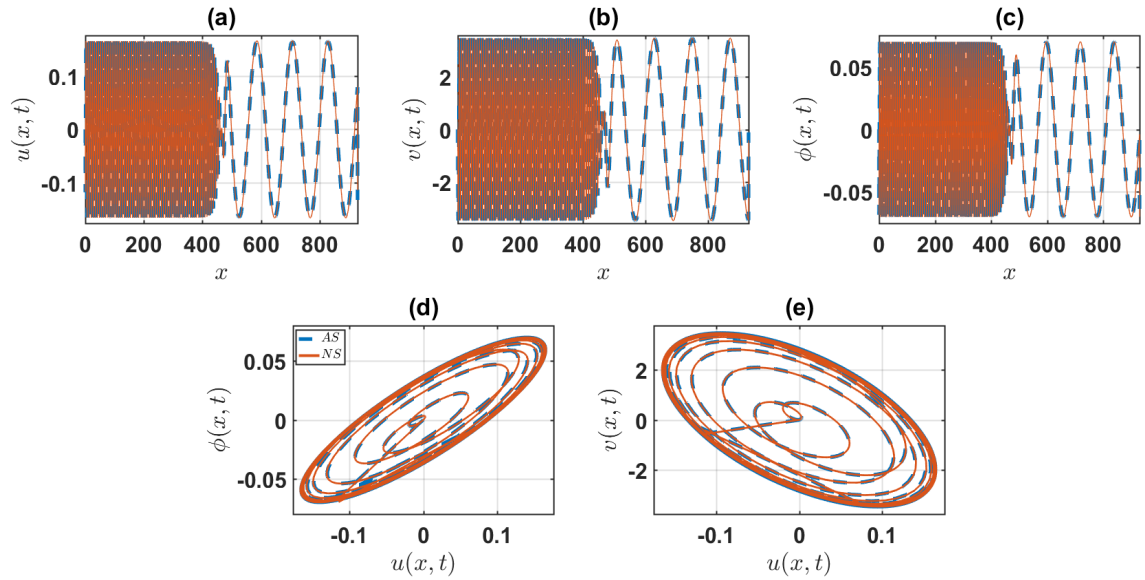

Figure 3.23: Comparison of the analytical and numerical solutions Eqs (3.67a)-(3.67b)-(3.67c) for 6000 cells and for a fixed time $t = 0.0$, where the evolution of cardiac ionic wave of both solutions for u(x,t) is shown in panel (a), displays the plot for the ionic current v(x,t) in panel (b) and the flux variable $\phi(x,t)$ in panel (c) and the phase portray in panels (d) and (e). The features are captured for fixed values of a = 0.25, b = -0.15, $\gamma = 3.6$, $\epsilon_0 = 0.01$, $d_1 = 2.0$, $d_2 = 2.0$, K = 8.0, $\alpha = 1.0$, $\beta = -1/6$, $\Gamma = 1/120$, ka0 = 0.64, ka1 = 0.5, ka2 = 1.0.

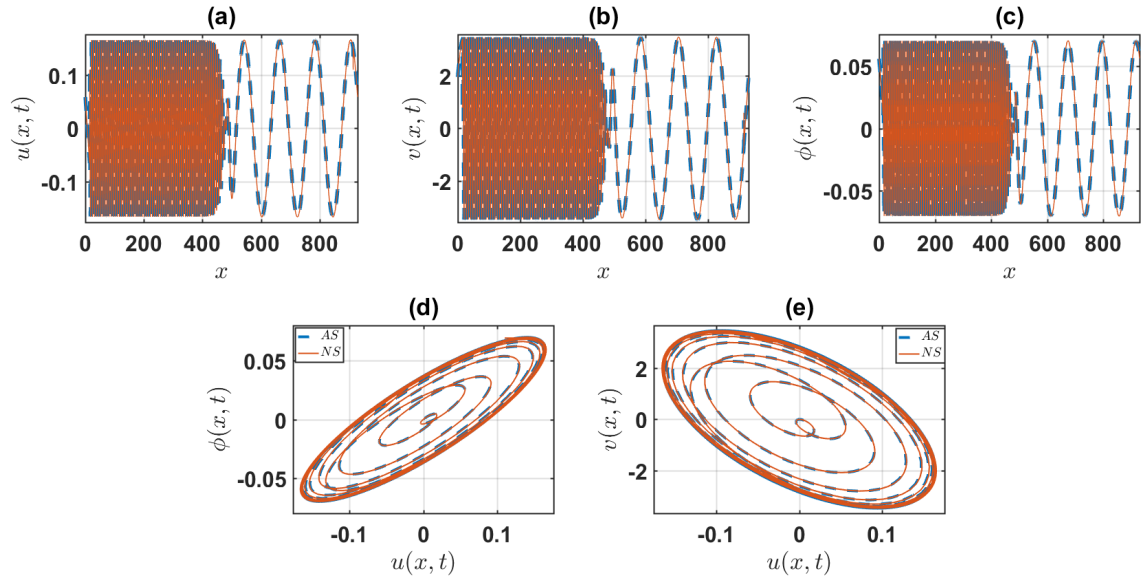

Figure 3.24: Comparison of the analytical and numerical solutions Eqs. (3.67a)-(3.67b)-(3.67c) for 6000 cells and for a fixed time $t = 100.0$, where the evolution of cardiac ionic wave of both solutions for u(x,t) is shown in panel (a), displays the plot for the ionic current v(x,t) in panel (b) and the flux variable $\phi(x,t)$ in panel (c) and the phase portray in panels (d) and (e). The features are captured for fixed values of a = 0.25, b = -0.15, $\gamma = 3.6$, $\epsilon_0 = 0.01$, $d_1 = 2.0$, $d_2 = 2.0$, K = 8.0, $\alpha = 1.0$, $\beta = -1/6$, $\Gamma = 1/120$, ka0 = 0.64, ka1 = 0.5, ka2 = 1.0.

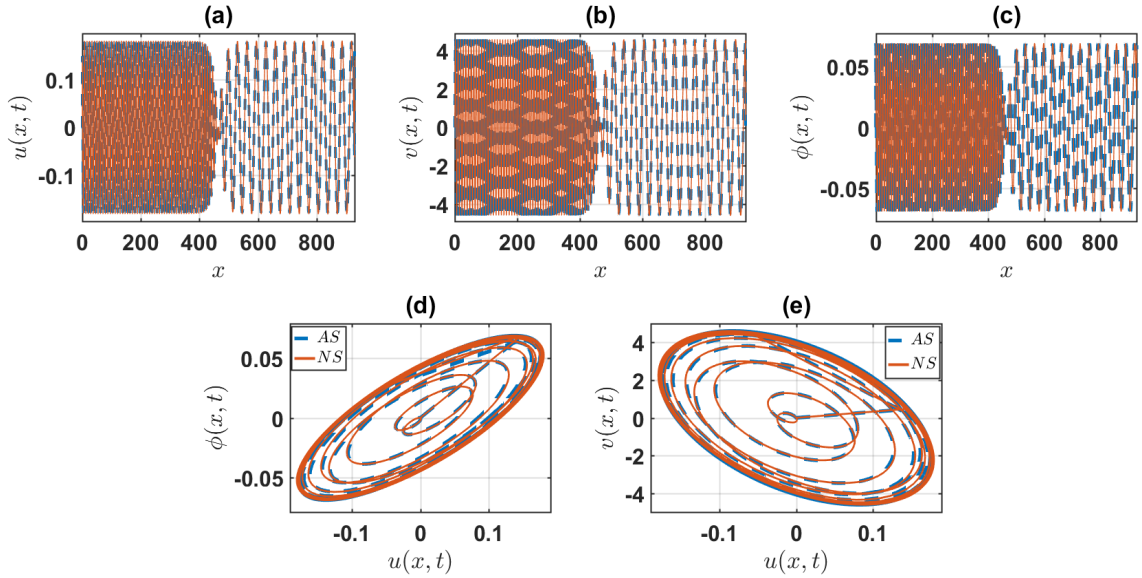

Figure 3.25: Comparison of the analytical and numerical solutions Eqs. (3.67a)-(3.67b)-(3.67c) for 6000 cells and for a fixed time t = 0.0, where the evolution of cardiac ionic wave of both solutions for u(x,t) is shown in panel (a), displays the plot for the ionic current v(x,t) in panel (b) and the flux variable $\phi(x,t)$ in panel (c) and the phase portray in panels (d) and (e). The features are captured for fixed values of a = 0.25, b = -0.15, $\gamma = 3.6$, $\epsilon_0 = 0.01$, $d_1 = 2.0$, $d_2 = 2.0$, K = 8.0, $\alpha = 1.0$, $\beta = -1/6$, Γ = 1/120, ka0 = 1.24, ka1 = 0.5, ka2 = 1.0.

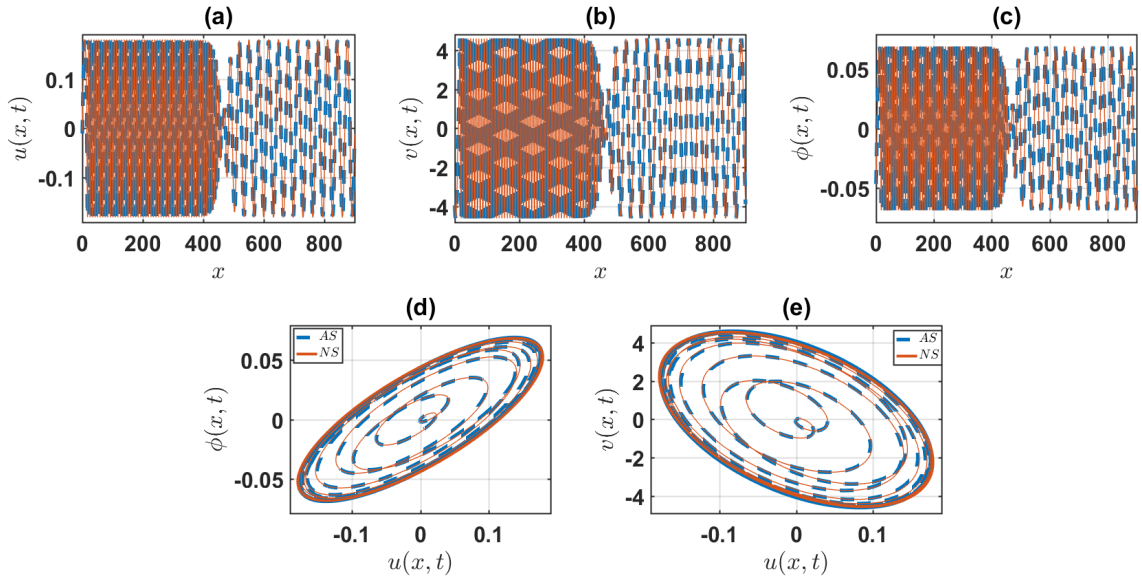

Figure 3.26: (Color online) Comparison of the analytical and numerical solutions Eqs. (3.67a)-(3.67b)-(3.67c) for 6000 cells and for a fixed time t = 100.0, where the evolution of cardiac ionic wave of both solutions for u(x,t) is shown in panel (a), displays the plot for the ionic current v(x,t) in panel (b) and the flux variable $\phi(x,t)$ in panel (c) and the phase portray in panels (d) and (e). The features are captured for fixed values of a = 0.25, b = -0.15, $\gamma = 3.6$, $\epsilon_0 = 0.01$, $d_1 = 2.0$, $d_2 = 2.0$, K = 8.0, $\alpha = 1.0$, $\beta = -1/6$, Γ = 1/120, ka0 = 1.24, ka1 = 0.5, ka2 = 1.0.

It can be seen that with the influence of the electromagnetic induction feedback gain, the amplitude of the oscillations grows up in panels (a), (b) and (c) and the lateral oscillations disappear completely in panels (d) and (e) of the phase portraits in Fig. 3.26. This shows that the greater the feedback gain, the more the heartbeat balance is restored.

3.5 Conclusion

The findings of this study have allowed us to explore how factors like diffusion, thermoelectric coupling, and feedback from electromagnetic induction affect the behavior of a modified FHN model. This model is based on the cqCGL equation and helps us understand how highly localized wave structures form due to a phenomenon called modulational instability.

Modulational instability suggests that nerve and cardiac impulses can be transmitted through a solitary wave, similar to a soliton. Fluctuations in thermoelectric coupling tend to increase modulational instability. However, when electromagnetic induction is strong, it can lead to turbulent behaviors and a decrease in modulational instability, resulting in synchronized patterns in the cardiac lattice.

Analytical approximations show that these dissipative solitonic structures resemble patterns seen in electrocardiograms (ECGs). Furthermore, numerical simulations suggest that these solitons are stable, and the periodic cycles of depolarization and repolarization are crucial for coordinating muscle contraction and ensuring efficient blood pumping.

Studying these effects helps us understand how cells communicate in both neural and cardiac networks.

General Conclusion

The main goal was to investigate how do bio-physical parameters (cross-diffusion, electromagnetic induction, temperature) influence the formation, propagation, stability, and behavior of dissipative solitons in RDs.

Pattern Formation and Nonlinear Effects: The study has demonstrated that the interplay between cross-diffusion, electromagnetic induction and temperature can lead to stationary solitons, traveling waves, and oscillatory patterns. These localized structures are crucial for understanding the stable propagation of electrical impulses in excitable environment. By employing the cubic-quintic Complex Ginzburg-Landau equation obtained via the multiple-scale expansion, we were able to capture the intricate balance between nonlinearity and dispersion, revealing how these factors contribute to the formation and stability of solitons. This equation has proven to be a robust tool for modeling the dynamic behaviors observed in cardiac tissues. From the stability analysis we have identified conditions under which the dissipative soliton remain stable. This stability is contingent on specific parameter ranges. Understanding these conditions is vital for predicting and potentially controlling abnormal cardiac rhythms, such as arrhythmias. Analytical methods such as Multiple-scale analysis and Hirota Bilinear methods have enabled to obtain the complex cubic-quintic Ginzburg-Landau equation, the solitary wave and the Hole-type soliton soltutions, respectively of this ODEs. Numerical methods such as finite difference, Fourth-order Runge-Kutta, and finite element methods, have enabled detailed simulations of reaction-diffusion systems, allowing us to explore the parameter space and observe soliton dynamics under various conditions.

Futhermore, we investigate the effect of the bio-physical parameters on the CQCGL model equation with physical (Linear Gain/Loss (γ), dispersion parameter (P), cubic nonlinearity (Q), quintic nonlinearity (R), self-diffusion coefficients (d_1,d_2), cross-diffusion coefficients (h_1,h_2)). It helps to explain how stable electrical impulses travel through heart tissue, maintaining consistent rhythms. Reveals how reentrant waves, are initiated and sustained in the heart media. Targeted interventions could be designed to disrupt pathological solitons and restore normal rhythm.

Electromagnetic induction can alter wave patterns and soliton in the system, influence the electrical activity of cardiac cells, identifying how certain arrhythmias are triggered and maintain, potentially leading to either stabilization or destabilization of heart rhythms. For the therapeutic approaches, targeted electromagnetic fields could also be used to modulate the properties of cardiac excitability and rhythm, such as the threshold, and the wave speed.

Thermoelectric coupling influence the excitability of cardiac cells by altering ion channels dynamics and potentially affecting the threshold for action potential initiation. it changes, can induce or exacerbate arrhythmias during fever or hypothermia. For the therapeutic interventions, localized heating or cooling could be used to stabilize cardiac tissue and prevent arrhythmic events such as during surgeries or in response to environmental stress. Thermal gradients can modulate wave propagation, stability, and interactions. Thermal and electrical effects can inject or remove energy, influencing the amplitude and the speed of nonlinear waves.

The MI growth rate appeared to be very sensitive relevant to the change of self-and-cross diffusion, temperature, and electromagnetic induction, thus attesting that these parameters are the best candidates to control and regulate the formation of nonlinear excitation within myocardial cells. Interaction between species with boundaries, lead to phenomena such as wave merging, annihilation and reflection. Wavefronts, patterns or pulse solitons profile, gives more insight into the comprehension of the cardiac signals, electrocardiogramm and magnetocardiogramm.

The insights gained from this study extend beyond theoretical interest. The ability to model and predict solitonic structures, can inform the development of new therapeutic strategies and technologies. For instance, targeted interventions could be designed to modulate these nonlinear excitations, potentially offering new avenues for treating cardiac disorders.

Limitations

- ☞ We are encountering performance issues with our computer due to the complex deployment of our system.
- ☞ We have been unable to test our solution in real-world scenarios.
- ☞ Our internet network is not sufficiently robust to access certain documents, which are paid resources.

- ☞ The use of certain analytical methods occasionally prevented us from identifying the poles.
- ☞ Experimental validation and refinement of the model to include more realistic boundary conditions and nonlinearities are needed.

futures directions

- ☞ Extended Models: Future research should explore the extension of this model into two and three-dimensional spaces. Investigating the stability of spiral wave formations and their interactions in higher dimensions will provide a more comprehensive understanding of cardiac dynamics.
- ☞ The phamarcology (Pharmacokinetics, Pharmacodynamics) modeling of cardiovascular diseases.

- ☞ Computational modeling of optogenetic cardiac stimulation.

In summary, dissipative solitons in reaction-diffusion systems with self-and-cross diffusion represent a rich area of research with significant theoretical, numerical, and experimental challenges. Key findings have advanced our understanding of soliton stability and pattern formation, while future directions point towards more comprehensive studies and practical applications.

APPENDIX

Appendix (A) :

$$r_0=-\frac{(i\omega+\mu_1-d_2k^2)}{\mu_2},r_1=\frac{k_1}{(k_2-i\omega)},r_2=\frac{\left(k^2\beta_1-2(\alpha_1+\gamma_0k^2)\right)}{\alpha_0},r_3=-\frac{\mu_1r_2}{\mu_2},$$

$$r_4=\frac{k_1r_2}{k_2},r_5=\frac{\left(i\omega\lambda_1-\alpha_1+\beta_1k^2+\gamma_0k^2\right)}{12j_6k^4-3\alpha_0},r_6=-\frac{\left(\mu_1+2\omega\right)}{\mu_2-4k^2d_2}r_5,r_7=\frac{k_1}{k_2-2\omega}r_5,r_8=0,$$

$$r_9=-\frac{v_gr_3}{\mu_2},r_{10}=\frac{v_gr_4}{k_2},r_{11}=\frac{2i\left(3k\beta_0-12k^3j_6\right)r_5}{\left(12k^4j_6-3\alpha_0\right)},r_{12}=-\frac{\left(\mu_1r_{11}+(v_g+2ikd_2)r_6\right)}{(2i\omega+\mu_2-4k^2d_2)},$$

$$r_{13}=\frac{\left(k_1r_{11}+v_gr_7\right)}{(k_2-2i\omega)},r_{14}=\frac{1}{(72k^4j_6-8\alpha_0)}(i\omega(3\lambda_1r_5+\lambda_2+\lambda_3)$$
$$-2\alpha_1r_5-\alpha_2r_1^2-\alpha_3r_1-\alpha_4+k^2(5\beta_1r_5+\beta_2r_1^2+\beta_3+\gamma_1+(j_0+j_2+j_4)r_1^2),$$

$$r_{15}=-\frac{\mu_1r_{14}}{(3i\omega+\mu_2-9k^2d_2)},r_{16}=\frac{k_1r_{14}}{(k_2-3i\omega)},$$

$$r_{17}=-\frac{1}{\alpha_0}(\alpha_1(3r_2^2+2|r_5|^2)+\alpha_2(r_2r_5^*+2r_1^*r_7+2r_2|r_1|^2)+\alpha_3$$
$$(2r_4+2r_1^*(r_2+r_5)+r_7^*)+\alpha_4(3r_5^*+3r_5+6r_2)+\alpha_5(6+12r_2+r_2^2)-k^2(\beta_1(2+8|r_5|^2)$$
$$-2\beta_2(r_1r_4-2r_5^*r_1^2-r_1^*r_7)+2\beta_3(r_2+2r_5^*+r_5)+3\beta_4+8\gamma_0|r_5|^2$$
$$-\gamma_1(2r_2+r_5+3r_5^*)-3\gamma_2-j_0(2r_5^*r_1^2+2r_5(r_1^*)^2+r_1^*(r_4+r_7)+r_1(r_4+r_7^*))$$
$$+j_2(r_1^2r_5^*+(r_1^*)^2r_5-2r_2|r_1|^2)+j_4(r_1^2r_5^*+r_1(5r_7^*+r_4)+r_1^*(r_4+5r_7$$
$$+r_1^*r_5)+2r_2|r_1|^2))),r_{18}=-\frac{\mu_1}{\mu_2}r_{17},r_{19}=\frac{k_1}{k_2}r_{17},$$

$$r_{20}=\frac{1}{(12j_6k^4-3\alpha_0)}(i\omega(2\lambda_1(r_2r_5+r_{14})+\lambda_2(2r_1r_4+2r_4r_5+r_5|r_1|^2)$$
$$+2\lambda_3(r_2r_5+r_2+2r_5)+3\lambda_4r_2)-2\alpha_1(r_2r_5+r_{14})-\alpha_2(2r_5|r_1|^2+r_2r_1^2)$$
$$-\alpha_3(r_4+2r_1r_2+r_1^*r_5+2r_7)-3\alpha_4(2r_5+r_2)-2\alpha_5(2+3r_2)+k^2(2\beta_1(2r_2r_5+5r_{14})$$
$$+2\beta_2(r_1(r_4+r_7)+4r_5|r_1|^2)+2\beta_3(r_2+6r_5)+4\beta_4-\gamma_1(2r_5-r_2)+j_0(r_1^*r_7+r_1(r_4-3r_7))$$
$$+j_2(r_1^2r_2-2|r_1|^2r_5)+j_4(r_1(r_4+5r_7)+r_1^2r_2+2|r_1|^2r_5))),$$

$$r_{21}=-\frac{\mu_1r_{20}}{(2i\omega+\mu_2-4d_2k^2)},r_{22}=\frac{k_1r_{20}}{(k_2-2i\omega)}r_{23}=\frac{96ik^3j_6r_{14}}{(72j_6k^4-8\alpha_0)},$$

$$r_{24}=-\frac{(\mu_1r_{23}+(v_g+6ikd_2)r_{15})}{(3i\omega+\mu_2-9k^2d_2)},r_{25}=\frac{(v_gr_{16}+k_1r_{23})}{(k_2-3i\omega)},$$

$$r_{26}=\frac{1}{(240k^4j_6-15\alpha_0)}(i\omega(2\lambda_1(2r_{14}+r_5^2)+2\lambda_2r_5r_1^2+4\lambda_3r_5+\lambda_4)$$

$$-\alpha_1(2r_{14}+r_5^2)-\alpha_2 r_8 r_1^2-\alpha_3(2r_1r_5+r_7)-3\alpha_4 r_5-\alpha_5+k^2(2\beta_1(2r_5^2+5r_{14})$$
$$-4\beta_2 r_1^2 r_5+6\beta_3 r_5+\beta_4+8\gamma_0 r_5^2+5\gamma_1 r_5+\gamma_2+j_0(2r_1^2r_5+r_1r_7)+j_2 r_1^2 r_5+j_4(5r_1r_7+r_1^2r_5))),$$

$$r_{27}=-\frac{\mu_1 r_{26}}{(4i\omega+\mu_2-16k^2d_2)}, r_{28}=\frac{k_1 r_{26}}{(k_2-4i\omega)}.$$

Appendix (B) : Coefficients of the matrix

$$a_{11}=-2R_i\phi_0^5-2iP_rq\Gamma\phi_0+P_i\Gamma^2\phi_0-Q_i\phi_0^3-i\phi_0\Omega_1, a_{12}=2\phi_0^4R_r-2iq\Gamma P_i-\Gamma^2P_r+\phi_0^2Q_r,$$
$$a_{13}=2\phi_0^5R_i+\phi_0^3Q_i, a_{14}=2\phi_0^4R_r+\phi_0^2Q_r, a_{21}=2R_r\phi_0^5-2iP_iq\Gamma\phi_0-P_r\Gamma^2\phi_0+Q_r\phi_0^3,$$
$$a_{22}=2\phi_0^4R_i+2Iq\Gamma P_r-\Gamma^2P_m+\phi_0^2Q_i+i\Omega_1, a_{23}=-2\phi_0^5R_r-\phi_0^3Q_r, a_{24}=2\phi_0^4R_i+\phi_0^2Q_i,$$
$$a_{31}=2\phi_0^5R_i+\phi_0^3Q_i, a_{32}=2\phi_0^4R_r+\phi_0^2Q_r,$$
$$a_{33}=-2\phi_0^5R_m+2iq\Gamma P_r\phi 0+\Gamma^2P_m\phi_0-\phi_0^3Q_m-i\phi_0\Omega_1, a_{34}=2\phi_0^4R_r+2iq\Gamma P_i-\Gamma^2P_r+\phi_0^2Q_r,$$
$$a_{41}=-2\phi_0^5R_r-\phi_0^3Q_r, a_{42}=2\phi_0^4R_i+\phi_0^2Q_i, a_{43}=2\phi_0^5R_r+2iq\Gamma P_i\phi_0-\Gamma^2P_r\phi_0+\phi_0^3Q_r,$$
$$a_{44}=2\phi_0^4R_i-2iq\Gamma P_r-\Gamma^2P_i+\phi_0^2Q_i+i\Omega_1,$$

Appendix (C) : Coefficients of the Polynomial equation

$$A_0=\phi_0^2, A_1=-8i\phi_0^6R_i+4i\Gamma^2P_i\phi_0^2-4iQ_m\phi_0^4,$$
$$A_2=-16{\phi_0}^{10}{r_m}^2+24\Gamma^2p_m{\phi_0}^6r_m+8\Gamma^2p_r{\phi_0}^6r_r-16{\phi_0}^8q_mr_m-6\Gamma^4{p_m}^2{\phi_0}^2-2\Gamma^4{p_r}^2{\phi_0}^2$$
$$+8\Gamma^2q^2{p_m}^2{\phi_0}^2-8\Gamma^2q^2{p_r}^2{\phi_0}^2+12\Gamma^2p_m{\phi_0}^4q_m+4\Gamma^2p_r{\phi_0}^4q_r-4{\phi_0}^6{q_m}^2,$$
$$A_3=8i\Gamma^4p_mp_r{\phi_0}^4q_r+8i\Gamma^4{p_r}^2{\phi_0}^6r_m-16i\Gamma^2p_r{\phi_0}^8q_rr_m+24i\Gamma^4{p_m}^2{\phi_0}^6r_m$$
$$-32i\Gamma^2p_m{\phi_0}^{10}{r_m}^2+16i\Gamma^2q^2{p_r}^2{\phi_0}^4q_m-8i\Gamma^2p_r{\phi_0}^6q_mq_r-32i\Gamma^2q^2{p_m}^2{\phi_0}^6r_m$$
$$+32i\Gamma^2q^2{p_r}^2{\phi_0}^6r_m+16i\Gamma^4q^2p_m{p_r}^2{\phi_0}^2-4i\Gamma^6p_m{p_r}^2{\phi_0}^2+16i\Gamma^4q^2{p_m}^3{\phi_0}^2$$
$$-4i\Gamma^6{p_m}^3{\phi_0}^2+4i\Gamma^4{p_r}^2{\phi_0}^4q_m-32i\Gamma^2p_m{\phi_0}^8q_mr_m+12i\Gamma^4{p_m}^2{\phi_0}^4q_m$$
$$-8i\Gamma^2p_m{\phi_0}^6{q_m}^2-64i\Gamma^2q^2p_mp_r{\phi_0}^6r_r+16i\Gamma^4p_mp_r{\phi_0}^6r_r-16i\Gamma^2p_r{\phi_0}^8q_mr_r$$
$$-32i\Gamma^2p_r{\phi_0}^{10}r_mr_r-16i\Gamma^2q^2{p_m}^2{\phi_0}^4q_m-32i\Gamma^2q^2p_mp_r{\phi_0}^4q_r,$$

$$A_4=16\Gamma^4{p_m}^2{\phi_0}^{10}{r_m}^2+32\Gamma^4p_mp_r{\phi_0}^{10}r_mr_r+16\Gamma^4{p_r}^2{\phi_0}^{10}{r_r}^2-64\Gamma^2q^2{p_m}^2{\phi_0}^{10}{r_m}^2$$
$$-128\Gamma^2q^2p_mp_r{\phi_0}^{10}r_mr_r-64\Gamma^2q^2{p_r}^2{\phi_0}^{10}{r_r}^2-8\Gamma^6{p_m}^3{\phi_0}^6r_m-8\Gamma^6{p_m}^2p_r{\phi_0}^6r_r$$
$$-8\Gamma^6p_m{p_r}^2{\phi_0}^6r_m-8\Gamma^6{p_r}^3{\phi_0}^6r_r+32\Gamma^4q^2{p_m}^3{\phi_0}^6r_m+32\Gamma^4q^2{p_m}^2p_r{\phi_0}^6r_r$$
$$+32\Gamma^4q^2p_m{p_r}^2{\phi_0}^6r_m+32\Gamma^4q^2{p_r}^3{\phi_0}^6r_r+16\Gamma^4{p_m}^2{\phi_0}^8q_mr_m+16\Gamma^4p_mp_r{\phi_0}^8q_mr_r$$
$$+16\Gamma^4p_mp_r{\phi_0}^8q_rr_m+16\Gamma^4{p_r}^2{\phi_0}^8q_rr_r-64\Gamma^2q^2{p_m}^2{\phi_0}^8q_mr_m-64\Gamma^2q^2p_mp_r{\phi_0}^8q_mr_r$$
$$-64\Gamma^2q^2p_mp_r{\phi_0}^8q_rr_m-64\Gamma^2q^2{p_r}^2{\phi_0}^8q_rr_r+\Gamma^8{p_m}^4{\phi_0}^2+2\Gamma^8{p_m}^2{p_r}^2{\phi_0}^2+\Gamma^8{p_r}^4{\phi_0}^2$$

$$-8\Gamma^6 q^2 {p_m}^4 {\phi_0}^2 - 16\Gamma^6 q^2 {p_m}^2 {p_r}^2 {\phi_0}^2 - 8\Gamma^6 q^2 {p_r}^4 {\phi_0}^2 - 4\Gamma^6 {p_m}^3 {\phi_0}^4 q_m$$
$$-4\Gamma^6 {p_m}^2 p_r {\phi_0}^4 q_r - 4\Gamma^6 p_m {p_r}^2 {\phi_0}^4 q_m - 4\Gamma^6 {p_r}^3 {\phi_0}^4 q_r + 16\Gamma^4 q^4 {p_m}^4 {\phi_0}^2 + 32\Gamma^4 q^4 {p_m}^2 {p_r}^2 {\phi_0}^2$$
$$+16\Gamma^4 q^4 {p_r}^4 {\phi_0}^2 + 16\Gamma^4 q^2 {p_m}^3 {\phi_0}^4 q_m + 16\Gamma^4 q^2 {p_m}^2 p_r {\phi_0}^4 q_r + 16\Gamma^4 q^2 p_m {p_r}^2 {\phi_0}^4 q_m$$
$$+16\Gamma^4 q^2 {p_r}^3 {\phi_0}^4 q_r + 4\Gamma^4 {p_m}^2 {\phi_0}^6 {q_m}^2 + 8\Gamma^4 p_m p_r {\phi_0}^6 q_m q_r + 4\Gamma^4 {p_r}^2 {\phi_0}^6 {q_r}^2$$
$$-16\Gamma^2 q^2 {p_m}^2 {\phi_0}^6 {q_m}^2 - 32\Gamma^2 q^2 p_m p_r {\phi_0}^6 q_m q_r - 16\Gamma^2 q^2 {p_r}^2 {\phi_0}^6 {q_r}^2,$$

Appendix (D) : Ferrari parameters

$$L = \frac{A_2}{A_0} - \frac{3}{8}\frac{A_1^2}{A_0^2}, M = -\frac{1}{2}\frac{A_2 A_1}{{A_0}^2} + \frac{1}{8}\frac{{A_1}^3}{{A_0}^3} + \frac{A_3}{A_0}, N = -\frac{1}{4}\frac{A_3 A_1}{{A_0}^2} + \frac{A_4}{A_0} + \frac{1}{16}\frac{A_2 {A_1}^2}{{A_0}^3} - \frac{3}{256}\frac{{A_1}^4}{{A_0}^4},$$

$$H = -\frac{1}{12}L^2 - N, E = -\frac{1}{108}L^3 + \frac{1}{3}LN - \frac{1}{8}M^2, R_0 = -\frac{1}{2}E + \sqrt{\frac{H^3}{27} + \frac{E^2}{4}}, U = {R_0}^{1/3},$$

$$Y = -\frac{5}{6}L + U - \frac{1}{3}\frac{H}{U}, \qquad U \neq 0, W = \sqrt{L + 2Y},$$

$$\Omega_1 = -\frac{1}{4}\frac{A_1}{A_0} + \frac{1}{2}W - \frac{1}{2}\sqrt{-3L - 2Y + 2\frac{M}{W}}, \Omega_2 = -\frac{1}{4}\frac{A_1}{A_0} + \frac{1}{2}W + \frac{1}{2}\sqrt{-3L - 2Y + 2\frac{M}{W}},$$

$$\Omega_3 = -\frac{1}{4}\frac{A_1}{A_0} - \frac{1}{2}W - \frac{1}{2}\sqrt{-3L - 2Y - 2\frac{M}{W}}, \Omega_4 = -\frac{1}{4}\frac{A_1}{A_0} - \frac{1}{2}W + \frac{1}{2}\sqrt{-3L - 2Y - 2\frac{M}{W}},$$

BIBLIOGRAPHY

[1] Miura, R. M. Analysis of excitable cell models. J. Comput. Appl. Math. **144**, 29-47 (2002). doi: 10.1016/S0377-0427(01)00550-7

[2] Enns-Ruttan, J., Miura, R. M. Spontaneous secondary spiking in excitable cells. J. Theor. Biol. **205**, 181-199 (2000).doi: 10.1006/jtbi.2000.2056

[3] Butler, S. Review: From Neuron to Brain: A Cellular and Molecular Approach to the Function of the Nervous System (Third Edition). Sage Pub. **22**, 755-756 (1983). doi: 10.1068/p220755

[4] Holden, A. V., Markus, M., Othmer, H. Nonlinear wave processes in excitable media. 244, (2013). doi: 10.1007/978-1-4899-3683-7

[5] Fisher, R.A. The wave of advance of advantageous genes. Ann. Eugenics **7**, 355-369 (1937). doi:10.1111/j.1469-1809.1937.tb02153.x

[6] Kolmogorov, A., Petrovskii, I., Piskunov, N. Study of a diffusion equation that is related to the growth of a quality of matter and its application to a biological problem. Moscow Univ. Math. Bull. **1**, 1-26 (1937).

[7] Turing, A. The chemical basis of morphogenesis. Philos. Trans. R. Soc. Lond. B Biol. Sci. **237**, 37-72 (1952). doi:10.1098/rstb.1952.0012

[8] FitzHugh, R. Impulses and physiological states in theoretical models of nerve membrane. Biophys. J. **1**, 445-466 (1961). doi:10.1016/S0006-3495(61)86902-6

[9] Nagumo, J., Arimoto, S., Yoshizawa, S. An active pulse transmission line simulating nerve axon. IEEE Trans. **50**, 2061-2070 (1962). doi:10.1109/JRPROC.1962.288235

[10] Vanag, V. K., Epstein, I. R. Stationary and oscillatory localized patterns, and subcritical bifurcations. Phys. Rev. Lett. **92**, 128301 (2004)

[11] Lobanova, E. S., Ataullakhanov, F. I. Running pulses of complex shape in a reaction-diffusion model. Phys. Rev. Lett. **93**, 098303 (2004). doi.org/10.1103/PhysRevLett.93.098303

[12] Zeldovich, Ya. B., Frank-Kamenetskii, D. A. A theory of thermal propagation of flame. Acta Physicochim. USSR **9**, 341-350 (1938).

[13] Noble, M. W., Tonks, M. R., Fitzgerald, S. P. Turing instability in the solid state: void lattices in irradiated metals. Phys. Rev. Lett. **124**, 167401 (2020). doi.org/10.1103/PhysRevLett.124.167401

[14] Belousov, V. A periodic reaction and its mechanism. In: Oscillations and traveling waves in chemical systems, edited by Field, R., Burger, M. Wiley J, New York, 1985, pp. 605; Zhabotinskii, A. M. Periodic course of the oxidation of malonic acid in a solution (Studies on the kinetics of Belousov's reaction). Biofizika **9**, 306 (1964)

[15] Vanag, V. K., Epstein, I. R. Cross-diffusion and pattern formation in reaction-diffusion systems. Phys. Chem. Phys. **11**, 897 (2009). doi.org/10.1039/B813825G

[16] Zemskov, E. P., Kassner, K., Hauser, M. J. B. Wavy fronts and speed bifurcation in excitable systems with cross diffusion. Phys. Rev. E **77**, 036219 (2008). doi.org/10.1103/PhysRevE.77.036219

[17] Zemskov, E. P., Tsyganov, M. A., Kassner, K., Horsthemke, W. Nonlinear waves in a quintic FitzHugh-Nagumo model with cross-diffusion: fronts, pulses and wave trains. Chaos **31**, 033141 (2021). doi:10.1063/5.0043919

[18] Tsyganov, M. A., Biktashev, V. N., Brindley, J., Holden, A. V., Ivanitsky, G. R. Waves in systems with cross-diffusion as a new class of nonlinear waves. Phys. Uspekhi **50**, 263 (2007). doi:10.1070/PU2007v050n03ABEH006114

[19] Ouyang, Q., Swinney, H. L. Transition from a uniform state to hexagonal and striped Turing patterns. Nature **352**, 610 (1991).

[20] Lenk, M., Einax, J., Köhler, M. J., Maass, P. Complex oscillation modes in the Belousov-Zhabotinsky reaction by weak diffusive coupling. Phys. Rev. E **99**, 022202 (2019). doi.org/10.1103/PhysRevE.99.022202

[21] Gambino, G., Giunta, V., Lombardo, M. C., Rubino, G. Cross-diffusion effects on stationary pattern formation in the FitzHugh-Nagumo model. Am. Inst. Math. Sci. **27**, 7783-7816 (2022). doi:10.3934/dcdsb.2022063

[22] Kostianko, A., Sun, C., Zelik, S. Reaction-diffusion systems with supercritical nonlinearities revisited. Math. Ann. **384**, 1-45 (2022). https://doi.org/10.1007/s00208-021-02222-6

[23] Zipes, D. P., Jalife, J., Stevenson, W. G. Cardiac Electrophysiology: From Cell to Bedside E-Book. Elsevier Health Sciences (2021).

[24] Madzvamuse, A., Ndakwo, H. S., Barreira, R. Cross-diffusion-driven instability for reaction-diffusion systems: analysis and simulations. J. Math. Biol. **70**, 709 (2015).

[25] Tsyganov, M. A., Brindley, J., Holden, A. V., Biktashev, V. N. Quasisoliton interaction of pursuit-evasion waves in a predator-prey system. Phys. Rev. Lett. **91**, 218102 (2003). https://doi.org/10.1103/PhysRevLett.91.218102

[26] Tsyganov, M. A., Brindley, J., Holden, A. V., Biktashev, V. N. Soliton-like phenomena in one-dimensional cross-diffusion systems: a predator-prey pursuit and evasion example. Physica D. **197**, 18 (2004). doi.org/10.1016/j.physd.2004.06.004

[27] Guin, L. N. Spatial patterns through Turing instability in a reaction-diffusion predator-prey model. Math. Comput. Simul. **109**, 174 (2015). doi.org/10.1016/j.matcom.2014.102002

[28] Biktashev, V. N., Tsyganov, M. A. Spontaneous traveling waves in oscillatory systems with cross-diffusion. Phys. Rev. E **80**, 056111 (2009). doi.org/10.1103/PhysRevE.80.05611

[29] Shi, J., Xie, Z., Little, K. Cross-diffusion induced instability and stability in reaction-diffusion systems. J. Appl. Anal. Comput. **24**, 95-119 (2010)

[30] Hodgkin, A. L., Huxley, A. F. A quantitative description of membrane current and its application to conduction and excitation in nerve. J. Physiol. **117**, 500-544 (1952). doi:10.1113/JPHYSIOL.1952.SP004764

[31] Knight, B. W. Dynamics of encoding in a population of neurons. J. Gen. Physiol. **59**, 734-766 (1972). doi:10.1085/jgp.59.6.734

[32] Morris, C., Lecar, H. Voltage oscillations in the barnacle giant muscle fiber. Biophys. J. **35**, 193-213 (1981). doi:10.1016/S0006-3495(81)84782-0

[33] Rajagopal, K. A model for the nerve impulse propagation using two first-order differential equations. Phys. Lett. A **59**, 734-766 (1972). doi:10.1016/0375-9601(83)90552-2

[34] Bernstein, J. Pfluegers Arch. Gesamte Physiol. Menschen Tiere **92**, 521 (1902).

[35] Stefanu, B. The temperature-induced changes in membrane potential. Riv. Bio. **102**, 199 (2009). doi:10.1400/122127

[36] Lengyel, I., Epstein, I. R. Modeling of Turing structures in the chlorite-iodide-malonic acid-starch reaction system. Science **251**, 650-652 (1991). doi: 10.1126/science.251.4994.650

[37] Tsyganov, M. A., Biktashev, V. N. Classification of wave regimes in excitable systems with linear cross-diffusion. Phys. Rev. E **90**, 062912 (2014). doi.org/10.1103/PhysRevE.90.062912

[38] Zemskov, E. P., Tsyganov, M. A., Horsthemke, W. Oscillatory pulses and wave trains in a bistable reaction-diffusion system with cross-diffusion. Phys. Rev. E **95**, 012203 (2017). doi.org/10.1103/PhysRevE.95.012203

[39] Biktashev, V. N., Tsyganov, M. A. Solitary waves in excitable systems with cross-diffusion. Proc. R. Soc. **461**, 3711 (2005). doi.org/10.1098/rspa.2005.1529

[40] Zemskov, E. P., Epstein, I. R., Muntean, A. Oscillatory pulses in FitzHugh-Nagumo type systems with cross-diffusion. Math. Med. Biol. **28**, 217-226 (2011). https://doi.org/10.1093/imammb/dqq012

[41] Zemskov, E. P., Tsyganov, M. A., Horsthemke, W. Oscillatory pulse-front waves in a reaction-diffusion system with cross diffusion. Phys. Rev. E **97**, 062206 (2018). doi.org/10.1103/PhysRevE.95.012203

[42] Mvogo, A., Takembo, C. N., Ekobena Fouda, H. P., Kofané, T. C. Pattern formation in diffusive excitable systems under magnetic flow effects. Phys. Lett. Sect. A Gen. At. Solid State Phys. **381**, 2264-2271 (2017). doi:10.1016/j.physleta.2017.05.020

[43] Sobel, E., Davanipour, Z. Electromagnetic field exposure may cause increased production of amyloid beta and eventually lead to Alzheimer's disease. Neurology. **47**, 1594-1600 (1996). doi:10.1212/WNL.47.6.1594

[44] Takembo, C. N., Mvogo, A., Ekobena Fouda, H. P., Kofané, T. C. Autaptic regulation of electrical activities in neuron under electromagnetic induction. Inter Journal of Mod Phys B. **32**, 1850165 (2018). doi:10.1142/S0217979218501655

[45] Nkeh, O. N., Patrick, G. G., Francois-Marie, M. K. Localized nonlinear waves in a myelinated nerve fiber with self-excitable membrane. Chinese Physics B. **32**, 020504 (2023). doi:10.1088/1674-1056/ac720d

[46] Xu, D., Roth, B. J. The magnetic field produced by heart and its influence on MRI. Math Prob Eng. **2017**, 3035479 (2017). doi.org/10.1155/2017/3035479

[47] Xu, Y., Ying, H., Jia, Y. et al. Autaptic regulation of electrical activities in neuron under electromagnetic induction. Sci Rep. **7**, 43452 (2017). doi:10.1038/srep43452

[48] Zhang, G., Wang, C., Alzahrani, F., Wu, F., An, X. Investigation of dynamical behaviors of neurons driven by memristive synapse. Chaos, Solitons and Fractals **108**, 15-24 (2018). doi:10.1016/j.chaos.2018.01.017

[49] Ghosn, R., Villégier, A.nS., Selmaoui, B., Thuróczy, G., de Sèze, R. Effets des radiofréquences sur le système nerveux central chez l'homme: EEG, sommeil, cognition, vascularisation. Comptes Rendus Phys. **14**, 395-401 (2013). doi:10.1016/j.crhy.2013.02.004

[50] Tabi, C. B., Etémé, A. S., Kofané, T. C. Unstable cardiac multi-spiral waves in a FitzHugh-Nagumo soliton model under magnetic flow effect. Nonli Dyn. **100**, 3799-3814 (2020). doi:10.1007/s11071-020-05750-z

[51] Farashi, S., Savadkoohi, P., Ranjbar, H. Computational modeling of the effect of temperature variations on human pancreatic β-cell activity. Journal of Thermal Biology **75**, 69-80 (2018). doi:10.1016/j.jtherbio.2018.05.006

[52] Jose, A. D., Collison, D. The normal range and determinants of the intrinsic heart rate in man. Cardiovasc. Res. **4**, 160-167 (1970). doi:10.1093/cvr/4.2.160

[53] Takembo, C. N., Ekobena Fouda, H. P. Effect of temperature fluctuation on the localized pattern of action potential in cardiac tissue. Sci Rep. **10**, 15087 (2020). doi:10.1038/s41598-020-72188-z

[54] Alonso, S., Bar, M., Echebarria, B. Nonlinear physics of electrical wave propagation in the heart: A review. Reports Prog. Phys. **79** (2016). doi:10.1088/0034-4885/79/9/096601

[55] Barkley, D., Kness, M. and Tuckerman, L. S. Spiral-wave dynamics in a simple model of excitable media: The transition from simple to compound rotation. Phys. Rev. A. **42**, 2489-2492 (1990). doi:10.1103/PhysRevA.42.2489

[56] Zeeman, E. C. Differential equations for the heartbeat and nerve impulse. Biol. Process Living Syst. 8-67 (2018). doi:10.4324/9781351297165-2

[57] Oral, P., Merdan, M. and Bekäryaz, Z. Analysis of a Random Zeeman Heartbeat Model with Differential Transformation Method. **40**, 285-298 (2019). doi:10.17776/csj.460984

[58] Butler, S. Review: From Neuron to Brain: A Cellular and Molecular Approach to the Function of the Nervous System (Third Edition). Perception **22**, 755-756 (1993). doi:10.1068/p220755

[59] Johnston, D. and Wu, S. M.-S. Foundations of Cellular Neurophysiology. MIT Press, 676 (1995).

[60] Hindmarsh, J. L., Rose, R. M. A model of neuronal bursting using three coupled first order differential equations. Proc. R. Soc. Lond. B Biol. Sci. **221**, 87-102 (1984). doi:10.1098/rspb.1984.0024

[61] Rose, R. M., Hindmarsh, J. L. The assembly of ionic currents in a thalamic neuron. III. The seven-dimensional model. Proc. R. Soc. B Biol. Sci. **237**, 313-334 (1989). doi:10.1098/rspb.1989.0051

[62] Hindmarsh, J. and Cornelius, P. The development of the Hindmarsh-Rose model for bursting. Bursting Genes. Rhythm Nerv. Syst. 3 – 18(2005). doi:10.1142/9789812703231$_0$001

[63] Stenzinger, R. V., Scalvin, T. E., Morelo, P. A., and Tragtenberg, M. H. R. Cardiac behaviors and chaotic arrhythmias in the Hindmarsh-Rose model. Chaos, Solitons and Fractals. **175**, 113983 (2023). doi:10.1016/j.chaos.2023.113983

[64] Aliev, R. R., Panfilov, A. V. A Simple Two-variable Model of Cardiac Excitation. Chaos, Solitons and Fractals **7**, 293-301 (1996). doi:10.1016/0960-0779(95)00089-5

[65] Pertsov, A. M., Ermakova, E. A., Panfilov, A. V. Rotating spiral waves in a modified Fitz-Hugh-Nagumo model. Phys. D Nonlinear Phenom. **14**, 117-124 (1984). doi:10.1016/0167-2789(84)90008-3

[66] Panfilov, A. V., Müller, S. C., Zykov, V. S., Keener, J. P. Elimination of spiral waves in cardiac tissue by multiple electrical shocks. Phys. Rev. E **61**, 4644-4647 (2000). doi:10.1103/PhysRevE.61.4644

[67] Bernus, O., Verschelde, H., and Panfilov, A. V. Reentry in an anatomical model of the human ventricles. Int. J. Bifurcat. Chaos. **13**, 3693-3702 (2003). doi:10.1142/S021812740300896X

[68] Courtemanche, M., and Winfree, A. T. Re-entrant rotating waves in a Beeler-Reuter based model of two-dimensional cardiac electrical activity. Int. J. Bifurcat. Chaos. **1**, 431-444 (1991). doi:10.1142/s0218127491000336

[69] Pravdin, S. F., Dierckx, H., Katsnelson, L. B., Solovyova, O., Markhasin, V. S., and Panfilov, A. V. Electrical wave propagation in an anisotropic model of the left ventricle based on analytical description of cardiac architecture. PLoS One. **9**, 24817308 (2014). doi:10.1371/journal.pone.0093617

[70] Wulff, C., Doedel, E. J., and Turaev, D.: CGL and CGLE revisited: new bifurcations in space-time modulated planar waves. Journal of Dynamics and Differential Equations, **18(1)**, 227-275 (2006).

[71] Murray, J. D. Mathematical Biology I: Spatial models and biomedical applications, 3rd ed. Springer-Verlag, Berlin, (2003). doi:10.1007/b98869

[72] FitzHugh, R. Mathematical models of threshold phenomena in the nerve membrane. Bull. Math. Biophys. **17**, 257-278 (1955). doi:10.1007/BF02477753

[73] FitzHugh, R. Biological Engineering. Edited by Herman P. Schwan. McGraw-Hill Companies **9**, 556 pages (1969).

[74] Noble, D., and Rudy, Y. Models of cardiac ventricular action potentials: Iterative interaction between experiment and simulation. Philos. Trans. R. Soc. A Math. Phys. Eng. Sci. **359**, 1127-1142 (2001). doi:10.1098/rsta.2001.0820

[75] Starobin, J. M., Zilberter, Y. I., Rusnak, E. M., and Starmer, C. F. Wavelet formation in excitable cardiac tissue: The role of wavefront-obstacle interactions in initiating high-frequency fibrillatory-like arrhythmias. Biophys. J. **70**, 581-5942 (1996). doi:10.1016/S0006-3495(96)79624-8

[76] Scott, A. C., Chu, F. Y. F., McLaughlin, D. W. The Soliton: A New Concept in Applied Science. Proceedings of the IEEE 61, 1443-1483 (1973). doi:10.1109/PROC.1973.9296

[77] Korteweg, D. J., de Vries, G. On the change of form of long waves advancing in rectangular canal and on a new type of long stationary waves. Philos. Mag. Ser. **5**, 422-443 (1895).

[78] P. G. Drazin and R. S. Johnson.: Solitons: An Introduction. (1983)

[79] Yuri. S., Kivshar., and Govind P. Agrawal.: Optical Solitons: From Fibers to Photonic Crystals. (2003)

[80] Roger K. Dodd, et al.: Solitons and Nonlinear Wave Equations. (1982)

[81] Fermi, A., Pasta, J., Ulam, S. Studies of non-linear problems, I. Los Alamos Report LA 1940 (1955).

[82] Zabusky, N. J., Kruskal, M. D. Interaction of solitons in a collisionless plasma and the recurrence of initial states. Phys. Rev. Lett. **15**, 240-243 (1965). doi: 10.1103/PhysRevLett.15.240

[83] Gardner, C. S., Greene, J. M., Kruskal, M. D., Miura, R. M. Method for solving the Korteweg-de Vries equation. Phys. Rev. Lett. **19**, 1095-1097 (1967).

[84] Hodgkin-Huxley electrical circuit. Available at: https://i1.wp.com/upload.wikimedia.org/wikipedia/commons/thumb/1/1f/ MembraneCircuit.svg/448px-MembraneCircuit.svg.png?w=560 (2024).

[85] Structure of the heart. url:https://thescienceandmathszone.com/structure-of-the-heart/. January (2024)

[86] Thiriet, M. Heart Wall. Pages: 271-348 (2013). url:https://upload.wikimedia.org/wikipedia/commons/ $thumb/6/6f/Blausen_0470_HeartWall.png$. January (2024)

[87] Filament cross section. Available at: $https://content.byui.edu/file/a236934c-3c60-4fe9-90aa-d343b3e3a640/1/module7/readings/skel_muscle_org.html$ (2024).

[88] Blood conduction. Available at: https://www.shutterstock.com/zh/image-vector/human-circulatory-system-stylized-heart-anatomy-1474700549 (2024).

[89] Wikimedia Commons. Pulmonary Circuit. Creative Commons License. Available at: $https://commons.wikimedia.org/wiki/File:2119_Pulmonary_Circuit.jpg$ (2024).

[90] Chung, D. D. L. Electrical Conduction Behavior. Funct. Mater. Available at: https://cvphysiology.com/s9v2f-3r4p7/share/conduction-system-2022.png (2024).

[91] Action potential of heart nodal cells. Available at: *https://www.moleculardevices.com/applications/patch – clamp – electrophysiology/media*$_1$*c6efa9f5f7a50e4dab68c492527445b7fdabda54.jpeg?width=750format=jpegoptimize=medium* (2024).

[92] Action potential of cardiac muscle cells. Available at: https://basicmedicalkey.com/wp-content/uploads/2016/07/*B9780323073622500206f16 – 03 – 9780323073622.jpg* (2024).

[93] Cardiopathies. Available at: https://pbs.twimg.com/media/FKbaDNaUUAQ7-AR.png (2024).

[94] Neuron. Available at: https://training.seer.cancer.gov/images/anatomy/nervous/neuron-structure.jpg (2024).

[95] Structural categories of neurons. Available at:

[96] Erps, B. Neuron Action Potential Synapse. Available at: https://www.sciencefacts.net/wp-content/uploads/2023/03/Action-Potential-Graph-Chart.jpg (2024).

[97] Ions flow. Available at: https://media.springernature.com/lw685/springer-static/image/chp

[98] Purves, D., Augustine, G. J., Fitzpatrick, D., Hall, W. C., LaMantia, A. S., McNamara, J.O. and White, L.E. Neuroscience, 4th ed. 26 (2008).

[99] Hodgkin, A. L. Evidence for electrical transmission in nerve: Part I. J. Physiol. **90**, 183-210 (1937). doi:10.1113/jphysiol.1937.sp003507

[100] Comparison between Electrical and Chemical synapses. Available at: https://o.quizlet.com/lWH-nxyISldIL2KTrsmzUw.jpg (2024)

[101] S*ü*dhof, T. C. Neurotransmitter release. Handb. Exp. Pharmacol. **184**, 1-21 (2008). doi:10.1007/978 – 3 – 540 – 74805 – 2$_1$

[102] Rusakov, D. A. Ca^{2+}-dependent mechanisms of presynaptic control at central synapses. Neuroscientist **12**, 317-326 (2006). doi:10.1177/1073858405284672

[103] Zoidl, G. and Dermietzel, R. On the search for the electrical synapse: A glimpse at the future. Cell Tissue Res. **310**, 137-142 (2002). doi:10.1007/s00441-002-0632-x

[104] Brink, P. R., Cronin, K. and Ramanan, S. V. Gap junctions in excitable cells. J. Bioenerg. Biomembr. **28**, 351-358 (1996). doi:10.1007/BF02110111

[105] Maestú, F., de Haan, W., Busche, M. A. and DeFelipe, J. Neuronal excitation/inhibition imbalance: Core element of a translational perspective on Alzheimer pathophysiology. Ageing Res. Rev. **69** (2021). doi:10.1016/j.arr.2021.101372

[106] Neurodegenerative Diseases. https://www.creativebiolabs.net/static/img/Neurodegenerative-Diseases-1.png (2024)

[107] Wenk, G. L.: Neuropathologic changes in Alzheimer's disease. The Journal of Clinical Psychiatry. **64**, 7-10 (2003)

[108] Lock, M. M.: The Alzheimer conundrum : entanglements of dementia and aging (2013)

[109] Elbaz, A., Carcaillon, L., Kab, S., Moisan, F.: Epidemiology of Parkinson's disease. Revue Neurologique. **172 (1)**, 14-26 (2016). doi:10.1016/j.neurol.2015.09.012

[110] Parkinson's Disease Mechanism Discovered. (2006)

[111] Min, Y.G., Choi, S.J., Hong, Y.H., Kim, S.M., Shin, J.Y., Sung, J.J.: Dissociated leg muscle atrophy in amyotrophic lateral sclerosis/motor neuron disease: the split-leg sign. Scientific Reports. **10 (1)**, 15661 (2020) doi:10.1038/s41598-020-72887-7

[112] Quinn, C., Edmundson, C., Dahodwala, N., Elman, L.: Reliable and efficient scale to assess upper motor neuron disease burden in amyotrophic lateral sclerosis. Muscle and Nerve. **61 (4)**, 508?511 (2020). doi:10.1002/mus.26764

[113] Purves, D., Augustine, G.A., Fitzpatrick, D., Hall, W., LaMantia, A.S., McNamara, J.O., Williams, S.M.: Circuits within the Basal Ganglia System. In Purves D (ed.). Neuroscience (2nd ed.). Sunderland, MA: Sinauer Associates (2001).

[114] Barnat, Monia; Capizzi, Mariacristina; Aparicio, Esther; Boluda, Susana; Wennagel, Doris, K., Radhia, K., Rayane, L., Sophie, A., Fabienne, B., Barbara Y., Liu, Jeh-Ping. Huntington's disease alters human neurodevelopment. Science. **369 (6505)**, 787-793 (2020) doi:10.1126/science.aax3338

[115] Nishinari, K., Abe, K., and Satsuma, J. A new type of soliton behavior of the Davey-Stewartson equations in a plasma system. Theor. Math. Phys. **99**, 745-753 (1994). doi:10.1007/BF01017062

[116] Nozaki, K., Bekki, N. Exact solutions of the generalized Ginzburg-Landau equation. The Physical Society of Japan. **53**, 1581-1582 (1984). doi.org/10.1143/JPSJ.53.1581

[117] Alidou, M., Ayissi, B. E., and Kofane, T. C. Instability criteria and pattern formation in the complex Ginzburg-Landau equation with higher-order terms. Phys. Rev. E. **74**, 046604 (2006).doi.org/10.1103/PhysRevE.74.046604

[118] Etienne, W., Alidou, M., and Kofane, T. C. Modulational instability of a trapped Bose-Einstein condensate with two- and three-body interactions. Phys. Rev. E. **77** (2008). doi:10.1103/PhysRevE.74.046604

[119] Yomba, E., and Kofane, T. C. Exact solutions of the one-dimensional generalized modified complex Ginzburg-Landau equation. Chaos Solitons Fractals. **17**, 847-860 (2003). doi:10.1016/S0960-0779(02)00488-5

[120] Conte, R., and Musette, M. Linearity inside nonlinearity: Exact solutions to the complex Ginzburg-Landau equation. Phys. D Nonlinear Phenom. **69**, 1-17 (1993). doi:10.1016/0167-2789(93)90177-3

[121] Yomba, E., Kofane, T. C., and Pelap, F. B. On exact solutions of the generalized modified Ginzburg-Landau equation using Hirota?s method. J. Phys. Soc. Jpn. **65**, 2337-2338 (1996). doi:10.1143/JPSJ.65.2337

[122] Cross, M. C., and Hohenberg, P. C. Pattern formation outside of equilibrium. Rev. Mod. Phys. 65, 851 (1993). https://doi.org/10.1103/RevModPhys.65.851

[123] Zemskov, E. P. and Tsyganov, M. A. Using a two-step extension of a well-known epidemic model with multiple seeds. Phys. Rev. E. (2017). doi:10.1142/S0217979218501655

[124] Tabi, C. B., Etémé, A. S., and Kofané, T. C. Unstable cardiac multi-spiral waves in a FitzHugh-Nagumo soliton model under magnetic flow effect. Nonlinear Dyn. **100**, 3799-3814 (2020). doi:10.1007/s11071-020-05750-z

[125] B. D. Tabi, A. S. Etémé, A. Mvogo, C. B. Tabi, H. P. Ekobena Fouda, and T. C. Kofané, *"Soliton-like nonlinear excitation in the FitzHugh-Nagumo cardiac model through the cubic-quintic Complex Ginzburg-Landau equation,"* Nonlinear Dynamics **112**, 11399-11418 (2024).

[126] A. Gizzi, A. Loppini, R. Ruiz-Baier, A. Ippolito, A. Camassa, A. La Camera, E. Emmi, L. Di Perna, V. Garofalo, C. Cherubini, and S. Filippi, *"Nonlinear diffusion and thermo-electric coupling in a two-variable model of cardiac action potential,"* Chaos. **27**, 093919 (2017).

[127] F. H. Fenton, A. Gizzi, C. Cherubini, N. Pomella, and S. Filippi, *"Role of temperature on nonlinear cardiac dynamics,"* Phys. Rev. E **87**, 042717 (2013).

[128] S. Filippi, A. Gizzi, C. Cherubini, S. Luther, and F. H. Fenton, *"Mechanistic insights into hypothermic ventricular fibrillation: the role of temperature and tissue size,"* Europace. **16(3)**, 424-434 (2014).

[129] D. Binia, C. Cherubinib, S. Filippi, *"On vortices heating biological excitable media,"* Chaos. Solitons and Fractals. **42**, 2057?2066 (2009).

[130] R. FitzHugh, K. S. Cole, *"Theoretical potassium loss from squid axons as a function of temperature,"* Biophys J. **4**,257 (1964).

[131] R. FitzHugh, *"Impulse and physiological states in models of nerve membrane,"* Biophys. J. **1**, 445-446 (1961).

[132] Tabi, C. B., Fewu, M., Ekobena, H. P., Fouda, A., Mohamadou, A., and Kofane, T. C.: Nonlinear wave trains in three-strand ? helical protein models. Euro. Phys. Jour. B **86**, 374 (2013). doi: 10.1140/epjb/e2013-40467-6

[133] Hirota, R. Direct Methods in Soliton Theories. Springer. 255-263 (1991). doi:10.1007/978-3-642-84570-3-32

[134] Hirota, R. The Direct Method in Soliton Theory. Cambridge University Press. (2004). doi:10.1017/cbo9780511543043

[135] Hirota, R. Exact Envelope-Soliton Solutions of a Nonlinear Wave Equation. Journal of Mathematical Physics **14**, 805-809 (1973). doi:10.1063/1.1666399

[136] Nozaki, K., Bekki, N. Pattern selection and spatiotemporal transition to Chaos in the Ginzburg-Landau equation. Phys. Rev. Lett. **51**, 2171-2174 (1983). doi:10.1103/PhysRevLett.51.2171

[137] Hirota, R., Iwanami, S. Direct method in soliton theory. Cambridge University Press, (1992).

[138] Bender, C. M. and Orszag, S. A. Advanced mathematical methods for scientists and engineers. 544-576 (1978). doi:10.1007/978-1-4757-3069-2

[139] Nayfeh, A. H. Perturbation Methods. IEEE Transactions on Systems Man and Cybernetics. doi:10.1109/TSMC.1978.4309986

[140] Leon, J. and Manna, M. Discrete Instability in Nonlinear Lattices. Phys. Rev. Lett. **83**, 2324 (1999). doi:10.1103/PhysRevLett.83.2324

[141] Remoissenet, M. Low-amplitude breather and envelope solitons in quasi-one-dimensional physical models. Phys. Rev. B **33**, 2386-2392 (1986). doi:10.1103/PhysRevB.33.2386

[142] Dauxois, T., Peyrard, M. Physics of Solitons, Chapter 3. Cambridge University Press, Cambridge (2006).

[143] N.N. Rao, Nonlinear wave modulations in plasmas, *Pramana*, 49(2):109-127, 1997.

[144] T.B. Benjamin, J.E. Feir, The disintegration of wave trains on deep water, *J. Fluid Mech.*, 27(3):417-430, 1967. doi:10.1017/S002211206700045X

[145] A.R. Seadawy, T.R. Rizvi, B. Mustafa, K. Ali, S. Althubiti, Chirped periodic waves for a cubic-quintic nonlinear Schrödinger equation with self steepening and higher-order nonlinearities, *Chaos Solitons Fractals*, 156:111191, 2022.

[146] E. Kengne, R. Vaillancourt, B.A. Malomed, Bose-Einstein condensates in optical lattices: The cubic-quintic nonlinear Schrödinger equation with a periodic potential, *J. Phys. B: At. Mol. Opt. Phys.*, 41(20):205202, 2008.

[147] Ndzana II, F., Mohamadou, A., Kofané, T.C., English, L.Q. Modulated waves and pattern formation in coupled discrete nonlinear LC transmission lines. Phys. Rev. E **78**, 016606 (2008). doi:10.1103/PhysRevE.78.016606

[148] Seadawy, A. Modulation instability analysis for the generalized derivative higher order nonlinear Schrödinger equation and its bright and dark soliton solutions. J. Electromagn. Waves Appl. **31(14)**, 1353-1362 (2017). doi:10.1016/j.ijleo.2019.02.027

[149] Belobo, D. B., Ekogo, T. B., Ben-Bolie, G. H., Tiofack, C. G. L., Kofané, T. C. Modulational Instability of a Bose-Einstein Condensate Beyond the Fermi Pseudopo-

tential with a Time-Dependent Complex Potential. International J. Mod. Phys. B **26(30)**, 1250164(17) (2012). doi:10.1142/S0217979212501640

[150] Afanasjev, V. V. Dynamics of Ion Acoustic Waves in Electronegative Plasmas. Opt. Lett. **18**, 790-793 (1993).

[151] Tabapsi, R., Kamdem, D. B., Belobo, et al. Energy localization in microtubules with radial dislocation. Eur. Phys. J. Plus **138**, 433 (2023). doi:10.1140/epjp/s13360-023-04051-9

[152] Etémé, A. S., Tabi, C. B., Mohamadou, A. Long-range patterns in Hindmarsh?Rose networks. Commun. Nonlinear Sci. Numer. Simul. **43**, 211-219 (2017). doi:10.1016/j.cnsns.2016.07.005

[153] Maina, I., Tabi, C. B., Mohamadou, A., Ekobena, H.P.F., Kofané, T.C. Discrete impulses in ephaptically coupled nerve fibers. Chaos **25**, 043118 (2015). doi:10.1063/1.4919077

[154] Tabi, C. B., Ondoua, R. Y., Ekobena, H. P., Mohamadou, A., Kofané, T. C. Energy patterns in coupled α-helix protein chains with diagonal and off-diagonal couplings. Phys. Lett. A **380**, 2374 (2016). doi:10.1016/j.physleta.2016.05.033

[155] Hussain, S., Shan, S. A., Akhtar, N., Masud, M. M. Investigation of the properties of electrostatic IA solitary wave structures in negative ion magnetoplasmas with superthermal electrons. Astrophys. Space Sci. **352**, 605-612 (2014). doi:10.1007/s10509-014-1977-9

[156] Shan, S. A., Akhtar, N. Astrophys and Space Science. **346**, 367 (2013).

[157] Tabi, C. B., Maina, I., Mohamadou, A., Ekobena, H.P.F., Kofané, T.C. EPL **106**, 18005 (2014). doi.org/10.1209/0295-5075/106/18005

[158] Mohamadou, A., Kofané, T.C. Modulational instability and pattern formation in discrete dissipative systems. Phys. Rev. E **73**, 046607 (2006). doi:10.1103/PhysRevE.73.046607

[159] Orazio, D., Servet, M., Enrique, T. Thermodynamic potentials for non-equilibrium systems. Chaos, Solitons Fractals **12**, 2619-2630 (2001). doi:10.1016/S0960-0779(01)00077-7

[160] Etémé, A. S. Consistency between modulational instability and energy localization in time-delay-memristive neural network. Europhys. Lett. **143**, 42002 (2023). doi:10.1209/0295-5075/acee1b

[161] McAllister, R. E., Noble, D., Tsien, R. W. Reconstruction of the electrical activity of cardiac Purkinje fibres. J. Physiol. 251, 1-59 (1975). doi:10.1113/jphysiol.1975.sp011080

[162] Ghomsi, P. G., Tameh, T. J. B., Moukam, F. M. K.: Ionic wave propagation and collision in an excitable circuit model of microtubules. Chaos **28**, 023106 (2018). doi: 10.1063/1.5001066.

[163] Draper, M. H., and Weidmann, S.: Cardiac resting and action potentials recorded with an intracellular electrode. J. Physiol. **115**, 74-94 (1951). doi: 10.1113/jphysiol.1951.sp004653

[164] MacGrogan, D., Luna-Zurita, L., and de la Pompa, J. L.: Notch signaling in cardiac valve development and disease. **91(6)**, 449-59 (2011). doi: 10.1002/bdra.20815

[165] Jongsma, H. J., and Wilders, R.: Gap junctions in cardiovascular disease. Circ Res. **86**, 1193-1197 (2000). doi: 10.1161/01.res.86.12.1193

[166] Almirantis, Y., and Papageorgiou, S.: Cross-diffusion effect on chemical and biological pattern formation. J. Theor. Biol **151**, 289-311 (1991). doi: 10.1016/S0022-5193(05)80379-0

[167] Zemskov, E. P., Tsyganov, M. A., Ivanitsky, G. R., and Horsthemke, W.: Solitary pulses and periodic wave trains in a bistable FitzHugh-Nagumo model with cross-diffusion and cross advection. Phys. Rev. E **105**, 014207 (2022). doi: 10.1103/PhysRevE.105.014207

[168] Noble, D., and Rudy, Y.: Models of cardiac ventricular action potentials: iterative interaction between experiment and simulation. Phil. Trans. R. Soc. A **359**, 1127-42 (2001). doi: 10.1098/rsta.2001.0820

[169] Panguetna, C. S., Tabi, C. B., Kofané, T. C. Low relativistic effects on the modulational instability of rogue waves in electronegative plasmas. J. Theor. Appl. Phys. **13**, 237-249 (2019). doi:10.1007/s40094-019-00342-8

[170] Panguetna, C. S., Tabi, C. B., Kofané, T. C. Two-dimensional modulated ion-acoustic excitations in electronegative plasmas. Phys. Plasmas **24**, 092114 (2017). doi:10.1063/1.5001725

[171] Madimabe, E. B., Tabi, C. B., Latchio, T. C. G., and Kofane, T. C.: Modulational instability in vector exciton-polariton condensates with photonic spin-orbit coupling. Phys. Rev. B **107**, 184502 (2023). doi: 10.1103/PhysRevB.107.184502

[172] Tabi, C. B., Maina, I., Mohamadou, A., Ekobena, H. P. F., and Kofane, T. C.: Long-range intercellular Ca^{2+} wave patterns. Physica A **435**, 1 (2015). doi: 10.1016/j.physa.2015.04.022

[173] Tabi, C. B., Maina, I., Mohamadou, A., Ekobena, F. H. P., and Kofane, T. C.: Wave instability of intercellular Ca^{2+} oscillations. EPL **106**, 18005 (2014). doi: 10.1209/0295-5075/106/18005

[174] Tabi, C. B., Etémé, A. S., Mohamadou, A., and Kofané, T. C.: Oscillating two-dimensional Ca^{2+} waves in cell networks with bidirectional paracrine signaling. Waves Rand. Complex Media **31**, 1028 (2021). doi: 10.1080/17455030.2019.1644465

[175] Zaoro, N. R., Tabi, C. B., Etémé, A. S., and Kofane, T. C.: Unstable cAMP wave patterns during aggregation of Dictyostelium discoideum cells. Phys. Lett. A **384**, 126133 (2020). doi: 10.1016/j.physleta.2019.126133

[176] Legoya, P., Etémé, A. S., Tabi, C. B., Mohamadou, A., and Kofane, T. C.: Frequency modes of unstable spiral waves in two-dimensional Rosenzweig-MacArthur ecological networks. Chaos Solit. Fract. **146**, 112599 (2022). doi: 10.1016/j.chaos.2022.112599

[177] Kivshar, Y. S., Peyrard, M. Synchronization behaviors of coupled neurons under electromagnetic radiation. Phys. Rev. A **46**, 3198-3205 (1992). doi:10.1103/PhysRevA.46.3198

[178] Pelap, F. B., and Kofane, T. C.: Modulational instability in some Physical systems. Physica. Scripta. **64**, 410-412 (2001). DOI: 10.1238/Physica.Regular.064a00410

[179] Daumont, I., Dauxois, T., Peyrard, M. Modulational instability: first step towards energy localization in nonlinear lattices. Nonlinearity **10(3)** (1997). PII: S0951-7715(97)77016-6

[180] Ferrari, L., and Cardano, G.: Ferrari's Method in his Artis Magnae, Sive de Regulis Algebraicis. 1545.

[181] A. L. F. Casas, G. M. D. Santos, N. B. Chiocheti, and M. de Andrade, *"Effect of temperature variation on the human cardiovascular system: A systematic review,"* Climate change and Health (2016).

[182] S. Modi and T. C. Krahn, *"Sudden cardiac arrest without overt heart disease,"* Circulation **123**, 2994-3008 (2011).

[183] R. E. Klabunde, *"Cardiac electrophysiology: normal and ischemic ionic current and the ECG,"* Adv. Physiol. Educ. **41**, 29-37 (2017).

[184] D. DiFrancesco, *"Pacemaker mechanisms in cardiac tissue,"* Annu. Rev. Physiol. **55**, 455-72 (1993).

[185] Takembo, C. N., Mvogo, A., Ekobena, H. P., and Kofane, T. C.: Effect of electromagnetic radiation on the dynamics of spatiotemporal patterns in memristor-based neuronal network. Nonlinear Dyn. **95(2)**, 1067-1078 (2019).doi:10.1007/s11071-018-4616-0

[186] Fuqiang, W., Chunni, W., Ying, X., and Jun, M.: Model of electrical activity in cardiac tissue under electromagnetic induction. Sci. Rep. **6**, 28 (2016).doi: 10.1038/s41598-016-0031-2.

[187] Liu, W., Yu, W., Yang, C., Liu, M., Zhang, Y., and Lei, M. Analytic solutions for the generalized complex Ginzburg-Landau equation in fiber lasers. Nonlinear Dyn. **89**, 2933-2939 (2017). doi:10.1007/s11071-017-3636-5

[188] Tomaselli, G. F., and Marban, E.: Electrophysiological remodeling in hypertrophy and heart failure. Cardiovascular Research **42**, 270-283 (1999).https://doi.org/10.1016/S0008-6363(99)00017-6

[189] Molkentin, J. D., Lu, J. R., Antos, C. L., Markham, B., Richardson, J., Robbins, J., et al.: A calcineurin-dependent transcriptional pathway for cardiac hypertrophy. Cell **93**, 215-228 (1998).doi: 10.1016/s0092-8674(00)81573-1

[190] Pelap, F. B., and Kofané, T. C.: The Revised Modulational Instability Criterion: I -The Mono-Inductance Transmission Line. Physica. Scripta. **57**, 410 (1998). 10.1088/0031-8949/57/3/011

[191] Nakaya, Y.: Magnetocardiography: a comparison with electrocardiography. J Cardiogr Suppl **3**, 31-40 (1984).

[192] Strukov, D. B., Snider, G. S., Stewart, D. R., et al.: The missing memristor found. Nature **453**, 80-83 (2008).doi.org/10.1038/nature06932

[193] Hershberger, R. E.: The dilated, restrictive and infiltrative cardiomyopathies. Braunwald's Heart Disease: A Textbook of Cardiovascular Medicine. 12th ed. Philadelphia, PA, Elsevier **52**, 1031-1051 (2002).

List of publication

1. B. Tabi Dzou, A. S. Etémé, A. Mvogo, C. B. Tabi, H. P. Ekobena Fouda, and T. C. Kofané, "*Soliton-like nonlinear excitation in the FitzHugh-Nagumo cardiac model through the cubic-quintic complex Ginzburg-Landau equation*" Nonlinear Dynamics **112**, 11399-11418 (2024), https://doi.org/10.1007/s11071-024-09629-1

Nonlinear Dyn
https://doi.org/10.1007/s11071-024-09629-1

ORIGINAL PAPER

Soliton-like nonlinear excitation in the FitzHugh–Nagumo cardiac model through the cubic–quintic complex Ginzburg–Landau equation

B. Tabi Dzou · A. S. Etémé · A. Mvogo · C. B. Tabi · H. P. Ekobena Fouda · T. C. Kofané

Received: 24 December 2023 / Accepted: 12 April 2024

Abstract The article exclusively discusses how the cubic–quintic complex Ginzburg–Landau equation governs the dynamics of dissipative soliton in the FitzHugh–Nagumo model combined with linear self- and cross-diffusion terms. Then, based on the linear stability analysis, a set of equations describing the evolution of the perturbation amplitude is derived, and a detailed analysis of the modulational instability gain spectrum is presented. Moreover, the exact dissipative soliton of the cubic–quintic complex Ginzburg–Landau equation is found using Hirota's bilinear method. Furthermore, as an input condition to our simulations, we use the obtained dissipative soliton solution to check the stability of the moving pulse solution by solving the quintic FitzHugh–Nagumo model numerically with self- and cross-diffusion terms. As a result, numerical findings are in perfect correlation with analytical investigations, thus attesting that cardiac cell dynamics through the quintic FitzHugh–Nagumo model is the support of soliton-pulse-like solutions.

Keywords FitzHugh–Nagumo model · Cubic–quintic complex Ginzburg–Landau equation · Modulational instability · Dissipative solitons · Action potential

B. Tabi Dzou · A. S. Etémé · A. Mvogo · H. P. Ekobena Fouda
Laboratory of Biophysics, Department of Physics, Faculty of Science, University of Yaoundé I, University of Yaoundé, P.O. Box 812, Yaoundé, Cameroon
e-mail: dzoublaise@gmail.com

A. S. Etémé
e-mail: etemearmand@yahoo.fr

A. Mvogo
e-mail: mvogal_2009@yahoo.fr

H. P. Ekobena Fouda
e-mail: hekobena@gmail.com

C. B. Tabi ( ) · T. C. Kofané
Department of Physics and Astronomy, Botswana International University of Science and Technology, Private Bag 16, Palapye, Botswana
e-mail: tabic@biust.ac.bw

T. C. Kofané
e-mail: tckofane@gmail.com

1 Introduction

There is a long-standing interest in excitable media, which are spatially distributed systems of locally excitable elements. The interaction of neighbouring elements by diffusive coupling can produce travelling waves of chemical, physical or biological activity. Many types of travelling waves, such as phase waves and trigger waves, are possible in excitable media waves in excitable media have been studied from experimental, numerical, topological and analytical points of view [1]. Experimentally observed features of waves of excitation in media of chemical, biochemical, and biophysical origin can be studied with the help of reaction-diffusion (RD) equations, in general, and by the concept of diffusion-driven instability, also known as the Turing instability, in particular. Turing instability leads to patterns that are stationary in time and periodic in space

Published online: 06 May 2024

[2]. In this concept, the inhibitor must diffuse faster than the activator, fulfilling one of the necessary conditions for forming spatial structure. Interest in spatial patterns in chemical systems has been growing with the observation by Zhabotinsky of spatial patterns in the Belousov–Zhabotinsky reaction [3–5]. The chemical patterns arise from the interplay between diffusion and the local chemical kinetics.

Several generalizations of the RD theory for pattern formation involve the introduction of domain growth as well as cross-diffusion, according to which gradients of the other field drive the flux of one of the fields. Many research works have been performed to investigate RD systems with various forms of diffusion, such as self-diffusion, cross-diffusion, mutual-diffusion, tracer-diffusion, intra-diffusion, inter-diffusion, uphill-diffusion and negative- or incongruent-diffusion, depending on the biological problem at hand [6]. In particular, RD systems with and without cross-diffusion for pattern formation have been studied in many theoretical papers [6,7] and then realized experimentally [8–12]. For instance, supercritical and subcritical solutions which depend on the parameter values of the model have been examined in the cross-diffusion transport in biological systems [13]. With the help of amplitude equations and numerical simulations in the vicinity of the Turing bifurcation curve, it has been shown that cross-diffusion plays a significant role in the determination and selection of patterns in the spatiotemporal prey-predator model with cross-diffusion terms [14] and ratio-dependent functional response [15]. Moreover, cross-diffusion-driven instability conditions for a two-component RD system with activator-depleted reaction kinetics have been derived, and cross-diffusion-induced parameter spaces have been computed. It appeared that the parameter spaces without cross-diffusion are sub-spaces of the cross-diffusion-induced parameter spaces [16]. Also, cross-diffusion-driven Turing instability, as well as Turing–Hopf conditions, have been investigated in the non-dimensional form of Schnakenberg model, which has been proposed as a typical activator-depleted substrate chemical RD model, leading to spatial and spatiotemporal pattern formation [17].

For predator–prey systems with negative and positive taxis, represented by nonlinear cross-diffusion terms, quasi-soliton interaction has been demonstrated, with the dependence of the velocity of wave propagation on the taxis having parabolic and linear forms [18,19]. On the one hand, a prey-dependent predator–prey model subject to self as well as cross-diffusion has been used to generate complex pattern replication in the two-dimensional space [20]. Indeed, it has been observed that spatially uniform oscillations in two predator–prey models with cross-diffusion terms of pursuit-evasion mutual taxis, such as the Truscott-Brindley model [21], and the Rosenzweig-MacArthur model [22–24] are unstable with respect to small perturbations [25]. Furthermore, it has been shown that cross-diffusion can induce the instability of an equilibrium, which is stable for the kinetic system and the self-diffusion–reaction ecosystem [26]. At the same time, cross-diffusion can also stabilize a uniform equilibrium, which is stable for the kinetic system but unstable for the self-diffusion reaction system in the predator–prey system with preytaxis and vegetation pattern formation in a water-limited ecosystem [27]. Based on multiple time and space scales expansion, the Turing amplitude equation in the case of Turing instability, and the complex Ginzburg–Landau (CGL) equation in the case of Hopf instability have been derived [28] for the Oregonator [29,30] and Brusselator [31] models with cross-diffusion terms. In addition, envelope quasi-solitons where amplitudes and speeds are fixed by parameters of the models have been reported in dissipative two-component models, supplemented with cross-diffusion, rather than self-diffusion terms [32]. In the same line of ideas, the cubic and the quintic Stuart-Landau equations, respectively describing the shape and the amplitude of the pattern near marginal stability, have been derived in an RD system with nonlinear diffusion.

In early research efforts, due to their complex external and internal properties, various mathematical neuron models have been proposed in order to describe the dynamical bursting-spiking behaviour of the membrane potential, such as the Hodgkin-Huxley neuron [33], the Hindmarsh-Rose model [34–38], the Izhikevich neuron [39], the Morris-Lecar neuron [40], the Chay model [41], the Hopfield neural network model [42], the Rulkov model [43], epileptor model [44], and the FitzHugh–Nagumo (FHN) model [45,46]. The FHN model has been introduced by FitzHugh [45] with the equivalent circuit by Nagumo et al. [46], which is a generalization of the Van der Pol oscillator. The effect of electromagnetic induction through the memristor coupling has been reported in the modified FHN model [47]. By using a reductive perturbation expansion in the

semi-discrete approximation, it has been shown that the dynamics of localized nonlinear excitations in an improved diffusive FHN model are described by the modified CGL equation [48]. The possibility to generate modulated spiral-like structures in a 2D FHN model under the activation of modulational instability (MI), also known as Benjamin–Feir instability, and the impact of the electromagnetic induction on spiral-like waves has been addressed in the framework of the 2D-CGL equation [49]. The effect of temperature fluctuation on wave localization during intercellular communication has been explored in the improved FHN myocardial model driven by a constant external current [50]. A chain memristive FHN network has been constructed, and monitor information patterns via MI as driven by autaptic coupling have been analysed [51]. Bifurcation diagrams, Lyapunov exponents, and time series have been used to characterize regular and irregular patterns in an improved photosensitive memristive FHN neural circuit [52].

Despite the great progress in FHN systems in recent years, most existing literature mainly focuses on local reactions or self-diffusion. Much less attention, however, has been devoted to analyzing the combined action of the linear self-diffusion and the linear cross-diffusion terms. Recently, it has been noticed that solitary waves in FHN system with cross-diffusion terms have properties that are different from the FHN system with classical self-diffusion coefficients [53]. Moreover, a bifurcation of excitation fronts, whose spatial profiles are characterized by oscillating tails, has been discovered in two-component bistable RD systems with cross-diffusion [18,54]. Subsequently, traveling pulses with oscillatory tails and fronts have been found in RD systems of the FHN type with linear cross-diffusion, which may be useful in exploring the effects of certain drugs on the neuron firing process [55]. It should be pointed out that the properties of various wave regimes, namely, fixed-shape propagating waves, envelope waves, multi-envelope waves, and quasi-solitons in two spatial dimensions have been observed in numerical simulations of two-component excitable media with cross-diffusion, such as the FHN kinetics and the Lengyel–Epstein [56] model of a chlorite-iodide-malonic acid-starch auto-catalytic reaction system [57]. In subsequent investigations, the effect of cross-diffusion on wave profiles and speed of propagation of solitary pulses and periodic solution has been analyzed in the bistable cross-diffusive FHN system [58]. Numerical simulations have generated the pulse-front waves constructed of fronts and pulses in a bistable piecewise linear RD system of the FHN type with linear cross diffusion [59]. Fast and slow wave solutions of the FHN model with cross-diffusion connection between the potential and recovery variables have been found [60].

In this paper, we consider the quintic FHN model with linear self- and cross-diffusion terms [61,62]. Contrary to the well-studied bistable regime of a piecewise linear of the standard FHN model, where the Heaviside step function replaces the cubic nonlinearity, we know little about the quintic FHN model with linear cross-diffusion terms. In fact, previous studies on the quintic generalization of the standard FHN model have focused on the interplay of a tristable kinetics [61] and self-diffusion as well as cross-diffusion terms on the formation and stability of nonlinear waves [62]. Notably, for a piecewise-linear McKean-type approximation of the quintic equation, the pulse solution with a zigzag-shaped profile has been generated [63], as opposed to the cubic FHN model where only the standard kink fronts, solitary pulses, and wave trains occur [64–66]. By considering quintic RD equations for two variables, exploding dissipative solitons can propagate for long times for a given range of parameters [62]. Consequently, starting from the quintic FHN model combined with self- and cross-diffusion terms, it is the main purpose of this paper to carry out a weakly nonlinear analysis to deduce the cubic–quintic CGL equation by the use of the multiple scales method. Furthermore, the standard linear stability is formulated, the expression for the MI gain spectrum is obtained, and the main characteristic is analyzed. Next, we address the problem of finding solutions to the FHN model, a basic model used to describe excitation and propagation in various active physical, chemical, and biological media. However, the FHN model is not easily analytically integrable and requires extended methods for its solutions to be characterized [67–69]. To solve this problem, we use the perturbative reduction method to establish the relationship between reaction-diffusion systems and the CGL equation, particularly its cubic–quintic version. This version has well-known analytical solutions.

It is also appropriate to mention that the MI is a nonlinear process of common occurrence in various fields of physics, such as fluids [70], plasmas [71–73], nonlinear optics [74–80], metamaterials [81,82], discrete

nonlinear systems [83–90], and Bose-Einstein condensates (BECs) [91–95], just to name a few. The MI phenomenon manifests itself in the exponential growth of weak perturbations through the amplification of sideband frequencies, which break up the otherwise uniform wave and generate fine localized structures [96–98]. Next, based on the Hirota's bilinear method [99–105], the bilinear equation for the cubic–quintic CGL equation is obtained by applying an appropriate dependent variable transformation associated with a modified bilinear operator. Then, a spatially localized dissipative soliton solution of the obtained nonlinear amplitude equation is derived by the perturbation technique. This analytical dissipative soliton solution is chosen as an initial condition of the quintic FHN model with linear self- and cross-diffusion terms to check the stability of the moving pulse solution in our numerical experiments.

The paper is organized as follows: Sect. 2 sets the problem, introduces the quintic FHN model combined with linear self- and cross-diffusion terms, and derives the cubic–quintic CGL equation using a multiple-scale perturbation theory. Section 3 investigates the linear stability analysis of uniform steady states and the MI gain spectrum. Then, Sect. 4 discusses the existence of dissipative soliton of the cubic–quintic CGL equation based on Hirota's bilinear formulation. Section 5 reports the results of numerical investigations on dissipative soliton dynamics. Finally, Sect. 6 gives some concluding remarks.

2 Model, multiple-scale expansion and derivation of the cubic–quintic CGL equation

The FHN model is a universal mathematical model that describes the dynamics of most excitable cells and tissues, including neurons, cardiac cells, and amoebae cells. In the following, we investigate the dynamics of cardiac cells. The following system of RD equations governs the process in agreement with the framework of our interest:

$$\frac{\partial u}{\partial t} = -u^5 + (a+b)u^4 + (1-ab)u^3 - (a+b)u^2 + abu - v + d_1\frac{\partial^2 u}{\partial x^2} + h_1\frac{\partial^2 v}{\partial x^2}, \tag{1}$$

$$\frac{\partial v}{\partial t} = \sigma u - \sigma\gamma v + d_2\frac{\partial^2 v}{\partial x^2} - h_2\frac{\partial^2 u}{\partial x^2}, \tag{2}$$

which is an extension of the FHN model [45,46,106], recently proposed by Zemskov et al. [63], in which a and b are the excitation thresholds that control the amplitude and the shape of the pulse ($0 < a < 1/2, -1/2 < b < 0$). The parameter ($\sigma \ll 1$), which is the ratio of the time scales and γ a free positive parameter, are taken both according to these conditions inter alia $((1-a-a^2)/3 - \sigma\gamma) > 0$, and $((1/\gamma) - (1-a-a^2)/3) > 0$. In Eqs.(1) and (2), the parameters d_1 and d_2 stand for the self-diffusion coefficients, while h_1 and h_2 represent the positive and negative cross-diffusion coefficients. The variable $u = u(x,t)$ represents the fast variable trans-membrane potential and $v = v(x,t)$ is the recharge variable ionic current. Although Eq. (2) does not contain any nonlinearity, the corresponding property is brought by the term $-u^5 + (a+b)u^4 + (1-ab)u^3 - (a+b)u^2$ in Eq. (1) which denotes the trans-membrane ionic currents per unit area [49,63]. We rewrite Eqs.(1) and (2) in the more general forms

$$\frac{\partial u}{\partial t} = \lambda_5 u^5 + \lambda_4 u^4 + \lambda_3 u^3 + \lambda_2 u^2 + \lambda_1 u + \lambda_0 v + d_1\frac{\partial^2 u}{\partial x^2} + h_1\frac{\partial^2 v}{\partial x^2}, \tag{3}$$

$$\frac{\partial v}{\partial t} = \mu_1 u + \mu_2 v + d_2\frac{\partial^2 v}{\partial x^2} - h_2\frac{\partial^2 u}{\partial x^2}, \tag{4}$$

where auxiliary parameters are given by $\lambda_0 = -1$, $\lambda_1 = ab$, $\lambda_2 = -(a+b)$, $\lambda_3 = 1-ab$, $\lambda_4 = a+b$, $\lambda_5 = -1$, $\mu_1 = \sigma$, and $\mu_2 = -\sigma\gamma$.

Solutions for the above system can be investigated using the general trial functions

$$u(x,t) = \sum_{n=1}^{\infty}\epsilon^n \sum_{\ell=-n}^{n} u_n^{(\ell)}(\xi_1,\xi_2,\tau_1,\tau_2)A^{(\ell)}(x,t), \tag{5}$$

$$v(x,t) = \sum_{n=1}^{\infty}\epsilon^n \sum_{\ell=-n}^{n} v_n^{(\ell)}(\xi_1,\xi_2,\tau_1,\tau_2)A^{(\ell)}(x,t), \tag{6}$$

where terms in $u_n^{(\ell)}$ and $v_n^{(\ell)}$ are given such a way that $u_n^{(-\ell)} = (u_n^{(\ell)})^*$ and $v_n^{(-\ell)} = (v_n^{(\ell)})^*$, with * being the complex conjugate. The new independent variables ξ_p and τ_p, are defined as $\xi_p = \epsilon^p(x - v_g t)$ and $\tau_p = \epsilon^{2p}t$, with $p = 1, 2$ and $\epsilon \ll 1$ being a small perturbation parameter. $A^{(\ell)}(x,t) = e^{i\ell\theta(x,t)}$ represents the carrier wave, where the phase $\theta = kx - \omega t$, with k and ω being its wavenumber and angular frequency, respectively.

By utilizing the trial solutions (5) and (6), we obtain sets of equations at different orders of ϵ for all terms in u and their derivatives. These equations must be solved at different order ϵ^n by considering different harmonics related to ℓ. As such, the leading order $(1, \ell)$, for $\ell = 0$, yields a homogeneous set of equations with non-zero determinant. Consequently, only the trivial solutions exist, so that $u_1^{(0)} = v_1^{(0)} = 0$. At the same order, for $\ell = 1$, we obtain a linear system for $u_1^{(1)}$ and $v_1^{(1)}$, yielding the following dispersion relation:

$$(i\omega)^2 + \big(\mu_2 + \lambda_1 - (d_1 + d_2)k^2\big)(i\omega) + (d_1d_2 + h_1h_2)k^4 + (\mu_1h_1 - \mu_2d_1 - \lambda_1d_2)k^2 + \lambda_1\mu_2 = 0, \tag{7}$$

where the solutions $u_1^{(1)} \equiv \psi$, $v_1^{(1)} = \alpha_0 u_1^{(1)}$, $\alpha_0 = \frac{i\omega+\lambda_1-d_1k^2}{h_1k^2} = \frac{-(\mu_1+h_2k^2)}{i\omega+\mu_2-d_2k^2}$ are found. It is worth noting that $u_1^{(1)}$ is an arbitrary function which will be defined later.

The order $(2, \ell)$, when $\ell = 0$, admits the solutions

$$u_2^{(0)} = \alpha_1|\psi|^2, \quad \text{and} \quad v_2^{(0)} = \alpha_2|\psi|^2, \tag{8}$$

with $\alpha_1 = \frac{-2\lambda_2}{\lambda_1}$ and $\alpha_2 = \frac{-\mu_1}{\mu_2}$. The case $\ell = 1$ leads to an inhomogeneous linear system for $u_2^{(1)}$ and $v_2^{(1)}$. As the determinant of the associated homogeneous system is equal to zero due to the dispersion relation (7), the system will have a solution under the Fredholm solvability condition, which is satisfied for

$$v_g = \frac{1}{(2i\omega + \mu_2 + \lambda_1 - (d_1 + d_2)k^2)} \times (4ik^3(d_1d_2 + h_1h_2) + 2k((d_1 + d_2)\omega + i(h_1\mu_1 - d_1\mu_2 - d_2\lambda_1))), \tag{9}$$

with v_g being the group velocity. The corresponding solutions are given by

$$u_2^{(1)} = u_2^{(1)}, v_2^{(1)} = \alpha_0 u_2^{(1)} + \frac{(2ih_2k - (v_g + 2id_2k)\alpha_0)}{(i\omega\mu_2 - d_2k^2)}\frac{\partial\psi}{\partial\xi_1}, \tag{10}$$

where $u_2^{(1)}$ is an another arbitrary function. Obviously, the angular frequency (ω) and the group velocity (v_g) are complex, i.e., they both contain real and imaginary parts. The plots of panels $(\text{aj})_{j=1,2}$ in Fig. 1 display the real and imaginary parts of the angular frequency versus the wavenumber k, while the plots of

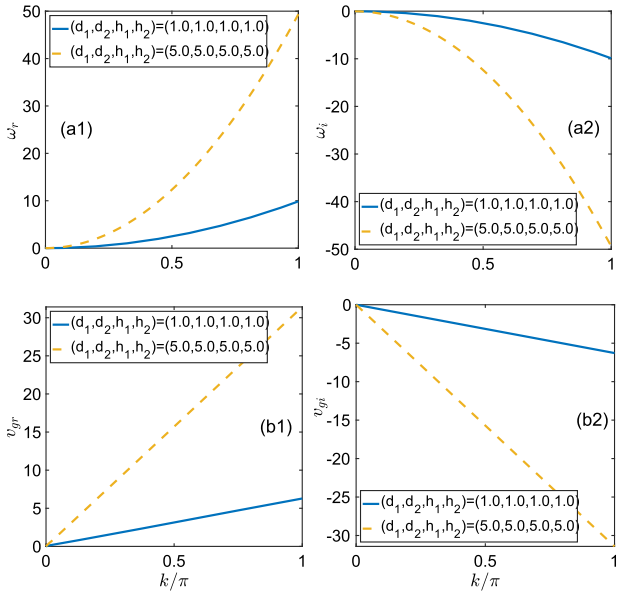

Fig. 1 (Color online) Panels $(\text{aj})_{j=1,2}$ show plots of the real and imaginary parts of the frequency ω, while panels $(\text{bj})_{j=1,2}$ display real and imaginary parts of the group velocity v_g versus the wavenumber k. The plots are generated by changing values of self- and cross-diffusion coefficients with $a = 0.25$, $b = -0.15$, $\gamma = 3.6$ and $\sigma = 0.01$. Real parts of ω and v_g are increasing functions of d_1, d_2, h_1 and h_2, while their imaginary components decrease when the self- and cross-diffusion coefficients are increased

panels $(\text{bj})_{j=1,2}$ show the real and imaginary parts of the group velocity, also against the wavenumber k. At this stage, changing the values of the self- and cross-diffusion coefficients importantly impacts the parametric behaviours of the two quantities. In general, ω_r and v_{gr} are increasing functions of the diffusion coefficients, while their imaginary parts decrease with increasing such coefficients. Precision should be made that the solid blue line in Fig. 1 corresponds to $(d_1, d_2, h_1, h_2) = (1.0, 1.0, 1.0, 1.0)$ and the dashed yellow line is obtained for $(d_1, d_2, h_1, h_2) = (5.0, 5.0, 5.0, 5.0)$. For the same order, it remains to consider $\ell = 2$, where one obtains the solutions

$$u_2^{(2)} = \alpha_3\psi^2, \quad \text{and} \quad v_2^{(2)} = \alpha_4\psi^2, \tag{11}$$

where $\alpha_3 = -\frac{(2i\omega+\mu_2-4d_2k^2)\lambda_2}{\Delta_1}$, $\alpha_4 = \frac{(\mu_1+4h_2k^2)\lambda_2}{\Delta_1}$, $\Delta_1 = (2i\omega)^2 + (\mu_2 + \lambda_1 - 4(d_1 + d_2)k^2)(2i\omega) + 16(d_1d_2+h_1h_2)k^4+4(\mu_1h_1-\mu_2d_1-\lambda_1d_2)k^2+\lambda_1\mu_2$. Similarly, calculations at the order $(3, \ell)$, when $\ell = 0$, lead to the solutions

$$u_3^{(0)} = \alpha_5\frac{\partial|\psi|^2}{\partial\xi_1}, \quad v_3^{(0)} = \alpha_6\frac{\partial|\psi|^2}{\partial\xi_1}, \tag{12}$$

where $\alpha_5 = -\frac{\alpha_0 v_g}{\lambda_1}$ and $\alpha_6 = \frac{(\alpha_0\mu_1-\alpha_1\lambda_1)v_g}{\lambda_1\mu_2}$. At the same order ϵ^3, for $\ell = 1$ we obtain an inhomogeneous system of equations in $u_3^{(1)}$ and $v_3^{(1)}$. As the determinant of the associated homogeneous system cancels out due to the dispersion relation, non-trivial solutions are expected if the Fredholm solvability condition is fulfilled. Thus, we obtain a nonlinear equation in which the terms in $u_3^{(1)}$ on the one hand, and the terms in $\frac{\partial u_2^{(1)}}{\partial \xi_1}$ and $\frac{\partial \psi}{\partial \xi_2}$ on the other hand cancel out due to the dispersion relation and the Fredholm solvability condition, respectively. Taking into account the previous results, we therefore obtain the cubic CGL equation, which reads

$$i\frac{\partial \psi}{\partial \tau_1} + p\frac{\partial^2 \psi}{\partial \xi_1^2} + q|\psi|^2\psi = 0, \tag{13}$$

where the coefficients p and q can be found in **Appendix 1**

Still at the order (3, 1), the solutions of the obtained inhomogeneous system are given by

$$\begin{aligned} u_3^{(1)} &= u_3^{(1)}, \\ v_3^{(1)} &= \frac{1}{(i\omega\mu_2 - d_2k^2)}\Big(-(\mu_1 + h_2k^2)u_3^{(1)} \\ &\quad +\alpha_0\frac{\partial \psi}{\partial \tau_1} + (2ih_2k - (v_g + 2id_2k)\alpha_0)\frac{\partial \psi}{\partial \xi_2} \\ &\quad +((h_2 - d_2\alpha_0) - (v_g + 2id_2k) \\ &\quad \times\frac{(2ih_2k - (v_g + 2id_2k)\alpha_0)}{(i\omega + \lambda_1 - d_1k^2)})\frac{\partial^2 \psi}{\partial \xi_1^2} \\ &\quad (2ih_2k - (v_g + 2id_2k)\alpha_0)\frac{\partial u_2^{(1)}}{\partial \xi_1}\Big), \end{aligned} \tag{14}$$

where $u_3^{(1)}$ is an another arbitrary function. To remind, it has been demonstrated that the envelope quasi-solitons in one-dimensional RD systems, with linear cross-diffusion [32], share the same form of spatiotemporal oscillations with envelope solitons in the cubic CGL equation for a complex field $\psi = u - iv$ [107]. Further investigations have revealed various types of nonlinear waves in excitable cross-diffusion systems. We follow up in the same order, with $\ell = 2$ and $\ell = 3$, one obtains the solutions

$$\begin{aligned} u_3^{(2)} &= \frac{\det\left(u_3^{(2)}\right)}{\Delta_1}, \\ v_3^{(2)} &= \frac{1}{(2i\omega + \mu_2 - 4d_2k^2)}(-(\mu_1 + 4h_2k^2)u_3^{(2)} \\ &\quad +((4ih_2k\alpha_3 - v_g + 4id_2k)\alpha_4)\frac{\partial \psi^2}{\partial \xi_1}), \end{aligned} \tag{15}$$

with $\det\left(u_3^{(2)}\right) = (((2i\omega + \mu_2 - 4d_2k^2)\alpha_3 + 4h_1k^2\alpha_3\alpha_4)v_g + 16i\alpha_3(d_1d_2 + h_1h_2 + (h_1d_2 - h_1d_1)\alpha_4)k^3 + 4\alpha_3((2d_1 + 2h_1\alpha_4)\omega - i\mu_2(d_1 + h_1\alpha_4))k)\frac{\partial \psi^2}{\partial \xi_1}$, and

$$u_3^{(3)} = \alpha_7\psi^3, \quad v_3^{(3)} = \alpha_8\psi^3, \tag{16}$$

where $\alpha_7 = -\frac{(3i\omega+\mu_2-9d_2k^2)(\lambda_3+2\lambda_2\alpha_3)}{\Delta_2}$ and $\alpha_8 = \frac{(\mu_1+9h_2k^2)\alpha_7}{\Delta_2}$, with $\Delta_2 = (3i\omega)^2 + (\mu_2 + \lambda_1 - 9(d_1 + d_2)k^2)(3i\omega) + 81(d_1d_2 + h_1h_2)k^4 + 9(\mu_1h_1 - \mu_2d_1 - \lambda_1d_2)k^2 + \lambda_1\mu_2$.

At the order $(4, \ell)$, when $\ell = 0$, by neglecting the nonlinear terms of higher-order such as, $\frac{\partial u_3^{(0)}}{\partial \xi_1}$, $\frac{\partial u_2^{(0)}}{\partial \xi_2}$, $\frac{\partial u_2^{(0)}}{\partial \tau_1}$, $\frac{\partial^2 u_2^{(0)}}{\partial \xi_1^2}$ and $\frac{\partial^2 v_2^{(0)}}{\partial \xi_1^2}$, we get the solutions

$$u_4^{(0)} = \alpha_9|\psi|^4, \quad \text{and} \quad v_4^{(0)} = \alpha_{10}|\psi|^4, \tag{17}$$

where $\alpha_9 = -\frac{(6\lambda_4+3\lambda_3(2\alpha_1+\alpha_3^*+\alpha_3)+\lambda_2(2|\alpha_3|^2+\alpha_1^2))}{\lambda_1}$, and $\alpha_{10} = -\frac{\mu_1}{\mu_2}\alpha_9$. The order $(4, \ell)$, when $\ell = 1$, the obtained system of algebraic equations is such that setting its determinant to zero cancels the higher-order nonlinearities terms such that $\frac{\partial u_3^{(1)}}{\partial \xi_1}$, $\frac{\partial u_2^{(1)}}{\partial \xi_2}$ and $\frac{\partial |\psi|}{\partial \xi_1}\psi$, and yields

$$\begin{aligned} &i\frac{\partial u_2^{(1)}}{\partial \tau_1} + p\frac{\partial^2 u_2^{(0)}}{\partial \xi_1^2} = 0, \quad u_4^{(1)} = u_4^{(1)}, \\ &v_4^{(1)} = \frac{1}{(i\omega + \mu_2 - d_2k^2)}(-(\mu_1 + h_2k^2)u_4^{(1)} \\ &\quad -\alpha_0\frac{\partial u_2^{(1)}}{\partial \tau_1} + (2ih_2k - (v_g + 2id_2k)\alpha_0)\frac{\partial u_3^{(1)}}{\partial \xi_1} \\ &\quad +(2ih_2k - (v_g + 2id_2k)\alpha_0)\frac{\partial u_2^{(1)}}{\partial \xi_2} + \Big((h_2 - d_2\alpha_0) \\ &\quad -(v_g+2id_2k)\left(\frac{(2ih_2k-(v_g+2id_2k)\alpha_0)}{(i\omega + \mu_2 - d_2k^2)}\right)\frac{\partial^2 u_2^{(1)}}{\partial \xi_2^2}\Big), \end{aligned} \tag{18}$$

with $u_4^{(1)}$ another arbitrary function. In the same order, with $\ell = 2$, one gets

$$u_4^{(2)} = \alpha_{11}|\psi|^2\psi^2, \quad \text{and} \quad v_4^{(2)} = \alpha_{12}|\psi|^2\psi^2, \tag{19}$$

where $\alpha_{11} = -\frac{1}{\Delta_1}((4\lambda_4+3\lambda_3(2\alpha_3+\alpha_1)+\lambda_2(2\alpha_1\alpha_3+\alpha_7))(2i\omega + \mu_2 - 4d_2k^2))$ and $\alpha_{12} = \frac{(\mu_1+4h_2k^2)\alpha_{11}}{(2i\omega+\mu_2-4d_2k^2)}$. However, for $\ell = 3$ one obtains

$$u_4^{(3)} = \alpha_{13}\frac{\partial \psi^3}{\partial \xi_1}, \quad \text{and} \quad v_4^{(3)} = \alpha_{14}\frac{\partial \psi^3}{\partial \xi_1}, \tag{20}$$

with $\alpha_{13} = \frac{det(u_4^{(3)})}{(\Delta_2\frac{\partial \psi^3}{\partial \xi_1})}$, $\alpha_{14} = \frac{1}{(3i\omega+\mu_2-9d_2k^2)}(-(\mu_1 + 9h_2k^2)\alpha_{13}+(6ih_2k\alpha_7-(v_g+6id_2k)\alpha_8))$, $\det\left(u_4^{(3)}\right) =$

$(((3i\omega + \mu_2 - 9d_2k^2) + 9h_1k^2\alpha_8)v_g + 54i(h_2\alpha_7 - d_2\alpha_8)k^3 + 18\omega(d_1\alpha_7 + h_1\alpha_8)k + (6id_2k^3 - 6i\mu_2k)(d_1\alpha_7 + h_1\alpha_8))\frac{\partial\psi^3}{\partial\xi_1}$. Still at the same order, for $\ell = 4$, we get

$$u_4^{(4)} = \alpha_{15}\psi^4, \quad \text{and} \quad v_4^{(4)} = \alpha_{16}\psi^4, \tag{21}$$

with $\alpha_{15} = det(u_4^{(4)})/(\Delta_3\psi^4)$, $\alpha_{16} = -\frac{(\mu_1 + 16h_2k^2)\alpha_{15}}{(4i\omega + \mu_2 - 16d_2k^2)}$, $\Delta_3 = (4i\omega)^2 + (\mu_2 + \lambda_1 - 16(d_1 + d_2)k^2)(4i\omega) + 256(d_1d_2 + h_1h_2)k^4 + 16(\mu_1h_1 - \mu_2d_1 - \lambda_1d_2)k^2 + \lambda_1\mu_2$, and $\det(u_4^{(4)}) = -(4i\omega + \mu_2 - 16d_2k^2)(\lambda_4 + 3\lambda_3\alpha_3 + 2\lambda_2(\alpha_3^2 + \alpha_7))\psi^4$.

The order $(5, \ell)$, for $\ell = 0$ admits the solutions

$$u_5^{(0)} = \alpha_{17}\frac{\partial|\psi|^4}{\partial\xi_1}, \quad \text{and} \quad v_5^{(0)} = \alpha_{18}\frac{\partial|\psi|^4}{\partial\xi_1}, \tag{22}$$

where $\alpha_{17} = -\frac{\alpha_9 v_g}{\lambda_1}$ and $\alpha_{18} = -\frac{(\alpha_{10}v_g + \mu_1\alpha_{17})}{\mu_2}$. At the same order for $\ell = 1$, we obtain an inhomogeneous system in $u_5^{(1)}$ and $v_5^{(1)}$. The determinant of the latter is zero due to the dispersion relation. Therefore, such a system admits non-trivial solutions if the solvability condition is satisfied. This allows to derive a nonlinear partial differential equation in which the term in $u_5^{(1)}$ on the one hand and in $\frac{\partial u_3^{(1)}}{\partial\xi_2}$ and $\frac{\partial u_4^{(1)}}{\partial\xi_1}$ on the other hand cancel out due to the dispersion relation and the Fredholm solvability condition, respectively. Considering the previous results and making some simplifications, we obtain the following reduced equation.

$$i\frac{\partial\psi}{\partial\tau_2} + p\frac{\partial^2\psi}{\partial\xi_2^2} + i\frac{\partial\psi}{\partial\tau_1} + p\frac{\partial^2\psi}{\partial\xi_1^2} + r|\psi|^4\psi = i\gamma\psi \tag{23}$$

From Eq. (13), the expression $i\frac{\partial\psi}{\partial\tau_1} + p\frac{\partial^2\psi}{\partial\xi_1^2} = -q|\psi|^2\psi$. By letting, $\xi = \xi_2$, $\tau = \tau_2$ and $-q \longleftarrow q$, we derive the cubic–quintic CGL equation as

$$i\frac{\partial\psi}{\partial\tau} + p\frac{\partial^2\psi}{\partial\xi^2} + q|\psi|^2\psi + r|\psi|^4\psi = i\gamma\psi, \tag{24}$$

where ψ denotes the complex envelope of soliton-like solution. Herein, $p = p_r + ip_i$ denotes the complex dispersion coefficient, $q = q_r + iq_i$ represents the cubic complex nonlinearity coefficient, $r = r_r + ir_i$ is the quintic complex nonlinearity coefficient, and $\gamma = \gamma_r + i\gamma_i$ is the complex dissipation coefficient which is responsible for damping in the action potential of myocardial cells. While p and q are given in **Appendix 1**, the other coefficients, i.e., r and γ can be found in **Appendix 2**. It is important to note that the cubic–quintic CGL Eq. (24) and its various adaptations have been extensively studied due to their nonlinear nature. This equation is useful in understanding both qualitative and quantitative aspects of physical processes, such as nonlinear transmission lines [108] and fluid mechanics [109]. Here, this equation will be useful to exclusively describe the electrical current of soliton-like nonlinear excitation from the Sino-atrial (SA) node among myocardial cells in a biological context.

3 Linear stability analysis of a plane wave solution

As said earlier, the MI phenomenon is a physical process whereby a plane wave, under small perturbations, breaks into trains of solitons [110]. The process has been addressed, under different contexts, in a broad range of physical systems, including biophysics [83,109] to nonlinear optics [111–113], through electrical transmission line [33,45,114], plasma systems [115,116] and Bose–Einstein condensates [117,118]. In Ref. [113], authors have derived the MI criterion through the generalized cubic–quintic CGL equation. Here, we apply a similar approach to investigate the MI phenomenon through the cubic–quintic CGL equation (24). To proceed with our analysis, we assume the plane wave $\psi(\xi, \tau) = \psi_0 e^{i(\nu\xi - \eta\tau)}$ to be solution of Eq. (24), with ν and η corresponding to the wavenumber and angular frequency of the unperturbed plane wave that are related via the equation

$$-\eta - p\nu^2 + q|\psi_0|^2 + r|\psi_0|^4 = i\gamma, \tag{25}$$

which can also be expressed in the form

$$-\eta - p_r\nu^2 + q_r|\psi_0|^2 + r_r|\psi_0|^4 = -\gamma_i, \tag{26}$$

$$-p_i\nu^2 + q_i|\psi_0|^2 + r_i|\psi_0|^4 = \gamma_r, \tag{27}$$

after separating the real and imaginary parts. To examine the stability of the plane wave solution, we modulate it with a small perturbation as $\psi(\xi, \tau) = (\psi_0 + \delta\psi)\, e^{i(\nu\xi - \eta\tau)}$, where $\delta\psi$ accounts for the perturbation and its amplitude is supposed to be small in comparison to the plane wave amplitude ψ_0. Inserting the perturbed solution into Eq. (24), linearizing around the unperturbed plane wave and taking into account Eq. (25), we obtain the following equation for the perturbation field:

$$i\frac{\partial\delta\psi}{\partial\tau} + p\frac{\partial^2\delta\psi}{\partial\xi^2} + 2i\nu p\frac{\partial\delta\psi}{\partial\xi} + q\psi_0(\psi_0\delta\psi^* + \psi_0^*\delta\psi) + 2r|\psi_0|^2\psi_0(\psi_0\delta\psi^* + \psi_0^*\delta\psi) = 0. \tag{28}$$

A solution to the above equation can be taken in the form $\delta\psi = \delta\psi_1 e^{i(\Gamma\xi+\Omega\tau)} + \delta\psi_2^* e^{-i(\Gamma\xi+\Omega^*\tau)}$, where Γ and Ω represent the wavenumber and the angular frequency of the perturbation, respectively. Making use of this in the perturbation Eq. (28), one obtains the following homogeneous system for $\delta\psi_1$ and $\delta\psi_2$:

$$2(\Omega + c_{11})\delta\psi_1 + c_{12}\delta\psi_2 = 0, \tag{29}$$

$$c_{21}\delta\psi_1 + (\Omega + c_{22})\delta\psi_2 = 0, \tag{30}$$

where

$$c_{11} = (2\nu\Gamma + \Gamma^2)p - (q + 2r|\psi_0|^2)|\psi_0|^2,$$
$$c_{12} = -(q + 2r|\psi_0|^2)\psi_0^2,$$
$$c_{21} = (q^* + 2r^*|\psi_0|^2)(\psi_0^*)^2,$$
$$c_{22} = (2\nu\Gamma - \Gamma^2)p^* + (q^* + 2r^*|\psi_0|^2)|\psi_0|^2.$$

The above system will admit non-trivial solutions under the condition that its determinant equal to zero, which allows obtaining the nonlinear dispersion relation

$$\Omega^2 + X\Omega + Y = 0, \tag{31}$$

where $X = c_{11} + c_{22}$ and $Y = c_{11}c_{22} - c_{12}c_{21}$. Solutions of Eq. (31) are investigated via its discriminant $\Delta = \Delta_r + i\Delta_i$, where Δ, Δ_r and Δ_i are expressed in **Appendix 3**.

Based on the above, the solution of Eq. (31) giving the perturbation angular frequency is a complex function that can be written in a simplified way as:

$$\Omega = (\chi \pm e_1) + i(\phi \pm e_2), \tag{32}$$

where $\chi = 2\nu\Gamma p_r, \phi = \left(\Gamma^2 p_i - q_i|\psi_0|^2 - 2r_i|\psi_0|^4\right)$, with

$$e_1 = \sqrt{\frac{1}{2}\left(\Delta_r + \sqrt{\Delta_r^2 + \Delta_i^2}\right)},$$

$$e_2 = \sqrt{\frac{1}{2}\left(-\Delta_r + \sqrt{\Delta_r^2 + \Delta_i^2}\right)}.$$

The previously determined expression of Ω allows us to examine two cases that are related to the sign of Δ_i. So, when $\Delta_i < 0$, the solutions of Eq. (31) are Ω_1 and Ω_2 on the one hand. On the other hand, when $\Delta_i > 0$, solutions of Eq. (31) are $\Omega_1^{'}$ and $\Omega_2^{'}$. Therefore, the two pairs of solutions are expressed by

$$\Omega_1 = (\chi + e_1) + i(\phi - e_2),$$
$$\Omega_2 = (\chi - e_1) + i(\phi + e_2),$$
$$\Omega_1^{'} = (\chi - e_1) + i(\phi - e_2),$$
$$\Omega_2^{'} = (\chi + e_1) + i(\phi + e_2). \tag{33}$$

It is important to stress that solutions $\Omega_1^{'}$ and $\Omega_2^{'}$ have the same asymptotic behavior as those of Ω_1 and Ω_2. As it is well known, the sign of the imaginary part of the perturbation angular frequency allows assessing the development of the MI in the system under study [113]. For a better understanding, let us insert the first relation of Eq. (33) into the expression of the perturbation $\delta\psi$ and doing so, we obtain

$$\delta\psi = \delta\psi_1 e^{i(\Gamma\xi+(\chi+e_1)\tau)}e^{-(\phi-e_2)\tau} + \delta\psi_2^* e^{-i(\Gamma\xi+(\chi+e_1)\tau)}e^{(\phi-e_2)\tau}. \tag{34}$$

Obviously, the behavior of the $\delta\psi$-function is influenced by the sign of $(\phi - e_2)$, which represents $\mathrm{Im}(\Omega_1)$. Upon analyzing the sign of $(\phi - e_2)$, we observe that if $\phi < 0$, then $(e_2 - \phi) > 0$. Consequently, the cubic–quintic CGL equation experiences exponential growth over time, leading to the instability of the plane wave under modulation. However, if $\phi > 0$, we have $(\phi - e_2) < 0$, i.e., $\mathrm{Im}(\Omega_1) < 0$, the cubic–quintic CGL equation diverges without limit as τ increases, and the system is considered to be modulationally unstable. The explicit expression of the imaginary part of Ω_1 is given by

$$\phi - e_2 = \phi - [\frac{1}{2}\{e_3 + 2\Gamma^2(p_r q_r + p_i q_i)|\psi_0|^2 + 4\Gamma^2(p_r r_r + p_i r_i)|\psi_0|^4 + e_4\}]^{1/2}, \tag{35}$$

with, $e_3 = -4\nu^2\Gamma^2 p_r^2 - \Gamma^4|p|^2$, $e_4 = (\Gamma^2 p_i - (q_i + 2r_i|\psi_0|^2)|\psi_0|^2)^2 + 4\nu^2\Gamma^2|p|^2 + \sqrt{\Delta_r^2 + \Delta_i^2}$. As the quantity $e_4 > 0$, it happens that $\phi - e_2 \leq \phi - [\frac{1}{2}\{e_3 + 2\Gamma^2(p_r q_r + p_i q_i)|\psi_0|^2 + 4\Gamma^2(p_r r_r + p_i r_i)|\psi_0|^4\}]^{1/2}$. Moreover, the inequality $\mathrm{Im}(\Omega_1) < 0$ is satisfied if $\phi - [\frac{1}{2}\{e_3 + 2\Gamma^2(p_r q_r + p_i q_i)|\psi_0|^2 + 4\Gamma^2(p_r r_r + p_i r_i)|\psi_0|^4\}]^{1/2} < 0$. By giving that, $\phi > 0$ and $e_3 < 0$, the above condition is fulfilled as soon as we have

$$(p_r q_r + p_i q_i) + 2(p_r r_r + p_i r_i)|\psi_0|^2 > 0. \tag{37}$$

The inequality (37) which represents the MI criterion is similar to that found by Mohamadou et al. [113] while investigating pattern formation in the generalized cubic–quintic CGL equation. From Eq. (37), the threshold amplitude of an unstable monochromatic wave above which the plane wave breaks into nonlinear patterns is found as

$$|\psi_0|^2 > |\psi_{0,cr}|^2 = -\frac{(p_r q_r + p_i q_i)}{2(p_r r_r + p_i r_i)}. \tag{38}$$

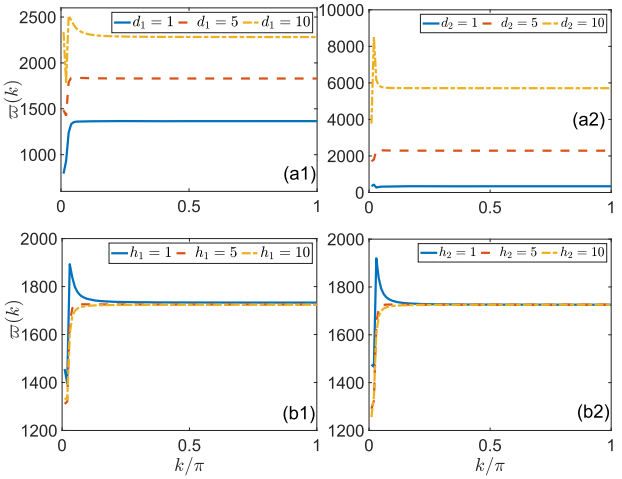

Fig. 2 (Color online) The panels show plots of the instability function $\varpi(k) = (p_r q_r + p_i q_i) + 2(p_r r_r + p_i r_i)|\psi_0|^2$ against the wavenumber k, under the respective effects of the self-diffusion coefficients [panels (**a1**) and (**a2**)] and cross-diffusion coefficients [panels (**b1**) and (**b2**)]. For (**a1**), $d_2 = h_1 = h_2 = 1$, for (**a2**) $d_1 = h_1 = h_2 = 1$, for (**b1**) $d_1 = d_2 = h_2 = 1$ and (**b2**) $d_1 = d_2 = h_1 = 1$, with the other parameter values being: $a = 0.25$, $b = -0.15$, $\gamma = 3.6$ and $\sigma = 0.01$

It is worth noticing that the plane wave amplitude expressed in Eq. (27) as

$$|\psi_0|^2 = (-q_i - \sqrt{q_i^2 + 4r_i(\nu^2 p_i + \gamma_r)})/2r_i$$

verifies the above condition (38), when $\nu > 2.8\pi$. In Fig. 2, the instability function $\varpi(k) = (p_r q_r + p_i q_i) + 2(p_r r_r + p_i r_i)|\psi_0|^2$, according to Eq. (37), is plotted versus the wavenumber k of the carrier wave for different values of the self- and cross-diffusion coefficients. As shown, the $\varpi(k)$-function remains positive regardless of the value of the wavenumber k along with the diffusion coefficients, thus attesting that the plane wave is trivially modulationally unstable. Obviously, $\varpi(k)$ increases with both self-diffusion coefficients [see panels (a1) and (a2)]. This suggests that these parameters can be used to monitor the appearance of nonlinear localized structures for the action potential within the cardiac cells. On the other hand, when the cross-diffusion coefficients h_1 and h_2 are increased in panels (b1) and (b2), respectively, the instability function decreases, which predicts a decrease of the MI growth rate [119]. Concerning the model under study, the projection is indicative of the membrane trying to adjust for the perturbation to bring the potential back down to the steady state. For the completeness of this linear stability analysis, the MI growth rate is expressed as

$$\mathbf{G}(\Gamma) = \Big|\Gamma^2 p_i - q_i|\psi_0|^2 - 2r_i|\psi_0|^4 - \sqrt{\frac{1}{2}\left(-\Delta_r + \sqrt{\Delta_r^2 + \Delta_i^2}\right)}\Big|. \tag{39}$$

Some features of the MI growth rate, using Eq. (39), are displayed in Fig. 3, where different combinations of self- and cross-diffusion parameter values have been used as in Fig. 2. Our discussion in this part emphasizes the maximum growth rate of instability that appears to be very sensitive to changes in d_1, d_2, h_1, and h_2. For example, the impact of varying d_1 is given by Fig. 3(aj)$_{j=1,2,3}$, where it is clear that increasing d_1 amplifies the maximum growth rate, in a context where nonlinear patterns are likely to appear in regions of weak wavenumber Γ. Similar calculations are repeated in Fig. 3 (bj)$_{j=1,2,3}$, where d_1, h_1, and h_2 are fixed with d_2 changing. We also observe the same spectrum of behaviors which can be specifically attributed to the variations of self-diffusion coefficients. Now, fixing d_1, d_2, and h_2, the impact of h_1 is pictured in Fig. 3 (cj)$_{j=1,2,3}$, where increasing its value does not importantly impact the growth rate magnitude, but rather contribute to reducing its parametric expansion in the Γ-direction. The same behavior of the growth rate remains ostensible when h_2 is changed, keeping d_1, d_2, and h_1 constant as shown in Fig. 3 (dj) $_{j=1,2,3}$. When parameters are chosen properly within the instability zone, the transmembrane potential is expected to exhibit nonlinear oscillations. These oscillations are crucial in understanding cardiac signals and electrocardiograms. If the magnitude of the MI growth rate decreases, the instability tends to disappear. Since the SA node generates the soliton train, energy decreases over time, preventing wave pattern formation in the cardiac tissue. Tabi et al. [49] discussed plane wave perturbation's importance in generating spiral waves in the FHN cardiac model, celebrating balanced contributions from nonlinear and dispersive effects. However, instead of cross-diffusion, the application of an induced magnetic field was shown to drastically modify the appearance of MI through the growth rate and spatiotemporal evolution. This reinforces the idea that MI and solitary waves are straightforwardly related and share the same parameter space [120]. That constitutes a profound motivation to look for exact envelope solutions for the studied model as proposed in the next section.

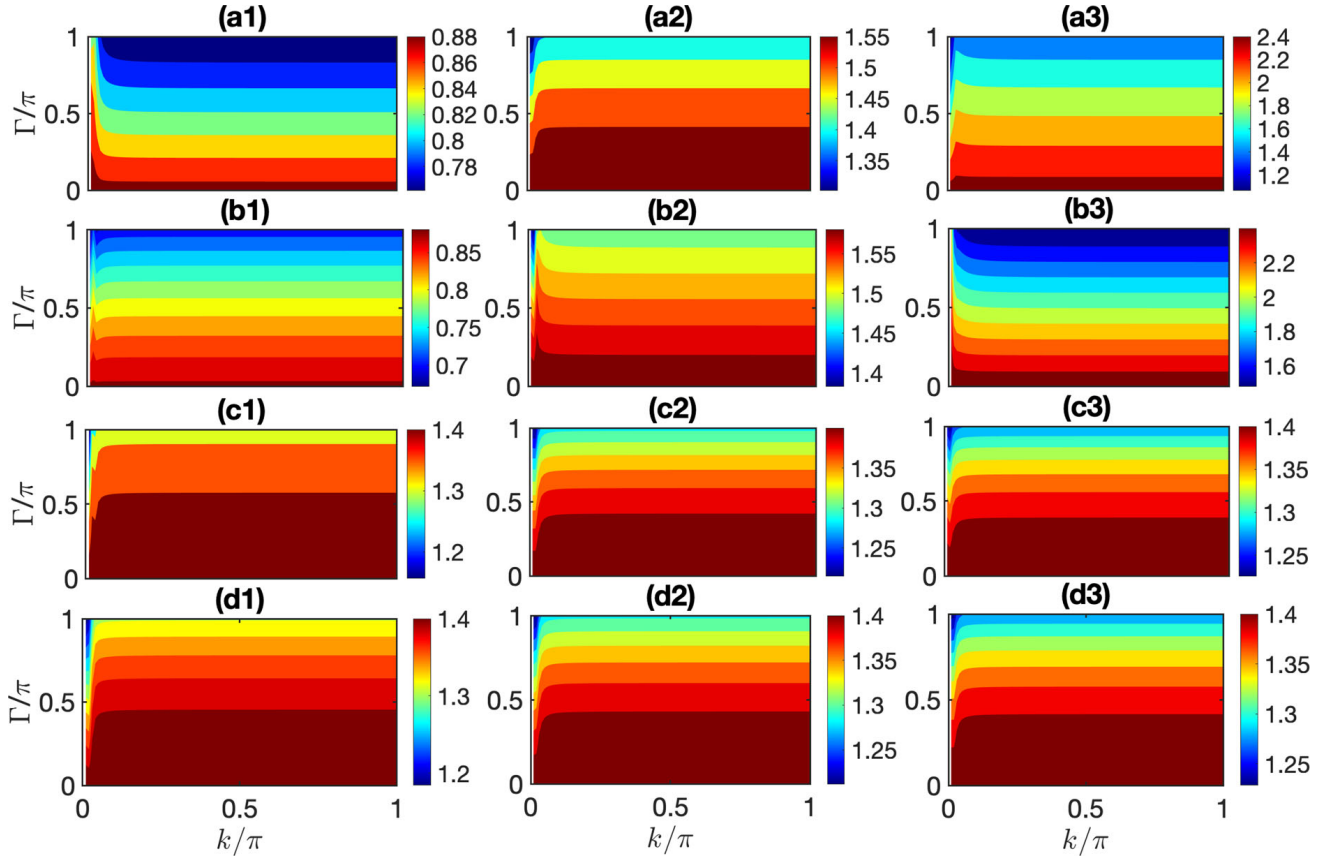

Fig. 3 (Color online) Panels $(\mathrm{aj})_{j=1,2,3,}$ and $(\mathrm{bj})_{j=1,2,3,}$ show the growth rate of MI versus the wavenumbers k and Γ, under the effect of the self-diffusion coefficients d_1 and d_2, respectively. Panels $(\mathrm{cj})_{j=1,2,3,}$ and $(\mathrm{dj})_{j=1,2,3,}$ display the MI growth rate under the impact of the cross-diffusion coefficients h_1 and h_2, respectively. It is worth noticing that when one of the self- or cross-diffusion coefficients varies, its values are selected in the $\{1, 5, 10\}$ range and the remaining coefficients are fixed to 4. The other parameters are given by: $a = 0.25$, $b = -0.15$, $\gamma = 3.6$ and $\sigma = 0.01$

4 Nonlinear solution of the cubic–quintic CGL equation using Hirota's method

The application of the Hirota method via the use of the modified Hirota operator $D^m_{n,\xi}$ is one of the most regular and handy techniques implemented, which produces analytical solutions of the cubic–quintic CGL equation [121–123]. Hirota's bilinear method was first introduced in Ref. [99,100] and used by Nozaki and Bekki [101,102], who have made an ad hoc modification of the definition of the differential operator of Hirota, with a convenient choice of variables. Here, the solution of Eq. (24) is taken in the form $\psi(\xi,\tau) = \frac{g(\xi,\tau)}{f^n(\xi,\tau)}$ [121], where g and f are two differentiable functions of complex-valued and real-valued, respectively. The power $n = 1 + i\alpha$ is a complex constant and n^* its complex conjugate so that $n + n^* = 2$; where the real parameter α will be determined later. Inserting above solution into Eq. (24) and decoupling the obtained relation, we arrive at

$$\left(iD_{n,\tau} + pD^2_{n,\xi} - \lambda - \mu\right)(g\cdot f) = 0, \tag{40}$$

$$f^2\left\{\left(\frac{n(n+1)pD^2_{n,\xi}}{2r} + \frac{i\gamma-\lambda}{r}\right)(f\cdot f) + \frac{(q-\mu)|g|^2}{r}\right\} - |g|^4 = 0, \tag{41}$$

where the two complex constant parameters $\lambda = \lambda_r + i\lambda_i$ and $\mu = \mu_r + i\mu_i$ were introduced as the decoupling parameters. According to Hirota's method [99], the bilinear operator $D^m_{n,\xi}(g\cdot f)$ is defined by

$$D^m_{n,\xi}(g\cdot f) = \left[\left(\frac{\partial}{\partial\xi} - n\frac{\partial}{\partial\xi'}\right)^m g(\xi,\tau)f(\xi',\tau')\right]_{\xi=\xi',\tau=\tau'}, \tag{42}$$

where $m = 0, 1, 2$ is an integer. Accordingly, the constitutive derivatives, in terms of Hirota's operator, can be written as

$$\begin{aligned}
&D_{n,\tau}(g\cdot f)\\
&\quad=\left[\left(\frac{\partial}{\partial\tau}-n\frac{\partial}{\partial\tau'}\right)g(\xi,\tau)f(\xi',\tau')\right]_{\xi=\xi',\tau=\tau'},\\
&D^2_{n,\xi}(g\cdot f)\\
&\quad=\left[\left(\frac{\partial}{\partial\xi}-n\frac{\partial}{\partial\xi'}\right)^2 g(\xi,\tau)f(\xi',\tau')\right]_{\xi=\xi',\tau=\tau'},\\
&D^2_{\xi}(f\cdot f)\\
&\quad=\left[\left(\frac{\partial}{\partial\xi}-n\frac{\partial}{\partial\xi'}\right) f(\xi,\tau)f(\xi',\tau')\right]_{\xi=\xi',\tau=\tau'}.
\end{aligned}\tag{43}$$

As we seek for the solitary wave solution, the functions f and g are supposed to be in the form

$$g = g_0 e^{\theta_3}, \quad \text{and} \quad f = 1 + e^{\theta_3+\theta_3^*}, \tag{44}$$

where $\theta_3 = \kappa\xi - \Lambda\tau$, $\theta_3^* = \kappa^*\xi - \Lambda^*\tau$, $\kappa = \kappa_r + i\kappa_i$ and $\Lambda = \Lambda_r + i\Lambda_i$ being a complex constant. The presence of the term $|g|^4$ on the right-hand side of Eq. (41) implied that all coefficients of the corresponding equation should be real. Therefore, $\mathrm{Im}\left(\frac{n(n+1)p}{2r}\right) = \mathrm{Im}\left(\frac{i\gamma-\lambda}{r}\right) = \mathrm{Im}\left(\frac{q_r-\mu}{r}\right) = 0$, which leads to

$$\begin{aligned}
&\alpha = -\beta \pm \sqrt{\beta^2+2}, \quad \beta = \frac{3(p_r r_r + p_i r_i)}{2(p_r r_i - p_i r_r)},\\
&r_i(\lambda_r+\gamma_i) = r_r(\lambda_i-\gamma_r),\\
&r_r(q_i-\mu_i) = r_i(q_r-\mu_r).
\end{aligned}\tag{45}$$

Here, we assume that $\lambda_r = -\gamma_i$, $\lambda_i = \gamma_r$, $\mu_i = q_i$ and $\mu_r = q_r$. Furthermore, solving the remainder of Eq. (41) at the order $e^{2(\theta_3+\theta_3^*)}$ yields

$$|g_0|^4 = \frac{8\kappa_r^2}{A}, \quad A = \frac{(p_r r_r + p_i r_i)}{|p|^2(2-\alpha^2)}. \tag{46}$$

On the other hand, Eq. (40) at the order $e^{2\theta_3+\theta_3^*}$, taking into account the order e^{θ_3}, leads to

$$\Lambda_r - 2p\kappa_r\kappa_i + 2p\kappa_r^2\alpha = 0. \tag{47}$$

After separating Eq. (47) into real and imaginary parts one obtains $\kappa_i = \alpha\kappa_r$, $\Lambda_r = 0$. Moreover, at the order e^{θ_3}, the same Eq. (40) yields

$$\begin{aligned}
&\Lambda_i = \kappa_r^2(2p_i\alpha - p_r\left(1-\alpha^2\right)) - \gamma_i + q_r,\\
&\kappa_r^2 = \frac{(\gamma_r+q_i)}{2p_r\alpha + p_i\left(1-\alpha^2\right)}.
\end{aligned}\tag{48}$$

We finally get the solitary wave solution as

$$\psi(\xi,\tau) = \frac{g_0 e^{((\kappa_r+i\kappa_i)\xi - i\Lambda_i\tau)}}{(1+e^{((\kappa_r+i\kappa_i)\xi - i\Lambda_i\tau)} + e^{((\kappa_r-i\kappa_i)\xi + i\Lambda_i\tau)})^{1+i\alpha}}, \tag{49}$$

Based on the above results on the Hirota's scheme and taking into consideration Eqs. (5) and (6), the solutions for the generic model Eqs. (1) and (2) are expressed as

$$\begin{aligned}
u(x,t) &= 2\epsilon(\cos(kx-\omega_r t)\psi_r\\
&\quad - \sin(kx-\omega_r t)\psi_i)e^{\omega_i t} + O(\epsilon^2),
\end{aligned}\tag{50}$$

$$\begin{aligned}
v(x,t) &= 2\epsilon((\alpha_r\psi_r - \alpha_i\psi_i)\cos(kx-\omega_r t)\\
&\quad - (\alpha_r\psi_i + \alpha_i\psi_r)\sin(kx-\omega_r t))e^{\omega_i t} + O(\epsilon^2),
\end{aligned}\tag{51}$$

with $\psi_r = \mathrm{Re}(\psi)$ and $\psi_i = \mathrm{Im}(\psi)$. Moreover, the relationship between the pair of variables (ξ,τ) and (x,t) is given by $(\xi,\tau) = \left(\epsilon^2(x-v_g t), \epsilon^4 t\right)$ which implied that above solutions (50) only depends on the state variables (x,t).

Obviously, the solutions given by Eqs.(50) are solitary pulses propagating from left to right. Etémé previously found a similar form of solutions [120] in the context of MI and energy localization in a time-delayed memristive neural network. As shown in Fig. 4, the corresponding analytical solutions are clearly depicted where panels (a) and (b) show the activator variable $u(x,t)$, and inhibitor variable $v(x,t)$, respectively. In other words, the recorded diagrams deliver the features of the fast variable trans-membrane potential $u(x,t)$ and slow variable potential in a spatiotemporal context, where the self- and cross-diffusion constants (d_1, d_2, h_1, h_2) have equal values, with $k = 0.01\pi$. The solution exhibits two peaks, normal and inverted,

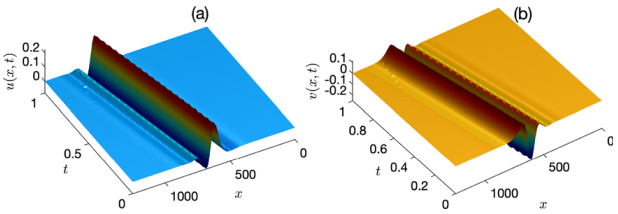

Fig. 4 (Color online) Space-time plots of the analytical solutions (50), where the evolution of cardiac ionic wave of analytical solutions for $u(x,t)$ is shown in panels (**a**), and panels (**b**) displays the plot for the ionic current $v(x,t)$. The features are captured for fixed values of self- and cross diffusion parameters $(d_1, d_2, h_1, h_2 = 10, 10, 10, 10)$

resulting from a change in the sign of the same coefficients. These envelope solitons have an oscillatory profile and transmit information between nodes for better coordination of important cardiac functions downstream and pathological situations upstream [124,125]. Additionally, the action potential starts with a sudden change in membrane potential to -0.05V, followed by a rapid upstroke approaching the sodium equilibrium potential. Finally, there is a fairly quick depolarisation to approximately -0.05V. The potential then moves in a positive direction to $+0.2$V, generating the characteristic "notch" that regulates cardiomyocyte electrical differentiation and intracellular signaling mechanism, as observed in many experimental records [126,127].

5 Numerical simulations

Electrical processes in the heart are initiated in the SA node due to the ionic flow. These processes spread to other components of the heart under various factors, including self- and cross-diffusive effects. Meanwhile, from a physical point of view, dissipative effects affect information stability and the energy that propagates across the cardiac tissue. The purpose of this section is to test the accuracy of the proposed solution by numerically integrating Eqs. (1) and (2) of the generic cubic–quintic FHN model using the standard fourth-order Runge–Kutta computational scheme. The time-step $\Delta t = 10^{-3}$, the spatial dimension coordinate step $\Delta x = 0.25$, the carrier wavenumber $k = 0.01\pi$, and the speed of propagation $v_0 = 0.1/\Delta t$ have been adopted. The parameter v_0 has been introduced here to regulate the propagation speeds of both analytical and numerical solutions. As said so far, the initial conditions are given by Eqs. (50) and (51), and the numerical integration is conducted using Neumann boundary conditions for both $u(x,t)$ and $v(x,t)$. For technical purposes, analytical results are superposed to numerical ones under the context where the phase plane of the global dynamics is unveiled.

To start, Fig. 5 displays the space evolution of the two components $u(x,t)$ and $v(x,t)$, which are the fast traveling pulse and the slow traveling pulse, at different instants $t = 0$ [panels $(\text{aj})_{j=1,2}$], $t = 86$ [panels $(\text{bj})_{j=1,2}$] and $t = 300$ [panels $(\text{cj})_{j=1,2}$]. For $t = 0$ and $t = 86$, there is an accurate correlation between analytical and numerical results, which confirms the effectiveness of our solution. As predicted, the propagation features show direct pulses for $u(x,t)$ and inverted pulses for $v(x,t)$, with additional oscillations. In this case, when $(d_1, d_2, h_1, h_2) = (6, 6, 6, 6)$, there is a slight mismatch between the analytical and numerical pulses of $u(x,t)$ at $t = 300$, but the resulting zigzag-shaped profiles are still recognized as the normal propagation of electrical impulses throughout the medium, with familiar wave regimes such as depolarization, repolarization, and hyperpolarization, which help restore the pulse to its normal state by resetting the blocking mechanism in the system. The panels illustrate the scenario where the upper peaks occur at critical values lower than the lower peak. The graph of $v(x,t)$ in each panel $(\text{bj})_{j=1,2,3}$ shows two upper peaks that have a substantially smaller amplitude than the lower, bigger peak. This indicates an equilibrium of ionic particle random movement across the membrane level. Optical solitonic waves show a similar shape represented by the bright and dark soliton. There is no specific requirement for small values of σ for wave propagation. Due to ion regulation at gap junctions, analytical and numerical solutions have no amplitude gap.

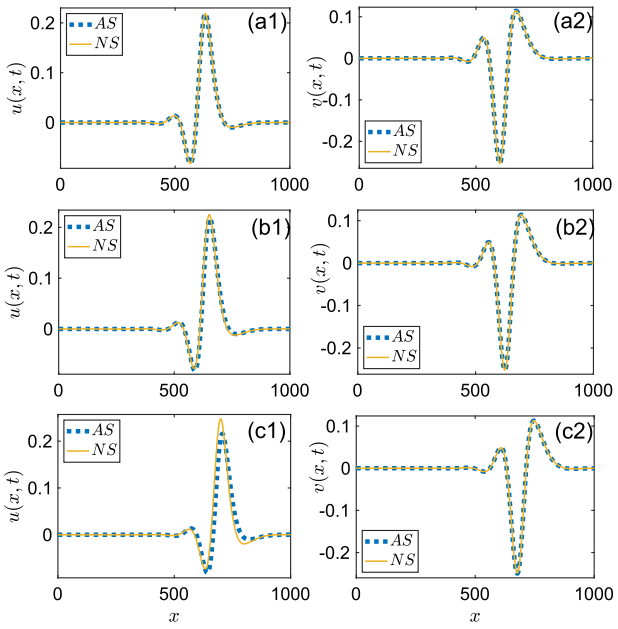

Fig. 5 (Color online) The panels compare analytical and numerical solitary pulses from solutions (50–51) giving $u(x,t)$ and $v(x,t)$. Plots **a1**–**a2** are generated at time $t = 0$. Panels **b1** and **b2** are obtained at time $t = 86$ and panels **c1**–**c2** are obtained at time $t = 300$, with the other parameters being $(d_1, d_2, h_1, h_2) = (6, 6, 6, 6)$, $k = 0.01\pi$, $a = 0.25$, $b = -0.15$, $\gamma = 3.6$ and $\sigma = 0.01$. AS refers to analytical solution (dotted blue line) and NS refers to numerical solution (solid yellow line)

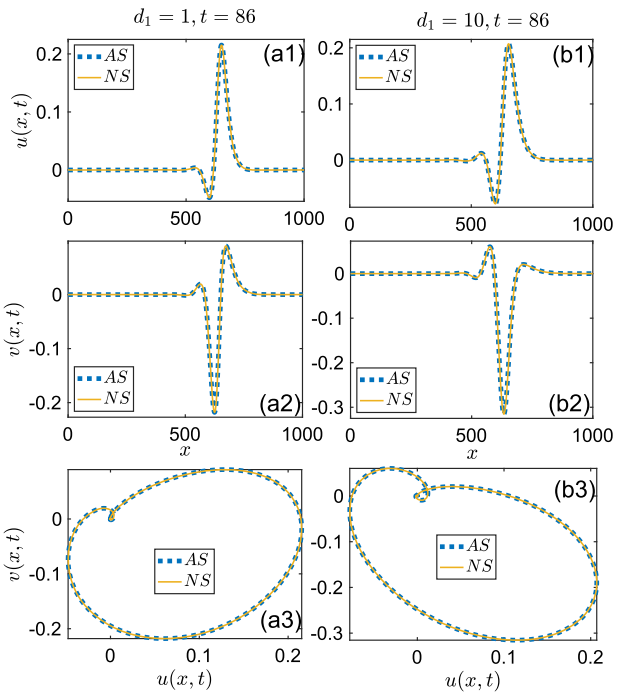

Fig. 6 (Color online) Comparison between analytical and numerical solitary pulse profiles of $u(x,t)$ and $v(x,t)$ under the impact of the self-diffusion coefficient d_1, with $d_1 = 1$ [panels (aj)$_{j=1,2,3}$] and $d_1 = 10$ [panels (bj)$_{j=1,2,3}$]. Panels **a3** and **b3** give the phase planes, respective to values of d_1, with the other parameter values being: $(d_2, h_1, h_2 = 6, 6, 6)$, $k = 0.01\pi$, $a = 0.25$, $b = -0.15$, $\gamma = 3.6$, and $\sigma = 0.01$. AS refers to analytical solution (dotted blue line) and NS refers to numerical solution (solid yellow line)

Figure 6 shows that the effect of the self-diffusion parameter d_1 on membrane potentials is stable upon propagation, meaning there is a perfect correlation between numerical and analytical results, for $d_1 = 1$ [panels (aj)$_{j=1,2}$] and $d_1 = 10$ [panels (bj)$_{j=1,2}$]. The difference in the sharpnesses of the profiles also testifies to the sensitivity of the analytical and numerical solutions to changes in d_1. Obviously, the regimes of solitons are different in terms of amplitudes and increase progressively, i.e., $u(x,t)$ and $v(x,t)$ are increasing functions. From another angle, we can say that the medium may absorb the inward and the outward concentration of ion currents among the gap junction of the cell membrane. However, in some cardiac diseases, there is an expansion of the protein molecules forming the gate channels from intercalated disc to lateral cell borders and reduces conduction velocity [128]. The phase planes of the corresponding components also show some propagative features, from which oscillations in the pulse profiles are materialized by minor nodes along with some manifestations of asymmetric profiles, also sensitive to changes in d_1 [see Fig. 6a3, b3].

For the case displayed in Fig. 7, all other parameters are kept constant, except d_2 that takes the respective values $d_2 = 1$ [panels (aj)$_{j=1,2}$] and $d_2 = 10$ [panels (bj)$_{j=1,2}$]. In general, as the self-diffusion coefficient d_2 increases, so does the amplitude of cardiac impulse $u(x,t)$. Additionally, the more random the distribution of the ions across the membrane, the narrower the width of the action potential and the larger its amplitude [129]. The random wavering in the sequence of cardiac firing times induces this phenomenon. Moreover, we notice an exact correlation between the analytical and numerical solutions whose amplitude increases, therefore confirming the results in Figs. 5 and 6. In addition, the phase planes of Fig. 7a3 and b3 support the fact that increasing d_2 tends to suppress lateral oscillations around the main pulses, a behavior that is mainly triggered by the dynamics of the slow component $v(x,t)$. However, the dynamics remains periodic in both cases.

Figure 8 points out the impact and contribution of changing the cross-diffusion parameter h_1. Like in Figs. 6 and 7, analytical results and numerical simulations are confronted, where $h_1 = 1$ is supported by Fig. 8(aj)$_{j=1,2}$ and $h_1 = 10$ is depicted in Fig. 8(bj)$_{j=1,2}$. While the pulses' dynamics remains robust for the compound of the FHN model, one notices an increase in the pulse amplitudes, which clearly shows that the action potential of the cardiac tissue is an increasing function of the cross-diffusion coefficient h_1. However, further increasing h_1 leads to slight oscillations around the main pulse peaks as shown in Fig. 8(bj)$_{j=1,2}$. On confronting the behaviors of the phase planes corresponding to the two used values of h_1, the phase plane between $u(x,t)$ and $v(x,t)$ shows one cycle for $h_1 = 1$, while the main loop is complemented by a minor inner one for $h_1 = 10$, showing the appearance of additional oscillations around the main pulses (see Figs. 8a3, b3) as discussed earlier. Along the same line, the impact of the cross-diffusion coefficient is addressed in Fig. 9, where panels (aj)$_{j=1,2}$ and (bj)$_{j=1,2}$ correspond to the respective values $h_2 = 1$ and $h_2 = 10$, with all the other parameters being kept fixed. Indeed, the same spectrum of behaviors as in Fig. 8 is delivered and confirms the cross-diffusive effects to bring about more oscillations into the pulse profiles, as testified by the enclosed phase planes. Such behaviours also give the room to discuss the bistability

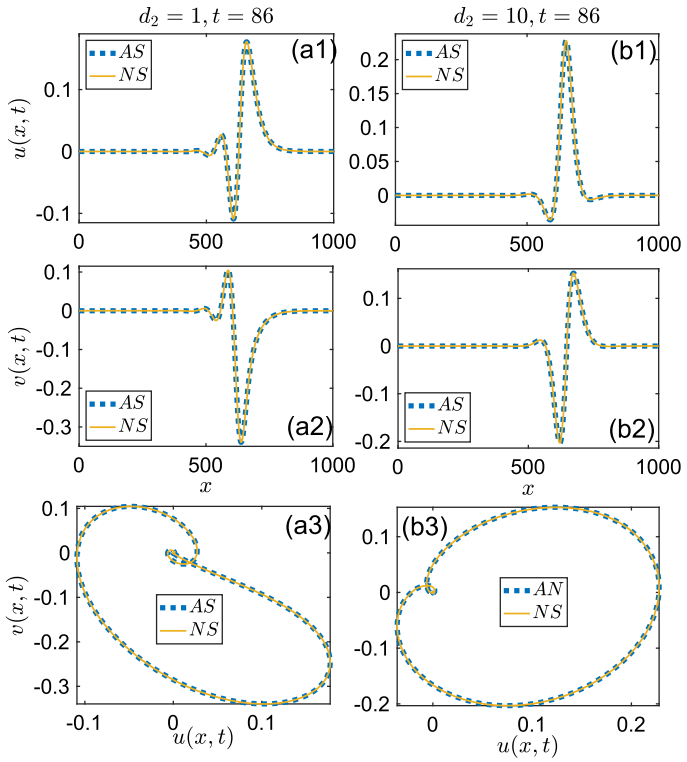

Fig. 7 (Color online) Comparison between analytical and numerical solitary pulse profiles of $u(x,t)$ and $v(x,t)$ under the impact of the self-diffusion coefficient d_2, with $d_2 = 1$ [panels (aj)$_{j=1,2,3}$] and $d_2 = 10$ [panels (bj)$_{j=1,2,3}$]. Panels (a3) and (b3) give the phase planes, respective to values of d_1, with the other parameter values being: $(d_1, h_1, h_2 = 6, 6, 6)$, $k = 0.01\pi$, $a = 0.25$, $b = -0.15$, $\gamma = 3.6$, and $\sigma = 0.01$. AS refers to the analytical solution (dotted blue line), and NS refers to the numerical solution (solid yellow line)

brought by the cross-dispersion that was already identified in Ref. [130] as a direct signature of asymmetric wave trains, also known as caused by some fluctuations in the sequences of myocardial cells firing instants [131].

In order to assess the nontrivial effects of the cross-diffusion described so far, we have switched off self-diffusive effects, i.e., $d_1 = d_2 = 0$, in the system for the results of Fig. 10 to be recorded. In such a context, when $h_1 = h_2 = 1$, one observes the features of Fig. 10(aj)$_{j=1,2}$, where the action potential dynamics is governed by a breather soliton, also known in many physical systems, in the reductive perturbation method, as the solution of the nonlinear Schrödinger equation [115,116,132]. Compared to other results in the paper, the number of oscillations in the pulse's profile has increased due to the absence of the self-diffusions. The same behaviour is also perceptible in the profile of $v(x,t)$, and more interestingly, in their subsequent phase plane that shows a curved single orbit, characteristics of complex periodic dynamics. On the other hand, the panels of Fig. 10(bj)$_{j=1,2}$ display extended breather solitons along with their asymmetric character, with oscillations in their profiles. This gives rise to two inner loops in their typical phase plane of Fig. 10b3. One may therefore suspect that the smaller h_1 and h_2, the faster the action potential in the studied model. Indeed, as

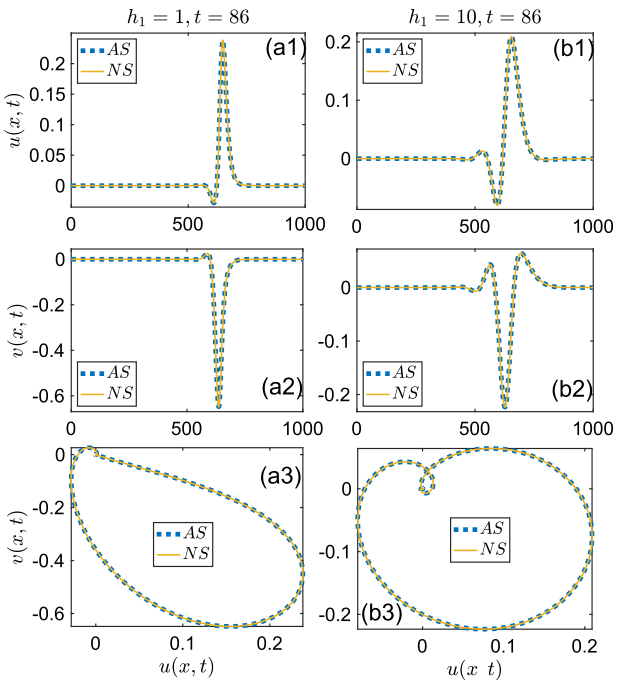

Fig. 8 (Color online) Comparison between analytical and numerical solitary pulse profiles of $u(x,t)$ and $v(x,t)$ under the impact of the cross-diffusion coefficient h_1, with $h_1 = 1$ [panels (aj)$_{j=1,2,3}$] and $h_1 = 10$ [panels (bj)$_{j=1,2,3}$]. Panels **a3** and **b3** give the phase planes, respective to values of h_1, with the other parameter values being: $(d_1, d_2, h_2 = 6, 6, 6)$, $k = 0.01\pi$, $a = 0.25$, $b = -0.15$, $\gamma = 3.6$, and $\sigma = 0.01$. AS refers to analytical solution (dotted blue line) and NS refers to numerical solution (solid yellow line)

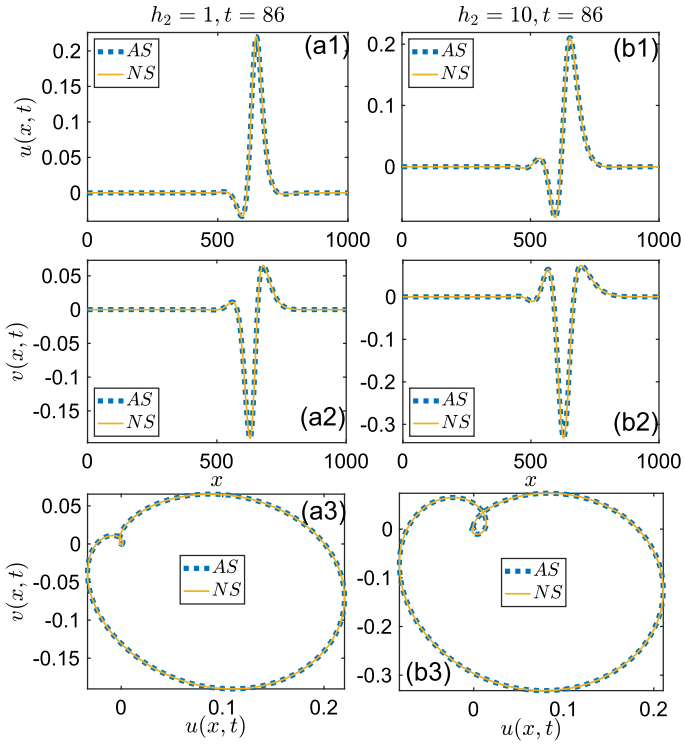

Fig. 9 (Color online) Comparison between analytical and numerical solitary pulse profiles of $u(x,t)$ and $v(x,t)$ under the impact of the cross-diffusion coefficient h_2, with $h_2 = 1$ [panels $(\text{aj})_{j=1,2,3}$] and $h_2 = 10$ [panels $(\text{bj})_{j=1,2,3}$]. Panels **a3** and **b3** give the phase planes, respective to values of h_2, with the other parameter values being: $(d_1, d_2, h_1 = 6, 6, 6)$, $k = 0.01\pi$, $a = 0.25$, $b = -0.15$, $\gamma = 3.6$, and $\sigma = 0.01$. AS refers to analytical solution (dotted blue line) and NS refers to numerical solution (solid yellow line)

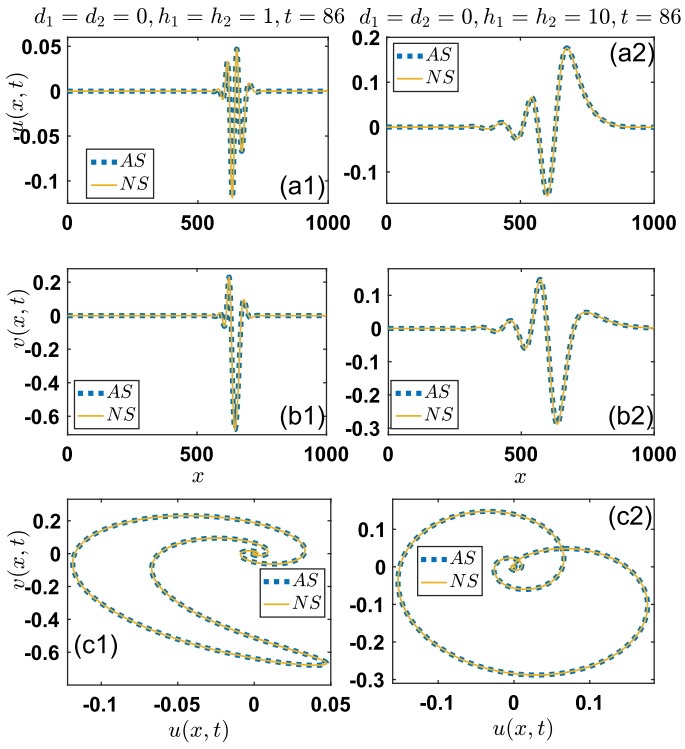

Fig. 10 (Color online) Comparison between analytical and numerical solitary pulse profiles of $u(x,t)$ and $v(x,t)$ under the impact of the cross-diffusion coefficients h_1 and h_2 in the absence of self-diffusive effects, i.e., $d_1 = d_2 = 0$, with $h_1 = h_2 = 1$ [panels $(\text{aj})_{j=1,2,3}$] and $h_1 = h_2 = 10$ [panels $(\text{bj})_{j=1,2,3}$]. Panels **a3** and **b3** give the phase planes, respective to values of $h_1 = h_2$, with the other parameter values being: $k = 0.01\pi$, $a = 0.25$, $b = -0.15$, $\gamma = 3.6$, and $\sigma = 0.01$. AS refers to analytical solution (dotted blue line) and NS refers to numerical solution (solid yellow line)

predicted so far in the linear stability of a plane wave, one may conclude that the obtained patterns may share the same parameter areas with the unstable plane wave solution in the context of MI. This, once more, brings about the evidence shared by the soliton and MI concepts. In the meantime, the reader should be aware that for the MI phenomenon to be efficiently assessed, one should use a perturbed plane wave as the initial condition and observe its longtime evolution. This has been performed in a broad range of RD systems [86,133–

136], with exciting results, and does not constitute the primary objective of this work.

6 Concluding remarks

In the framework of the quintic FHN model combined with linear self-and cross-diffusion, we have used a multiple-scale perturbation theory to exclusively show that the cubic–quintic CGL equation governs the dynamics of nonlinear excitations. Under the standard linear stability analysis of a uniform steady-state solution, instability zones and the analytic expressions of the gain spectrum of MI have been obtained. Using a modified bilinear operator, we derived the bilinear equation for the cubic–quintic CGL equation. Thereafter, we deduced an exact localized dissipative soliton solution and demonstrated its remarkable stability on the quintic FHN model with linear self- and cross-diffusion terms in numerical simulations. As a result, the MI growth rate appeared to be very sensitive to the changes of self- and cross-diffusion coefficients, thus attesting that these space parameters can be the best candidates to control and regulate the formation of nonlinear excitation within myocardial cells. Moreover, a correlation between the analytical and numerical solutions with pulse solitons profiles has been observed. This work gives more insight into the comprehension of the behaviour of the cardiac signals and electrocardiogram. The model studied here can be extended into two-dimensional space to investigate the stability of spiral wave formation as the self- and cross-diffusion coefficients change.

Funding The authors have not disclosed any funding.

Data Availability Statement The simulation data related to the current study are not publicly available but can be obtained from the corresponding author, CBT, on reasonable request.

Declarations

Conflict of interest: The authors declare that they have no Conflict of interest.

Appendices

Appendix 1: Coefficients of Eq. (13)

$$
\begin{aligned}
p = \frac{1}{(2\omega - i(\mu_2+\lambda_1-(d_1+d_2)k^2))}(h_1\mu_1 \\
- (i\omega+\mu_2-d_2k^2)d_1 - (i\omega+\lambda_1-d_1k^2)d_2 \\
+ 6h_1h_2k^2 + 2ih_1k\alpha_0(v_g+2id_2k) \\
- \frac{(v_g+2id_2k)^2(i\omega+\lambda_1-d_1k^2)^2}{(\mu_1+h_2k^2)h_1k^2} \\
+ 2ih_2k\frac{(v_g+2id_2k)(i\omega+\lambda_1-d_1k^2)}{(\mu_1+h_2k^2)}), \\
q = -\frac{(i\omega+\mu_2-d_2k^2)(3\lambda_3+2\lambda_2(\alpha_1+\alpha_3))}{(2\omega-i(\mu_2+\lambda_1-(d_1+d_2)k^2))}.
\end{aligned}
$$

Appendix 2: Coefficients of Eq. (24)

$$
\begin{aligned}
r = \frac{-1}{(2\omega - i(\mu_2+\lambda_1-(d_1+d_2)k^2))}((i\omega+\mu_2 \\
- d_2k^2)(10\lambda_5 + 4\lambda_4(\alpha_3^* + 3(\alpha_1+\alpha_3)) + 3\lambda_3 \\
\times (2|\alpha_3|^2 + \alpha_1^2 + \alpha_7) + 2\lambda_2(\alpha_{11}+\alpha_9+\alpha_7))), \\
\gamma = \frac{(\omega - i(\mu_2+d_2k^2))\lambda_0\alpha_0}{(2\omega-i(\mu_2+\lambda_1-(d_1+d_2)k^2))}.
\end{aligned}
$$

Appendix 3: Expressions of Δ, Δ_r and Δ_i

$$
\begin{aligned}
\Delta = (2\nu\Gamma p_r)^2 + (\Gamma^2 p_i - (q_i + 2r_i|\psi_0|^2)|\psi_0|^2)^2 \\
+ (4\nu^2\Gamma^2 - \Gamma^4)|p|^2 - 2\Gamma^2(p_rq_r + p_iq_i)|\psi_0|^2 \\
- 4\Gamma^2(p_rr_r + p_ir_i)|\psi_0|^2 \\
+ 4i\nu\Gamma p_r(\Gamma^2 p_i - (q_i + 2r_i|\psi_0|^2))|\psi_0|^2 \\
+ 4i\nu\Gamma[(p_iq_r - p_rq_i) + 2(p_ir_r - p_rr_i)|\psi_0|^2]|\psi_0|^2, \\
\Delta_r = (2\nu\Gamma p_r)^2 + (\Gamma^2 p_i - (q_i + 2r_i|\psi_0|^2)|\psi_0|^2)^2 \\
+ (4\nu^2\Gamma^2 - \Gamma^4)|p|^2 - 2\Gamma^2(p_rq_r + p_iq_i)|\psi_0|^2 \\
- 4\Gamma^2(p_rr_r + p_ir_i)|\psi_0|^2, \\
\Delta_i = 4\nu\Gamma p_r(\Gamma^2 p_i - (q_i + 2r_i|\psi_0|^2)|\psi_0|^2) \\
+ 4\nu\Gamma[(p_rq_i - p_iq_r) + 2(p_ir_r - p_rr_i)|\psi_0|^2]|\psi_0|^2.
\end{aligned}
$$

References

1. Tyson, J.J., Keener, J.P.: Singular perturbation theory of traveling waves in excitable media (a review). Physica D **32**, 327 (1988)
2. Turing, A.M.: The chemical basis of morphogenesis. Phil. Trans. R Soc. B **237**, 37 (1952)
3. Zhabotinskii, A.M.: The early period of systematic studies of oscillations and waves in chemical systems. In: Field, R., Burger, M. (eds.) Oscillations and Traveling Waves in Chemical Systems, vol. 1. Wiley, New York (1985)

4. Belousov, V.: A periodic reaction and its mechanism. In: Field, R., Burger, M. (eds.) Oscillations and Traveling Waves in Chemical Systems, vol. 605. Wiley, New York (1985)
5. Zhabotinskii, A.M.: Periodic course of the oxidation of malonic acid in a solution (Studies on the kinetics of Beolusovs reaction). Biofizika **9**, 306 (1964)
6. Vanag, V.K., Epstein, I.R.: Cross-diffusion and pattern formation in reaction-diffusion systems. Phys. Chem. Phys. **11**, 897 (2009)
7. Tsyganov, M.A., Biktashev, V.N., Brindley, J., Holden, A.V., Ivanitsky, G.R.: Waves in systems with cross-diffusion as a new class of nonlinear waves. Phys. Usp. **50**, 263 (2007)
8. Castets, V., Dulos, E., Boissonade, J., De Kepper, P.: Experimental evidence of a sustained standing Turing-type nonequilibrium chemical pattern. Phys. Rev. Lett. **64**, 2953 (1990)
9. Ouyang, Q., Swinney, H.L.: Transition from a uniform state to hexagonal and striped Turing patterns. Nature **352**, 610 (1991)
10. Vanag, V.K., Epstein, I.R.: Pattern formation in a tunable medium: the Belousov-Zhabotinsky reaction in an aerosol at microemulsion. Phys. Rev. Lett. **87**, 228301 (2001)
11. Tyrrell, H.J.V., Harris, K.R.: Diffusion in Liquids: A Theoretical and Experimental Study. Butterworths, London (1984)
12. Lenk, C., Einax, M., Kohler, J.M., Maass, P.: Complex oscillation modes in the Belousov-Zhabotinsky reaction by weak diffusive coupling. Phys. Rev. E **99**, 022202 (2019)
13. Almirantis, Y., Papageorgiou, S.: Cross-diffusion effects on chemical and biological pattern formation. J. Theor. Biol. **151**, 289 (1991)
14. Ling, Z., Zhang, L., Lin, Z.: Turing pattern formation in a predator-prey system with cross-diffusion. Appl. Math. Model. **38**, 5022 (2014)
15. Banerjee, M., Ghorai, S., Mukherjee, N.: Study of cross-diffusion induced Turing patterns in a ratio-dependent prey-predator model via amplitude equations. Appl. Math. Model. **55**, 383 (2018)
16. Madzvamuse, A., Ndakwo, H.S., Barreira, R.: Cross-diffusion-driven instability for reaction-diffusion systems: analysis and simulations. J. Math. Biol. **70**, 709 (2015)
17. Yang, R.: Cross-diffusion induced spatiotemporal patterns in Schnakenberg reaction-diffusion model. Nonl. Dyn. **110**, 1753 (2022)
18. Tsyganov, M.A., Brindley, J., Holden, A.V., Biktashev, V.N.: Quasisoliton interaction of pursuit-evasion waves in a predator-prey system. Phys. Rev. Lett. **91**, 218102 (2003)
19. Tsyganov, M.A., Brindley, J., Holden, A.V., Biktashev, V.N.: Soliton-like phenomena in one-dimensional cross-diffusion systems: a predator-prey pursuit and evasion example. Physica D **197**, 18 (2004)
20. Guin, L.N.: Spatial patterns through Turing instability in a reaction-diffusion predator-prey model. Math. Comput. Simul. **109**, 174 (2015)
21. Truscott, J.E., Brindley, J.: Equilibria, stability and excitability in a general class of plankton population models. Philos. Trans. R. Soc. Lond.-Ser. A **347**, 703 (1994)
22. Britton, N.F.: Essential Mathematical Biology. Springer, New York (2003)
23. Sherratt, J.A., Smith, M.J.: Periodic traveling waves in cyclic populations: field studies and reaction-diffusion models. J. R. Soc.-Interface **5**, 483 (2008)
24. Rosenzweig, M.L., MacArthur, R.H.: Graphical representation and stability conditions of predator-prey interactions. Am. Nat. **97**, 209 (1963)
25. Biktashev, V.N., Tsyganov, M.A.: Spontaneous traveling waves in oscillatory systems with cross-diffusion. Phys. Rev. E **80**, 056111 (2009)
26. Tian, C., Lin, Z., Pedersen, M.: Instability induced by cross-diffusion in reaction-diffusion systems. Nonl. Anal. **11**, 1036 (2010)
27. Shi, J., Xie, Z., Little, K.: Cross-diffusion induced instability and stability in reaction-diffusion systems. J. Appl. Anal. Comput. **24**, 95 (2010)
28. Zemskov, E.P., Vanag, V.K., Epstein, I.R.: Amplitude equations for reaction-diffusion systems with cross-diffusion. Phys. Rev. E **84**, 036216 (2011)
29. Field, R.J., Noyes, R.M.: Oscillations in chemical systems. IV. Limit cycle behavior in a model of a real chemical reaction. J. Chem. Phys. **60**, 1877 (1974)
30. Tyson, J.J., Fife, P.C.: Target patterns in a realistic model of the Belousov-Zhabotinskii reaction. J. Chem. Phys. **73**, 2224 (1980)
31. Nicolis, G., Prigogine, I.: Self-Organization in Nonequilibrium Systems. Wiley-Interscience, New York (1977)
32. Biktashev, V.N., Tsyganov, M.A.: Envelope quasisolitons in dissipative systems with cross-diffusion. Phys. Rev. Lett. **107**, 134101 (2011)
33. Hodgkin, A.L., Huxley, A.F.: A quantitative description of membrane current and its application to conduction and excitation in nerve. J. Physiol. **117**, 500 (1952)
34. Hindmarsh, J.L., Rose, R.: A model of the nerve impulse using two first-order differential equations. Nature **296**, 162 (1982)
35. Hindmarsh, J.L., Rose, R.: A model of neuronal bursting using three coupled first order differential equations. Proc. R. Soc. Lond.-Ser. B **221**, 87 (1984)
36. Dtchetgnia, S.R.D., Yamapi, R., Kofané, T.C., Aziz-Alaoui, M.A.: Deterministic and stochastic bifurcations in the Hindmarsh-Rose neuronal model. Chaos **23**, 033125 (2013)
37. Tabi, C.B., Etémé, A.S., Mohamadou, A., Kofané, T.C.: Unstable discrete modes in Hindmarsh-Rose neural networks under magnetic flow effect. Chaos Solit. Fract. **123**, 116 (2019)
38. Tene, A.G., Kofané, T.C., Tchoffo, M.: Generalized synchronization of the extended Hindmarsh-Rose neuronal model with fractional order derivative. Chaos Solit. Fract. **118**, 311 (2019)
39. Izhikevich, E.M.: Simple model of spiking neurons. IEEE Trans. Neural Net. **14**, 1569 (2003)
40. Tsumoto, K., Kitajima, H., Yoshinaga, T., Aihara, K., Kawakami, H.: Bifurcations in Morris-Lecar neuron model. Neurocomput. **69**, 293 (2006)
41. Chay, T.R.: Chaos in a three-variable model of an excitable cell. Physica D **16**, 233 (1985)
42. Njitacke, Z.T., Isaac, S.D., Nestor, T., Kengne, J.: Hamiltonian energy computation and complex behavior of a small heterogeneous network of three neurons: circuit implementation. Neural Comput. Appl. **1**, 20 (2020)

43. Xu, Q., Liu, T., Feng, C.T., Bao, H., Wu, H.G., Bao, B.C.: Continuous non-autonomous memristive Rulkov model with extreme multistability. Chin. Phys. B **30**, 128702 (2021)
44. Tene, A.G., Tchoffo, M., Tabi, C.B., Kofané, T.C.: Generalized synchronization of regulate seizures dynamics in partial epilepsy with fractional-order derivatives. Chaos Solit. Fract. **132**, 109553 (2020)
45. FitzHugh, R.: Impulses and physiological states in theoretical models of nerve membrane. Biophys. J. **1**, 445 (1961)
46. Nagumo, J., Animoto, S., Yoshizawa, S.: An active pulse transmission line simulating nerve axon. Proc. Inst. Radio Eng. **50**, 2061 (1962)
47. Takembo, C.N., Mvogo, A., Fouda, H.P.E., Kofané, T.C.: Localized modulated wave solution of diffusive FitzHugh-Nagumo cardiac networks under magnetic flow effect. Nonl. Dyn. **95**, 1079 (2019)
48. Takembo, C.N., Mvogo, A., Fouda, H.P.E., Kofané, T.C.: Effect of electromagnetic radiation on the dynamics of spatiotemporal patterns in memristor-based neuronal network. Nonl. Dyn. **95**, 1067 (2019)
49. Tabi, C.B., Etémé, A.S., Kofané, T.C.: Unstable cardiac multi-spiral waves in a FitzHugh-Nagumo soliton model under magnetic flow effect. Nonl. Dyn. **100**, 3799 (2020)
50. Takembo, C.N., Fouda, H.P.E.: Effect of temperature fluctuation on the localized pattern of action potential in cardiac tissue. Sci. Rep. **10**, 15087 (2020)
51. Njitacke, Z.T., Takembo, C.N., Awrejcewicz, J., Fouda, H.P.E., Kengne, J.: Hamilton energy, complex dynamical analysis and information patterns of a new memristive FitzHugh-Nagumo neural network. Chaos Solit. Fract. **160**, 112211 (2022)
52. Njitacke, Z.T., Ramadoss, J., Takembo, C.N., Rajagopal, K., Awrejcewicz, J.: Hamilton energy, complex dynamical analysis and information patterns of a new memristive FitzHugh-Nagumo neural network. Chaos Solit. Fract. **167**, 113014 (2023)
53. Biktashev, V.N., Tsyganov, M.A.: Solitary waves in excitable systems with cross-diffusion. Proc. R. Soc. **461**, 3711 (2005)
54. Zemskov, E.P., Kassner, K., Hauser, M.J.B.: Wavy fronts and speed bifurcation in excitable systems with cross diffusion. Phys. Rev. E **77**, 036219 (2008)
55. Zemskov, E.P., Epstein, I.R., Muntean, A.: Oscillatory pulses in FitzHugh-Nagumo type systems with cross-diffusion. Math. Med. Biol. **28**, 217 (2011)
56. Lengyel, I., Epstein, I.R.: Modeling of Turing structures in the chlorite-iodide-malonic acid-starch reaction system. Science **251**, 650 (1991)
57. Tsyganov, M.A., Biktashev, V.N.: Classification of wave regimes in excitable systems with linear cross-diffusion. Phys. Rev. E **90**, 062912 (2014)
58. Zemskov, E.P., Tsyganov, M.A., Horsthemke, W.: Oscillatory pulses and wave trains in a bistable reaction-diffusion system with cross-diffusion. Phys. Rev. E **95**, 012203 (2017)
59. Zemskov, E.P., Tsyganov, M.A., Horsthemke, W.: Oscillatory pulse-front waves in a reaction-diffusion system with cross diffusion. Phys. Rev. E **97**, 062206 (2018)
60. Berezovskaya, F., and Toni, B. (ed.): Mathematical sciences with multidisciplinary applications. Springer Proceedings in Mathematics and Statistics 157
61. Zemskov, E.P.: Front bifurcation in a tristable reaction-diffusion system under periodic forcing. Phys. Rev. E **69**, 036208 (2004)
62. Descalzi, O., Akhmediev, N., Brand, H.R.: Exploding dissipative solitons in reaction-diffusion systems. Phys. Rev. E **88**, 042911 (2013)
63. Zemskov, E.P., Tsyganov, M.A., Kassner, K., Horsthemke, W.: Nonlinear waves in a quintic FitzHugh-Nagumo model with cross-diffusion: fronts, pulses and wave trains. Chaos **31**, 033141 (2021)
64. Koga, S., Kuramoto, Y.: Localized patterns in reaction-diffusion systems. Prog. Theor. Phys. **63**, 106 (1980)
65. van Saarloss, W.: Front propagation into unstable states. II. Linear versus nonlinear marginal stability and rate of convergence. Phys. Rev. A **39**, 6367 (1989)
66. Descalzi, O., Hayase, Y., Brand, H.R.: Analytical approach to localized structures in a simple reaction-diffusion system. Phys. Rev. E **69**, 026121 (2004)
67. Ma, W.-X., Chen, M.: Direct search for exact solutions to the nonlinear Schrodinger equation. Appl. Math. Comput. **215**, 2835 (2009)
68. Ma, W.-X.: Matrix integrable fourth-order nonlinear Schrödinger equations and their exact soliton solutions. Chin. Phys. Lett **39**, 100201 (2022)
69. Wu, Y., Zhang, J., Cao, J., Abdel-Aty, M.: Hybrid $L_1 \times \ell_1$-gain performance analysis and synthesis of hybrid positive systems. Commun. Nonlinear Sci. Numer. Simul. **126**, 107493 (2023)
70. Benjamin, T.B., Feir, J.E.: The disintegration of wave trains on deep water. J. Fluid Mech. **27**, 417 (1967)
71. Panguetna, C.S., Tabi, C.B., Kofané, T.C.: Two-dimensional modulated ion-acoustic excitations in electronegative plasmas. Phys. Plasmas **24**, 092114 (2017)
72. Tabi, C.B., Panguetna, C.S., Kofané, T.C.: Electronegative (3+1)-dimensional modulated excitations in plasmas. Phys. B **545**, 370 (2018)
73. Panguetna, C.S., Tabi, C.B., Kofané, T.C.: Electronegative nonlinear oscillating modes in plasmas. Commun. Nonl. Sci. Numer. Simul. **55**, 326 (2018)
74. Ndebele, K.K., Tabi, C.B., Kofané, T.C.: Modulational instability in nonlinear doped optical fiber induced by the cubic-quintic-septic complex Ginzburg-Landau equation with higher-order dispersions. J. Opt. Soc. Am. B **37**, A214 (2020)
75. Ndebele, K.K., Tabi, C.B., Tiofack, C.G.L., Kofané, T.C.: Higher-order dispersion and nonlinear effects of optical fibers under septic self-steepening and self-frequency shift. Phys. Rev. E **104**, 044208 (2021)
76. Zanga, D., Fewo, S.I., Tabi, C.B., Kofané, T.C.: Generation of dissipative solitons in a doped optical fiber modeled by the higher-order dispersive cubic-quintic-septic complex Ginzburg-Landau equation. Phys. Rev. A **105**, 023502 (2022)
77. Tabi, C.B., Tagwo, H., Kofané, T.C.: Modulational instability in nonlinear saturable media with competing nonlocal nonlinearity. Phys. Rev. E **106**, 054201 (2022)
78. Souleymanou, A., Alphonse, H., Lanre, A., Mustafa, I., Serge, Y.D., Kofané, T.C.: Synchronized wave and modu-

lation instability gain induce by the effects of higher-order dispersions in nonlinear optical fibers. Opt. Quantum Electron **54**, 642 (2022)
79. Souleymanou, A., Youssoufa, S., Alphonse, H., Lanre, A., Mustafa, I., Thomas, B.B.: Modulated wave and modulation instability gain brought by the cross-phase modulation in birefringent fibers having anti-cubic nonlinearity. Phys. Lett. A **442**, 128191 (2022)
80. Hamadou, H., Souleymanou, A., Alphonse, H., Lanre, A., Mustafa, I., Thomas, B.B.: Rational W-shape solitons on a nonlinear electrical transmission line with Josephson junction. Phys. Lett. A **430**, 127951 (2022)
81. Abemgnigni, N.M., Tabi, C.B., Kofané, T.C.: Few-cycle optical pulses in negative index materials with dispersive permittivity and permeability. J. Opt. Soc. Am. B **37**, A331 (2020)
82. Megne, L.T., Tabi, C.B., Kofané, T.C.: Modulation instability in nonlinear metamaterials modeled by a cubic-quintic complex Ginzburg-Landau equation beyond the slowly varying envelope approximation. Phys. Rev. E **102**, 042207 (2020)
83. Kivshar, Y.S., Peyrard, M.: Modulational instabilities in discrete lattices. Phys. Rev. A **46**, 3198 (1992)
84. Hennig, D.: Next-nearest neighbor interaction and localized solutions of polymer chains. Eur. Phys. J. B **20**, 419 (2001)
85. Tabi, C.B., Koko, A.D., Doko, R.D., Fouda, H.P.E., Kofané, T.C.: Modulated charge patterns and noise effect in a twisted DNA model with solvent interaction. Phys. A **442**, 498 (2016)
86. Tabi, C.B., Maïna, I., Mohamadou, A., Ekobena, H.P.F., Kofané, T.C.: Long-range intercellular Ca^{2+} wave patterns. Phys. A **435**, 1 (2015)
87. Tabi, C.B., Mohamadou, A., Kofané, T.C.: Modulational instability of charge transport in the Peyrard-Bishop-Holstein model. J. Phys. Condens. Matter **21**, 335101 (2009)
88. Ndzana, F., II., Mohamadou, A., Kofané, T.C.: Discrete Lange-Newell criterion for dissipative systems. Phys. Rev. E **79**, 056611 (2009)
89. Mohamadou, A., Jiotsa, A.K., Kofané, T.C.: Modulational instability and unstable patterns in the discrete complex cubic Ginzburg-Landau equation with first and second neighbor couplings. Phys. Rev. E **72**, 036220 (2005)
90. Alphonse, H., Abbagari, S., Lanre, A., Serge, Y.D., Mustafa, I.: Discrete breathers incited by the intra-dimers parameter in microtubulin protofilament array. Eur. Phys. J. Plus **137**, 465 (2022)
91. Otlaadisa, P., Tabi, C.B., Kofané, T.C.: Modulation instability in helicoidal spin-orbit coupled open Bose-Einstein condensates. Phys. Rev. E **103**, 052206 (2021)
92. Tabi, C.B., Veni, S., Kofané, T.C.: Generation of matter waves in Bose-Bose mixtures with helicoidal spin-orbit coupling. Phys. Rev. A **104**, 033325 (2021)
93. Tabi, C.B., Veni, S., Kofané, T.C.: (2+1)-dimensional unstable matter waves in self-interacting pseudospin-1/2 BECs under combined Rashba and Dresselhaus spin-orbit couplings. Phys. Lett. A **442**, 128192 (2022)
94. Tabi, C.B., Otlaadisa, P., Kofané, T.C.: Modulation instability of two-dimensional Bose-Einstein condensates with helicoidal and a mixture of Rashba-Dresselhaus spin-orbit couplings. Phys. Lett. A **449**, 128334 (2022)
95. Alphonse, H., Souleymanou, A., Lanre, A., Mustafa, I., Serge, Y.D.: Wave propagation in discrete cold bosonic atoms zig-zag optical lattice. Eur. Phys. J. Plus **137**, 1029 (2022)
96. Shao-Wen, Y., Raheela, M., Asim, Z., Mustafa, I., Souleymanou, A., Alphonse, H.: Exact soliton solutions to the Cahn-Allen equation and Predator-Prey model with truncated M-fractional derivative. Results Phys. **37**, 105455 (2022)
97. Agrawal, G.P.: Nonlinear Fiber Optics, 4th edn. Academic Press, San Diego (2006)
98. Tai, K., Hasegawa, A., Tomita, A.: Observation of modulational instability in optical fibers. Phys. Rev. Lett. **56**, 135 (1986)
99. Hirota, R.: Direct methods in soliton theory. In: Bullough, R.K., Caudrey, P. (eds.) Solitons. Topics in current physics, vol. 17. Springer, Berlin (1980)
100. Hirota, R., Iwanami, S.: Direct Method in Soliton Theory 1992. Cambridge University Press, Cambridge (2004)
101. Nozaki, K., Bekki, N.: Exact solutions of the generalized Ginzburg-Landau equation. J. Phys. Soc. Jpn. **53**, 1581 (1984)
102. Nozaki, K., Bekki, N.: Pattern selection and spatiotemporal transition to chaos in the Ginzburg-Landau equation. Phys. Rev. Lett. **51**, 2171 (1983)
103. Ma, Y.-L., Wazwaz, A.-M., Bang-Qing, L.: Soliton resonances, soliton molecules, soliton oscillations and heterotypic solitons for the nonlinear Maccari system. Nonl. Dyn. **111**, 18331 (2023)
104. Ma, Y.-L., Bang-Qing, L.: Soliton interactions, soliton bifurcations and molecules, breather molecules, breather-to-soliton transitions, and conservation laws for a nonlinear (3+1)-dimensional shallow water wave equation. Nonl. Dyn. **112**, 2851 (2024)
105. Ma, Y.-L., Wazwaz, A.-M., Bang-Qing, L.: A new (3+1)-dimensional Sakovich equation in nonlinear wave motion: Painlevé integrability, multiple solitons and soliton molecules. Qual. Theory Dyn. Syst. **21**, 158 (2022)
106. Cross, M.C., Hohenberg, P.C.: Pattern formation outside of equilibrium. Rev. Mod. Phys. **65**, 851 (1993)
107. Akhmediev, N.N., Ankiewicz, A., Soto-Crespo, J.M.: Multisoliton solutions of the complex Ginzburg-Landau equation. Phys. Rev. Lett. **79**, 4047 (1997)
108. Pelap, F.B., Kofané, T.C., Flytzanis, N., Remoissenet, M.: Wave modulations in the nonlinear bi-inductance transmission line. J. Phys. Soc. Jpn. **70**, 2568 (2001)
109. Benjamin, T.B., Feir, J.E.: The disintegration of wave trains on deep water Part 1. Theory. J. Fluid Mech. **27**, 417 (1967)
110. Tabi, C.B., Mohamadou, A., Kofané, T.C.: Formation of localized structures in the Peyrard-Bishop-Dauxois model. J. Phys. Cond. Matter **20**, 415104 (2008)
111. Tiofack, C.G.L., Mohamadou, A., Kofané, T.C., Moubissi, A.B.: Generation of pulse trains in nonlinear optical fibers through the generalized complex Ginzburg-Landau equation. Phys. Rev. E **80**, 066604 (2009)
112. Mohamadou, A., Kofané, T.C.: Modulational instability and pattern formation in discrete dissipative systems. Phys. Rev. E **73**, 046607 (2006)

113. Mohamadou, A., Ayissi, B.E., Kofané, T.C.: Instability criteria and pattern formation in the complex Ginzburg-Landau equation with higher-order terms. Phys. Rev. E **74**, 046604 (2006)
114. Ndzana, F., II., Mohamadou, A., Kofané, T.C., English, L.Q.: Modulated waves and pattern formation in coupled discrete nonlinear LC transmission lines. Phys. Rev. E **78**, 016606 (2008)
115. Panguetna, C.S., Tabi, C.B., Kofané, T.C.: Low relativistic effects on the modulational instability of rogue waves in electronegative plasmas. J. Theor. Appl. Phys. **13**, 237 (2019)
116. Panguetna, C.S., Tabi, C.B., Kofané, T.C.: Electronegative nonlinear oscillating modes in plasmas. Commun. Nonl. Sci. Numer. Simul. **55**, 326 (2018)
117. Seadawy, A.: Modulation instability analysis for the generalized derivative higher order nonlinear Schrödinger equation and its bright and dark soliton solutions. J. Electromagn. Waves Appl. **31**, 1353 (2017)
118. Belobo, D.B., Ekogo, T.B., Ben-Bolie, G.H., Tiofack, C.G.L., Kofané, T.C.: Modulational instability of a Bose-Einstein condensate beyond the Fermi pseudopotential with a time-dependent complex potential. Int. J. Mod. Phys. B **26**, 1250164 (2012)
119. Orazio, D., Servet, M., Enrique, T.: Thermodynamic potentials for non-equilibrium systems. Chaos Solit. Fract. **12**, 2619 (2001)
120. Etémé, A.S.: Consistency between modulational instability and energy localization in time-delay-memristive neural network. EPL **143**, 42002 (2023)
121. Liu, W., Yu, W., Yang, C., Liu, M., Zhang, L., Lei, M.: Analytic solutions for the generalized complex Ginzburg-Landau equation in fiber lasers. Nonl. Dyn. **89**, 2933 (2017)
122. Yomba, E., Kofané, T.C.: Exact solutions of the one-dimensional generalized modified complex Ginzburg-Landau equation. Chaos Solit. Fract. **17**, 847 (2003)
123. Yomba, E., Kofané, T.C.: Solutions of the lowest order complex Ginzburg-Landau equation. J. Phys. Soc. Jpn. **69**, 1027 (2000)
124. McAllister, R.E., Noble, D., Tsien, R.W.: Reconstruction of the electrical activity of cardiac Purkinje fibres. J. Physiol. **251**, 1 (1975)
125. Ghomsi, P.G., Tameh, T.J.B., Moukam, F.M.K.: Ionic wave propagation and collision in an excitable circuit model of microtubules. Chaos **28**, 023106 (2018)
126. Draper, M.H., Weidmann, S.: Cardiac resting and action potentials recorded with an intracellular electrode. J. Physiol. **115**, 74 (1951)
127. MacGrogan, D., Luna-Zurita, L., de la Pompa, J.L.: Notch signaling in cardiac valve development and disease. Birth Defects Res.-Part A **91**, 449 (2011)
128. Jongsma, H.J., Wilders, R.: Gap junctions in cardiovascular disease. Circ. Res. **86**, 1193 (2000)
129. Almirantis, Y., Papageorgiou, S.: Cross-diffusion effects on chemical and biological pattern formation. J. Theor. Biol. **151**, 289 (1991)
130. Zemskov, E.P., Tsyganov, M.A., Ivanitsky, G.R., Horsthemke, W.: Solitary pulses and periodic wave trains in a bistable FitzHugh-Nagumo model with cross-diffusion and cross advection. Phys. Rev. E **105**, 014207 (2022)
131. Noble, D., Rudy, Y.: Models of cardiac ventricular action potentials: iterative interaction between experiment and simulation. Phil. Trans. R. Soc. A **359**, 1127 (2021)
132. Madimabe, E.B., Tabi, C.B., Latchio, T.C.G., Kofané, T.C.: Modulational instability in vector exciton-polariton condensates with photonic spin-orbit coupling. Phys. Rev. B **107**, 184502 (2023)
133. Tabi, C.B., Maïna, I., Mohamadou, A., Ekobena, F.H.P., Kofané, T.C.: Wave instability of intercellular Ca^{2+} oscillations. EPL **106**, 18005 (2014)
134. Tabi, C.B., Etémé, A.S., Mohamadou, A., Kofané, T.C.: Oscillating two-dimensional Ca^{2+} waves in cell networks with bidirectional paracrine signaling. Waves Rand. Complex Media **31**, 1028 (2021)
135. Zaoro, N.R., Tabi, C.B., Etémé, A.S., Kofané, T.C.: Unstable cAMP wave patterns during aggregation of Dictyostelium discoideum cells. Phys. Lett. A **384**, 126133 (2020)
136. Legoya, P., Etémé, A.S., Tabi, C.B., Mohamadou, A., Kofané, T.C.: Frequency modes of unstable spiral waves in two-dimensional Rosenzweig-MacArthur ecological networks. Chaos Soliton Fract. **146**, 112599 (2022)